Modèles effectifs de nouvelle physique au Large Hadron Collider

Jérémie Llodra-Perez

N° d'ordre 127-2011
LYCEN – T 2011-08

Thèse

présentée devant

l'Université Claude Bernard Lyon-I

École Doctorale de Physique et d'Astrophysique

pour l'obtention du

DIPLÔME de DOCTORAT
Spécialité : Physique des Particules / Physique Théorique

(arrêté du 7 août 2006)

par

Jérémie LLODRA-PEREZ

Modèles effectifs de nouvelle physique au Large Hadron Collider

Soutenue le 1er juillet 2011
devant la Commission d'Examen

Jury :	M.	A.	Deandrea	Directeur de thèse
	M.	G.	Cacciapaglia	Directeur de thèse
	M.	D.	Tsimpis	Président du jury
	Mme	G.	Servant	Rapporteur
	M.	E.	Dudas	Rapporteur
	M.	G.	Moreau	Examinateur

N°d'ordre: 127-2011 Année 2011

THÈSE DE DOCTORAT DE L'UNIVERSITÉ DE LYON

délivrée par L'UNIVERSITÉ CLAUDE BERNARD LYON 1

ÉCOLE DOCTORALE DE PHYSIQUE ET
D'ASTROPHYSIQUE DE LYON

DIPLÔME DE DOCTORAT

(arrêté du 7 août 2006)

Spécialité

Physique théorique / Physique des particules

Présentée par

M. Jérémie LLODRA-PEREZ

Modèles effectifs de nouvelle physique au Large Hadron Collider

Soutenue publiquement le 01 Juillet 2011 devant la commission d'examen formée de:

M.	D.	Tsimpis	*Président du jury*	-	IPN Lyon
M.	E.	Dudas	*Rapporteur*	-	CPHT Palaisau
Mme.	G.	Servant	*Rapporteur*	-	CERN Genève
M.	G.	Moreau	*Examinateur*	-	LPT Orsay
M.	G.	Cacciapaglia	*Directeur de thèse*	-	IPN Lyon
M.	A.	Deandrea	*Directeur de thèse*	-	IPN Lyon

N°d'ordre: 127-2011 Year 2011

PHD THESIS of the UNIVERSITY of LYON

Delivered by the UNIVERSITY CLAUDE BERNARD LYON 1

Subject:

Theoritical Physics / Particles Physics

submitted by

Mr. Jérémie LLODRA-PEREZ

for the degree of

DOCTOR OF PHILOSOPHY

Effective Models of new physics at the Large Hadron Collider

---

defended July 1st, 2011 in front of the following Examining Committee:

Mr.	D.	Tsimpis	*President*	-	IPN Lyon
Mr.	E.	Dudas	*Reviewer*	-	CPHT Palaiseau
Mrs.	G.	Servant	*Reviewer*	-	CERN Geneva
Mr.	G.	Moreau	*Examiner*	-	LPT Orsay
Mr.	G.	Cacciapaglia	*Supervisor*	-	IPN Lyon
Mr.	A.	Deandrea	*Supervisor*	-	IPN Lyon

Résumé

Grâce à l'exploitation du Large Hadron Collider, débutée en 2010, le monde de la physique des particules espère enfin avoir une compréhension plus précise du mécanisme de brisure de la symétrie électrofaible et résoudre certaines questions expérimentales et théoriques que soulèvent encore le modèle standard. S'inscrivant dans cette effervescence scientifique, nous allons présenter dans ce manuscrit une paramétrisation largement indépendante des modèles afin de caractériser les effets d'une éventuelle nouvelle physique sur les mécanismes de production et de désintégration du boson de Higgs. Ce nouvel outil pourra aisément être utilisé dans les analyses des grandes expériences généralistes comme CMS et ATLAS afin de valider ou d'exclure de manière significative certaines théories au delà du modèle standard.

Ensuite, dans une approche différente, fondée sur la construction de modèles, nous avons considéré un scenario où les champs du modèle standard peuvent se propager dans un espace plat possédant six dimensions. Les nouvelles directions spatiales supplémentaires sont compactifiées sur un Plan Projectif Réel. Cet *orbifold* original est l'unique géométrie à six dimensions qui présente des fermions chiraux et un candidat de matière noire dit *naturel*. Le photon scalaire, particule la plus légère du premier mode de Kaluza-Klein, est en effet stabilisé par une symétrie résiduelle de l'invariance de Lorentz à six dimensions. En utilisant les contraintes actuelles fournies par les observations cosmologiques, nous avons déterminé l'ordre de grandeur de la masse de cette particule aux alentours d'une centaine de GeV. De ce fait les nouveaux états présents dans cette théorie sont suffisamment légers pour produire des signatures claires et observables au Large Hadron Collider. Avec une étude plus poussée du spectre de masses et des couplages du modèle, incluant les corrections radiatives à une boucle, nous avons pu ainsi donner les premières prédictions et contraintes sur la phénoménologie attendue au Large Hadron Collider.

Mots-clés :

Large Hadron Collider, Phénoménologie, Boson de Higgs, Dimensions supplémentaires, Compactification, Corrections radiatives, Matière noire.

Abstract

With the start of the Large Hadron Collider runs, in 2010, particle physicists will be soon able to have a better understanding of the electroweak symmetry breaking. They might also answer to many experimental and theoretical open questions raised by the Standard Model. Surfing on this really favorable situation, we will first present in this thesis a highly model-independent parametrization in order to characterize the new physics effects on mechanisms of production and decay of the Higgs boson. This original tool will be easily and directly usable in data analysis of CMS and ATLAS, the huge generalist experiments of LHC. It will help indeed to exclude or validate significantly some new theories beyond the Standard Model.

In another approach, based on model-building, we considered a scenario of new physics, where the Standard Model fields can propagate in a flat six-dimensional space. The new spatial extra-dimensions will be compactified on a Real Projective Plane. This orbifold is the unique six-dimensional geometry which possesses chiral fermions and a *natural* Dark Matter candidate. The scalar photon, which is the lightest particle of the first Kaluza-Klein tier, is stabilized by a symmetry relic of the six dimension Lorentz invariance. Using the current constraints from cosmological observations and our first analytical calculation, we derived a characteristic mass-range around few hundred GeV for the Kaluza-Klein scalar photon. Therefore the new states of our Universal Extra-Dimension model are light enough to be produced through clear signatures at the Large Hadron Collider. So we used a more sophisticated analysis of particle mass spectrum and couplings, including radiative corrections at one-loop, in order to establish our first predictions and constraints on the expected LHC phenomenology.

Keywords:

Large Hadron Collider, Phenomenology, Higgs boson, Extra-dimensions, Compactification, Radiatives corrections, Dark matter.

Remerciements

Je tiens à remercie tout d'abord tous les membres de mon jury de thèse, pour leur relecture attentive de ce manuscrit, leurs commentaires et les échanges très agréables et intéressants que nous avons eus lors de la soutenance. Je souhaite aussi remercier très vivement mes deux directeurs de thèse : Aldo D. et Giacomo C. pour les beaux projets de recherche qu'ils m'ont proposés d'étudier durant ces trois années, pour leurs discussions si riches d'enseignements, pour l'expérience de recherche et l'autonomie qu'ils m'ont permis d'acquérir et les opportunités qu'ils m'ont offertes pour présenter mes travaux dans le monde entier. J'espère sincèrement que nous aurons encore l'occasion de partager ensemble sur la physique dans les années à venir.

Je tiens aussi à adresser mes remerciements à Sacha D. pour les riches discussions que nous avons pu avoir sur la physique des particules mais aussi sur l'avenir d'un jeune doctorant. Un grand merci aussi à Corinne A., tu as été une tutrice pédagogique extraordinaire et je peux te dire que tu continueras à m'inspirer tout au long de ma carrière.

Je veux aussi remercier très chaleureusement tous mes amis sans qui ce manuscrit n'aurait jamais pu exister :

Merci à Bogna K. et Grégoire G. qui ont eu le courage d'affronter et de supporter au quotidien mon stress et mes râleries, merci pour les supers moments que l'on a passés ensemble à discuter de physique, de musique, de sémantique,... Un merci immense à mes amis de troisième année : à Nicolas C., l'homme des étoiles et à Vincent J., le roi des lasers pour leur bonne humeur et leur supers soirées raclettes !!! A Gaëlle G., la plus grande spécialiste des fours et des porcelaines, pour sa bonne humeur, sa sagacité et ses conseils précieux. A Hugues B., le roi des cristaux de CMS, pour sa gentillesse naturelle, sa simplicité et sa finesse d'esprit. Et enfin merci à Laure M., alias Alice, Claire ou la reine des plasmas, ton amitié inconditionnelle et ton soutien indéfectible m'ont été d'une aide gigantesque durant ces trois années ! Je ne doute pas une seconde que vous deviendrez tous de brillants chercheurs !!!

Je voudrais remercier aussi les post-doc (en particulier Luca P. et Antonio U.) et tous les thésards passés, présents et futurs de l'IPNL et du LASIM ainsi que les gens géniaux avec qui j'ai eu le plaisir de partager mes repas de midi ! Une pensée spéciale pour Claire-Émilie V., spécialiste des crayons de papier radioactifs, qui m'a inspiré et fait tant rêver le jour où je l'ai surprise à revenir de la thermocolleuse! Merci aussi à tous les chercheurs et tout le personnel de l'IPNL.

Je voudrais aussi remercier grandement mes amis musiciens qui m'ont permis de vivre durant ces trois années des aventures musicales exceptionnelles, mes amis de l'ENS Cachan, mes amis de classes préparatoires avec une pensée spéciale pour Laura D. et mes amis du lycée tout particulièrement mes deux chéries Miranda M. et Émilie S.. Enfin je voudrais remercier infiniment toute ma famille et surtout les trois personnes les plus chères à mes yeux : mon papa,

ma maman et ma petite sœur. Sans vous je n'aurais jamais pu réussir de telles études. Je vous serai donc toujours infiniment reconnaissant d'avoir cru en moi et d'avoir été des appuis sans faille durant toutes ces années, malgré mes craintes, mes inquiétudes et mes doutes incessants ! Cette thèse, je vous la dédie.

Contents

Introduction

Above the attometer scale (10^{-18}m), descriptions of matter and of its interactions are extremely well realized by the Standard Model of particle physics. Since the middle of the 20th Century, experimentalists have been measuring the parameters of this effective theory with great accuracy and no significant deviation from predictions has been observed yet. However some experimental and theoretical puzzles remain and tend to open a new path toward physics beyond the Standard Model.

In order to study the limits of this theory, new experiments in high energy physics and in observational cosmology have been developed in the last decade. The Large Hadron Collider (LHC), which is a proton-proton collider located at CERN, is one of these promising apparatus, built to understand a crucial question raised by the Standard Model: how is generated the electroweak symmetry breaking? Moreover with current collisions at 7 TeV energy in the center of mass, the LHC generalist experiments, ATLAS and CMS, will explore a totally new energy scale where new physics can arise.

However, because of the complicated chromodynamical background, experimentalists using proton-proton collider, will need to be guided by phenomenologists in order to look at the data yielded by the detectors. A huge effort is actually made by the theorist community to produce predictions as precise as possible for the Standard Model observables and to suggest what could be the nature of new physics, soon visible at LHC. As a part of this contribution, this thesis will give new directions and new ideas that can be studied within next years at the LHC.

Using effective models, we followed two main axes to investigate phenomenological effects of physics beyond the Standard Model. At the beginning of this doctorate, we worked on Higgs boson phenomenology. The decay of this scalar boson into two high-energetic photons is a crucial process for light Higgs detection at the LHC, because it leads to a clear signature in the CMS and ATLAS calorimeters. For theorists, this decay presents also a nice property: generated by radiative corrections, it is very sensitive to new heavy particles which could couple to the Higgs bosons. In our study, we develop a new model-independent parametrization of these new physics effects which can help experimentalists to discriminate between different scenarios of physics beyond the Standard Model. We apply this formalism to various effective models present in the literature in 4 and 5 dimensions to emphasize the potential of this new tool.

At a later time, we focused on extra-dimensional effective theories. We built a new model where fields can propagate in a six-dimensional space with two flat extra-dimensions compactified on a Real Projective Plane. The geometry of this 6D orbifold is the only one reproducing the Standard Model chiral fermions and possessing a *natural* dark matter candidate. In this framework, because of the compactification, 6D field momenta along the extra-dimensions will

be quantized. Therefore fundamental objects of the theory will be "infinite" towers of four-dimensional fields labelled by their integer momenta k and l along the two new dimensions. In this case, the tree level masses of (k, l) tier will be given by: $m^2 = k^2/R_5^2 + l^2/R_6^2$ where R_5 and R_6 are the radii of the extra-dimensions. Then radiative corrections and electroweak symmetry breaking effects will break the mass degeneracy of the different particles within a same tier. The stabilization of the lightest particle of the first Kaluza-Klein tier (1,0) (or (0,1)) is actually generated by a discrete symmetry, called KK-parity, relic of the 6D Lorentz invariance. Using data from cosmological observations, we will contrain the mass-range of this scalar photon around few hundred GeV. This has important consequences on the phenomenology of the new heavy states: their pretty "low" masses will make them detectable at the LHC. Therefore we investigated the phenomenology of the (2,0) (or (0,2)) level which is even under the KK-parity and which would produce clear signatures at proton-proton colliders. Combining LHC and cosmological observations, we predict that this Universal Extra-dimensional model can be confirmed or ruled out within next year.

In order to present all these results, we divided this thesis in five parts:

- Chapter 1 will present the current context of this work and will introduce the reader to the main concepts necessary to understand the following sections. We will present a general review of the Standard Model of particle physics and of cosmology. We will also develop the general idea of effective models and show how powerful they can be to extend physics beyond the Standard Model. In particular, we will focus on the physics of extra-dimensional models which will be the main topic of our study.

- Chapter 2 will be mainly dedicated to the model building of the Universal Extra-Dimension in 6D on the Real Projective Plane. We will describe the space topology and its consequences on field propagation. Then we will detail the techniques we developed to compute radiative corrections in this framework and we will present the mass spectrum of the first Kaluza-Klein tier. Finally we will show how this one-loop spectrum has been used to perform our analytical calculation of the Dark Matter relic abundance and how we deduced constraints on the size of the extra-dimension radii.

- In chapter 3 and 4, we will carry on the work based the one-loop renormalization of the model. In particular, we will emphasize how crucial it is to understand the interactions generated on the singular points of the orbifold in order to predict the structure of the effective vertices allowed on the Real Projective Plane. Then we will use this study of couplings and masses on the Real Projective Plane to investigate LHC phenomenology. After we present the rich potential signatures of this model, we will focus on the specific level (2,0) (or (0,2)). Using `FEYNRULES` and `CALCHEP` codes, we have implemented our 6D model and performed first cross-section calculations for the LHC. Considering the mass-range preferred by the constraints on Dark Matter relic density, we observed that processes involving dilepton production, lepton + missing transverse energy, top pair and 4-tops can be tested soon at LHC.

- In chapter 5, we will present our JHEP publication concerning the original parametrization of new physics effects on Higgs decay into photons. We choose to keep this first PhD work as "synthetic" as possible although this project can turn out to be very useful tool for experimentalists.

Chapter 1 and 5 are independent from the three central chapters. Finally some appendices will help the reader to find details on technical calculations performed in the main chapters.

Chapter 1

General context and overview

1.1 The Standard Model and beyond

1.1.1 Introduction to Effective Field Theories

What is an Effective Field Theory?

Physics, as an experimental science, is highly based on measurements. When an experiment is carried out, possibilities of measurements are limited by the resolution of the apparatus, therefore below a scale predefined by experiment, no observation of physical behaviors can be realized and no physical information can be extracted anymore. In this context, as we will see, in order to describe physical phenomena, we have to introduce effective theories based on the statement that low energy dynamics (also called long-distances or infrared) does not depend on the details of high energy dynamics (also called short distances or ultraviolet). This approach is used in numerous fields of physics from atomic physics to astrophysics. For instance, let us quote the multipole expansion in electromagnetism, the neglected planet size effects on study of solar system motion and the use of Newtonian mechanics to describe dynamics of bodies whose speed is much smaller that the speed of light. Similarly, we can compute the energy levels of the hydrogen atoms with a "good" accuracy by considering only charges and masses of the proton and of the electron. Nevertheless, in current experiments which can probe atoms hyperfine structure, their 1/2-spin and their magnetic momentum need to be taken into account. From a numerical point of view, we can do a rough estimate of the experimental precision needed to see hyperfine effects: $\Delta E_{hyperfine}/E_{bound} \sim 10^{-6}$. If we continue to increase experimental precision more details of the structure of the proton will be required for a more accurate prediction.

This approach can also be used in the context of field theory where high energy E_H effects are suppressed at low energy (E_L) by powers of E_L/E_H and this is the general idea we will follow during all this thesis to describe the eventual new physics that could be expected at the TeV scale. However, in effective field theory, notice that the decoupling between scales may be more subtle because radiative corrections involve all scales through integration over momenta running into loops.

Interesting properties of Effective Field Theory

Effective Field Theory (EFT) can be a very useful tool to describe physics at low scale (1). In the case of known perturbative UV-theory, it will help to simplify calculations. For an unknown or non-perturbative theory it will permit to estimate the magnitude of the interactions, to classify and parametrize them; the UV-physics being taken into account indirectly in the coupling with light degrees of freedom. Nevertheless, we have to notice that EFT describe the IR-physics which can be quite far from the fundamental underlying theory. Let us mention quantum chromodynamics for instance and its description in term of chiral theories with mesons and baryons. This is not problematic when the high energy physics is already known, even if the matching between the two theories can be really challenging. However often in particle physics, the short-distance physics is still hidden so it will be *really* difficult, only knowing the IR-behaviors, to figure out what could be the characteristic UV-scale and what would be the physics at short distances.

In this section, for the purpose of this thesis, we will only focus on weakly coupled effective field theories. Here new degrees of freedom will be relevant when the energy scale will be high enough for the particles to be produced on-shell. From this point of view, for instance, the Standard Model can be seen as an EFT since we do not know its content from TeV scale to

Planck scales. Technically this means that the Lagrangian of EFT can be expanded in a finite sum of operators with dimension four or less and an infinite set of higher dimensional operators.

$$\mathcal{L}_{eff} = \mathcal{L}_{d\leq 4} + \sum_i \frac{\mathcal{O}_i}{\Lambda^{\dim(\mathcal{O}_i)-4}} \tag{1.1}$$

where Λ is an energy scale related to the physical scale where the EFT is not valid anymore (new on-shell contributions) and $\dim(\mathcal{O}_i)$ is the dimension of the operator $\mathcal{O}_i$. As we are working with weakly coupled theory, the dimension of the operator can be deduced by using the usual power counting. In practice, in formula 1.1, only a subset of operators with low dimensions is relevant to describe the experimental results. This pragmatic approach can be very useful to put model independent constraints on new phenomena coming from specific sectors of the theory at higher energy as we will see in chapter 5. On the other hand, instead of using the most general operator structures which are allowed by the low energy theory, we could prefer to add assumptions on the UV-theory and work with EFT which include new degrees of freedom and parts of the underlying UV-symmetries. This will be indeed the approach we will follow throughout the thesis when working with extra-dimensional model for instance.

Finally let us mention the non-trivial question of the EFT renormalization and renormalizability. In general, since $\mathcal{L}_{eff}$ contains operators with dimension higher than 4, these theories are not renormalizable. Nevertheless *the EFT still has a predictive power as far as we want results with finite accuracy but also as long as we have an idea of what the scale Λ is.* In high energy physics, we do not know at all the scale where the theory will break down but we can still estimate it and also constrain the contributions coming from the higher dimensional operators.

Simple example of tree level matching in EFT

A well-known example of EFT is the Fermi theory of electroweak interactions. Historically, in the 1930s, Fermi proposed to explain the decay of $n \to p + e^- + \bar{\nu}_e$ by introducing in the QED Lagrangian, a 4-fermion interaction operator:

$$\mathcal{L}_{Fermi} \supset -\frac{4G_F}{\sqrt{2}}(\bar{n}\gamma^\mu p)(\bar{\nu}_e\gamma_\mu e_L) \tag{1.2}$$

where $G_F \sim 10^{-5}\text{GeV}^{-2}$ is the dimensionful Fermi constant. Here the index L refers to the fact that only the left-handed part of the electron couples to the neutrino through the weak interaction. This point will be develop more in detail in section 1.1.2. From the previous discussion, we can see that this description, efficient at low energy, will break down when the proton energy will be close to $\Lambda \sim \frac{1}{\sqrt{G_F}} \sim 100$ GeV. Nowadays this result is not surprising because we know that this effective description has to be replaced at high energy by the electroweak theory. In this model, we introduce new massive degrees of freedom, W and Z with a mass m_W and m_Z. To remove the complication of the QCD effects due to the presence of hadrons, we will illustrate the *tree level matching* of this two theories using the muon μ decay into electron e and neutrinos ν_μ and ν_e. First let us give the two interactions which are parts of the Lagrangian of the IR- and UV-theory:

$$\begin{aligned}\mathcal{L}_{Fermi} &\supset -\frac{4G_F}{\sqrt{2}}(\bar{\mu_L}\gamma^\alpha\nu_\mu)(\bar{\nu}_e\gamma_\alpha e_L)\\ \mathcal{L}_{electroweak} &\supset -\frac{g_w}{\sqrt{2}}(\bar{e_L}\gamma^\alpha\nu_e + \bar{\mu_L}\gamma^\alpha\nu_\mu)W^-_\alpha\end{aligned} \tag{1.3}$$

To perform the matching, we have actually to extract from the UV-theory, the value of the IR-theory coupling as a function of the high energy parameters. This coupling can be derived from the calculation of the Feynman diagram with W-exchange in the t-channel (Figure 1.1).

After calculation, we obtain the matrix element in both theories for the 4-fermion interaction:

$$i\mathcal{M}_{Fermi} = -i\frac{4G_F}{\sqrt{2}}(\bar{\mu_L}\gamma^\alpha\nu_\mu)(\bar{\nu}_e\gamma_\alpha e_L) \tag{1.4}$$

$$\begin{aligned} i\mathcal{M}_{electroweak} &= \left(\frac{ig_w}{2}\right)^2(\bar{\nu}_e\gamma_\alpha e_L)\frac{-ig^{\alpha\beta}}{(p_1-p_3)^2-m_W^2}(\bar{\mu_L}\gamma^\beta\nu_\mu) \\ &= -i\left(\frac{g_w}{2m_W}\right)^2(\bar{\nu}_e\gamma_\alpha e_L)(\bar{\mu_L}\gamma^\alpha\nu_\mu) + O\left(\frac{(p_1-p_3)^2}{m_W^2}\right) \end{aligned} \tag{1.5}$$

p_1 and p_3 are respectively the incoming momentum of the muon and outcoming momentum of muonic neutrino (Figure 1.1). For the muon decay, we consider that the muon is almost at rest which means that $|p_i| \ll m_W$. The ratio $\frac{(p_1-p_3)^2}{m_W^2}$ is the expansion parameter of the UV-theory. At the zeroth-order, the W-field is integrated out and we can match the two theories:

$$\frac{G_F}{\sqrt{2}} = \frac{g_w^2}{8m_W^2} \tag{1.6}$$

Renormalization group running

In the previous section, we have shown that the effective coupling G_F does not depend on the energy scale of the process at tree level but we will soon understand that the matching has been performed at the m_W scale so that: $\frac{G_F}{\sqrt{2}}(\mu = m_W) = \frac{g_w^2}{8m_W^2}$. The last point we need to mention about EFT is how to renormalize them. This will be a crucial discussion for the chapter 3 of this thesis when we will consider the renormalization of couplings in our extra-dimensional model. To illustrate it, we will present a toy model based on the previous idea and detailed in reference (2). The tree level Lagrangian (1.7) represents a simple effective theory where we integrated out a massive vector field with a mass M. The remaining degrees of freedom are only one fermionic degree of freedom ψ, one extra light scalar ϕ with a mass $m \ll M$ and their coupling through a Yukawa interaction.

$$\mathcal{L}_{tree} = i\bar{\psi}\gamma_\mu\partial^\mu\psi + \frac{c_V}{2}\bar{\psi}\gamma_\mu\psi\bar{\psi}\gamma^\mu\psi + \frac{1}{2}(\partial_\mu\phi)^2 - \frac{m^2}{2}\phi^2 - \eta\bar{\psi}\psi\phi \tag{1.7}$$

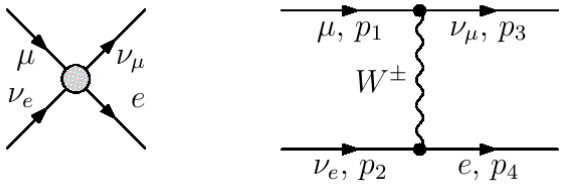

Figure 1.1: Left: 4-fermions amplitude from the Fermi theory. Right: t-channel amplitude with W-boson exchange.

This Lagrangian has been obtained after a matching has been done at the typical high-energy scale M. Notice that we can show after a quick power-counting that $\overline{\psi}\gamma_\mu\psi\overline{\psi}\gamma^\mu\psi$ is a dimension 6 operator. Then, if we compute the 4-fermion scattering amplitude at the low scale characterized by m, we need to take into account radiative corrections. These corrections will affect masses and couplings and the amplitude will be enhanced by large contributions in $\log(M/m)$, as we will see in the following. This logarithmic term can be taken into account by means of the Renormalization Group Equations (RGE) of parameters. For the low-energy scattering study, we will focus only on the evolution of the 4-fermions coupling c_V. To obtain the RGE, first we have to compute the 1-loop correction to the self-energy of the fermion and then the scattering amplitude corrections. Without going into all the details of computation, using dimensional regularization[1], we obtain for the self energy:

$$i\Sigma(p) = \frac{i\eta^2 \not{p}}{2(4\pi)^2}\frac{1}{\epsilon} + \text{finite} \tag{1.8}$$

where p is the momentum of the fermion line and $d = 4 - 2\epsilon$ where d is the dimension of space. Only the pole in $1/\epsilon$ will enter in the RGE. For the correction to the 4-fermions vertex, the calculation is more subtle. For the contribution of the ϕ exchange (Figure 1.2), the diagram (a) will give divergent contribution to the $\overline{\psi}\gamma_\mu\psi\overline{\psi}\gamma^\mu\psi$ operator but (b) and (c) will introduce contributions which are proportional to a new tensorial operator : $\overline{\psi}\sigma_{\mu\nu}\psi\overline{\psi}\sigma^{\mu\nu}\psi$ where $\sigma^{\mu\nu} = \frac{i}{2}[\gamma^\mu, \gamma^\nu]$. This situation is due to the fact that these two operators have the same dimension, the same particles and respect the same allowed symmetries of the problem. So loop effects will mix these two operators. To be more accurate, the tree level Lagrangian should be written as:

[1]This regularization technique consists in integrating over a Minkowski space with dimension $d = 4 - 2\epsilon$ instead of $d = 4$. The main advantage of this method is to preserve the Lorentz and gauge symmetries of the space contrary to the regularization by cut-off on the momenta.

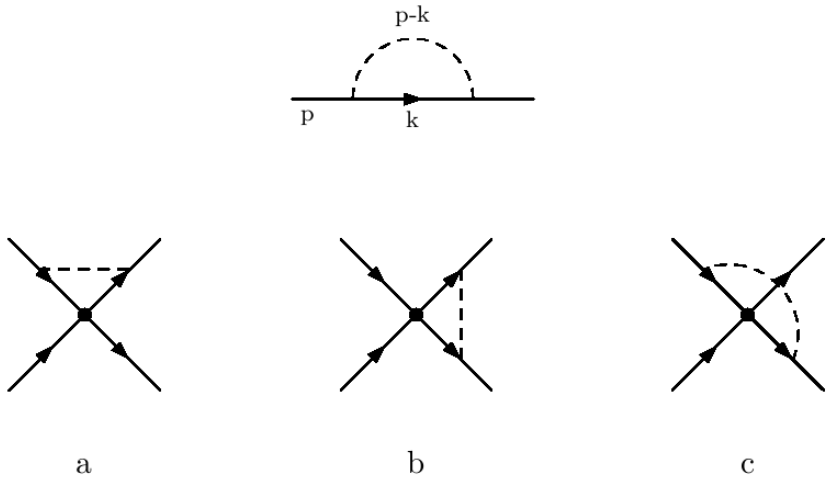

Figure 1.2: Top: Self energy diagram for fermions. Bottom: Topologies of one-loop corrections to 4-fermions scattering. Dashed line represents ϕ scalar exchange.

$$\mathcal{L}_{tree} = i\overline{\psi}\gamma_\mu\partial^\mu\psi + \frac{c_V}{2}\overline{\psi}\gamma_\mu\psi\overline{\psi}\gamma^\mu\psi + \frac{c_T}{2}\overline{\psi}\sigma_{\mu\nu}\psi\overline{\psi}\sigma^{\mu\nu}\psi + \frac{1}{2}(\partial_\mu\phi)^2 - \frac{m^2}{2}\phi^2 - \eta\overline{\psi}\psi\phi \tag{1.9}$$

with $c_V(\mu = M) \neq 0$ and $c_T(\mu = M) = 0$. At low energy these coefficients will be both non-zero. The one-loop calculations will then give for the amplitude:

$$\begin{aligned} i\mathcal{M} =& \frac{i\eta^2}{(4\pi)^2}\frac{1}{\epsilon}(-c_V + 6c_T)\overline{u}(p_3)\gamma_\mu u(p_1)\overline{u}(p_4)\gamma^\mu u(p_2) \\ &+ \frac{i\eta^2}{(4\pi)^2}\frac{1}{\epsilon}(c_V)\overline{u}(p_3)\sigma_{\mu\nu}u(p_1)\overline{u}(p_4)\sigma^{\mu\nu}u(p_2) \end{aligned} \tag{1.10}$$

Now we can rewrite the Lagrangian of the theory in terms of bare (with zero index) and of renormalized fields and couplings at the one-loop.

$$\begin{aligned} \mathcal{L} &= i\overline{\psi_o}\gamma_\mu\partial^\mu\psi_o + \frac{c_{V,o}}{2}\overline{\psi_o}\gamma_\mu\psi\overline{\psi_o}\gamma^\mu\psi_o + \frac{c_{T,o}}{2}\overline{\psi_o}\sigma_{\mu\nu}\psi\overline{\psi_o}\sigma^{\mu\nu}\psi_o + ... \\ &= iZ_\psi\ \overline{\psi}\gamma_\mu\partial^\mu\psi + \frac{c_V}{2}Z_V Z_\psi^2\mu^{2\epsilon}\ \overline{\psi}\gamma_\mu\psi\overline{\psi}\gamma^\mu\psi + \frac{c_T}{2}Z_T Z_\psi^2\mu^{2\epsilon}\ \overline{\psi}\sigma_{\mu\nu}\psi\overline{\psi}\sigma^{\mu\nu}\psi + ... \\ &= i\overline{\psi}\gamma_\mu\partial^\mu\psi + \frac{c_V}{2}\mu^{2\epsilon}\ \overline{\psi}\gamma_\mu\psi\overline{\psi}\gamma^\mu\psi + \frac{c_T}{2}\mu^{2\epsilon}\ \overline{\psi}\sigma_{\mu\nu}\psi\overline{\psi}\sigma^{\mu\nu}\psi + i(Z_\psi - 1)\ \overline{\psi}\gamma_\mu\partial^\mu\psi \\ &+ \frac{c_V}{2}\mu^{2\epsilon}(Z_V Z_\psi^2 - 1)\ \overline{\psi}\gamma_\mu\psi\overline{\psi}\gamma^\mu\psi + \frac{c_T}{2}\mu^{2\epsilon}(Z_T Z_\psi^2 - 1)\ \overline{\psi}\sigma_{\mu\nu}\psi\overline{\psi}\sigma^{\mu\nu}\psi + ... \end{aligned}$$

where $\psi_o = \sqrt{Z_\psi}\psi$ defines the renormalized field and $c_{i,o} = Z_i\mu^{2\epsilon}c_i$, the renormalized couplings. $\mu^{2\epsilon}$ is a scale factor which ensures homogeneity of the Lagrangian as in dimensional regularization the space-time dimension is $d = 4 - 2\epsilon$. From here we can impose that the introduced counter-terms remove the divergences calculated previously. In such case we get:

$$\begin{aligned} c_V(Z_V Z_\psi^2 - 1) =& \frac{i\eta^2}{(4\pi)^2}\frac{1}{\epsilon}(-c_V + 6c_T) \\ c_T(Z_T Z_\psi^2 - 1) =& \frac{i\eta^2}{(4\pi)^2}\frac{1}{\epsilon}(c_V) \end{aligned} \tag{1.11}$$

which can be related to the evolution of the coupling with the scale (2):

$$\begin{aligned} &\mu\frac{d}{d\mu}\begin{pmatrix} c_V \\ c_T \end{pmatrix} = \frac{2\eta^2}{(4\pi)^2}\begin{pmatrix} 0 & 6 \\ 1 & 1 \end{pmatrix}\begin{pmatrix} c_V \\ c_T \end{pmatrix} \\ &\text{with}\begin{cases} c_V(\mu = M) \neq 0 \\ c_T(\mu = M) = 0 \end{cases} \end{aligned} \tag{1.12}$$

As we can see, μ-dependence of the coupling η is needed to solve the differential equation. This can be obtained in a similar way, by considering the correction to Yukawa vertex. In this case we get:

$$\begin{aligned} \mu\frac{d\eta}{d\mu} = \frac{5\eta^3}{(4\pi^2)} \implies& \frac{d\mu}{\mu} = \frac{5}{(4\pi)^2}\frac{d\eta}{\eta^3} \\ \implies& \frac{1}{\eta(m)^2} - \frac{1}{\eta(M)^2} = \frac{10}{(4\pi)^2}\log\left(\frac{M}{m}\right) \end{aligned} \tag{1.13}$$

After changing variables in equation (1.11), diagonalizing and expanding for large logarithms, we can solve the RGE and extract the scale dependence of the c_V and c_T operators:

$$\begin{aligned} c_V(m) &= c_V(M) + O(\log(M/m)^2) \\ c_T(m) &= -c_V(M)\frac{10}{(4\pi)^2}\log\left(\frac{M}{m}\right) \end{aligned} \tag{1.14}$$

Notice that, here, at the end of the calculation, the contribution in $\log\left(\frac{M}{m}\right)$ cancels for the coupling c_V. However this is not the case in general as we can see for the other coupling c_T which is only generated by this log-contribution. So it is now apparent that radiative corrections will generate at low scale all the terms allowed by symmetries even if some tree level couplings are vanishing.

To conclude this discussion on the EFT, we have to keep in mind that we still have benefits from constructing such theories. Despite their lack of renormalizability, we can always give an estimate of coefficients for the theory and therefore keep a certain predictivity. This will be crucial to understand the motivation and the prediction we will have in chapter 2 and 3 with the extra-dimensional model we built. Relying on our review of EFT, we can now go a step further and start presenting the Standard Model of particle physics and its possible extensions.

1.1.2 The Standard Model of particle physics

Description of the model

The Standard Model (SM) of particles physics is a renormalizable quantum field theory describing the "elementary" particles of matter and their fundamental interactions. Introduced by Glashow, Salam and Weinberg (3; 4; 5) in the early 1970's in order to explain the electroweak interactions, this model has been widely accepted after the discovery of the particles mediating neutral and charged currents, Z and W, at the beginning of the 1980's. In parallel, the theory of strong interaction has also been developed and validate by experiments along the end of the century and up to the TeV scale[2]. This Yang-Mills theory is based on a non-abelian gauge symmetry group $G_{SM} = SU(3)_C \times SU(2)_W \times U(1)_Y$. $SU(3)_C$ group is the quantum chromodynamics (QCD) gauge group. These non-abelian interactions will lead to the strongly coupled sector of the theory and will be mediated by the gluon fields g. Then the $SU(2) \times U(1)_Y$ is here to describe the weakly coupled sector known as the electroweak sector. The associated gauge fields are respectively $W^{1,2,3}$ and B. This gauge symmetry will be broken into $U(1)_{EM}$ at the hundred GeV scale by the Higgs-Brout-Englert mechanism (6; 7), introducing masses for three new mass-eigenstates: $W^{\pm}$ and Z. One eigenstate will remain massless; the photon γ (or A for convenience)[3]. The matter fields will carry charges under this gauge symmetry group G_{SM}, which will determine their interactions. In the table 1.1, we give the SM field content and their charges under the three different gauge groups and their electric charges.

For convenience, the Standard Model Lagrangian can be split into different parts. In order to introduce the notations used in this thesis, the gauge sector $\mathcal{L}_G$, the Higgs sector $\mathcal{L}_H$, the fermion sector $\mathcal{L}_F$ and the Yukawa sector $\mathcal{L}_y$ will be detailed in the following.

$$\mathcal{L}_{SM} = \mathcal{L}_G + \mathcal{L}_H + \mathcal{L}_F + \mathcal{L}_y \tag{1.15}$$

[2]In this sense, as we mentioned, the Standard Model is also an EFT because its content and its interactions at energy from TeV to Planck scales are still unknown.

[3]The diagonalization of $W^{1,2,3}$ and B will be detailed in **Higgs sector** section.

Field	Notation	$SU(3)_C$	$SU(2)_W$	$U(1)_Y$	$U(1)_{EM}$
Quarks (s=1/2)	$Q_L = \begin{pmatrix} u_L \\ d_L \end{pmatrix}, \begin{pmatrix} c_L \\ s_L \end{pmatrix}, \begin{pmatrix} t_L \\ b_L \end{pmatrix}$	3	2	1/6	$\begin{pmatrix} 2/3 \\ -1/3 \end{pmatrix}$
	$u_R,\ c_R,\ t_R$	3	1	2/3	2/3
	$d_R,\ s_R,\ b_R$	3	1	$-1/3$	$-1/3$
Leptons (s=1/2)	$L_L = \begin{pmatrix} \nu_e \\ e_L \end{pmatrix}, \begin{pmatrix} \nu_\mu \\ \mu_L \end{pmatrix}, \begin{pmatrix} \nu_\tau \\ \tau_L \end{pmatrix}$	1	2	$-1/2$	$\begin{pmatrix} 0 \\ -1 \end{pmatrix}$
	$e_R,\ \mu_R,\ \tau_R$	1	1	-1	-1
Gauge (s=1)	g	8	1	0	0
	$W^3,\ W\pm$	1	3	0	$0,\ \pm 1$
	B	1	1	0	0
Higgs (s=0)	$\Phi = \begin{pmatrix} \phi^+ \\ \phi_0 = \frac{1}{\sqrt{2}}(v + h + i\varphi_0) \end{pmatrix}$	1	2	1/2	$\begin{pmatrix} 1 \\ 0 \end{pmatrix}$

Table 1.1: The SM fields with their representations under $SU(3)_C$ and $SU(2)_W$ and their charges under $U(1)_Y$ and $U(1)_{EM}$. Here, the electric charge is given by $Q = T_3 + Y$ ans s, the spin of the field.

Gauge sector

The first term is the kinetic term of the gauge fields:

$$\mathcal{L}_G = -\frac{1}{4} B^{\mu\nu} B_{\mu\nu} - \frac{1}{4} \sum_{a=1}^{3} W^{a,\mu\nu} W_{a,\mu\nu} - \frac{1}{4} \sum_{A=1}^{8} G^{A,\mu\nu} G_{A,\mu\nu} \tag{1.16}$$

where $B^{\mu\nu}$, $W^{a,\mu\nu}$ and $G^{A,\mu\nu}$ are the field strength of the associated gauge fields given by:

$$\begin{aligned} B^{\mu\nu} &= \partial^\mu B^\nu - \partial^\nu B^\mu \\ W^{a,\mu\nu} &= \partial^\mu W^{a,\nu} - \partial^\nu W^{a,\mu} + g_w\ \epsilon^{abc}\ W^{b,\mu} W^{c,\nu} \\ G^{A,\mu\nu} &= \partial^\mu G^{A,\nu} - \partial^\nu G^{A,\mu} + g_s\ f^{ABC}\ G^{B,\mu} G^{C,\nu} \end{aligned} \tag{1.17}$$

g_s, g_w and g_1 are the coupling constants associated to $SU(3)_C$, $SU(2)_W$ and $U(1)_Y$. ϵ^{abc} and f^{ABC} are the structure constants of $SU(2)$ and $SU(3)$. They are defined by the commutation relation between the generators t^a for $SU(2)$ or T^A for $SU(3)$ [4], where $a = 1..3$ and $A = 1..8$.

$$[t^a, t^b] = i\epsilon^{abc} t^c \text{ and } \quad [T^A, T^B] = i f^{ABC} T^C \tag{1.18}$$

In this section, we will not detail the gauge-fixing term neither the ghost term. When they will be needed in the thesis, they will be given for a generic $SU(N)$ non-abelian theory.

[4] $t^a = \sigma^a/2$ with $a = 1..3$ for the fundamental representation of $SU(2)$. Here σ^a are the Pauli matrices.

Fermion sector

The gauge interaction of fermions can be derived from the covariant derivative, once the various charges of the fields are known. The peculiarity of the SM is that the left-handed part of a fermion has a different coupling compared to the right-handed one. For instance, only left-handed fields couple to W bosons. In this case, the notation in terms of Weyl spinors is more appropriate for the chiral fermions of the Standard Model[5].

$$\begin{aligned}\mathcal{L}_F =& Q_{Li}^\dagger i\bar{\sigma}_\mu D^\mu Q_{Li} + u_{Ri}^\dagger i\sigma_\mu D^\mu u_{Ri} + d_{Ri}^\dagger i\sigma_\mu D^\mu d_{Ri} \\ &+ L_{Li}^\dagger i\bar{\sigma}_\mu D^\mu L_{Li} + e_{Ri}^\dagger i\sigma_\mu D^\mu e_{Ri}\end{aligned} \tag{1.19}$$

The index $i = 1..3$ is a flavor index which takes into account the three families of quarks and leptons, $\sigma_\mu = (1, \sigma_i)$ and $\bar{\sigma}_\mu = (1, -\sigma_i)$ (8). The color indices have been removed for more readability and the covariant derivative is given by:

$$D^\mu = \partial^\mu - ig_s\theta_S G^{\mu,A}T^A - ig_w\theta_W W^{\mu,a}t^a - ig_1 Y B^\mu \tag{1.20}$$

$\theta_S = 0, 1$ for singlets or triplets of $SU(3)_C$, $\theta_W = 0, +1$ for singlets or for doublets of $SU(2)_W$ and Y is the charge under $U(1)_Y$.

Higgs sector

This part of the Lagrangian will generate the spontaneous symmetry breaking of $SU(2)_W \times U(1)_Y$ into $U(1)_{EM}$ by giving masses to three bosons of the weak interactions, as it has been experimentally confirmed. We may think of adding directly a mass term by hand for the gauge boson. This would break explicitly the gauge symmetry. While it can be accepted experimentally, it leads to inconsistencies in the theory as we will discuss in section 1.1.3. In the Standard Model, this problem is solved by introducing a new scalar field Φ whose Lagrangian will respect all the symmetry of the SM but whose vacuum expectation value will not:

$$\langle\Phi\rangle = \frac{1}{\sqrt{2}}\begin{pmatrix} 0 \\ v \end{pmatrix} \tag{1.21}$$

If we consider the complete gauge transformation $\Phi \to e^{i\alpha^a t^a} e^{i\beta/2}\Phi$, only a transformation with $\alpha_1 = \alpha_2 = 0$ and $\beta = \alpha_3$ leaves $\langle\Phi\rangle$ invariant. This direction in the $SU(2)_W \times U(1)_Y$ space will be directly related to the massless gauge boson by the gauge transformation. The Lagrangian of the Higgs field is thereby built:

$$\mathcal{L}_H = (D^\mu\Phi)^\dagger(D_\mu\Phi) - \mu^2\Phi^\dagger\Phi + \lambda(\Phi^\dagger\Phi)^2 \tag{1.22}$$

where $D^\mu = \partial^\mu - ig_w W^{\mu,a}t^a - ig_1 Y_h B^\mu$. This expression of the potential is the easiest renormalizable possibility. For $\mu^2 < 0$ and $\lambda > 0$ we can show that it will generate the vacuum expectation value (vev) for the Higgs field $v = \sqrt{\frac{\mu^2}{\lambda}}$.

[5]The Dirac notation with 4 component fields could have also been used, two of the component would have been equal to zero. $\Psi_R = P_R\Psi = \begin{pmatrix} 0 \\ \bar{\eta} = \psi_R \end{pmatrix}$ and $\Psi_L = P_L\Psi = \begin{pmatrix} \chi = \psi_L \\ 0 \end{pmatrix}$, where $P_{R/L} = \frac{1\pm\gamma_5}{2}$, and in this case, Pauli's matrices are replaced by Dirac's ones in the Lagrangian.

Then we can write the Higgs field as:

$$\Phi = \begin{pmatrix} \phi^+ \\ \phi_0 = \frac{1}{\sqrt{2}}(v + h + i\varphi_0) \end{pmatrix} \tag{1.23}$$

By expanding the kinetic term of the Lagrangian, we will generate mass terms for the gauge bosons:

$$\mathcal{L}_{H,\text{bilinear}} = \frac{1}{8}\left| \begin{pmatrix} g_w W_\mu^3 + g_1 B_\mu & g_w\sqrt{2}W_\mu^+ \\ g_w\sqrt{2}W_\mu^- & -g_w W_\mu^3 + g_1 B_\mu \end{pmatrix} \begin{pmatrix} 0 \\ v \end{pmatrix} \right|^2 \tag{1.24}$$

$$= \frac{g_w^2 v^2}{4} W_\mu^+ W^{\mu-} + \frac{v^2}{8}(W_\mu^3 \; B_\mu) \begin{pmatrix} g_w^2 & -g_w g_1 \\ -g_w g_1 & g_1^2 \end{pmatrix} \begin{pmatrix} W^{3,\mu} \\ B^\mu \end{pmatrix} \tag{1.25}$$

$$= \frac{g_w^2 v^2}{4} W_\mu^+ W^{\mu-} + \frac{v^2}{8}(Z_\mu \; A_\mu) \begin{pmatrix} g_w^2 + g_1^2 & 0 \\ 0 & 0 \end{pmatrix} \begin{pmatrix} Z^\mu \\ A^\mu \end{pmatrix} \tag{1.26}$$

where $W_\mu^\pm = \frac{1}{\sqrt{2}}(W_\mu^1 \mp i W_\mu^2)$. The diagonalization of the mass matrix of the gauge fields gives the eigenstates Z^μ and A^μ of the theory:

$$\begin{pmatrix} Z_\mu \\ A_\mu \end{pmatrix} = \begin{pmatrix} \cos\theta_W & -\sin\theta_W \\ \sin\theta_W & \cos\theta_W \end{pmatrix} \begin{pmatrix} W_\mu^3 \\ B_\mu \end{pmatrix} \tag{1.27}$$

where θ_W is the Weinberg angle given by:

$$\cos\theta_W = \frac{g_w}{\sqrt{g_w^2 + g_1^2}} \quad \text{and} \quad \sin\theta_W = \frac{g_1}{\sqrt{g_w^2 + g_1^2}} \tag{1.28}$$

The eigenvalues, which are the masses of bosons, are noted m_W, m_Z and m_A. We can then extract the electromagnetic coupling e by identification with the photon coupling:

$$m_W = \frac{g_w v}{2}, \quad m_Z = \frac{\sqrt{g_w^2 + g_1^2}\, v}{2} \quad m_A = 0 \quad \text{and} \quad e = \frac{g_w g_1}{\sqrt{g_w^2 + g_1^2}} \tag{1.29}$$

Finally, only the Higgs boson h remains physical. The other fields φ_0, $\phi^\pm$ are Goldstone bosons associated with the symmetry breaking. They will be "eaten", in unitary gauge, by the Z, $W^\pm$ to create the longitudinal polarization of the heavy gauge bosons.

Yukawa sector

The Yukawa sector is responsible for generating fermionic field masses by using the Higgs field interactions. It will also introduce the mixing between different families. Actually to preserve gauge invariance, we have to use the Higgs doublet in order to write down a mass term which connects right-handed and left-handed components which are respectively singlets and doublets of $SU(2)_W$.

$$\mathcal{L}_Y = -\sum_{i=1}^{3} Y_{ij}^u Q_{Li}^\dagger (i\sigma_2 H^*) u_{Rj} - \sum_{i=1}^{3} Y_{ij}^d Q_{Li}^\dagger H d_{Rj} - \sum_{i=1}^{3} Y_{ij}^e L_{Li}^\dagger H e_{Rj} + h.c. \tag{1.30}$$

Then by expanding the Higgs field around its vacuum expectation value in the Lagrangian, we will generate mass terms for the fermions. The Yukawa matrices are 3×3 complex matrices. To

diagonalize them and define the real mass eigenstates, we introduce six unitary matrices such that:

$$Y^e_{diag} = V^e_L Y^e V^{e\dagger}_R, \quad Y^u_{diag} = V^u_L Y^u V^{u\dagger}_R, \quad Y^d_{diag} = V^d_L Y^d V^{d\dagger}_R \tag{1.31}$$

In the leptonic sector, when considering the $\mathcal{L}_F$ part of the Lagrangian, this rotation is reabsorbed in the redefinition of fields and does not affect the interactions. In this original version of the SM, there was no right-handed neutrino and the left-handed one was massless. This consideration has changed after the observation of neutrino oscillations as we will discuss in section 1.1.3.

But in the quark sector, u_L transforms differently from d_L, and this affects the interactions containing both quark types with $W^{\pm}$. The interaction term is modified and becomes:

$$\mathcal{L}_F \supset g_w u^{\dagger}_{Li} \mathcal{V}_{ij} \bar{\sigma}^{\mu} d_{Li} W^{+}_{\mu} + h.c. \tag{1.32}$$

where $\mathcal{V} = V^u_L V^{d\dagger}_L$ is a unitary matrix called the Cabibbo-Kobayashi-Maskawa mixing matrix (CKM). We can show that this non diagonal term is the only term in SM which ensures couplings between different generations of quarks.

CKM matrix definition contains only one physical phase. This can be seen in the following parametrization:

$$\mathcal{V} = \begin{pmatrix} 1 & 0 & 0 \\ 0 & c_{23} & s_{23} \\ 0 & -s_{23} & c_{23} \end{pmatrix} \begin{pmatrix} c_{13} & 0 & s_{13}e^{i\delta} \\ 0 & 1 & 0 \\ -s_{13}e^{i\delta} & 0 & c_{13} \end{pmatrix} \begin{pmatrix} c_{12} & s_{12} & 0 \\ -s_{12} & c_{12} & 0 \\ 0 & 0 & 1 \end{pmatrix} \tag{1.33}$$

where $c_{ij} = \cos\theta_{ij}$ and $s_{ij} = \sin\theta_{ij}$. Experimentally $s_{13} \ll s_{23} \ll s_{12}$. The phase δ is the source of CP-violation in the quark sector of the Standard Model. The magnitude of the CKM matrix elements have been measured with an extreme precision thanks to experiments studying mesons mixings like BELLE (9) and BABAR (10) for B-mesons.

Standard Model renormalizability and electroweak tests.

The success of the Standard Model Lagrangian lies in the accuracy of its description of physics from atomic scales down to scales around 10^{-18} m. The predictions of the SM have been probed by LEP and TEVATRON up to the scales of the order of few hundred GeV.

From a dimensional analysis of the standard Lagrangian, we can see that all the introduced terms are renormalizable. We will not develop the renormalization procedure in this section and we advice the reader to refer to the appendix B for more details. Nevertheless we have to emphasize that it is renormalizability that ensures the impressive predictivity of the model. In order to compare theoretical predictions of the Standard Model with the experimental data only three different input parameters are needed [6]: which are the Z-mass determined by LEP1, the fine structure constant α, extracted from measurement of the anomalous magnetic moment of the electron, and the Fermi constant extracted from the muon lifetime:

[6] This is without counting the Higgs mass m_h and the fermions masses and mixings.

$$m_Z = 91.1876 \pm 0.0021 \text{ GeV}$$
$$\alpha = \frac{1}{137.035999084(51)}$$
$$G_F = 1.166364(5) \times 10^{-5} \text{ GeV}^{-2}$$

All the other observables of the electroweak sector can be predicted with a high precision from these three inputs by including quantum correction effects and can be now observed with high accuracy in the colliders. The main advance in this domain was produced by the LEP, an e^+e^- collider, in the 1990's and it has already permitted to give bounds on the top and Higgs masses using fits of these so-called electroweak precision observables. The TEVATRON, a $p\bar{p}$ collider, has confirmed the presence of the top and has improved the precision of the top and W mass measurements (11). As top and Higgs masses are also inputs for the fits of electroweak precision data, these combined data from LEP and TEVATRON are used to give a preferred range of mass for the SM Higgs around $100-200$ GeV (see figure 1.3) , which is still compatible with no direct-observation limits from LEP and TEVATRON (12; 13). In the figure (1.4), we show how the precision of these measurements allows deviation which are often under the percent level. Therefore they can also be used to constrain eventual deviations from the Standard Model.

The radiative effects on all the electroweak observables are not independent and are mainly dominated by the radiative corrections to the gauge bosons self-energies[7]. This is due to the fact

[7]There exists also non-oblique corrections which are more specifics like the vertex correction to $Z \to b\bar{b}$ due to top and large bottom mass effects .

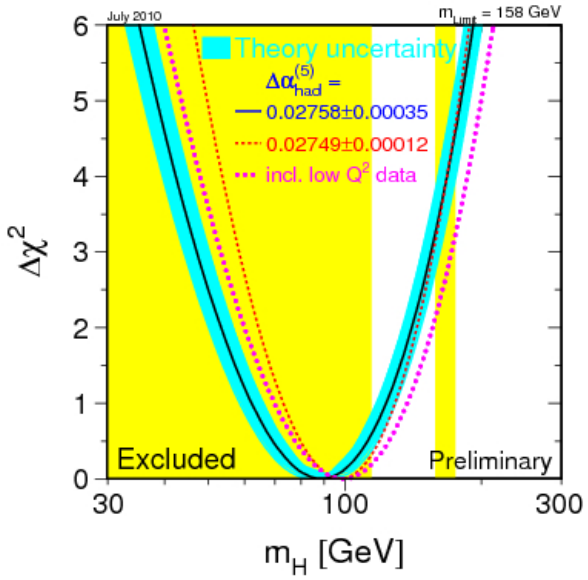

Figure 1.3: This plot presents the $\Delta\chi^2$ of the Standard Model fit of the electroweak precision observables as a function of the Higgs mass. The minimum of this curve, at 89 GeV, is the mass of the Higgs bosons which is preferred by EWPT with an experimental uncertainty of +35 and -26 GeV (at 68 percent confidence level). This has been taken from (14).

Quantity	Value	Standard Model	Pull	Dev.
M_Z [GeV]	91.1876 ± 0.0021	91.1874 ± 0.0021	0.1	0.0
Γ_Z [GeV]	2.4952 ± 0.0023	2.4954 ± 0.0009	-0.1	0.1
Γ(had) [GeV]	1.7444 ± 0.0020	1.7418 ± 0.0009	—	—
Γ(inv) [MeV]	499.0 ± 1.5	501.69 ± 0.07	—	—
$\Gamma(\ell^+\ell^-)$ [MeV]	83.984 ± 0.086	84.005 ± 0.015	—	—
σ_{had}[nb]	41.541 ± 0.037	41.484 ± 0.008	1.5	1.5
R_e	20.804 ± 0.050	20.735 ± 0.010	1.4	1.4
R_μ	20.785 ± 0.033	20.735 ± 0.010	1.5	1.6
R_τ	20.764 ± 0.045	20.780 ± 0.010	-0.4	-0.3
R_b	0.21629 ± 0.00066	0.21578 ± 0.00005	0.8	0.8
R_c	0.1721 ± 0.0030	0.17224 ± 0.00003	0.0	0.0
$A_{FB}^{(0,e)}$	0.0145 ± 0.0025	0.01633 ± 0.00021	-0.7	-0.7
$A_{FB}^{(0,\mu)}$	0.0169 ± 0.0013		0.4	0.6
$A_{FB}^{(0,\tau)}$	0.0188 ± 0.0017		1.5	1.6
$A_{FB}^{(0,b)}$	0.0992 ± 0.0016	0.1034 ± 0.0007	-2.7	-2.3
$A_{FB}^{(0,c)}$	0.0707 ± 0.0035	0.0739 ± 0.0005	-0.9	-0.8
$A_{FB}^{(0,s)}$	0.0976 ± 0.0114	0.1035 ± 0.0007	-0.6	-0.4
$\bar{s}_\ell^2(A_{FB}^{(0,q)})$	0.2324 ± 0.0012	0.23146 ± 0.00012	0.8	0.7
	0.2316 ± 0.0018		0.1	0.0
m_t [GeV]	173.1 ± 1.3	173.2 ± 1.3	-0.1	-0.5
M_W [GeV]	80.420 ± 0.031	80.384 ± 0.014	1.2	1.5
	80.376 ± 0.033		-0.2	0.1

Figure 1.4: This table is extracted from PDG review (11) on electroweak precision test. The *Pull* column give the deviation considering the Higgs mass as a free parameter and the *Dev* column is given for $m_h = 117$GeV. Γ's represent the partial and total width of the Z and $R_x = \Gamma_{had}/\Gamma_x$, A_{FB} the forward-backward asymmetry in the distribution of $f\bar{f}$ production which originates from interferences between the vector and the axial-vector couplings.

that all species of fermions in the Standard Model couple to weak gauge fields. From a theoretical point of view, it means that these, so called "oblique corrections", are parametrized by a limited set of variables which characterize the properties of electroweak symmetry breaking and which can be used to constrain the physics beyond the Standard Model. We can quote for instance the STU-parametrization (15) which introduces the S and T-parameters where T measures the difference between the new physics contributions of neutral and charged current processes at low energies (it is sensitive to the custodial isospin violation) and S (and U) describe new physics contributions to neutral (charged) current processes at different energy scales. Setting STU equal to zero in the SM case, present limits on these parameters are given by (11):

$$\begin{cases} S = 0.01 \pm 0.10 \\ T = 0.03 \pm 0.11 \quad \text{where} \quad m_h = 117 \text{ GeV} \\ U = 0.06 \pm 0.10 \end{cases}$$

STU-variables still depend on the Higgs mass but they give quite stringent bounds on some exotic SM extension by constraining masses and couplings of extra-particles that can be added

to the theories. Let us mention the simple example is a heavy degenerate family of fermions. In this case we have $S = 0.21$ which leads to a 6σ deviation and thereby to an exclusion of such extension.

1.1.3 Beyond the Standard Model

Behind its success, some curiosities remain

In the experimental data from low energy experiments, some 2-3 standard deviations discrepancies exist between electroweak data and SM predictions. We can quote for instance the anomalous momentum of the muon, the forward backward asymmetries in hadronic and leptonic decays **of the top (16)** and B_s-mesons oscillations. However, such effects can also be due to some experimental or theoretical artifacts or just to statistical fluctuations.

Other hints of beyond the Standard Model physics can be found in cosmology. In order to explain the asymmetry between matter and antimatter, cosmological theories require a CP-violation which is much stronger than the Standard Model one. This can be explained by new sources of CP-violation at higher energies. Another hint from cosmology is given by the evidences of Dark Matter that we will discuss in section 1.2. Dark Matter abundance can be explained by a new stable and Weakly Interacting Massive Particle (WIMP). Although such new particles has not been yet detected directly, this hypothesis seems to be the most promising one. There exists also other alternatives to the presence of new massive stable particles in the Universe, such as MOdified Newtonian Gravity models (MOND) (17) or MAssive Compact Halo Objects (MACHOs) (18) but they are not satisfactory to describe the current cosmological observations.

Finally, the undeniable evidence of neutrino oscillations shows that we need new states which are not included yet in the Standard Model. The Standard Model requires actually massless and left-handed neutrinos (due to maximal parity violation of electroweak interaction). However, by now, many experiments with solar, atmospheric, reactor and accelerator neutrinos have collected a lot of data showing the oscillation of the three flavors of neutrinos ν_e, ν_μ, ν_τ, caused by non zero masses and neutrinos mixing. For quarks we have used the CKM matrix to describe this mixing. Here we introduce a new matrix: the Pontecorvo-Maki-Nakagawa-Sakata (PMNS) matrix:

$$U = \begin{pmatrix} 1 & 0 & 0 \\ 0 & c_{23} & s_{23} \\ 0 & -s_{23} & c_{23} \end{pmatrix} \begin{pmatrix} c_{13} & 0 & s_{13}e^{i\delta} \\ 0 & 1 & 0 \\ -s_{13}e^{i\delta} & 0 & c_{13} \end{pmatrix} \begin{pmatrix} c_{12} & s_{12} & 0 \\ -s_{12} & c_{12} & 0 \\ 0 & 0 & 1 \end{pmatrix} \begin{pmatrix} e^{i\alpha_1} & 0 & 0 \\ 0 & e^{i\alpha_2} & 0 \\ 0 & 0 & 0 \end{pmatrix} \tag{1.34}$$

Then, the new mass eigenstates ν_1, ν_2, ν_3 will be related to the flavor eigenstates as follows:

$$\begin{pmatrix} |\nu_1\rangle \\ |\nu_2\rangle \\ |\nu_3\rangle \end{pmatrix} = U \begin{pmatrix} |\nu_e\rangle \\ |\nu_\mu\rangle \\ |\nu_\tau\rangle \end{pmatrix} \tag{1.35}$$

where $c_{ij} = \cos\theta_{ij}$ and $s_{ij} = \sin\theta_{ij}$, δ is the CP-violating phase. α_i are non-zero if the neutrinos are Majorana particles. The generation of such masses and phases remains an open question. By including right-handed neutrinos into the Standard Model, it is possible to explain the neutrino masses with SM Higgs mechanism only. However the Yukawa couplings of neutrinos will be very small. In this context, theorists develop already some models, like the *see-saw* model (19), which address the smallness of the neutrino masses by giving large masses to right-handed neutrinos that will couple with left-handed neutrinos through Yukawa couplings. Moreover many properties of the PMNS matrix, like unitarity or majorana phases, need to be understood.

Theoretical puzzles

In addition to all these experimental hints, we have to stress that some theoretical questions remain unsolved (20).

First, the Standard Model does explain neither the gravitational interactions, nor the choice of the gauge groups. Moreover, the existence of three different gauge couplings, the anomaly cancellation occurring in the SM and the quantized charges tend to lead physicists towards theories with unification of all forces. This idea of interaction unification at high energy scale has already been developed successfully in physics with electromagnetism or electroweak theories and it is reinforced by the fact that if we consider the running of coupling constants at a scale around $10^{14} - 10^{16}$GeV, the three constants seem to converge roughly close to same value.

Secondly, in the QCD sector, a coupling proportional to $\epsilon^{\mu\nu\rho\sigma} G^A_{\mu\nu} G^A_{\rho\sigma}$ for gluon fields, allowed by SM symmetries, could be written but this CP-violating term is not present. This absence has been measured with a extremely good precision and gives rise the so-called CP-strong problem.

Another puzzle is the large mass hierarchy in the matter sector of Standard Model: there exits a difference of 5 orders of magnitude between the electron mass which is less than the 0.51 MeV and the top mass which is around 172 GeV, and this is without considering neutrinos. Therefore, the generation of masses by the Yukawa couplings introduce a lot of free parameters in the Standard Model theory.

Finally, another issue arises with the quantum corrections to the Higgs mass from its self-couplings and the couplings to $W^{\pm}$, Z and top quark (figure 1.5). Such corrections are quadratically divergent and therefore very sensitive to the UV physics: from the renormalization procedure, we get the correction to the Higgs mass:

$$\Delta m_h^2 \sim \frac{1}{32\pi^2}((\frac{1}{4}(3g_w^2 + g_1^2) + 6\lambda - 6y_t^2)\Lambda^2 + \mathcal{O}(\log \Lambda)) \tag{1.36}$$

This means that if the Standard Model were valid up to the Planck scale ($M_P = 1.22 \times 10^{19}$ GeV), radiative corrections would be important because of the quadratic dependence in the cut-off scale in equation (1.36). As the physical mass is obtained by adding the bare mass and the one-loop correction, this would imply a "fine-tuning" with a precision of 10^{-32} between the bare mass and Δm_h^2 to cancel this quadratic effect and to get a mass for the Higgs around 100 GeV. This problem is known as the "naturalness" problem. In the end, as the Higgs has not been yet observed, we have to think of both possibilities: either there is a Higgs or not but in any case, we have to understand the unitarization of the $WW \longrightarrow WW$ scattering. The absence

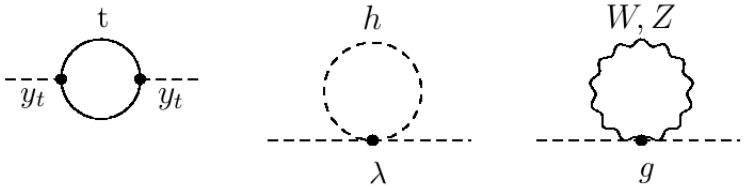

Figure 1.5: Radiative corrections to Higgs mass in SM from W, Z, top and Higgs self-interaction.

of new weakly coupled particles (as the Higgs boson) would actually lead the growth of this cross-section. The theory would not be perturbative anymore at around 1.2 TeV and new strong dynamics should arise to soften the UV divergences.

How to go beyond?

We can use different approaches to work on the physics beyond the Standard Model. The EFT is interesting because the number of operators we can write down and which respect Standard Model symmetries is limited. All new physics effects at low energy will be parametrized by these new operators. The problem is that the trace of the underlying and more fundamental symmetries that could have been presnet in the "full" UV-theory, is lost in the EFT approach.

Therefore, we can try to elaborate new theories valid at higher energies which will introduce new heavy degrees of freedom at around the TeV scale. So we can hope to see their effects in experiments like the Large Hadron Collider. On the other hand, these theories generate effects which have to be compatible with the low energy observables. For new scenarios beyond the Standard Model, we need then to work out the matching between the ultraviolet and infrared theory and to check it against the experimental data. Once we have presented this procedure, we can start looking at the various classes of models beyond the SM. Most of these theories (except for the minimal supersymmetric model which is renormalizable) are based on EFT which will break down at higher scales around few tens of TeV.

The tremendous list of possible extensions of the SM will be bounded by the creativity of model builders. However, in order to introduce the models used in the chapter 5, we will give a brief overview of the main axes of researches for new physics[8].

Supersymmetry

The appealing supersymmetric models, introduced in the 1970s, have been used in the 1980s to extend the SM and to try to address the fine-tuning "problem" of the Higgs mass.

To illustrate the principle of these models, let us consider for instance the top correction to Higgs in equation (1.37):

[8] Lee-Wick models, based on peculiar modifications of field propagator will be discussed in chapter 5.

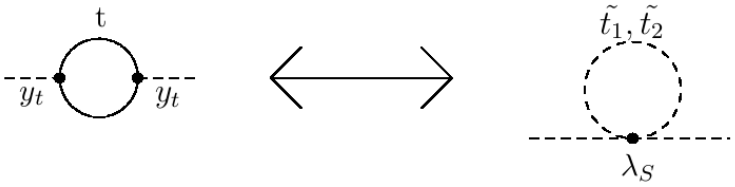

Figure 1.6: Radiative corrections to Higgs mass in SM from the top quark and new cancelling contribution from the two top partners: $\tilde{t_1}, \tilde{t_2}$.

$$\Delta m_h^2 \sim -\frac{y_t^2}{16\pi^2}(2\Lambda^2 + 6m_t^2 \log\left(\frac{\Lambda}{m_t}\right) + ...) \tag{1.37}$$

Here Λ is the cut-off scale of the Standard Model which is expected to be around the Planck mass M_P. Then we can think of adding two new scalars to the SM, with the same quantum number as the top quark; one superpartner for each top's chirality as it is shown in the figure 1.6. We denote λ_S their couplings with the Higgs and m_S, their masses. They will give corrections to the Higgs mass:

$$\Delta m_h^2 \sim 2 \times \left(\frac{\lambda_S}{16\pi^2}(\Lambda^2 + 2m_{\tilde{t}}^2 \log\left(\frac{\Lambda}{m_{\tilde{t}}}\right) + ...)\right) \tag{1.38}$$

If $\lambda_S = y_t^2$, there is a compensation between the two loops and the divergence is now logarithmic.

As we just see with this naive example, such models are based on a new symmetry between fermionic and bosonic degrees of freedom. From a technical point of view, this can be formulated in the following way: the new generators of this transformation will extend the Poincaré algebra into a superalgebra. This is allowed by Coleman-Mandula theorem only by adding also anticommuting generators. In the minimal extension, we add to the translation generator P^μ and Lorentz transformation generator $M^{\mu\nu}$, one new fermionic generator $Q = \left(Q_\alpha, \bar{Q}^{\dot{\alpha}}\right)^T$ which transforms like a spin-1/2 (21) [9]. The new superalgebra becomes:

$$\begin{aligned}
[P_\mu, P_\nu] = 0,\ [M_{\mu\nu}, P_\rho] &= i(g_{\mu\rho}P_\nu - g_{\nu\rho}P_\mu), \\
[M_{\mu\nu}, M_{\rho\sigma}] &= i(M_{\mu\sigma}g_{\nu\rho} + M_{\nu\sigma}g_{\mu\rho} - M_{\mu\rho}g_{\nu\sigma} - M_{\nu\sigma}g_{\mu\rho}) \\
[M_{\mu\nu}, Q_\alpha] = (\sigma_{\mu\nu})_\alpha^\beta Q_\beta,\ \text{and}\quad [P_\mu, Q_\alpha] &= 0 \\
\{Q_\alpha, Q_\beta\} = 0,\ \text{and}\quad \{Q_\alpha, \bar{Q}_{\dot{\beta}}\} &= 2\sigma^\mu_{\alpha\dot{\beta}} P_\mu
\end{aligned} \tag{1.39}$$

where $g_{\mu\nu}$ is Minkowski's metric, the $\alpha, \beta, \dot{\alpha}, \dot{\beta}$ indices take the values 1 or 2. $\sigma_\mu = (1, \sigma_i)$ are Pauli's matrices and $\sigma_{\mu\nu} = \frac{1}{4}[\sigma_\mu, \sigma_\nu]$.

In this minimal supersymmetric model (MSSM), which is a renormalizable theory, the content of particles is at least twice the Standard Model one. If supersymmetry is not broken, the SM particles and their partners have the same mass. Therefore the phenomenology of such model should be rich but none of these superpartners have yet been observed at colliders, like LEP or TEVATRON. Moreover the precision measurements done at low energy through rare decays like $b \to s\gamma$, $\mu \to e\gamma$, neutral meson mixings, anomalous magnetic moment of the muon have already excluded some models or at least part of their parameter space.

This means that supersymmetry, if it exists, is broken at a scale M_{SUSY} few times higher than the electroweak scale implying that the Higgs boson receives corrections in the following form:

$$\Delta m_h^2 \sim M_{SUSY}^2 \left(\frac{\lambda}{16\pi^2} \log\left(\frac{\Lambda}{m_{SUSY}}\right) + ...\right) \tag{1.40}$$

A lot of possible scenarios can explain this supersymmetry breaking mechanism, for instance gravity-, anomaly- or gauge- mediation, but the number of new free parameters is huge in

[9] Let us stress that adding such new symmetry of the space-time can be actually seen as adding a new Grassmannian extra-dimension.

those models making them difficult to constrain. Nevertheless a quite general prediction of supersymmetric models is the presence of a light Higgs boson with a mass below 150 GeV that can potentially be observed at the LHC. Another appealing feature in supersymmetric models is the "R-parity". This parity is introduced to avoid the proton decay through new, allowed, baryon number violating vertices. We can show that $P_R = +1$ for SM fields and $P_R = -1$ for supersymmetric partners. If this parity is exact it will also prevent the decays of "s-particles" into SM ones. As we will see in section 1.2, the lightest supersymmetric particle (LSP) could thereby become a viable Dark Matter candidate.

Little Higgs Model

Another alternative to supersymmetric scenarios are the Little Higgs (LH) models. They were proposed originally by Arkani-Hamed, Cohen and Georgi (22) and they protect the Higgs mass from quadratic divergences at one loop thanks to a spontaneously broken global symmetry. These effective field theories introduce a Higgs boson which is a pseudo-Nambu-Goldstone Boson (NGB). The symmetry breaking is realized in a subtle way called "collective symmetry breaking", which means that the symmetry of the Lagrangian is broken only if at least two couplings are not vanishing. Technically, this implies that the mass term for the Higgs can arise only if we consider two different NGB. Without entering into the details of such model buildings, the interesting phenomenological features of Little Higgs models are their new degrees of freedom. To each SM field will be associated a "heavy" field with the same spin and with a mass of the order of the breaking scale f. Their couplings with the Higgs will be such as they will soften the divergences of the Higgs mass (Figure 1.7). This is enough to solve the hierarchy problem,

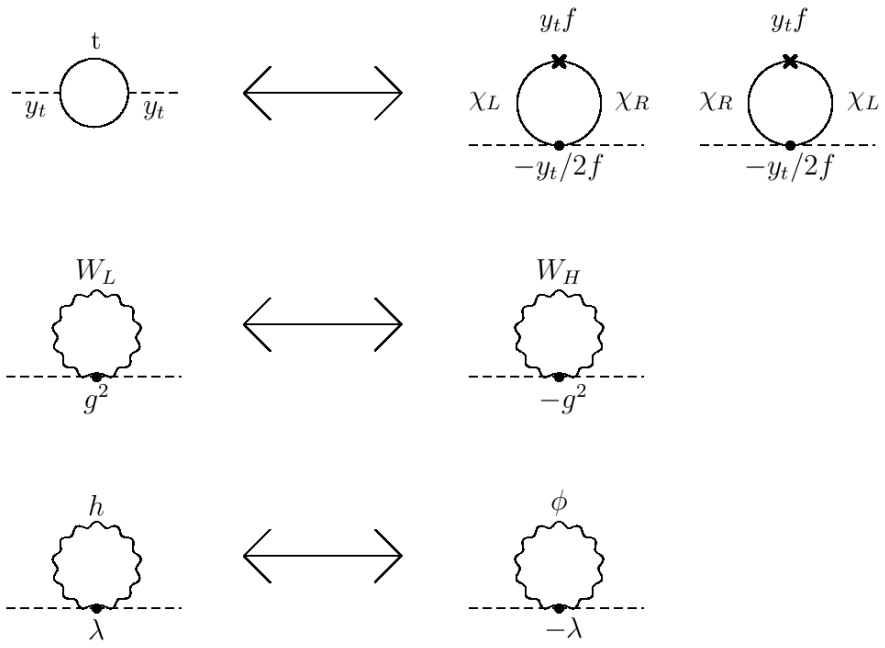

Figure 1.7: Radiative corrections to Higgs mass in SM and new contributions from Little Higgs model. W_H, is the heavy partner of the SM W_L,χ_L and χ_R are two vector like quarks which are introduced in the top sector, and ϕ is a pseudo-goldstone partner of the Higgs field.

because the scale of new physics required beyond the Little Higgs mechanism is pushed above 10 TeV.

This bound can be lowered once we introduce a new parity called *T-parity* (23) which avoids tree level contribution of new partners to electroweak observables. This symmetry will also prevent the decay of heavy partners and force them to be pair-produced which could have an interesting implication in cosmology (see section 1.2). This class of models has also interesting signatures for collider because of the rich number of new charged particles. Even if the pair production is needed, the couplings of heavy partners with SM particles are sizable (24). Typical bounds for such models, set around the TeV scale, leave open the possibility to observe it at the LHC collider.

Strongly coupled theories

Strongly coupled theories have also been thought of as extensions of Standard Model. One of the most discussed are the technicolor (TC) and the extended technicolor (ETC) (25). Proposed in the 1980s, those models give a dynamical approach to electroweak and flavor symmetry breaking effects. The underlying idea is that all the fundamental mass scales present in a theory have to be generated dynamically. In such models, the electroweak scale associated to the Higgs boson vacuum expectation value $v = 246$ GeV would arise from a new strong interaction, like in QCD, where the pion decay constant $f_\pi = 93$ MeV is linked to $\Lambda_{QCD} \sim 200$ MeV. In this case, a new non-abelian gauge structure and new "technifermions" are added to the SM particle content but we do not need new elementary scalar fields. Like in QCD, the chiral symmetry will be broken, a technifermion condensate will arise and Goldstone bosons will appear. The so-called "technipions" will be eaten by the $W^\pm$ and Z to become their longitudinal polarizations. The characteristic scale Λ_{TC} will be related to the decay constant of the "technipion" and so to the masses of $W^\pm$ and Z. From a phenomenological point of view, the interest is based on the potential observation of spin-zero technipions or of spin-one isovector technirhos. Nevertheless in TC and ETC, a lot of challenging problems such as flavor-changing neutral current effects, large mass of the top and compatibility with the electroweak precision tests are still present. For more information on technicolor models, we invite the reader to refer to the review of K.Lane (25).

In the same spirit, we find more recent developments on more model-independent approaches (26) which tend to describe theories with a light Higgs boson associated with a strong dynamics at higher scales. In this reference (26), the author describes for instance how these effective theories with composite Higgs can be related to some existing scenarios like Little Higgs Models. In all cases, we have to stress that the main technical issue with these strongly coupled theories, like in Chromodynamics, is the difficulty of extracting prediction from them. Computations in this framework are very challenging even if new techniques like ADS/CFT correspondence (27) and lattice calculations, as proposed in (28), start to give some promising results.

Extradimensional models

Another class of models that can be explored to extend the physics beyond the Standard Model will based on the modification of the properties of the usual 4-dimensional Minkowski space-time. As we will see later in section 1.3, it is possible to add new compact spatial dimensions to the 4D Minkowski metric. In this case, the propagation of the fields will be affected; the characteristic size of those new dimensions will determine the typical energy scale where new phenomenology will arise. Playing with the topology, the curvature and the boundaries of

the extra-space, we will see that effective field theories written in these new frameworks can be used to address numerous and various problems of the Standard Model.

1.2 Cosmological constraints on Dark Matter

1.2.1 The Standard Model of cosmology

At the beginning of the 20th century, Einstein developed a mathematical formulation of General Relativity expressing the gravitational interactions as a consequence of the space-time geometry. Then, few years later Friedmann, Lemaître, Robertson and Walker proposed a solution of Einstein equations describing the dynamics of our universe. This FLRW model is based on an universe background which is homogeneous, isotropic and non-stationnary. These assumptions, which are pretty well observed at scales larger than the hundred megaparsecs, will lead to a solution known as the Robertson-Walker's metric:

$$ds^2 = dt^2 - a(t)^2 \left[\frac{dr^2}{1-kr^2} + r^2(d\theta^2 + \sin^2\theta d\phi^2) \right] \tag{1.41}$$

where t is the time, r is the co-moving distance and k is the spatial curvature. Without loss of generality we can show that $k = -1, 0, +1$, which corresponds to open, flat or closed universe. The scale factor $a(t)$ will describe the curvature of the space-time and will make the link between physical distances at a given time and co-moving ones: $dl = a(t)dr$. We can introduce the Hubble paramater H which characterizes the rate of universe expansion at given time:

$$H(t) = \frac{\dot{a}(t)}{a(t)} \tag{1.42}$$

Actually we find that in the limit of low redshifts and low distances, the separation velocity v between two objects is linked to their relative distance r by the linear relation: $v = Hr$. This observation was made originally by Hubble and was a hint about such non-static universe.

In the FLRW model, the universe is filled by different perfect fluids with pressure p and density ρ which follow an equation of state of the form: $p = w\rho$. For relativistic gases: $w = 1/3$, for non-relativistic matter: $w \simeq 0$ and for dark energy, which is characterized by the cosmological constant Λ ($\rho_\Lambda = \frac{\Lambda}{8\pi G}$), $w = -1$. After solving the Einstein equations, we show that:

$$H^2 = \frac{8\pi G}{3}\rho_R + \frac{8\pi G}{3}\rho_M + \frac{8\pi G}{3}\rho_\Lambda - \frac{k}{a^2} \quad \text{with} \quad \rho \propto a^{-3(w+1)} \tag{1.43}$$

where G is Newton's gravitation constant. After introducing the critical density, $\rho_c = \frac{3H^2}{8\pi G}$, and the ratio $\Omega_i = \frac{\rho_i}{\rho_c}$, this "budget" equation (1.43) becomes for our flat universe:

$$1 = \Omega_{tot} = \Omega_R + \Omega_M + \Omega_\Lambda \quad \text{with} \quad k = 0 \tag{1.44}$$

The experimental determination of the five parameters $\{\Omega_R, \Omega_M, \Omega_\Lambda, H_0, k\}$ will be sufficient to describe the evolution of the FLRW universe and this is the reason why precise measurements of these parameters have been performed in observational cosmology for the last 30 years.

Moreover, from the observations of the last decades, it is possible also to propose a scenario for the history of the universe which is quite robust: the *Hot Big Bang* model. It is based on the fact that the universe was denser and hotter at early time. At this epoch, all particles were produced at thermal equilibrium. Then, progressively, the universe expansion cooled down this primordial plasma, unstable particles decayed but stopped being produced. On the other hand, stable particles stopped interacting with the rest of plasma and started evolving freely: this situation is known as *decoupling*. As an example, we can quote the last decoupling of the photons. At $T \sim 4000K$, the recombination of electrons and nucleons formed bound stable neutral states which stop interacting with photons. Since this time, the black body distribution of those thermal photons has been frozen and their "temperature" has just dropped because of expansion. Firstly observed by Penzias and Wilson (29), the temperature distribution of those photons has been extremely well measured at 2.725K by experiment of Cosmical Microwave Background (CMB) detection. As we will see, the CMB is a probe of the early universe structure and will contain information of the content of matter and radiation in the earlier universe (figure 1.9).

1.2.2 Evidences of Dark Matter

In this section, we will focus on the observations which suggest the presence of Dark Matter in our description of the universe. This new matter constituent has been introduced to explain gravitational effects at various scales, which were not understandable with the observed amount of baryonic matter in the universe (at least in the FLRW paradigm): $\Omega_M = \Omega_{nb} + \Omega_b$. We will present briefly some of those effects from astrophysical to cosmological scale:

At galaxy scale

The first evidences of Dark Matter come from the observations of galaxies. We expect that the orbits of the stars in such structures follow Kepler's laws. If we consider a mass $M(R)$ inside a sphere of radius R, the equilibrium between kinetic and gravitational energies can be written as:

$$\frac{v^2}{R} = \frac{GM(R)}{R^2} \quad \Rightarrow \quad v = \sqrt{\frac{GM(R)}{R}} \tag{1.45}$$

where G is the gravitational constant and v the velocity of the stars. As it can be seen in figure 1.8 on the so-called "disk" profile, we know that v decreases as $1/\sqrt{R}$ when we go away from the galaxy center for large distances ($R \gtrsim R_G = 5\text{kpc}$) if all the mass of the galaxy is included in the sphere of radius R_G. On the other hand, measurements of the speed distribution in spiral galaxies can be performed by spectroscopy of Doppler effects in hydrogen clouds. Thus, the rotation curves of galaxies (figure 1.8) obtained with this technique of radioastronomy (30), have shown a flat velocity profile at large distances from the center of galaxy. The discrepancy between the expected "Keplerian" behavior and the observations can be explained by the existence of a halo of non-visible matter which will play a gravitational role.

At the scale of galaxies and galaxy clusters

Historically the idea of "Dark Matter" in galaxy clusters comes from Zwicky, in 1933. By studying the speed distribution of galaxies in the Coma cluster, he estimated with the Virial theorem, the gravitational mass of the cluster. He compared it with the mass which could be extracted from observations of the luminosity of thousand of nebulae in the cluster. With this

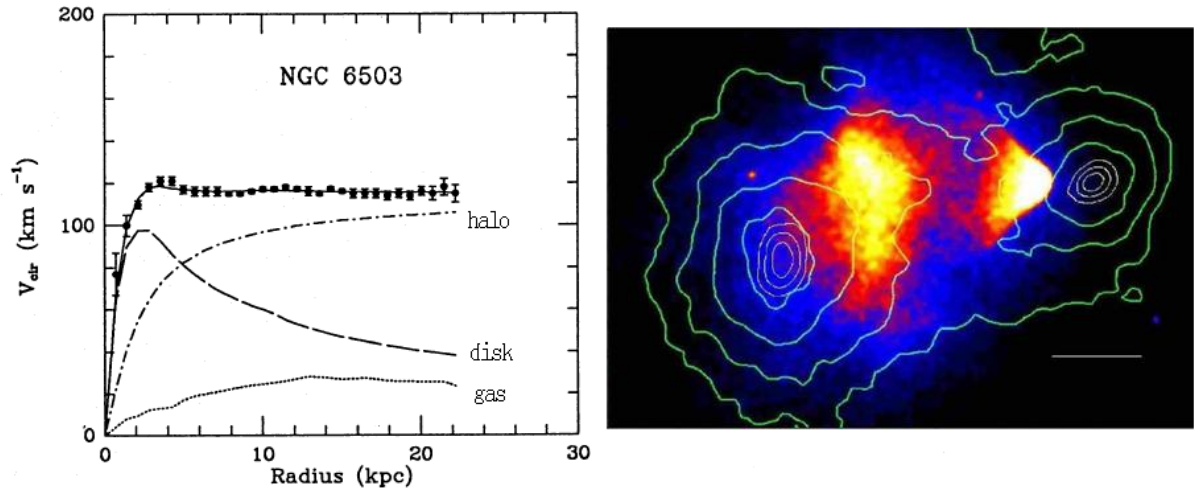

Figure 1.8: Left: Rotation curve for the spiral galaxy NGC6530, extracted from (30). Right: Direct evidence for Dark Matter in the "bullet cluster"(1E0657-56). In this plot reproduced from (31): the visible matter (red and yellow), observed in X-rays by the CHANDRA satellite, only contributes little to the total mass of the two colliding clusters (density contours in green). This total mass has been measured by gravitational lensing with VLT and Hubble satellites.

technique, he found that only 2% of the mass of the cluster came from "visible" matter, the rest was non-luminous matter. Now we know that roughly 10% of the cluster is made of invisible gases but the problem still remains.

The techniques of mass determination has evolved; not only the velocity distribution is used but also the gravitational lensing, based on General Relativity effects. By observing the deformation of galaxies located beyond the cluster, we can extract information on the mass of the cluster in the foreground which has modified the path of light. These observations show also the existence of large amount of Dark Matter in the clusters (32). Finally the last famous hint of Dark Matter evidence at this scale comes from the observation of the "Bullet cluster" (31). In figure (1.8), we see the collision of two galaxy clusters: in red and yellow, the famous bullet shape represents the X-rays emissions coming from the heating of interacting baryonic matter. On the other hand, the green contours show the distribution of mass which is quite isotropic and seems not affected by the collisions. This observation is difficult to explain with modified gravity while it can be understood by the presence of massive and weakly interacting kind of "invisible" matter.

At cosmological scale

The observations of the Cosmic Microwave Background (figure 1.9) show that the temperature of the universe at the time of photon decoupling, was homogeneous and isotropic up to perturbation smaller than 10^{-5}. Then we start seeing some anisotropies and fluctuations of the background that we can use to estimate the parameter set of cosmology introduced in section 1.2.3. The density fluctuations in the primordial plasma can lead to measurements of the baryonic matter density Ω_b which is very different from the one obtained for Ω_M (33).

$$\Omega_b h^2 = 0.02260 \pm 0.00053 \quad \text{and} \quad \Omega_M h^2 = 0.13334^{+0.0056}_{-0.0055} \tag{1.46}$$

where $h = H_0/100$ km.s^{-1}.Mpc^{-1} $= 0.704$. The accuracy of WMAP (Wilkinson Microwave Anisotropy Probe) measurements (34) has already allowed to constrain strongly the sum $\Omega_M + \Omega_\Lambda$ and forces us also to introduce a new non-baryonic matter-like component to our description of the universe. We can try to explain such effects with relic density of neutrinos which are also weakly interacting but WMAP estimates their relic abundance at $\Omega_\nu h^2 \leq 0.0145$[10] which is not sufficient.

Other studies on cosmological scale will help to improve our understanding of the Standard Model of cosmology also called Lambda-Cold Dark Matter (ΛCDM) paradigm. For instance, the Sloan Digital Sky Surveys has created a map of the sky with more than 900,000 galaxies, 120,000 quasars and 400,000 stars (36). The purpose of such maps is to look at the signatures of density perturbations which were in the primordial plasma (Baryonic Acoustic Oscillation) (37). The small fluctuations at early time have actually generated, through gravitational non-linear effects, the large scale structures observed nowadays. So, by measuring these structures, we can infer the power spectrum of those initial fluctuations. This leads to an estimate of matter abundance of $\Omega_M = 0.286 \pm 0.018$. Finally Supernovae of type Ia studies (33) can also be

[10]Note that this value is the WMAP measurement only, in table 1.2 we give the combined result.

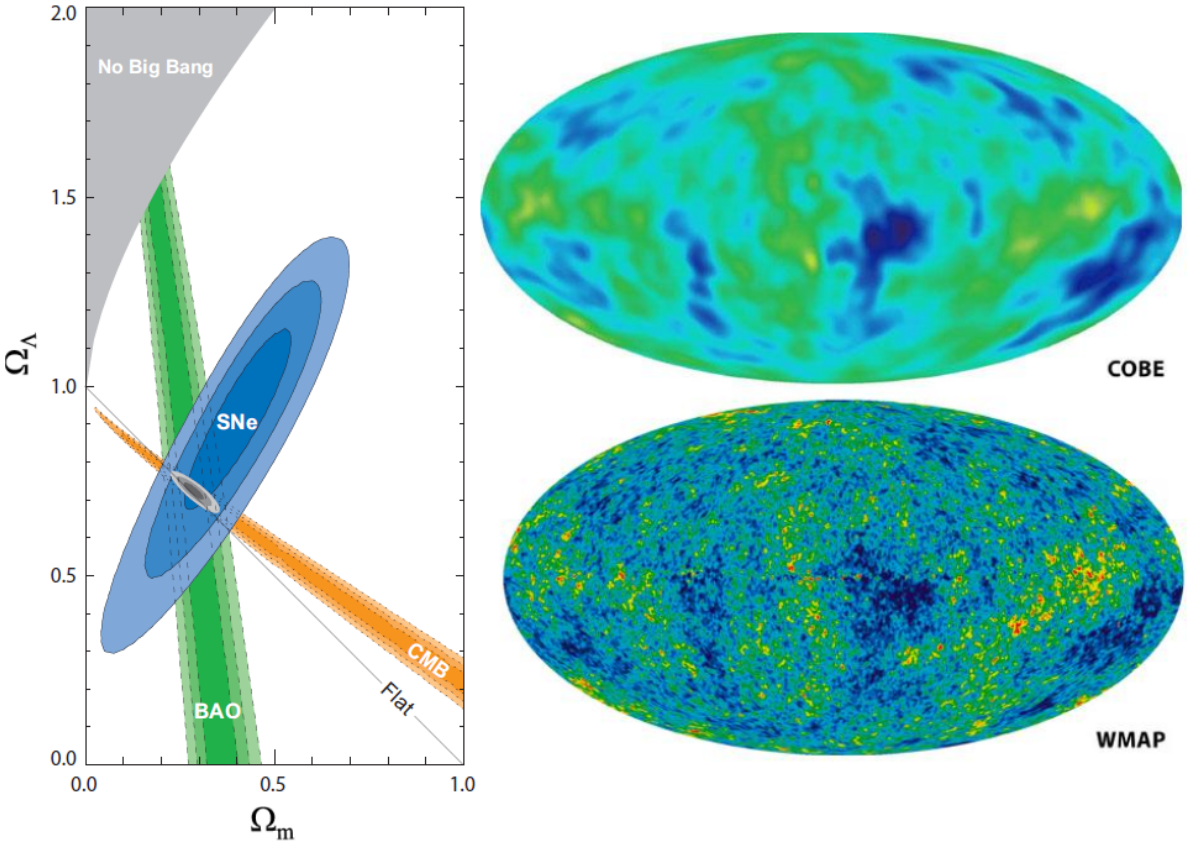

Figure 1.9: Left: 68.3%, 95.4% and 99.7% confidence level contours on Ω_Λ and Ω_M obtained from Cosmic Microwave Background, Baryonic Acoustic Oscillations and the SuperNovae Surveys as well as their combinations (assuming $w = -1$ for the dark energy), extracted from (33). Right: Cosmic Microwave Backgroup anisotropy measurements from COBE and WMAP-7 years with 30 times higher resolution (34). Those official plots are extracted from the WMAP collaboration website (35).

used. Luminosity curves of these standard candles are well understood and will allow accurate measurements of their distance luminosity as a function of their redshift. With these data, we can then estimate the deviations from Hubble law and constrain the Hubble parameter and $\Omega_M - \Omega_\Lambda$.

All these experiments will constrain the minimal set of parameters defining the ΛCDM model, as it is presented in table 1.2. In this table, the total density is $\Omega_{tot} = 1$ which means that we assume that the universe is flat ($k = 0$). We can relax this assumption and the fits of Ω_{tot} will still be in good agreement with the value $\Omega_{tot} = 1$. Then we remark that the dark energy component is quite important and "starts" dominating the dynamics of our present universe. The physical origin of such term is still a mystery which lies in the understanding of gravity and of early universe dynamics. Finally we can stress that the amount of baryonic matter is very small compared to the total matter density. As we already mentioned, a solution can be brought by particle physics by considering a Weakly Interacting Massive Particle (WIMP), whose abundance remains unchanged after decoupling from the primordial plasma.

Ω_γ	Ω_ν	Ω_b	Ω_{dm}	Ω_Λ	$H_0(\mathrm{km/s/Mpc})$
$4.6^{+0.5}_{-0.5} \times 10^{-5}$	< 0.0125	$0.0456^{+0.0016}_{-0.0016}$	$0.227^{+0.014}_{-0.014}$	$0.728^{+0.015}_{-0.016}$	$70.4^{+1.3}_{-1.4}$

Table 1.2: Constraints on ΛCDM model obtained combination of Cosmic Microwave Background, Baryonic Acoustic Oscillations and the SuperNovae Surveys assuming $\Omega_{tot} = 1$ (38).

1.2.3 Cold WIMP relic density calculation

In the previous section, we have presented the current model used to describe our universe and we have emphasized the fact that a Dark Matter component has to be added to our description. In the following we will present how Standard Model extensions can solve this problem and how Dark Matter can contribute to the total matter budget of the universe.

Solving the Boltzmann equation

In this part, we will review the standard calculation of the relic abundance of a particle species $\mathcal{Z}$ which can explain the observed matter density. We will explain how, because of the universe expansion, this massive stable particle went out of the thermal equilibrium and decoupled. The relic abundance of $\mathcal{Z}$ can be found by solving the Boltzmann equation[11] (39; 40):

$$\frac{dn}{dt} = -3Hn - \langle \sigma v \rangle (n^2 - n^{eq2}) \tag{1.47}$$

where n is the density of the relic particle and n^{eq} is the density at the thermal equilibrium. v is the relative velocity of the two $\mathcal{Z}$ and $\langle \sigma v \rangle = \langle \sigma(\mathcal{Z}\mathcal{Z} \to SM)v \rangle$ is the thermally averaged total annihilation cross-section. The first term corresponds to a dilution term of the relic $\mathcal{Z}$, the second one is the annihilation term and the third one is the production term from SM particles in the thermal bath. As we are interested in a cold Dark Matter, we have to look at two different regimes: at high temperature ($T \gg m$), $\mathcal{Z}$ is still relativistic and its equilibrium density is given by $n^{eq} \sim T^3$. At low temperature ($T \ll m$), n^{eq} is given by the non-relativistic limit:

[11] Here we suppose that the particle is stable or long-lived so that in the Boltzmann equation only the annihilation term is relevant.

$$n^{eq} = g\left(\frac{mT}{2\pi}\right)^{3/2} e^{-m/T} \tag{1.48}$$

Here m is the mass of the relic particle $\mathcal{Z}$, T is the temperature and g is the number of internal degrees of freedom such as spin, color, and so on. As it can be seen from the numerical solution in figure 1.10, at early time, $\mathcal{Z}$ annihilated (was created) with its own anti-particle into (from) Standard Model states. Then, because of the expansion, the temperature will drop ($a(t) \sim 1/T$) and the annihilation rate $\Gamma = n\langle\sigma v\rangle$ will be smaller than the Hubble parameter. In this case, the particles cannot annihilate anymore by default of reagents and their density will remain fixed. This decoupling of the stable particles from the thermal bath of the primordial plasma is called *freeze-out* and will occur at temperature denoted T_F which corresponds roughly to the time where $\Gamma \sim H$.

$\langle\sigma v\rangle$ is often approximated by its non-relativistic expansion:

$$\langle\sigma v\rangle = a + b\langle v^2\rangle + O(\langle v^4\rangle) \approx a + \frac{6b}{x} + O(1/x^2) \quad \text{where} \quad x = \frac{m}{T} \tag{1.49}$$

Then by solving the Boltzmann equation analytically with appropriate approximations, we ob-

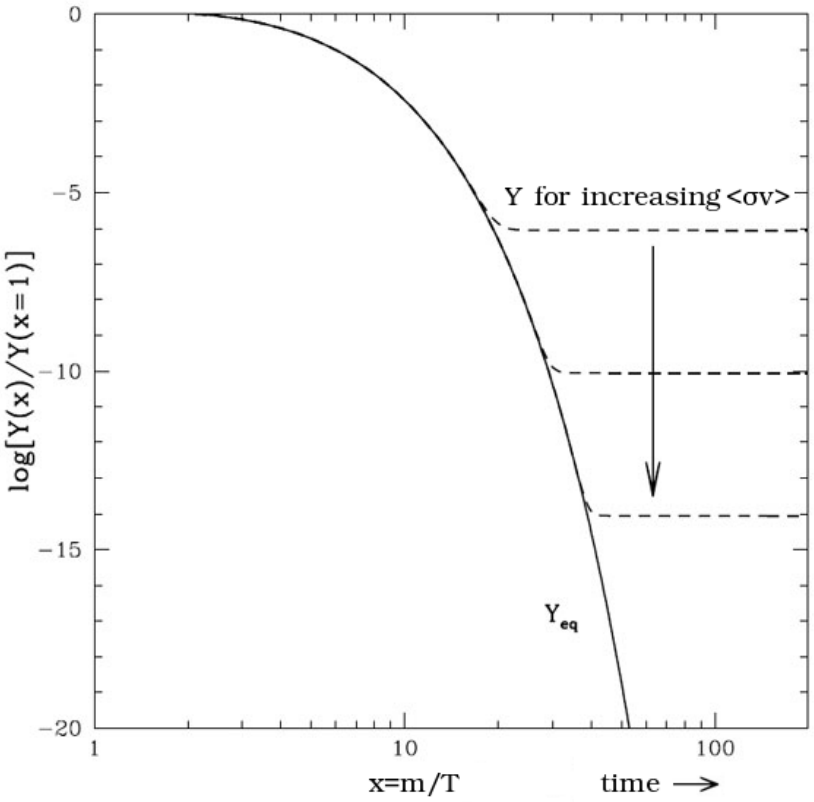

Figure 1.10: Numerical simulation for the evolution of the co-mobile relic density taken from (41). This co-mobile density $Y \propto nT^{-3}$ includes the dilution effect coming from the expansion of the universe. The solid line represents the equilibrium density and the dashed one the current density .

tain the relic density $\Omega_{\mathcal{Z}}$:

$$\Omega_{\mathcal{Z}}h^2 \approx \frac{1.04\times 10^9}{M_P}\frac{x_F}{\sqrt{g_*(x_F)}}\frac{1}{a+3b/x_F} \tag{1.50}$$

where $M_P = 1.22\times 10^{19}$ GeV is the Planck mass and g_* is the total number of effectively massless degrees of freedom and is given in first approximation by:

$$g_*(x) = \sum_{i=bosons} g_i + \frac{7}{8}\sum_{j=fermions} g_i \tag{1.51}$$

In g_*, the coefficient 7/8 comes from the Fermi-Dirac statistics and the dependence on temperature is due to the fact that the thermal bath will quickly lose a lot of massive species as the temperature will drop below their masses. The freeze-out "temperature", x_F, is found from the self-consistent equation:

$$x_F = \ln\left(c(c+2)\sqrt{\frac{45}{8}}\frac{g}{2\pi^3}\frac{mM_P(a+6b/x_F)}{\sqrt{g_*(x_F)x_F}}\right) \tag{1.52}$$

where the value of the constant c can be found after numerical computation. Usually we use $c = 1/2$ because of the weak dependence of x_F on its value. Finally, subleading effects can be taken into account (40; 42) like, for instance, relativistic corrections by the simple replacement $b \to b - \frac{1}{4}a$.

Coannihilation effects

In the previous section, we have considered only one single particle in the calculation of the relic abundance, but in extension of the Standard Model, we can have a richer spectrum of the new heavy states; in particular, other unstable particles are nearly degenerate with the lightest stable one. In this case, the new particles are almost as abundant as the relic $\mathcal{Z}$. If their masses is close to the freeze-out temperature, they will be accessible thermally and *coannihilation* processes involving those heavier particles will modify the prediction for the relic abundance. For this reason, we will consider the previous calculation including new heavier particles: $\mathcal{Z}_i$, $i = 1..N$ of masses m_i, with $\mathcal{Z}_1 \equiv \mathcal{Z}$ and where we have $m_i < m_j$ for $i < j$. Since the heavier particles which will not annihilate, will automatically decay into $\mathcal{Z}_1$, it will be relevant to consider the total density $n = \sum_{i=1}^{N} n_i$ to solve the Boltzmann equations. After some approximations described in (39; 40), we obtain the following expression:

$$\frac{dn}{dt} = -3Hn - \langle\sigma_{eff}v\rangle(n^2 - n^{eq2}) \tag{1.53}$$

where

$$\sigma_{eff}(x) = \sum_{ij}^{N}\sigma_{ij}\frac{g_ig_j}{g_{eff}^2}(1+\Delta_i)^{3/2}(1+\Delta_j)^{3/2}e^{-x(\Delta_i+\Delta_j)}$$
$$\text{and}\quad g_{eff} = \sum_{i=1}^{N} g_i(1+\Delta_i)^{3/2}e^{-x\Delta_i}\quad\text{where}\quad \Delta_i = \frac{m_i - m_1}{m_1} \tag{1.54}$$

Here we have $\sigma_{ij} = \sigma(\mathcal{Z}_i\mathcal{Z}_j \to SM)$ and g_i is the number of internal degrees of freedom of the particle $\mathcal{Z}_i$.

Similarly to the previous section, the freeze-out "temperature", x_F, is found from the self-consistent equation:

$$x_F = \ln\left(c(c+2)\sqrt{\frac{45}{8}}\frac{g}{2\pi^3}\frac{mM_P(a_{eff}(x_F)+6b_{eff}(x_F)/x_F)}{\sqrt{g_*(x_F)x_F}}\right) \tag{1.55}$$

Here a_{eff} and b_{eff} are the first terms in the velocity expansion of σ_{eff}:

$$\begin{aligned} &\langle\sigma_{eff}v\rangle(x) = a_{eff}(x) + b_{eff}v^2 + O(v^4) \\ \Longrightarrow &\begin{cases} a_{eff}(x) = \sum_{ij}^N a_{ij}\frac{g_ig_j}{g_{eff}^2}(1+\Delta_i)^{3/2}(1+\Delta_j)^{3/2}e^{-x(\Delta_i+\Delta_j)} \\ b_{eff}(x) = \sum_{ij}^N b_{ij}\frac{g_ig_j}{g_{eff}^2}(1+\Delta_i)^{3/2}(1+\Delta_j)^{3/2}e^{-x(\Delta_i+\Delta_j)} \end{cases} \end{aligned} \tag{1.56}$$

where a_{ij} and b_{ij} are obtained after expansion of $\sigma_{ij}v = a_{ij} + b_{ij}v^2 + O(v^4)$. After solving the Boltzmann equations, as we did previously, we get for the relic abundance:

$$\Omega_{\mathcal{Z}}h^2 \approx \frac{1.04\times10^9}{M_P}\frac{x_F}{\sqrt{g_*(x_F)}}\frac{1}{I_a+3I_b/x_F} \tag{1.57}$$

with

$$\begin{aligned} I_a &= x_F\int_{x_F}^{\infty} a_{eff}(x)x^{-2}dx \\ I_b &= 2x_F^2\int_{x_F}^{\infty} b_{eff}(x)x^{-3}dx \end{aligned} \tag{1.58}$$

This calculation can be performed for all models which predict a stable Dark Matter candidate and as an example, in the context of this thesis, we can quote the work done in extra-dimensional models like in the section 1.3.6 (39; 43) and in chapter 2. Those calculations can be refined by using numerical resolution of Boltzmann equations including for instance resonance effects (44).

To conclude this section on Dark Matter, let us perform a rough numerical estimate of relic density and annihilation cross section, we find:

$$\Omega_{\mathcal{Z}}h^2 \sim \frac{10^{-10}\ \text{GeV}^{-2}}{\langle\sigma v\rangle} \sim 0.1 \quad \text{and} \quad \langle\sigma v\rangle \sim \frac{\alpha^2}{m_W^2} \sim 10^{-9}\ \text{GeV}^{-2} \tag{1.59}$$

where $\alpha = 1/137$ is the fine structure constant and $m_W \sim 100$ GeV is the electroweak scale. So historically, it has been a puzzling coincidence that the annihilation cross-section of a massive particle with electroweak strength was compatible with relic density observations. This situation has indeed led to the commun idea of *Weakly Interacting Massive Particles* used to link beyond the Standard Model of particle physics and the ΛCDM Standard Model of cosmology.

1.3 Quantum field theory in extra-dimensional models

Finally, in the last review needed for our following discussions, we will present the main motivation for extra-dimensional models. We will show that extra-dimensions turn out to be an interesting tool for model building of new effective field theories and that they can bring new solutions to cure some of the Standard Model problems. Then we will introduce the reader to the basics of the field theory in this framework, which are essential for the understanding of this thesis.

1.3.1 Motivations

In the 1920s, Kaluza (1919) (45) and Klein (1926) (46) had the idea to add a fifth dimension to the usual four-dimensional space-time. Relying on the discovery of General Relativity, they proposed to unify the only two forces known at this time: electromagnetism and gravity. This can be realized by using a 5D Einstein's theory with one extra-dimension compactified on a circle. The $U(1)$ symmetry of the circle will correspond to the $U(1)$ symmetry of electromagnetism and the quadri-potential vector will be generated by the extra parts of the metric $g_{5\mu}$. Nevertheless this geometrical construction suffers of some phenomenological problems such as the prediction of light fermions.

Later in the 1970's and 1980's, the birth of supergravity and superstring theories renewed the interest in extra-dimensional models. However these dimensions are expected to be very small, at the order of $M_P^{-1} \sim 10^{-35}$m and will not be probed before a long time by experiments.

Then, at the beginning of the 1990's, new ideas started to emerge from theorist minds. For example, what will happen if these new extra-dimensions were larger that the Plank length? For instance, Antoniadis (47) proposed TeV^{-1} large extra-dimensions to explain the supersymmetry breaking. In string theory and M-theory, extra-dimensions can lead also to new features interesting for phenomenology at lower scales. But for our own concern, it is at the end of the 1990's that new phenomenological ideas arrived to address the hierarchy problem. We can actually wonder why the electroweak scale is so small compared to the gravity one: $M_P \gg m_W$. Unlike the point of view we have adopted in section 1.1.3, where we have looked for a stabilization of the Higgs mass, here we ask for a lowering of the EFT cut-off from the $M_P \approx 10^{19}$ GeV Planck scale down to TeV scale. In this case, gravitational effects will be observable at lower scales.

Large extra-dimension approach

Introduced by Arkani-Hamed, Dimopoulos and Dvali (ADD) (48), the large extra-dimensional models will consist in compactifing n flat extra-dimensions (with the same radius R for simplicity) on a torus. The volume of the extraspace is $V_n = (2\pi)^n R^n$ and the metric of the space will be:

$$ds^2 = g_{\mu\nu}dx^\mu dx^\nu - R^2 d\Omega^2_{(n)} \tag{1.60}$$

where $R^2 d\Omega^2_{(n)}$ is the metric element associated to the n-dimensional toroidal coordinates. Then the Standard Model is embedded on a 3-brane and gravity is present in the bulk space-time. After writing the Einstein-Hilbert action for 4+n dimensional gravity and integrating out over the extra-dimensions, we can find the matching with the 4-d gravity description:

$$M_P^2 = M_\star^{n+2} V_n \tag{1.61}$$

where $M_\star$ is now the fundamental scale of quantum gravity. For instance, to solve the hierarchy problem we can take $M_\star = 1$ TeV and in this case $R \sim 2.10^{-19} 10^{\frac{32}{n}}$ m. This underlying substructure of the space will affect gravitation, modifying for instance the Newton law. The dilution of gravitation at scale larger than R will not occur at smaller ones. For instance, if $n = 1$, effects will appear for $R \sim 10^8$ km which is bigger then the size of solar system. If $n = 2$, we have $R \gtrsim 0.1$ mm and in this case precision measurements of Newton's law by Cavendish-type experiment can rule out such models. However, this possibility was still valid when the model was proposed. For $n > 2$, we have $R \lesssim 10^{-8} m$, this is not yet reachable by those experiments. This

is due to the technical difficulty to measure such small gravitational effects. Nevertheless, as we will see in next section, propagation of gravity in this extra-dimension will produce excitation of the graviton field. So a tower of spin-2 particle will be produced at masses proportional to $m \sim 1/R$. Limits from collider are given by TEVATRON around the TeV scale and are already improved with LHC (49).

Randall-Sundrum approach

The ADD approach is not the only possibility we can use to dilute the gravity interaction and solve hierarchy problem. Another class of models, alternative to ADD, has been introduced by Randall and Sundrum (50) with only one extra-dimension. The new dimension is compactified on a finite interval $0 \leq y \leq L$. The endpoints of the interval are the so-called "3-branes". The brane at $y = 0$ is called UV-brane or Planck-brane, the brane at $y = L$, where the SM fields are localized is called the IR brane or TeV brane. Solution of Einstein's equations, the RS metric of the space between the 2 branes, so-called "bulk", is that of Anti-de-Sitter (ADS) in 5D and is given by:

$$ds^2 = e^{-2ky} g_{\mu\nu} dx^\mu dx^\nu - dy^2 \tag{1.62}$$

k is the curvature of the space. Without going into the details of solving Einstein's equation, we have to mention that the bulk and brane cosmological constants are compensating each other to stabilize the 4D theory with vanishing 4D cosmological constant. Similarly to the ADD matching, we can now identify at low energy the effective Plank mass M_P with the fundamental scale of gravity $M_\star$:

$$M_P^2 = \frac{M_\star^3}{k}(1 - e^{-2kL}) \sim \frac{M_\star^3}{k} \quad \text{for} \quad kL \sim O(10) \tag{1.63}$$

The Planck scale here does not depend strongly of the size of the extra-dimension; gravitational effects are principally localized close to the UV-brane but it depends only on the new scale $k \lesssim M_P$, the curvature of the space. It is different for SM fields, which are localized on the TeV brane. In this case, the local cut-off will be not be M_P but will be suppressed by:

$$\Lambda_L \sim M_\star e^{-kL} \tag{1.64}$$

M_star is of the order of the Planck scale but the effective cut-off scale Λ_L for the SM is now at the order of the TeV, as it is required by the hierarchy problem. Notice that to avoid to translate the hierarchy problem, we assume $kL \sim O(10)$ and the suppression on TeV remains sizeable without any important fine-tuning.

Like in ADD models, as gravity is propagating in the bulk, excitations of the 5D graviton field will be generated. The first massless one, so-called "zero-mode" is localized at the Planck brane and its coupling to SM fields will be suppressed by $1/M_P^2$. For the massive excitations, physics is different, the coupling with TeV brane fields is more important and in this case, the so-called KK-gravitons could be produced at collider through Drell-Yan process for instance. LHC experiments already constrain the mass of such particle around the TeV scale (51).

Finally, let us mention an interesting theoretical feature of the Anti-de-Sitter background which leads to a new field of research based on Anti-de Sitter / Conformal Field Theory correspondence, noticed by Maldacena (27) in the context of string theory. We could have actually defined the metric by using "conformal" coordinates $z = \frac{e^{-2ky}}{k}$. In this case the interval becomes $[R, R']$ where $R \sim 1/k$ the radius of ADS space and the metric is given by:

$$ds^2 = \left(\frac{R}{z}\right)^2 (g_{\mu\nu}dx^\mu dx^\nu - dz^2) \tag{1.65}$$

This metric has an additional rescaling invariance: $z \to \alpha z,\ x^\mu \to \alpha x^\mu$. A rescaling in 4D space-time of the field theory will lead to an inverted rescaling in energy. So moving along the extra-dimension will change the energy scale of the conformal theory. As a starting point, this property can be used to construct 5D weakly coupled theory which can help to describe 4D conformal theory which can be strongly coupled like QCD.

To conclude, we have seen that these models can pull down the scale of gravity to TeV scale which becomes the natural cut-off scale for the Standard Model. The main problem is that quantum gravity violates in general global symmetry, while we know that the Standard Model contains a lot of global symmetries preventing for instance proton decay, flavor changing neutral currents, excesses of CP violation and so on. Experimental limits on these phenomena rise the cut-off scale well above the TeV scale. So ADD and RS in their original version are incomplete to explain the smallness of those mechanisms. Generally to go further in the understanding of those phenomena, we need to open "Pandora's box" and allow some Standard Model fields propagate in the bulk of the dimension.

In more recent approaches, gravity is often left apart and we focus more on the possibilities that field theory in extra-dimensional background can bring from a phenomenological point of view. A lot of well-motivated models are considered to address various problems of the Standard Model and we will just concentrate on the ones needed for the understanding of this thesis. For more information, we invite the reader to look at the reviews (52; 53; 54; 55).

1.3.2 Scalar fields in flat extra-dimensions

In this section, we will go through the basic concept of extra-dimension field theory (52). We will consider for this purpose, the usual flat Minkowski space extended by only one compact and flat extra-dimension. The coordinates of a point in this space-time are given by:

$$x^M \equiv (x^\mu, y) = (x^\mu, x^5) \in \mathcal{M}^4 \times [0, \pi R] \tag{1.66}$$

The metric will be $g^{MN} = (+1, -1, -1, -1, -1)$ where $M = 0, 1, 2, 3, 5$. Greek letters μ, ν will denote the usual four dimensions. For a scalar field Φ, its bulk action will be given by:

$$\mathcal{S}_{bulk} = \int d^4x \int_0^{\pi R} \left(\frac{1}{2}\partial^M \Phi \partial_M \Phi - V(\Phi)\right) dy \tag{1.67}$$

We can now apply the variational principle to this action and we get:

$$\delta\mathcal{S}_{bulk} = \int d^4x \int_0^{\pi R} \left(\partial^M \Phi \partial_M \delta\Phi - \frac{\partial V(\Phi)}{\partial \Phi}\delta\Phi\right) dy \tag{1.68}$$

For simplicity we neglect localized actions in this section and postpone their introduction for the next paragraph.

Equation of motion and boundary conditions

We can then integrate by part the formula (1.68) along the four usual dimensions, by assuming the field vanishing at large distances. However, for the integral along the fifth dimension, we have to be careful because there is no physical reason for the field to vanish on the boundaries.

$$\delta\mathcal{S}_{bulk} = \int d^4x \int_0^{\pi R} \left(-\partial^M\partial_M\Phi - \frac{\partial V(\Phi)}{\partial\Phi}\right)\delta\Phi \; dy - \left[\int d^4x \; \partial_5\Phi\delta\Phi\right]_0^{\pi R} \tag{1.69}$$

Then to satisfy the variational principle, we have to impose $\delta\mathcal{S} = 0$ which leads to conditions on the bulk and boundary terms. First, the bulk equation of motion has to be satisfied by the 5D field:

$$\partial^M\partial_M\Phi + \frac{\partial V(\Phi)}{\partial\Phi} = 0 \tag{1.70}$$

Second, on the boundaries, two possibilities exist to satisfy $\delta\mathcal{S} = 0$:

- $\partial_5\Phi|_{y=(0,\pi R)} = 0$ which is called Neumann condition $(+)$.
- $\Phi|_{y=(0,\pi R)} = 0$ which is called Dirichlet condition $(-)$.

Neumann or Dirichlet conditions can be satisfied simultaneously on both ends but we can also have Neumann condition on one side and Dirichlet on the other.

Localized interactions

In the action, we considered only bulk contributions, but it is also possible to introduce the so-called *localized terms* on the boundary of the extra-dimension. In this section, we forget the potential in the bulk action, so the equation of motion of the 5D field is given by: $\partial_M^2\Phi = (\partial_\mu^2 - \partial_5^2)\Phi = 0$.

The first term, we can introduce, is a mass term:

$$\mathcal{S} = \mathcal{S}_{bulk} - \frac{1}{2}\int d^4x \int_0^{\pi R} dy \left(M_1^2\Phi^2\delta(y-0) + M_2^2\Phi^2\delta(y-\pi R)\right) \tag{1.71}$$

We obtain thereby the new boundary conditions:

$$\begin{aligned}\delta\mathcal{S}_{boundary} &= -\int d^4x\delta\Phi(\partial_5\Phi + M_2^2\Phi)|_{y=\pi R} + \int d^4x\delta\Phi(\partial_5\Phi - M_1^2\Phi)|_{y=0} \\ &\Longrightarrow \begin{cases} \Phi = 0 \text{ or } \partial_5\Phi + M_2^2\Phi = 0 \text{ at } y = \pi R \\ \Phi = 0 \text{ or } \partial_5\Phi - M_1^2\Phi = 0 \text{ at } y = 0 \end{cases}\end{aligned} \tag{1.72}$$

The reader will remark that these boundary conditions mix between Neumann and Dirichlet conditions. Moreover it is easy to see that we can have a continuous path between the two kinds of boundaries by sending the localized mass from zero to infinity. In this case, Dirichlet conditions can be interpreted as Neumann conditions with an infinitely heavy mass coupling on the branes.

Another possibility to extend the bulk action is to add a kinetic term on the boundaries. For simplicity, we will add only one term on the $y = 0$ brane, so that the action becomes:

$$\mathcal{S} = \mathcal{S}_{bulk} - \frac{1}{2M}\int d^4x \int_0^{\pi R} dy\ \partial_\mu\Phi\partial^\mu\Phi\ \delta(y-0) \tag{1.73}$$

The arbitrary parameter M is taken positive to avoid that tachionic states appear. We obtain the new boundary terms:

$$\begin{aligned}\delta\mathcal{S}_{boundary} &= -\int d^4x\delta\Phi(\partial_5\Phi - \frac{1}{M}\partial_\mu^2\Phi)|_{y=0} \\ &\Longrightarrow \partial_5\Phi - \frac{1}{M}\partial_\mu^2\Phi \overset{\text{bulk EOM}}{=} \partial_5\Phi - \frac{1}{M}\partial_5^2\Phi = 0\end{aligned} \tag{1.74}$$

This condition[12] is quite peculiar and requires some care because it involves second derivatives of the field. The main modification is coming from the scalar product of the theory. With this localized kinetic term, the scalar product of the theory has to be extended to preserve to hermiticity of the second derivative operator $< f, g'' >=< f'', g >$:

$$< f, g >= \int_0^{\pi R} f(y)g(y) \implies < f, g >= \int_0^{\pi R} f(y)g(y) + \frac{1}{M}f(0)g(0) \tag{1.75}$$

Orbifolding the space

The description of a compact extra-dimension as an interval is not the only possibility (52). Traditionally we prefer to use an orbifold description of the space. This method makes the underlying symmetry of the space more visible and consists in considering a manifold plus a set of identifications to reduce the fundamental domain of the extra-space. In 5D, the most general orbifolding is the quotient of the circle S^1 by the $\mathbb{Z}_2$ group. The circle compactification will identify points such as $y \to y + 2\pi Rn$ with $n \in \mathbb{Z}$. Then the $\mathbb{Z}_2$ reflexion will identify $y \to -y$. By this procedure it is easy to see that the obtained compact space is a line segment between 0 and πR. So fields are living in this interval $[0, \pi R]$ and we can show that they can be odd or even under the $\mathbb{Z}_2$ parity:

$$\begin{aligned}\text{even}\ \ \Phi_{(+)} \quad &: \quad \Phi_{(+)}(-y) = \Phi_{(+)}(y) \\ &\quad\ \Rightarrow \partial_5\Phi_{(+)}(0) = \partial_5\Phi_{(+)}(\pi R) = 0 \Leftrightarrow \text{ Neumann's BC} \\ \text{odd}\ \ \Phi_{(-)} \quad &: \quad \Phi_{(-)}(-y) = -\Phi_{(-)}(y) \\ &\quad\ \Rightarrow \Phi_{(-)}(0) = \Phi_{(-)}(\pi R) = 0 \Leftrightarrow \text{ Dirichlet's BC}\end{aligned} \tag{1.76}$$

This last equation shows the equivalence between the two approaches: interval and orbifold. We notice already that the boundary conditions are the same at both end points. Nevertheless the orbifold picture is not a restriction of the interval description because we can add localized

[12] The final form of this condition can be obtained by using KK expansion (section 1.3.2). If m_n is the mass of the n^{th} KK-mode $\phi^{(n)}$, it becomes $\partial_5\phi^{(n)} - \frac{m_n^2}{M}\phi^{(n)} = 0$ and the scalar product between wavefunctions is modified $\sum_n f_n(x)f_n(y) = \delta(x-y) - \frac{1}{M}\delta(x)\sum_n f_n(0)f_n(y)$. Then we have to be careful when considering orthogonality and completeness relations.

interactions on the orbifold fixed points ($y = 0$) and ($y = \pi R$) and as we have seen in the previous section, this prescription can help to obtain more complicated boundary conditions.

From now on, we will prefer for simplicity the interval notation to perform the integrations but we will always use the language of orbifolds to describe the properties of parity for the different fields. Boundary conditions will be deduced from the previous discussion.

Kaluza-Klein expansion

To describe physics of stationnary waves in linear physics (acoustic, electromagnetism, mechanics and so on), it is practical to use Fourier series expansion. In a similar way, to study the dynamics of 5D fields in a compact extra-dimension, it is convenient to introduce the so-called *Kaluza-Klein expansion* in order to get rid of the dependence on the fifth space coordinate:

$$\Phi(x^\mu, y) = \sum_{n=0}^{\infty} \phi_\mu^{(n)}(x^\mu) f^n(y) \tag{1.77}$$

$\phi^{(n)}(x^\mu)$ is a 4D field called *Kaluza-Klein mode* and $f^n(y)$ is the associated wavefunction which will describe the *profile* of the n-mode along the new extra-dimension and indicate how this mode is spread along the extra-dimension. Similarly to the potential well in quantum mechanics, we obtain here a *tower of resonances*. The mass of each resonance is determined by the equation of motion and by the boundary conditions defined for the 5D field. For instance, by considering a scalar field Φ with a 5D mass m_0 propagating in a $S^1/\mathbb{Z}_2$ orbifold, we get:

$$\partial^M \partial_M \Phi + m_0^2 \Phi = 0 \Longrightarrow f^{n\prime\prime} - p_{(n)}^2 f^n + m_0 f^n = 0 \tag{1.78}$$

$p_{(n)}$ is the usual fourmomentum of the $\phi^{(n)}$ 4D resonance which is defined by Fourier analysis as:

$$-\partial_\mu \partial^\mu \phi^{(n)}(x) = p_{(n)}^2 \phi^{(n)}(x) = m_n^2 \phi^{(n)}(x) \tag{1.79}$$

As we already mentioned, the S^1 compactification forces the form of the solution to be periodic:

$$\Phi(x, y + 2\pi R) = \Phi(x, y) \Longrightarrow f^n(y) = A_n \cos\frac{ny}{R} + B_n \sin\frac{ny}{R} \tag{1.80}$$

with $n \in \mathbb{N}$. A_n and B_n are coefficients which are chosen to satisfy canonical normalization condition for $\phi^{(n)}$ and boundary conditions. From the equation (1.80), we find the dispersion relation for the masses of KK-resonances:

$$m_n^2 = m_0^2 + \frac{n^2}{R^2} \tag{1.81}$$

Moreover, the 5D field Φ can be odd ($-$) or even ($+$) under the $\mathbb{Z}_2$ parity, in this case, wavefunctions are the ones given in table (1.3).

Notice that a scalar field which is even under the $\mathbb{Z}_2$ parity has a non-vanishing mode without momentum running along the extra-dimension. This zero-mode with a flat wavefunction becomes massless in the case of $m_0 = 0$. The properties of this mode will actually play a crucial role by defining 4D Standard Model fields in the extra-dimensional framework.

	$f^n_{(+)}$	$f^n_{(-)}$
$n=0$	$\frac{1}{\sqrt{2\pi R}}$	0
$n>0$	$\sqrt{\frac{1}{\pi R}}\cos\frac{ny}{R}$	$\sqrt{\frac{1}{\pi R}}\sin\frac{ny}{R}$

Table 1.3: Wavefunctions for a scalar field Φ propagating in the orbifold $S^1/\mathbb{Z}_2$.

1.3.3 Yang-Mills theory in extra-dimensions

The next step is now to consider pure gauge field in extra-dimensions. In this framework, a field A_M is a vector boson which contains 5 components. To the usual 4D gauge field A_μ is added a new polarization A_5 along the fifth dimension, which is a scalar field in 4D. After KK-expansion, A_μ vector gives a whole tower of massive states but we will see that A_5 does not lead to a tower of physical states. These KK-modes will be eaten (except for a possible zero mode) by the massive gauge fields to generate their longitudinal polarization, in a similar way to Goldstone bosons which are eaten in the Higgs mechanism by $W^\pm$ and Z gauge bosons.

Gauge fixing term and boundary conditions

The 5D bulk action for non-abelian gauge field is given on the orbifold $S^1/\mathbb{Z}_2$ or, in an equivalent way, on the interval $[0,\pi R]$, by:

$$\mathcal{S}_{YM} = \int d^4x \int_0^{\pi R} dy \left\{ -\frac{1}{4} F^a_{\mu\nu} F^{\mu\nu a} - \frac{1}{2} F^a_{\mu 5} F^{\mu 5 a} \right\} \tag{1.82}$$

where $F^a_{MN} = \partial_M A^a_N - \partial_N A^a_M + g_5 f^{abc} A^b_M A^c_N$ and g_5 is the 5D gauge coupling[13]. For antisymmetry reason, the F^{55} tensor is naturally vanishing. For the completeness of the description, the gauge fixing term has to be added to $\mathcal{S}_{YM}$. To determine it, we consider first the quadratic part of the mixing term between scalar and vector gauge fields:

$$\int d^4x \int_0^{\pi R} dy \; -\frac{1}{2} F^a_{\mu 5} F^{\mu 5 a} = -\int d^4x \int_0^{\pi R} dy \, \frac{1}{2} (\partial_\mu A^a_5 \partial^\mu A^{5a} + \partial_5 A^a_\mu \partial^5 A^{\mu a} - 2\partial_5 A^a_\mu \partial^\mu A^{5a}) \tag{1.83}$$

The gauge fixing term is chosen in such a way that it describes the usual 4D Lorentz gauge fixing term applies for the A_5-independent part and that it cancels moreover the term in $\partial_5 A^a_\mu \partial^\mu A^{5a}$ in the Yang-Mill Lagrangian. Therefore this allows to avoid the mixing between A_5 and A_μ KK-fields. The gauge fixing terms can be written as:

$$\mathcal{S}_{GF} = \int d^4x \int_0^{\pi R} dy \; -\frac{1}{2\xi} \left(\partial_\mu A^{\mu a} - \xi \partial_5 A^{5a} \right)^2 \tag{1.84}$$

And finally after integration by part, the bulk action for gauge fields becomes:

$$\mathcal{S}_{gauge} = \int d^4x \int_0^{\pi R} dy \left\{ A_\mu [(\partial^2_\alpha - \partial^2_5) g^{\mu\nu} - (1 - \frac{1}{\xi}) \partial^\mu \partial^\nu] A_\nu - A_5 [\partial^2_\alpha - \xi \partial^2_5] A_5 \right\} \tag{1.85}$$

[13] By dimensional analysis, we can notice that g_5 has a mass dimension of $-1/2$ which confirms the non-renormalizability nature of these extra-dimensional theories.

Wavefunctions and spectrum

From the bulk action (1.85), we deduce the equation of motion for A_μ and A_5:

$$\begin{cases} -\partial F_{\mu\nu} - \frac{1}{\xi}\partial^\mu\partial^\nu A_\mu + \partial_5^2 A_\nu = 0 \\ -\partial_\mu^2 A_5 + \xi\partial_5^2 A_5 = 0 \end{cases} \tag{1.86}$$

We will now expand the 5D fields in KK-modes (1.85):

$$A_\mu = \sum_{n=0}^{\infty} A_\mu^{(n)}(x) f^n(y) \quad \text{and} \quad A_5 = \sum_{n=0}^{\infty} A_5^{(n)}(x) g^n(y) \tag{1.87}$$

Thanks to the choice of gauge-fixing term, we have avoided the mixing between various polarizations of the 5D fields, which simplifies the description of the KK-tower. Then to extract the boundary conditions of the wavefunctions, let us consider the properties of the orbifold $S^1/\mathbb{Z}_2$.

$$A_M(x^\mu, y + 2\pi R) = A_M(x^\mu, y) \quad \text{and} \quad A_M(x^\mu, -y) = \begin{cases} \pm A_\mu(x^\mu, y) \\ \mp A_5(x^\mu, y) \end{cases} \tag{1.88}$$

From the equations of motion of the 4D n-mode, we extract the wavefunction equations:

$$\begin{aligned} -\partial F_{\mu\nu}^{(n)} - \frac{1}{\xi}\partial^\mu\partial^\nu A_\mu^{(n)} = p_{(n)}^2 A_\mu = m_n^2 A_\mu \Longrightarrow f^{n\prime\prime} + m_n^2 f^n = 0 \\ -\partial_\mu^2 A_5^{(n)} = p_{(n)}^2 A_5^{(n)} = m_n^2 A_5^{(n)} \Longrightarrow g^{n\prime\prime} + \xi m_n^2 g^n = 0 \end{aligned} \tag{1.89}$$

The equations (1.88) and (1.89) ensure that the wavefunctions are combinations of sines and cosines where $p_{(n)}^2 = m_n^2 = \frac{n^2}{R^2}$ with $n \in \mathbb{N}$. The relation (1.88) sets also that the parity of f_n and g_n which is opposite under $y \to -y$.

Finally, we summarize in table (1.4), the wavefunctions of vector and scalar fields depending on their parities under $\mathbb{Z}_2$.

In table (1.4) or in relation (1.89), we see that depending on the parity assigned to the gauge vector (equivalently BC conditions), the scalar part A_5 gets a physical zero mode or not. Moreover, in the Unitary gauge ($\xi \to \infty$), the massive modes of the fifth component A_5 are removed and they become the longitudinal polarization of the massive KK vectors. This possibility has led to new ideas of symmetry breaking of gauge group using boundary conditions. For instance we can mention GUT symmetry breaking models (56), Higgsless models (57; 58) or Gauge Higgs Unification models (59). Such models are introduced to solve the "hierarchy problem" by using the fifth polarization of gauge fields as a Higgs field. The "Higgs" mass is protected from quadratic divergences by the gauge invariance. These models will be discussed more in detail in chapter 5 and in appendix E.1.

	$f_{(+)}^n$	$g_{(-)}^n$	$f_{(-)}^n$	$g_{(+)}^n$
$n = 0$	$\frac{1}{\sqrt{2\pi R}}$	0	0	$\frac{1}{\sqrt{2\pi R}}$
$n > 0$	$\sqrt{\frac{1}{\pi R}}\cos\frac{ny}{R}$	$\sqrt{\frac{1}{\pi R}}\sin\frac{ny}{R}$	$\sqrt{\frac{1}{\pi R}}\sin\frac{ny}{R}$	$\sqrt{\frac{1}{\pi R}}\cos\frac{ny}{R}$

Table 1.4: Wavefunctions for a 5D gauge field A_M propagating in the orbifold $S^1/\mathbb{Z}_2$ in Feynman gauge $\xi = 1$.

1.3.4 Fermions in extra-dimensions

5D Clifford algebra

In 4D flat Minkowski space, the action for Dirac spinor Ψ is given by:

$$\mathcal{S}_{fermion} = \int d^4x \overline{\Psi}(i\gamma^\mu \partial_\mu - m)\Psi \tag{1.90}$$

where m is the mass of the fermion and γ_μ is a 4×4 matrix satisfying the Clifford algebra:

$$\{\gamma^\mu, \gamma^\nu\} = 2g^{\mu\nu} \tag{1.91}$$

Ψ Dirac spinor is a reducible spin-1/2 representation of Lorentz group. We can actually rewrite this spinor in terms of two Weyl spinors $\Psi = \Psi_R + \Psi_L$ where:

$$\begin{aligned} \Psi_L = P_L\Psi = \frac{1-\gamma_5}{2}\Psi = \begin{pmatrix} \chi \\ 0 \end{pmatrix} \\ \text{and} \quad \Psi_R = P_R\Psi = \frac{1+\gamma_5}{2}\Psi = \begin{pmatrix} 0 \\ \bar{\eta} \end{pmatrix} \end{aligned} \tag{1.92}$$

where $\gamma_5 = i\gamma_0\gamma_1\gamma_2\gamma_3$. P_L and P_R are two projectors, and Ψ_L and Ψ_R, so-called left-handed and right-handed spinors, are both irreducible spin-1/2 representations of the Lorentz group in 4D. The γ_5 matrix satisfies:

$$\{\gamma_\mu, \gamma_5\} = 0 \text{ and } \gamma_5^2 = 1 \tag{1.93}$$

In this thesis, we will usually use the chiral representation for γ matrices:

$$\gamma^\mu = \begin{pmatrix} 0 & \sigma^\mu \\ \overline{\sigma}^\mu & 0 \end{pmatrix} \text{ and } \gamma^5 = \begin{pmatrix} -1 & 0 \\ 0 & 1 \end{pmatrix} \tag{1.94}$$

where $\sigma_\mu = (1, \sigma^i)$ and $\overline{\sigma}_\mu = (1, -\sigma^i)$ (8). In 5D, the action becomes:

$$\mathcal{S}_{fermions} = \int d^4x \int_0^{\pi R} dy \ \left[\frac{i}{2}\left(\overline{\Psi}\Gamma^M \partial_M \Psi - \partial_M \overline{\Psi}\Gamma^M \Psi\right)\right] \tag{1.95}$$

To follow Csaki's notation (52), $\Gamma^0 = -\gamma^0$ and $\Gamma^i = \gamma^i$ are the same 4×4 matrices as in 4D. Nevertheless the algebra needs to be extended with the fifth matrix $\Gamma^5 = -i\gamma^5$:

$$\{\Gamma^M, \Gamma^N\} = 2g^{MN} \tag{1.96}$$

The main consequence is that now γ_5 is a part of the algebra and will mix the different chiralities. In 5D, the irreducible spin-1/2 representation of the Lorentz group is the 4-component Dirac representation $\Psi = \begin{pmatrix} \chi \\ \bar{\eta} \end{pmatrix}$. We could think that we cannot have chiral fermions anymore in 5D however we will see that after KK-expansion it is possible to mod out one of two chiralities for the zero mode.

Wavefunctions and mass spectrum

The action (1.95) of the Dirac fermion Ψ can be expressed in term of the Weyl spinors:

$$\mathcal{S}_{fermion} = \int d^4x \int_0^{\pi R} -i\ \bar{\chi}\ \bar{\sigma}^\mu \partial_\mu \chi - i\ \eta \sigma^\mu \partial_\mu \bar{\eta} - \frac{1}{2}(\bar{\chi}\partial_5 \bar{\eta} - \eta \partial_5 \chi + h.c.) \tag{1.97}$$

Then we can derive from (1.97), the equation of motion for 5D-fermions:

$$\begin{cases} -i\bar{\sigma}^\mu \partial_\mu \chi - \partial_5 \bar{\eta} = 0 \\ -i\sigma^\mu \partial_\mu \bar{\eta} + \partial_5 \chi = 0 \end{cases} \tag{1.98}$$

The next step consists in using the KK decomposition of the 5D spinors to extract the evolution along the fifth dimension. The components χ and ψ are defined by:

$$\chi(x,y) = \sum_n g_n(y)\chi^{(n)}(x) \quad \text{and} \quad \bar{\eta}(x,y) = \sum_n f_n(y)\bar{\eta}^{(n)}(x)\,, \tag{1.99}$$

where $\chi^{(n)}(x)$ and $\bar{\eta}^{(n)}(x)$ are the two 4D-components of the Dirac field with the mass m_n and satisfying the usual 4D Dirac equations:

$$\begin{cases} -i\bar{\sigma}^\mu \partial_\mu \chi^{(n)} + m_n \bar{\eta}^{(n)} = 0 \\ -i\sigma^\mu \partial_\mu \bar{\eta}^{(n)} + m_n \chi^{(n)} = 0 \end{cases} \tag{1.100}$$

The wavefunctions therefore will satisfy the following equations:

$$\begin{cases} g_n' - m_n f_n = 0 \\ f_n' + m_n g_n = 0 \end{cases} \Longrightarrow \begin{cases} g_n'' + m_n^2 g_n = 0 \\ f_n'' + m_n^2 f_n = 0 \end{cases} \tag{1.101}$$

Similarly to gauge bosons and scalars, the S^1 compactification and the equations of motion force the form of the solutions to be:

$$\Psi(x, y + 2\pi R) = \Psi(x,y) \Longrightarrow \begin{cases} g_n(y) = A_n \cos\frac{ny}{R} + B_n \sin\frac{ny}{R} \\ f_n(y) = B_n \cos\frac{ny}{R} - A_n \sin\frac{ny}{R} \end{cases} \tag{1.102}$$

A_n and B_n are coefficients, chosen to satisfy canonical normalization conditions for $\chi^{(n)}$ and $\eta^{(n)}$ and boundary conditions. Moreover we have the spectrum for the fermions which is $m_n = \frac{n\pi}{R}$. Concerning the $\mathbb{Z}_2$ parity: $y \to -y$, the upper part of the spinor χ can be odd or even under this parity. Then the sign of the parity for η is fixed by the invariance of the kinetic term under $\mathbb{Z}_2$ parity. The term $\eta\partial_5\chi$ in the action forces a flip of sign between the two components. Finally we can achieve to have chiral fermions by taking boundary conditions for the Dirac fields which allow light chiral zero modes, for instance:

$$\begin{aligned} \text{“even”} \quad &: \quad \begin{cases} \chi(-y) = \chi(y) \\ \eta(-y) = -\eta(y) \end{cases} \Leftrightarrow \text{left-handed zero mode} \\ \text{“odd”} \quad &: \quad \begin{cases} \chi(-y) = -\chi(y) \\ \eta(-y) = \eta(y) \end{cases} \Leftrightarrow \text{right-handed zero mode} \end{aligned} \tag{1.103}$$

We summarized in table (1.5), the wavefunctions of fermions depending on their parities under $\mathbb{Z}_2$.

	right-handed zero-mode		left-handed zero-mode	
	$f^n_{(+)}$	$g^n_{(-)}$	$f^n_{(-)}$	$g^n_{(+)}$
$n=0$	$\frac{1}{\sqrt{2\pi R}}$	0	0	$\frac{1}{\sqrt{2\pi R}}$
$n>0$	$\sqrt{\frac{1}{\pi R}}\cos\frac{ny}{R}$	$\sqrt{\frac{1}{\pi R}}\sin\frac{ny}{R}$	$\sqrt{\frac{1}{\pi R}}\sin\frac{ny}{R}$	$\sqrt{\frac{1}{\pi R}}\cos\frac{ny}{R}$

Table 1.5: Wavefunctions for a 5D fermion field Ψ propagating in the orbifold $S^1/\mathbb{Z}_2$.

Fermion masses and equations of motion

In the previous section, we did not consider any mass term in the bulk action for the fermions. There are different ways of writing such mass term in 5D. In this section, we will focus on two ways which will be interesting for the understanding of this thesis.

Odd bulk mass

$$\mathcal{S}_{mass} = -\int d^4x \int_0^{\pi R} dy\ \tilde{M}\overline{\Psi}\Psi = -\int d^4x \int_0^{\pi R} dy\ \tilde{M}(\bar{\chi}\ \bar{\eta} + \chi\eta) \tag{1.104}$$

$\tilde{M}$ is called "odd" bulk mass of the 5D fermion. We see actually that this mass needs to be odd under the $\mathbb{Z}_2$ symmetry to ensure the term $M\chi\eta$ to be invariant. This means that this peculiar mass term will undergo a discrete jump at the orbifold fixed points. With this mass term, the equations of motion are modified and the wavefunctions become:

$$\begin{cases} g_n' + \tilde{M} g_n - m_n f_n = 0 \\ f_n' - \tilde{M} f_n + m_n g_n = 0 \end{cases} \tag{1.105}$$

The solutions of those equations will be combinations of $\sin(\sqrt{m_n^2 - \tilde{M}^2}y)$ and $\cos(\sqrt{m_n^2 - \tilde{M}^2}y)$ (which become hyperbolic for the massless/light mode). The spectrum is thereby given by: $m_n = \frac{n\pi}{R} + \tilde{M}$, however as the zero mode is still chiral, its mass will be vanishing. The wavefunction of the zero mode of even field will be:

$$g_0 = \sqrt{\frac{2\tilde{M}}{1 - e^{-2\tilde{M}y}}} \tag{1.106}$$

This exponential dependence will be used to localize the field in the extra-dimension. By tuning the parameter $\tilde{M}$ we can control the overlapping between wavefunctions and thereby control the strength of the coupling between 4D modes. This technique can be used to generate a hierarchy for fermion masses in a "natural way" as we will see later in the chapter 5. But it is obvious that if we need to give a mass to zero mode, we have to consider other mechanisms.

Mass from Yukawa terms

Another solution to generate masses is through the usual Yukawa coupling. In this case, we consider a scalar field Φ, in the bulk or localized on the fixed points, which is doublet of

$SU(2)_W$. This field will pick up a non vanishing vacuum expectation value v. We need then to introduce for a same flavor, 2 Dirac fermions with opposite parities under $\mathbb{Z}_2$. The one with left-handed zero mode Ψ_D will be a part of a doublet of $SU(2)_W$ and the one with right-handed zero mode Ψ_S will be a singlet of $SU(2)_W$. For our purposes, we will assume that the Higgs field is propagating in the bulk but for localized Higgs the procedure is quite similar.

$$\mathcal{S}_{fermion} = \int d^4x \int_0^{\pi R} \frac{i}{2}\bar{\Psi}_{S/D}\gamma^M \partial_M \Psi_{S/D} - \frac{y_\Psi v}{\sqrt{2}}\overline{\Psi}_D \Psi_S + \ h.c. \tag{1.107}$$

If we expand the action (1.107) in KK modes, we get a mass term $m_\Psi = \frac{y_\Psi v}{\sqrt{2}}$ for the zero modes which are chiral. This feature can be needed in phenomenology to reproduce SM spectrum. Thus the tree level mass spectrum for the singlet and the doublet is simply given by:

$$m_n^2 = \frac{n^2}{R^2} + m_\Psi^2 \tag{1.108}$$

1.3.5 Fields in warped extra-dimensions

In the introduction to extra-dimensional models, we mentioned models where fields can evolve in a bulk ADS space. As we will present Higgs phenomenology in such model in chapter 5, let us give the basic elements, useful for our discussion. We will work on an interval $y \in [1/\Lambda, R']$ where Λ is associated to Planck scale and R'^{-1} to TeV one and where the metric is:

$$ds^2 = \left(\frac{R}{y}\right)^2 (g_{\mu\nu}dx^\mu dx^\nu - dy^2) \tag{1.109}$$

To obtain the action in such framework, we have to use field theory in curved space and redefine the covariant derivative. The connexions are indeed modified by the local space geometry (52).

Gauge fields

The action of a pure gauge theory in one extra-dimension, after fixing the R_ξ gauge, is given by:

$$\mathcal{S} = \int d^4x \int_{1/\Lambda}^{R'} dy \frac{R}{y}\left\{-\frac{1}{4}F^a_{\mu\nu}F^{\mu\nu a} - \frac{1}{2}F^a_{\mu 5}F^{\mu 5 a} - \frac{1}{2\xi}\left[\partial_\mu A^{\mu a} - \xi\frac{y}{R}\partial_5\left(\frac{R}{y}A^a_5\right)\right]^2\right\} \tag{1.110}$$

From this action, one can extract the equation of motion for the gauge fields in warped space:

$$f^{n\prime\prime} - \frac{1}{y}f^{n\prime} + m_n^2 f^n = 0 \Longrightarrow f_n(y) = y(A_n J_1(m_n y) + B_n Y_1(m_n y)) \tag{1.111}$$

The solutions of those equations in the warped case are a combination $J_1(m_n y)$ and $Y_1(m_n y)$ which are Bessel functions of first and second kind of order 1. The masses m_n are determined by the zeros of the Bessel functions. Finally, the zero mode has a flat wavefunction since the Bessel function can expended for low masses in $yJ_1(m_n y) \sim \frac{m_n y^2}{2}$ which is negligible for low masses and in $yY_1(m_n y) \sim -\frac{2}{m_n}$ which does not depend on y anymore.

Fermions

Here we are considering the minimal 5D bulk action for a fermionic field Ψ in ADS space:

$$\mathcal{S} = \int d^4x \int_{1/\Lambda}^{R'} dy \left(\frac{R}{y}\right)^4 \left[\frac{i}{2}\left(\overline{\Psi}\Gamma^M \partial_M \Psi - \partial_M \overline{\Psi}\Gamma^M \Psi\right) - \frac{R}{y}\tilde{M}\overline{\Psi}\Psi\right] \tag{1.112}$$

$\tilde{M}$ is the odd bulk mass of the 5D fermion. Then we can derive the equation of motion and find the wavefunctions of the KK-fermions:

$$\begin{cases} -i\bar{\sigma}^\mu \partial_\mu \chi - \partial_5 \bar{\eta} + \left(\frac{R}{y}\tilde{M} + \frac{2}{y}\right)\bar{\eta} = 0 \\ -i\sigma^\mu \partial_\mu \bar{\eta} + \partial_5 \chi + \left(\frac{R}{y}\tilde{M} - \frac{2}{y}\right)\chi = 0 \end{cases} \Longrightarrow \begin{cases} f_n' - \frac{c+2}{y} f_n + m_n g_n = 0 \\ g_n' + \frac{c-2}{y} g_n - m_n f_n = 0 \end{cases} \tag{1.113}$$

where $c = \tilde{M}R$ controls the localization of fermions along the extra-dimensions. The solutions of those equations in the warped case are a combination of Bessel functions $J_{1/2\pm c}(m_n y)$ and $J_{-1/2\pm c}(m_n y)$ (60). Similarly to gauge bosons, masses m_n are determined by the zeros of the Bessel functions and zero mode has the following wavefunction:

$$f_0 \sim \left(\frac{y}{R}\right)^{c+2} \text{ or } g_0 \sim \left(\frac{y}{R}\right)^{2-c} \tag{1.114}$$

Other details of field theory in warped case will be given in chapter 5 but now we will focus on a peculiar model of flat extra-dimension.

1.3.6 Universal Extra Dimensional model

In this last section, we will give some details on the easiest model we can construct with extra-dimension and which is called Universal Extra Dimension (UED). We will present its interesting features and introduce some limitations which motivated the work presented in chapters 2 and 3. UED models are effective field theories in which we allow to propagate all the Standard Model fields in the bulk of the extra-dimension. In these scenarios, we do not address either gravity questions or hierarchy problem. Nevertheless since the KK-modes will interact with SM gauge group, those models will have a very rich phenomenology. The simplest extension we can think of, is to add only one compactified flat extra-dimension but we can extend this discussion to six dimensional models (61; 62; 63). Here the chosen orbifolding will be $S^1/\mathbb{Z}_2$. We showed in the previous discussion that it is mandatory to have zero modes for the SM fields. For gauge bosons, we just need to impose even parity under $\mathbb{Z}_2$ to have a zero mode. For fermions, only the zero mode is chiral, so in order to reproduce SM phenomenology we need obviously two Dirac 5D-fermions for each SM fields in order to be able to write the SM Yukawa mass term. Therefore, the content of 5D fields is:

- The SM gauge bosons: G^A, B, W^a
- The Higgs field: H
- The SM fermions [14]: 2 Dirac spinors, $Q \equiv \begin{pmatrix} u_D \\ d_D \end{pmatrix}$ and $L \equiv \begin{pmatrix} \nu_L \\ l_L \end{pmatrix}$, doublets under $SU(2)_W$ and 3 Dirac spinors $U \equiv u_S$, $D \equiv d_S$ and $E \equiv e_R$, singlets under $SU(2)_W$.

where Q and L will be "even" under the $\mathbb{Z}_2$ parity and U, D and E will be "odd".

[14] The notation of the field in this thesis will be consistent with the notation in the program that we will use to study our own model.

KK-parity and interactions between fields

For models in $S^1/\mathbb{Z}_2$, the orbifolding will break the Lorentz invariance along the extra-dimension because of the orbifold fixed points. The conservation of the quantized momentum (KK number) along the extra-dimension will not be satisfied anymore, however a sub group of the symmetry group will remain unbroken. This so-called *KK-parity*, p_{KK}, is defined as $y \to y + \pi R$ and corresponds to a reflexion with respect to the center of the interval. We can see easily that this transformation induces a shift of $(-1)^n$ in the phase of the wavefunctions f_n (or g_n) of the KK-modes. This allows us to classify the KK-modes from their parity under p_{KK} which will constrain the possible interactions between KK-modes.

As an example, we take the case of the gauge coupling between a vector gauge bosons A_μ and a fermion Ψ both even under $\mathbb{Z}_2$. At tree level, the bulk Lagrangian contains interactions coming from the covariant derivative of the kinetic term:

$$\mathcal{L} \supset \; g_5 \int_0^{\pi R} dy \bar{\Psi} A_\mu \Gamma^\mu \Psi \supset \; g_5 \sum_{i,j,k} \int_0^{\pi R} dy \; g_i(y) g_j(y) f_k(y) \; \bar{\chi}^{(i)} \bar{\sigma}^\mu \chi^{(j)} A_\mu^{(k)} \tag{1.115}$$

We can then check easily that the integral along the y-direction is not vanishing if $i \pm j \pm k = 0$. This condition implies that the KK-parity of the coupling is $(-1)^{i+j+k} = +1$.

The localized terms will have the following form:

$$\begin{aligned} \mathcal{L}_{bound} \supset & c_0 \sum_{i,j,k} \int_0^{\pi R} dy \; \delta(y) \; g_i(y) g_j(y) f_k(y) \; \bar{\chi}^{(i)} \bar{\sigma}^\mu \chi^{(j)} A_\mu^{(k)} \\ & + c_\pi \sum_{i,j,k} \int_0^{\pi R} dy \; \delta(y - \pi R) \; g_i(y) g_j(y) f_k(y) \; \bar{\chi}^{(i)} \bar{\sigma}^\mu \chi^{(j)} A_\mu^{(k)} \end{aligned} \tag{1.116}$$

where c_i is a coupling constant defined on a boundary. Here, if $c_0 = c_\pi$, it is also necessary to consider couplings between modes such that $(-1)^{i+j+k} = +1$, in order to have a non-vanishing contribution.

For the first levels, we deduce for instance that:

- $(0,0,0)$ coupling is allowed and this is mandatory to reproduce SM phenomenology!
- $(1,0,0) - (0,1,0) - (0,0,1)$ couplings are not allowed and no single production and decays into SM particles of the first tier particles is possible.
- $(1,1,0) - (1,0,1) - (0,1,1)$ couplings are allowed also so that only pair production is possible.
- $(2,0,0) - (0,2,0) - (0,0,2)$ couplings are not there in the bulk Lagrangian but can appear on the boundaries. Moreover even if we assume that the coupling on the boundaries is vanishing, those terms will reappear at loop levels (see section 1.1.1).

This pair production of odd states will prevent the first tier to decay and the lightest particle from this tier could play the role of Dark Matter. The only "problem" with this construction is that KK-parity is a bulk symmetry but not necessarily a symmetry of the boundaries so that imposes for the boundary terms to be equal (for instance $c_0 = c_\pi$). This last condition will depend then on the UV-completion of the theory.

Mass spectrum in UED: Dark Matter and phenomenology

At tree level, all the particles of the first tier are degenerated. However, radiative corrections and electroweak symmetry breaking will split the masses of the level one, as it can be seen in figure (1.11) and in the following formula (64):

$$m_n^2 = \frac{k^2}{R^2} + m_0^2 + \delta_{1-loop} \tag{1.117}$$

where m_n is the mass of the n-mode, m_0 is the contribution generated by the bulk Higgs mechanism and δ_{1-loop} is the radiative correction to the self energy of the particles. The technical aspect of such mass spectrum calculation will be discussed more precisely in chapter 2 in our own framework.

We can show, in the case of the $S^1/\mathbb{Z}_2$ orbifold, if the KK-parity is preserved on the boundaries, that the vector photon $B^{(1)}$ is the lightest stable particle. Then using calculation of relic density (39; 43; 65; 66), it is possible to extract a bound on the radius of such extra-dimension which is around the TeV scale.

After this "short" introduction to Standard Model particle physics and to its extensions, after this presentation of the Standard Model of cosmology and of the calculation of relic density, the reader should be ready to start diving into the description of the work which has been realized during these three years.

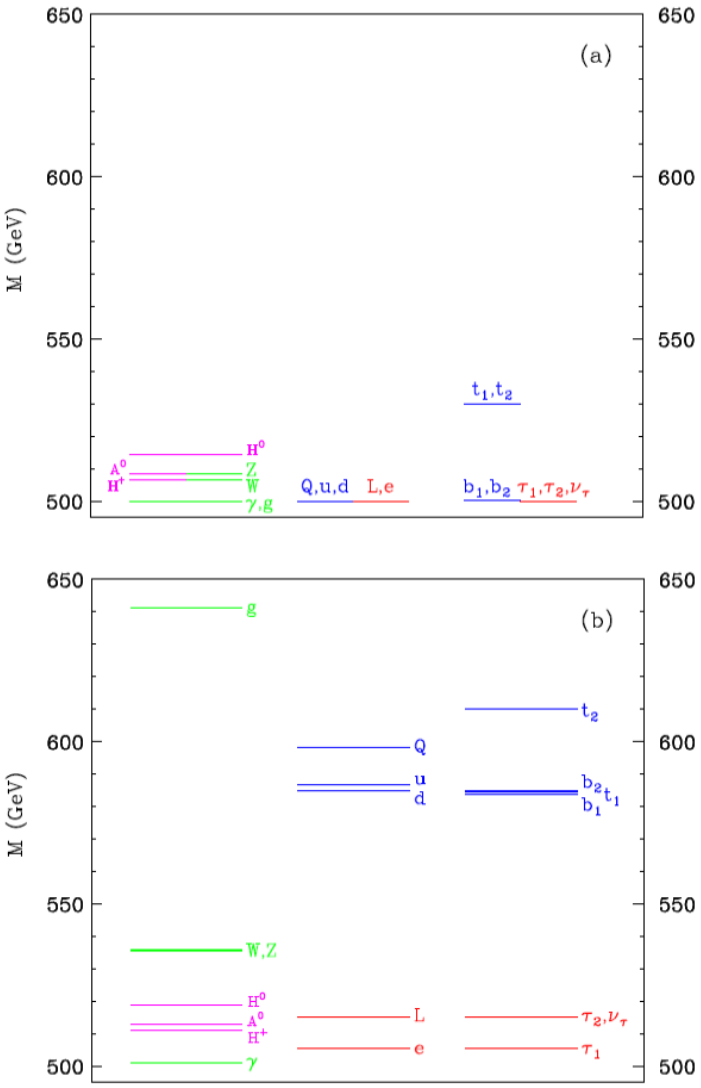

Figure 1.11: Spectrum for the first KK-level at tree level (a) and at one-loop (b) for $1/R = 500$ GeV in UED model in 5D. The cut-off scale Λ is chosen as $\Lambda R = 20$, $m_h^2 = 120$ GeV and the boundary terms are vanishing at the cut-off scale. Image reproduced from (64).

Chapter 2

A "natural" Dark Matter candidate from 6D Lorentz invariance

In the previous section 1.2, we have seen that cosmological observations tend to show that the universe is filled by a large amount of a non-baryonic kind of matter. The nature of this component can be explained with particle physics, by introducing a new kind of Weakly Interacting Massive Particle into the Standard Model. We have already discussed in section 1.3.6 that we can use flat extra-dimensions on an orbifold to address the Dark Matter problem. In those models, the stable particle is prevented to decay thanks to residual parities remaining after the breaking of Lorentz invariance by the orbifolding of the extra-dimension. In this sense, the Kaluza-Klein parity is well motivated from a theoretical point of view and can lead to a viable Dark Matter candidate. Nevertheless, in the model considered in (64), the $S^1/\mathbb{Z}_2$ compactification will generate two fixed points in the space. On these 4D branes, the KK-parity will not necessarily be conserved and in order to ensure the stability of the Dark Matter candidate, we will have to impose by hand the identification of the 4D-localized counter-terms. This assumption on the UV-completion can be seen as unsatisfactory and motivates the study we performed.

The presence of the localized terms is important from a model building point of view; we need to produce 4D-chiral fermions for instance and we have seen that it forces us to have a rotation symmetry which will automatically generate such fixed points. We can also need to localize fields in the extra-dimension to suppress some couplings for instance. Therefore we decided to investigate extra-dimensional models where KK-parity could be preserved in the bulk and also on the singular points. This will allow the presence of a "natural" Dark Matter candidate and also will increase the predictivity of the theory by limiting the UV sensitivity of our Effective Field Theory. In the following chapter, we will focus on work published in (63) where we studied the model building of such theory and presented our solution to address this problem.

2.1 Physics on the Real Projective Plane: definitions and motivations

2.1.1 Orbifolding the $\mathbb{R}^2$ extra-space

This section is highly based on the work presented in (67), where the reader will find a useful tool for model building in extra-dimensions.

In many models of extra-dimensions, the compactification of the space is realized by an orbifolding of the space. *Orbifolds* are quotient spaces of a manifold modulo a discrete group. Those discrete groups cannot be arbitrary but are restricted to so-called $n-$*dimensional space groups*, which are defined as cocompact groups of isometries of $\mathbb{R}^n$ [1]. In crystallography, the classification of such discrete groups is well-known; it exists in 1D, two possible orbifolds: the circle S^1 which is the quotient of $\mathbb{R}/\mathbb{Z}$ and the interval $S^1/\mathbb{Z}_2$. We already discuss these two orbifolds, the first one will not have fixed point but will not allow 4D-chiral fermions and the second will have two fixed points.

To go any further, we need to add to the 4D Minkowski space, two extra-dimensions. In this case, the possible isometries of the plane are given by:

- translations (t)

[1] In mathematics, the action of a group G on a topological space X is cocompact, if the quotient of the space X/G is compact.

- reflexions
- rotation (r) of $2\pi/n$ with n=2, 3, 4, 6
- glide-reflexions (g) which are combinations of translations and mirror reflexions.

In two dimensions, there are only 17 fundamental discrete groups which are called the wallpaper groups and only three of them are free from fixed points and fixed lines. The mapping of the entire $\mathbb{R}^2$ can be then obtained by acting with the generators of the group. Let us focus on this three possibilities which are:

- the Torus $\mathbb{R}$/p1 in figure 2.1

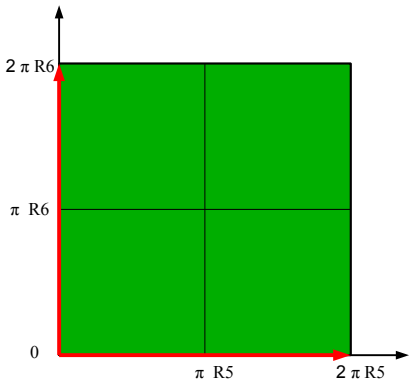

Figure 2.1: Torus: $T^2 = \mathbb{R}^2/\text{p1} = \mathbb{R}^2/\mathbb{Z}^2$. Fondamental domain of the torus (green). Generators of the 2D space group: translation (solid red arrow).

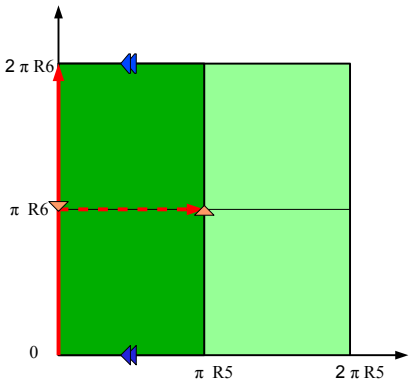

Figure 2.2: Klein Bottle: $\mathbb{R}^2$/pg. Fondamental domain of the orbifold (green) and the torus (light green). Generators of the 2D space group: translation (solid red arrow) and glide (dashed red arrow). The arrows on the edges indicate how they are identified by the orbifolds.

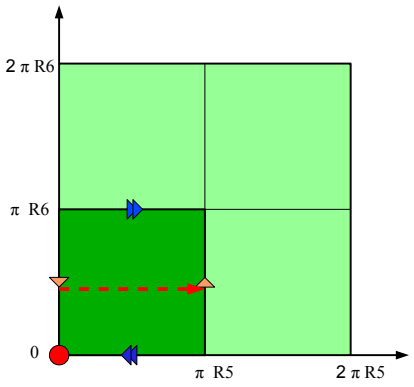

Figure 2.3: Real Proj. Plane: $\mathbb{R}^2$/pgg. Fondamental domain of the orbifold (green) and the torus (light green). Generators of the 2D space group: π-rotation (red circle) and glide (dashed red arrow). The arrows on the edges indicate how they are identified by the orbifolds.

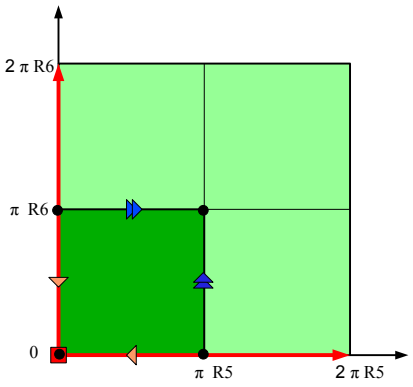

Figure 2.4: Chiral Square: $T^2/\mathbb{Z}_4$. Fondamental domain of the orbifold (green) and the torus (light green). Generators of the 2D space group: $\pi/2$-rotation (red square) and translations (solid red arrow). The black dots are fixed points of the orbifold.

- the Klein Bottle $\mathbb{R}$/pg in figure 2.2
- the Real Projective Plane (RPP) $\mathbb{R}$/pgg in figure 2.3.

Here the discrete group p1, pg and pgg[2] can be described in a purely algebraic way:

$$\begin{aligned} \text{p1} &\simeq \mathbb{Z}^2 = \langle t_1 \rangle \times \langle t_2 \rangle \\ \text{pg} &= \langle t_2, g | [g^2, t_2] = 0, t_2 g t_2 g^{-1} = \mathbf{1} \rangle \supseteq \mathbb{Z}^2 \\ \text{pgg} &= \langle r, g | r^2 = (g^2 r)^2 = \mathbf{1} \rangle \supseteq \mathbb{Z}^2, \mathbb{Z}_2 \end{aligned} \tag{2.1}$$

However, on the Torus and on the Klein Bottle, we cannot write down 4D-chiral fermions because there is no rotation in their discrete group definitions. Therefore, in the following, we will only focus on the Real Projective Plane and show how to generate chirality in such framework. We could have continued this study with more extra-dimensions but the number of orbifolds without fixed point increases strongly and the cut-off of the effective theory would be considerably low so that its range of validity would be too small.

As it is described in equation 2.1, the Real Projective Plane is defined by the transformations of the discrete group which are a $\pi-$rotation (r) and a glide (g). For studying field theory in this framework, it will be then very useful to characterize these transformations by their action on the extra-coordinates of the space:

$$r : \begin{cases} x_5 \sim -x_5 \\ x_6 \sim -x_6 \end{cases} \quad \text{and} \quad g : \begin{cases} x_5 \sim x_5 + \pi R_5 \\ x_6 \sim -x_6 + \pi R_6 \end{cases} \tag{2.2}$$

We see here that the RPP is not defined by translations unlike the Torus or the Klein Bottle, nevertheless they appear as combinations of the fundamental isometries of the Real Projective Plane:

$$t_5 = g^2 : \begin{cases} x_5 \sim x_5 + 2\pi R_5 \\ x_6 \sim x_6 \end{cases} \quad \text{and} \quad t_6 = (gr)^2 : \begin{cases} x_5 \sim x_5 \\ x_6 \sim x_6 + 2\pi R_6 \end{cases} \tag{2.3}$$

In this geometry, we can also define another glide (g') which is a combination of the discrete group generators:

$$g' = gr : \begin{cases} x_5 \sim -x_5 + \pi R_5 \\ x_6 \sim x_6 + \pi R_6 \end{cases} \tag{2.4}$$

Note here that the two radii R_5 and R_6 can be different: nevertheless for simplicity we will assume that $R_5 = R_6 = R$, and use $R = 1$ in formulas, except if we need to discuss the phenomenology of the model. In this case, the size of the radius will be reintroduced and will determine the overall mass scale for the KK modes, $m_{KK} = 1/R$.

In this framework, fields will also transform under the discrete group pgg. To illustrate this effect, we will consider the simple case of a 6D scalar field φ transforming under (r) and (g):

$$\begin{aligned} \varphi(g(x_5, x_6)) &= p_g \varphi(x_5, x_6) \\ \varphi(r(x_5, x_6)) &= p_r \varphi(x_5, x_6) \end{aligned}$$

[2]The notation of these discrete groups is the one used in (67).

From equation 2.1, we get directly the relation $p_r^2 = p_g^2 = 1$ and that implies:

$$p_r = \pm 1 \qquad \text{and} \qquad p_g = \pm 1 \tag{2.5}$$

For the other glide $g' = rg$, we have also $p_{g'} = p_r p_g = \pm 1$. Let us stress that, as the translation is deduced from the fundamental rotation and glide symmetry, we cannot write Scherk-Schwarz phases for the fields, so that all fields are periodic[3].

Finally let us mention a last possible orbifold with fixed points but on which we can also define and force a KK-parity: the Chiral Square $T^2/\mathbb{Z}_4$. The study of this other 6D framework, presented in figure 2.4 has been performed by the authors of (62; 68).

2.1.2 Chiral fermions on the Real Projective Plane

For the model building in extra-dimensions, the most stringent constraint often comes from the description of fermionic fields. Therefore we will focus here on the properties of fermions on the Real Projective Plane (RPP).

6D Diracology

In 4D and 5D we have seen that the minimal dimension for the representation of fermions is 4 but here in 6D we have to consider an 8 dimension field Ψ (69). This constraint is imposed by the construction of the Clifford algebra in 6D. We need actually six 8×8 Gamma matrices: $\Gamma^0 \dots \Gamma^3$, Γ^5 and Γ^6 which satisfy:

$$\{\Gamma^M, \Gamma^N\} = 2g^{MN} \tag{2.6}$$

In the following, we decided to choose the following representation for the Gamma matrices (69):

$$\Gamma^\mu = \begin{pmatrix} \gamma^\mu & 0 \\ 0 & \gamma^\mu \end{pmatrix}, \quad \Gamma^5 = \begin{pmatrix} 0 & i\gamma^5 \\ i\gamma^5 & 0 \end{pmatrix}, \quad \Gamma^6 = \begin{pmatrix} 0 & \gamma^5 \\ -\gamma^5 & 0 \end{pmatrix} \tag{2.7}$$

where

$$\gamma^\mu = \begin{pmatrix} 0 & \sigma^\mu \\ \overline{\sigma}^\mu & 0 \end{pmatrix} \text{ and } \gamma^5 = \begin{pmatrix} -1 & 0 \\ 0 & 1 \end{pmatrix} \tag{2.8}$$

with $\sigma_\mu = (1, \sigma^i)$ and $\overline{\sigma}_\mu = (1, -\sigma^i)$ using Peskin notations (8). The square of those matrices is given by:

$$\Gamma_\mu \Gamma^\mu = 4 \times \mathbf{1}_{8\times 8}, \quad (\Gamma^5)^2 = (\Gamma^6)^2 = -\mathbf{1}_{8\times 8} \quad \text{and} \quad \Gamma^M \Gamma_M = 6 \times \mathbf{1}_{8\times 8} \tag{2.9}$$

Similarly to the 4D field theory, in 6D, we can define a new matrix Γ^7 as a product of all the Gamma matrices of the algebra:

$$\Gamma^7 = \Gamma^0 \Gamma^1 \Gamma^2 \Gamma^3 \Gamma^5 \Gamma^6 \tag{2.10}$$

[3]Scherk-Schwarz phases are not allowed here because $p_{t5} = p_g^2 = +1$ and $p_{t6} = p_g^2 p_r^2 = +1$. This is not the case for instance on the circle S^1: $\varphi(t(x_5)) = \exp[i2\pi\rho]\varphi(x_5)$ with $\rho \in [0, 1) \subset \mathbb{Q}$.

This new matrix allows to define two 6D chiralities through the projectors:

$$P_\pm = \frac{1}{2}\left(1 \pm \Gamma^7\right) \tag{2.11}$$

Therefore the minimal spin-1/2 representation of the Lorentz group are 4-component chiral fermions: $\Psi = P_+\Psi + P_-\Psi = \Psi_+ + \Psi_-$. If we use the previous representation of Gamma matrices this can be written as:

$$\Gamma^7 = \begin{pmatrix} -\gamma^5 & 0 \\ 0 & \gamma^5 \end{pmatrix}, \quad \text{and} \quad P_\pm = \begin{pmatrix} \frac{1}{2}\left(1 \mp \gamma^5\right) & 0 \\ 0 & \frac{1}{2}\left(1 \pm \gamma^5\right) \end{pmatrix} = \begin{pmatrix} P_{L/R} & 0 \\ 0 & P_{R/L} \end{pmatrix} \tag{2.12}$$

where P_L and P_R are the projectors on the 4D chiralities. We notice here that the 6D-chiral fields contain two 4D-Weyl fermions of opposite chiralities.

In this basis, the 6D chiral fermions can be written in terms of 4D Weyl representation:

$$\Psi_+ = \begin{pmatrix} \psi_{L+} \\ \psi_{R+} \end{pmatrix}, \qquad \Psi_- = \begin{pmatrix} \psi_{R-} \\ \psi_{L-} \end{pmatrix} \tag{2.13}$$

with

$$\psi_{L\pm} = \begin{pmatrix} \chi_\pm \\ 0 \end{pmatrix}, \qquad \psi_{R\pm} = \begin{pmatrix} 0 \\ \bar{\eta}_\pm \end{pmatrix} \tag{2.14}$$

where ψ are Dirac spinors, χ and η are Weyl spinors.

We can also write this expression for the reducible 6D Dirac representation:

$$\Psi = \begin{pmatrix} \chi_+ \\ \bar{\eta}_- \\ \chi_- \\ \bar{\eta}_+ \end{pmatrix} \tag{2.15}$$

As we established the Clifford algebra in this framework, we can then derive the action for a massless 6D-chiral fermion:

$$\begin{aligned} S_\pm &= \iint dx_5\, dx_6\, \frac{i}{2}\Big\{\bar{\Psi}_\pm \Gamma^\alpha \partial_\alpha \Psi_\pm - \left(\partial_\alpha \bar{\Psi}_\pm\right)\Gamma^\alpha \Psi_\pm\Big\} = \\ &= \iint dx_5\, dx_6\, \Big\{\; i\bar{\psi}_{L\pm}\gamma^\mu \partial_\mu \psi_{L\pm} + i\bar{\psi}_{R\pm}\gamma^\mu \partial_\mu \psi_{R\pm} + \\ &\quad + \frac{1}{2}\left[\bar{\psi}_{L\pm}\gamma_5(\partial_5 \mp i\partial_6)\psi_{R\pm} + \bar{\psi}_{R\pm}\gamma_5(\partial_5 \pm i\partial_6)\psi_{L\pm} + h.c.\right]\Big\} \\ &= \iint dx_5 dx_6\; i\bar{\chi}_\pm \bar{\sigma}^\mu \partial_\mu \chi_\pm + i\eta_\pm \sigma^\mu \partial_\mu \bar{\eta}_\pm + \bar{\chi}_\pm(\partial_5 \mp i\partial_6)\bar{\eta}_\pm - \eta_\pm(\partial_5 \pm i\partial_6)\chi_\pm \end{aligned} \tag{2.16}$$

The only difference between the two chiralities is the sign in front of x_6 derivative; this feature will lead to interesting properties of fermions on the RPP. We can also have a mass term for those fermion fields:

$$\begin{aligned} S_{\text{mass}} &= \iint dx_5\, dx_6\; M\Big\{\bar{\Psi}_+\Psi_- + \bar{\Psi}_-\Psi_+\Big\} \\ &= \iint dx_5\, dx_6\; M\Big\{\bar{\psi}_{L+}\psi_{R-} + \bar{\psi}_{R+}\psi_{L-} + h.c.\Big\} \\ &= \iint dx_5\, dx_6\; M\Big\{\bar{\chi}_\pm \bar{\eta}_\mp + \eta_\pm \chi_\mp\Big\}. \end{aligned} \tag{2.17}$$

4D chirality for zero modes

To be viable, our model needs to possess a parity which provides at least chiral zero-modes for fermions.
Let us consider the glide parity (g). It transforms the x_6 coordinate by changing its sign. This implies that the two 6D-chirality are exchanged under (g) (up to a sign) to ensure the invariance of the Lagrangian:

$$\Psi(g(x)) = p_g \begin{pmatrix} \chi_- \\ \bar{\eta}_+ \\ \chi_+ \\ \bar{\eta}_- \end{pmatrix} = p_g \begin{pmatrix} 0 & 1 \\ 1 & 0 \end{pmatrix} \begin{pmatrix} \chi_+ \\ \bar{\eta}_- \\ \chi_- \\ \bar{\eta}_+ \end{pmatrix}$$

$$\Longrightarrow \Psi(g(x)) = p_g \Gamma_g \Psi(x) \quad \text{with} \qquad \Gamma_g = \Gamma^6 \Gamma^7 \tag{2.18}$$

Therefore the presence of the glide forces us to start with a non chiral 6D-theory and for both parities under the glide a non-chiral 4D massless mode is allowed. This is for instance, the reason why we cannot write down 4D chiral fermions on the Klein Bottle which is only defined by the glide.

For the rotation, the situation is slightly different. In fact, both coordinates change signs, so that the Lagrangian is invariant only if the two 4D chiralities have opposite sign under the rotation. The direct consequence is that one of the 4D chirality will possess a non-vanishing zero-mode. For a generic transformation, we have:

$$\Psi(r(x)) = p_r \begin{pmatrix} \chi_+ \\ -\bar{\eta}_- \\ \chi_- \\ -\bar{\eta}_+ \end{pmatrix} = p_r \begin{pmatrix} -\gamma_5 & 0 \\ 0 & -\gamma_5 \end{pmatrix} \begin{pmatrix} \chi_+ \\ \bar{\eta}_- \\ \chi_- \\ \bar{\eta}_+ \end{pmatrix}$$

$$\Longrightarrow \Psi(r(x)) = p_r \Gamma_r \Psi(x)\,, \qquad \Gamma_r = i\Gamma^5\Gamma^6\Gamma^7 \tag{2.19}$$

Here we choose $p_r = +1$ corresponding to a left-handed zero-mode and $p_r = -1$ to a right-handed one. Therefore, as for each fermion there is a massless chiral zero-mode, the Real Projective Plane is the unique (non-orientable) orbifold in 6D with chiral fermions and without fixed points! We stress also that like in 5D, the bulk mass term is odd under this rotation symmetry. To be complete let us mention also how fermions transform under the glide (g'):

$$\Psi(g'(x)) = p_r p_g \Gamma_{gr} \Psi(x)\,, \qquad \Gamma_{gr} = i\Gamma^5 \tag{2.20}$$

2.1.3 Kaluza-Klein parity and singularities

Now, it is clear that chiral fermions can be built on the RPP, but a question remains: is it possible to have a "natural" Dark Matter candidate in this framework? On the Real Projective Plane, there is no boundary but it exists two conical singularities, where all the curvature of this space is concentrated. Therefore, it is possible on these peculiar points to add localized

counter-terms. However, the special topology of the RPP will still allow a preserved KK-parity. As we discussed previously, this orbifold is defined by the rotation and the glide symmetries. Under rotation, there are 4 fixed points, mentioned on figure 2.5 by circles and stars, and there are not equivalent:

$$\begin{aligned} A: \quad (0,0) &\xrightarrow{r} (0,0), \qquad B: \quad (0,\pi) \xrightarrow{r} (0,\pi) \\ C: \quad (\pi,0) &\xrightarrow{r} (\pi,0), \qquad D: \quad (\pi,\pi) \xrightarrow{r} (\pi,\pi) \end{aligned} \tag{2.21}$$

But the glide symmetry will ensure an identification between those points:

$$\begin{aligned} A: \ (0,0) &\xrightarrow{g} D: \ (\pi,\pi) \\ B: \ (0,\pi) &\xrightarrow{g} C: \ (\pi,0) \end{aligned} \tag{2.22}$$

Therefore, from the orbifold point of view, no point stays invariant under the discrete group. This has an important consequence on localized interactions: they have to be identified by pairs and this global symmetry does not depend on the UV-completion of the model. For instance this is not the case on the Chiral Square where only two points are identified by pairs and one is left fixed (62).

This identification will extend a symmetry of the bulk and generate a KK-parity p_{KK} which will be always left unbroken by this framework: it can be seen from a geometrical point of view as a $\pi/2$-rotation with respect to the center of the fundamental domain $(\pi/2, \pi/2)$[4]:

$$p_{KK}: \begin{cases} x_5 \sim x_5 + \pi R_5 \\ x_6 \sim x_6 + \pi R_6 \end{cases} \tag{2.23}$$

This transformation ensures $A \leftrightarrow D$ and $B \leftrightarrow C$ and generates a phase $(-1)^{k,l}$, for KK-modes with quantized momenta (k,l) along the coordinates x_5 and x_6. As in models like supersymmetry or little higgs, this creates a distinction between odd and even KK-modes and constrains the possible decays between different tiers. For instance, the tiers with $(1,0)$ or $(0,1)$ momenta are odd under this KK-parity, they do not decay and play the role of Dark Matter candidate. On the other hand, modes like $(1,1)$ or $(2,0)$ are even and can decay into Standard Model particles.

Finally, let us mention a second bulk KK-parity p'_{KK} which is also a relic of Lorentz invariance:

$$p'_{KK}: \begin{cases} x_5 \sim x_5 + \pi R_5 \\ x_6 \sim x_6 \end{cases} \tag{2.24}$$

The main difference with p_{KK} is that this parity could be broken by the UV-completion on the boundaries and, in general, during our studies, as p'_{KK} is not a fundamental symmetry of the orbifold, we will not consider it and assume that it is broken. Nevertheless if p'_{KK} remains unbroken, the two tiers $(1,0)$ and $(0,1)$ would also pick different parity, and therefore contain two independent Dark Matter candidates and $(1,1)$ states would be odd and stable under this parity. Moreover the fact that p'_{KK} is a symmetry of the bulk has also an important consequence on quantum corrections of the theory. As the vertices appearing in the loops are generated by the bulk interactions, both KK-parities cannot be broken by radiative corrections. So the decay of $(1,1)$ states, for example, can only be generated by localized interactions introduced explicitly in the theory while $(2,0)$ decays will be already driven by loops.

[4]Notice that it corresponds to the same KK-parity as in (62).

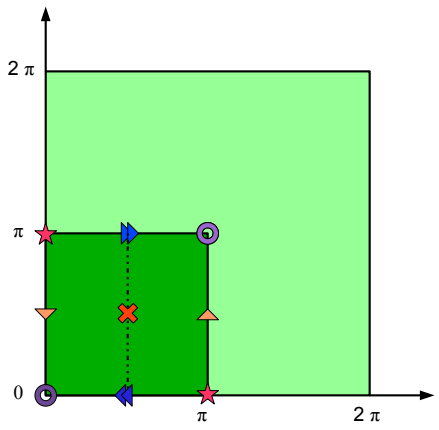

Figure 2.5: Residual parities and singular points on the Real Projective Plane. The parity with respect to the cross is the unbroken KK-parity p_{KK}. The dashed line represents the broken KK-parity p'_{KK} which is restored if we identify the four singular points.

2.2 The Standard Model on the Real Projective Plane

2.2.1 Scalar fields

The action for a scalar field Φ is (omitting the integral along the un-compact 4 dimensions and assuming $R_6 = R_5 = 1$):

$$S_{\text{scalar}} = \int_0^{2\pi} dx_5\, dx_6 \left\{ D_M \phi^\dagger D^M \phi - m_\phi^2 \phi^\dagger \phi \right\}, \tag{2.25}$$

where the index $M = (\mu, 5, 6)$ and where $D_M = \partial_M - igA_M^a t_r^a$. This leads to the equation of motion (EOM) for the free field:

$$\left(\partial_5^2 + \partial_6^2 + p^2 - m_\phi^2\right) \phi = 0\,, \tag{2.26}$$

where $p^2 = -\partial_\mu \partial^\mu$. After Fourier transforming along the two extra coordinates, the field can be expanded in a sum of KK modes:

$$\phi(p^2, x_5, x_6) = \sum_{k,l} f_{k,l}(x_5, x_6)\ \phi^{(k,l)}(p^2) \tag{2.27}$$

The wavefunctions $f_{k,l}(x_5, x_6)$ satisfy the previous equation with p^2 replaced by the mass squared of the (k,l)-mode $m_{k,l}^2$ which comes from the EOM of the 4D field $\phi^{(k,l)}$.

$$p^2 \phi^{(k,l)} = m_{k,l}^2 \phi^{(k,l)} \tag{2.28}$$

The solutions of this equation are usual combinations of sines and cosines (with frequencies determined by the 2π-periodicity):

$$\begin{aligned} f_{k,l}(x_5, x_6) = A_{k,l} \cos kx_5\ \cos lx_6 + B_{k,l} \sin kx_5\ \sin lx_6 \\ + C_{k,l} \sin kx_5\ \cos lx_6 + D_{k,l} \cos kx_5\ \sin lx_6 \end{aligned} \tag{2.29}$$

The coefficients $A_{k,l}$, $B_{k,l}$, $C_{k,l}$, $D_{k,l}$ will be chosen to satisfy the canonical normalization of fields and the boundary conditions of $\phi^{(k,l)}$. The wavefunctions can be labeled then with the parities under the rotation and glide:

$f^{(k,l)}$	p_r	p_g	spectrum
$\cos kx_5 \ \cos lx_6$	$+$	$(-1)^{k+l}$	$k,l \geq 0$
$\sin kx_5 \ \sin lx_6$	$+$	$(-1)^{k+l+1}$	$k,l > 0$
$\sin kx_5 \ \cos lx_6$	$-$	$(-1)^{k+l}$	$k > 0\,, l \geq 0$
$\cos kx_5 \ \sin lx_6$	$-$	$(-1)^{k+l+1}$	$k \geq 0\,, l > 0$

The masses are given by the formula:

$$m_{k,l}^2 = m_\phi^2 + k^2 + l^2 \tag{2.30}$$

and the mass eigenstates can be labeled by their parity assignment (p_r, p_g) and KK number (k,l). In table 2.1, we show the full classification of the modes (with normalized wave functions).

2.2.2 Gauge fields

For an SU(N) gauge group, the 6D Lagrangian can be written as:

$$\mathcal{L}_{\text{gauge}} = \int_0^{2\pi} dx_5\, dx_6 \left\{ -\frac{1}{4} F_{MN} F^{MN} - \frac{1}{2\xi} \left(\partial_\mu A^\mu - \xi(\partial_5 A_5 + \partial_6 A_6)\right)^2 \right\} \tag{2.31}$$

where $F_{MN} = \partial_M A_N - \partial_N A_M + g f^{abc} A_M^b A_N^c$, and the ξ-gauge fixing term is added to eliminate the mixing between A_μ and the extra polarizations A_5 and A_6 similarly to what we explain in section 1.3.3. If we consider a free propagating field, the equation of motion for the vector component is given by:

$$-\partial^\mu F_{\mu\nu} - \frac{1}{\xi}\partial_\nu \partial^\mu A_\mu + (\partial_5^2 + \partial_6^2) A_\nu = (p^2 + \partial_5^2 + \partial_6^2) A_\nu = 0 \tag{2.32}$$

which is the same as for a scalar field after assuming that each KK-mode satisfies the usual 4D equation in ξ-gauge:

$$-\partial^\mu F_{\mu\nu} - \frac{1}{\xi}\partial_\nu \partial^\mu A_\mu = p^2 A_\mu \tag{2.33}$$

(k,l)	p_{KK}	$(++)$	$(+-)$	$(-+)$	$(--)$
$(0,0)$	$+$	$\frac{1}{2\pi}$			
$(0,2l)$	$+$	$\frac{1}{\sqrt{2}\pi} \cos 2lx_6$			$\frac{1}{\sqrt{2}\pi} \sin 2lx_6$
$(0,2l-1)$	$-$		$\frac{1}{\sqrt{2}\pi} \cos(2l-1)x_6$	$\frac{1}{\sqrt{2}\pi} \sin(2l-1)x_6$	
$(2k,0)$	$+$	$\frac{1}{\sqrt{2}\pi} \cos 2kx_5$		$\frac{1}{\sqrt{2}\pi} \sin 2kx_5$	
$(2k-1,0)$	$-$		$\frac{1}{\sqrt{2}\pi} \cos(2k-1)x_5$		$\frac{1}{\sqrt{2}\pi} \sin(2k-1)x_5$
$(k,l)_{\text{k+l even}}$	$+$	$\frac{1}{\pi} \cos kx_5 \cos lx_6$	$\frac{1}{\pi} \sin kx_5 \sin lx_6$	$\frac{1}{\pi} \sin kx_5 \cos lx_6$	$\frac{1}{\pi} \cos kx_5 \sin lx_6$
$(k,l)_{\text{k+l odd}}$	$-$	$\frac{1}{\pi} \sin kx_5 \sin lx_6$	$\frac{1}{\pi} \cos kx_5 \cos lx_6$	$\frac{1}{\pi} \cos kx_5 \sin lx_6$	$\frac{1}{\pi} \sin kx_5 \cos lx_6$

Table 2.1: Normalized wavefunctions and parities for a scalar bulk field, where $(p_r, p_g) = (\pm, \pm)$

Once the parities are assigned, the spectrum and wavefunctions will be the same as for the scalar field (with $m_\phi = 0$):

$$m_{k,l}^2 = k^2 + l^2 \tag{2.34}$$

The A_5–A_6 scalar sector is more complicated: like in 5D, the massive vector modes acquire their longitudinal polarization by eating a tower of scalar components provided by a combination of A_5 and A_6, but in 6D a new feature appears: another combination will give rise to a single tower of physical scalar states. In ξ-gauge, this means that the bilinear kinetic term between A_5 and A_6 will mix and force to redefine new mass eigenstates:

$$\mathcal{L}_{A_5,A_6} = \int_0^{2\pi} dx_5\, dx_6\, \frac{1}{2}(A_5, A_6)\cdot \begin{pmatrix} -\partial_\mu^2 + \partial_6^2 + \xi\partial_5^2 & (\xi-1)\partial_5\partial_6 \\ (\xi-1)\partial_5\partial_6 & -\partial_\mu^2 + \partial_5^2 + \xi\partial_6^2 \end{pmatrix} \cdot \begin{pmatrix} A_5 \\ A_6 \end{pmatrix} \tag{2.35}$$

and in generic ξ-gauge, the EOMs given by:

$$-\partial_\mu^2 A_5 + \xi\partial_5(\partial_5 A_5 + \partial_6 A_6) + \partial_6(\partial_6 A_5 - \partial_5 A_6) = 0 \tag{2.36}$$

$$-\partial_\mu^2 A_6 + \xi\partial_6(\partial_5 A_5 + \partial_6 A_6) + \partial_5(\partial_5 A_6 - \partial_6 A_5) = 0 \tag{2.37}$$

First we will focus on two gauge choices: the Unitary gauge, where all non-physical degrees of freedom are removed, and the Feynman-'t Hooft gauge, which is more useful for 6D-loop calculations.

Feynman-'t Hooft gauge

In the Feynman-'t Hooft gauge $\xi = 1$, the equations of motion for A_5 and A_6 decouple:

$$(\partial_5^2 + \partial_6^2 - \partial_\mu^2)A_{5,6} = 0 \tag{2.38}$$

therefore the two components can be treated as two independent scalar fields with proper parities. The wavefunctions and masses are the same as in the scalar case presented in detail in Section 2.2.1.

Unitary gauge

In the unitary gauge $\xi \to \infty$, the combination

$$\partial_5 A_5 + \partial_6 A_6 = 0\,. \tag{2.39}$$

The two fields are not independent, and we can therefore expand both fields on the same tower of 4D scalars $A_\varphi^{(k,l)}$:

$$A_5 = \sum f_5(x_5, x_6) A_\varphi^{(k,l)}\,, \qquad A_6 = \sum f_6(x_5, x_6) A_\varphi^{(k,l)} \tag{2.40}$$

with $\partial_5\phi_5 + \partial_6\phi_6 = 0$. Using the latter relation in equations (2.36–2.37), the two wavefunctions respect the usual EOM of a scalar field:

$$(p^2 + \partial_5^2 + \partial_6^2) f_{5/6} = 0 \tag{2.41}$$

spectra and wavefunctions are again the same as in the scalar case, with the additional constraint from equation 2.39.

Parities

Moreover, the parities of the scalar components are determined by the fact that they are parts of a 6D vector:

$$A_M(p^2, p_r(x_5, x_6)) = \begin{cases} p_r A_\mu(x^\mu, y) \\ -p_r A_5(x^\mu, y) \\ -p_r A_6(x^\mu, y) \end{cases} \quad \text{and} \quad A_M(p^2, p_g(x_5, x_6)) = \begin{cases} p_g A_\mu(x^\mu, y) \\ p_g A_5(x^\mu, y) \\ -p_g A_6(x^\mu, y) \end{cases} \tag{2.42}$$

therefore if the vector component A_μ has parities (p_r, p_g), the parities of A_5 and A_6 components are respectively $(-p_r, p_g)$ and $(-p_r, -p_g)$. In the following tables, we list in detail the masses and normalized wave functions for the 4 possible parity assignments: in the $(++)$ case, the gauge symmetry is unbroken (table 2.2); in table 2.3 the gauge symmetry is broken by the glide, case $(+-)$ and there is no zero mode in the spectrum; then in table 2.4 the gauge symmetry is broken by the rotation (and the glide g'), then there is a zero mode living in the A_5 component, then in table 2.5 the gauge symmetry can be broken by both rotation and glide g; in this case the zero modes resides in A_6.

Generic ξ-gauge

Finally, for the calculation performed in chapter 3, we will have to consider the case of a generic ξ-gauge. In this case, we will have to diagonalize the bilinear term 2.35 and the only possibility to obtain the mass eigenstates, is to Fourier expand A_5 and A_6 fields and diagonalize

(k,l)	p_{KK}	$A_\mu^{(++)}$	$A_5^{(-+)}$	$A_6^{(--)}$
$(0,0)$	$+$	$\frac{1}{2\pi}$		
$(0,2l)$	$+$	$\frac{1}{\sqrt{2}\pi}\cos 2lx_6$		
$(0,2l-1)$	$-$		$\frac{1}{\sqrt{2}\pi}\sin(2l-1)x_6$	
$(2k,0)$	$+$	$\frac{1}{\sqrt{2}\pi}\cos 2kx_5$		
$(2k-1,0)$	$-$			$\frac{1}{\sqrt{2}\pi}\sin(2k-1)x_5$
$(k,l)_{\text{k+l even}}$	$+$	$\frac{1}{\pi}\cos kx_5\cos lx_6$	$\frac{l}{\pi\sqrt{k^2+l^2}}\sin kx_5\cos lx_6$	$-\frac{k}{\pi\sqrt{k^2+l^2}}\cos kx_5\sin lx_6$
$(k,l)_{\text{k+l odd}}$	$-$	$\frac{1}{\pi}\sin kx_5\sin lx_6$	$\frac{l}{\pi\sqrt{k^2+l^2}}\cos kx_5\sin lx_6$	$-\frac{k}{\pi\sqrt{k^2+l^2}}\sin kx_5\cos lx_6$

Table 2.2: Normalized wavefunctions for a $(+,+)$ gauge boson in unitary gauge.

(k,l)	p_{KK}	$A_\mu^{(+-)}$	$A_5^{(--)}$	$A_6^{(-+)}$
$(0,0)$	$+$			
$(0,2l)$	$+$		$\frac{1}{\sqrt{2}\pi}\sin 2lx_6$	
$(0,2l-1)$	$-$	$\frac{1}{\sqrt{2}\pi}\cos(2l-1)x_6$		
$(2k,0)$	$+$			$\frac{1}{\sqrt{2}\pi}\sin 2kx_5$
$(2k-1,0)$	$-$	$\frac{1}{\sqrt{2}\pi}\cos(2k-1)x_5$		
$(k,l)_{\text{k+l even}}$	$+$	$\frac{1}{\pi}\sin kx_5\sin lx_6$	$\frac{l}{\pi\sqrt{k^2+l^2}}\cos kx_5\sin lx_6$	$-\frac{k}{\pi\sqrt{k^2+l^2}}\sin kx_5\cos lx_6$
$(k,l)_{\text{k+l odd}}$	$-$	$\frac{1}{\pi}\cos kx_5\cos lx_6$	$\frac{l}{\pi\sqrt{k^2+l^2}}\sin kx_5\cos lx_6$	$-\frac{k}{\pi\sqrt{k^2+l^2}}\cos kx_5\sin lx_6$

Table 2.3: Normalized wavefunctions for a $(+,-)$ gauge boson in unitary gauge.

(k,l)	p_{KK}	$A_\mu^{(-+)}$	$A_5^{(++)}$	$A_6^{(+-)}$
$(0,0)$	$+$		$\frac{1}{2\pi}$	
$(0,2l)$	$+$		$\frac{1}{\sqrt{2}\pi}\cos 2lx_6$	
$(0,2l-1)$	$-$	$\frac{1}{\sqrt{2}\pi}\sin(2l-1)x_6$		
$(2k,0)$	$+$	$\frac{1}{\sqrt{2}\pi}\sin 2kx_5$		
$(2k-1,0)$	$-$			$\frac{1}{\sqrt{2}\pi}\cos(2k-1)x_5$
$(k,l)_{\text{k+l even}}$	$+$	$\frac{1}{\pi}\sin kx_5\cos lx_6$	$\frac{l}{\pi\sqrt{k^2+l^2}}\cos kx_5\cos lx_6$	$\frac{k}{\pi\sqrt{k^2+l^2}}\sin kx_5\sin lx_6$
$(k,l)_{\text{k+l odd}}$	$-$	$\frac{1}{\pi}\cos kx_5\sin lx_6$	$\frac{l}{\pi\sqrt{k^2+l^2}}\sin kx_5\sin lx_6$	$\frac{k}{\pi\sqrt{k^2+l^2}}\cos kx_5\cos lx_6$

Table 2.4: Normalized wavefunctions for a $(-,+)$ gauge boson in unitary gauge.

(k,l)	p_{KK}	$A_\mu^{(--)}$	$A_5^{(+-)}$	$A_6^{(++)}$
$(0,0)$	$+$			$\frac{1}{2\pi}$
$(0,2l)$	$+$	$\frac{1}{\sqrt{2}\pi}\sin 2lx_6$		
$(0,2l-1)$	$-$		$\frac{1}{\sqrt{2}\pi}\cos(2l-1)x_6$	
$(2k,0)$	$+$			$\frac{1}{\sqrt{2}\pi}\cos 2kx_5$
$(2k-1,0)$	$-$	$\frac{1}{\sqrt{2}\pi}\sin(2k-1)x_5$		
$(k,l)_{\text{k+l even}}$	$+$	$\frac{1}{\pi}\cos kx_5\sin lx_6$	$\frac{l}{\pi\sqrt{k^2+l^2}}\sin kx_5\sin lx_6$	$\frac{k}{\pi\sqrt{k^2+l^2}}\cos kx_5\cos lx_6$
$(k,l)_{\text{k+l odd}}$	$-$	$\frac{1}{\pi}\sin kx_5\cos lx_6$	$\frac{l}{\pi\sqrt{k^2+l^2}}\cos kx_5\cos lx_6$	$\frac{k}{\pi\sqrt{k^2+l^2}}\sin kx_5\sin lx_6$

Table 2.5: Normalized wavefunctions for a $(-,-)$ gauge boson in unitary gauge.

the mass matrix mode by mode. We will then get the mass eigenstate $A_\pi^{(k,l)}$ with a ξ-dependent mass corresponding to the Goldstone boson eaten in the unitary-gauge by the massive gauge boson. The other field $A_\varphi^{(k,l)}$ will be the physical new degree of freedom. For (k,l) mode, it can be shown by considering for instance a $(++)$ gauge field that the bilinear term (2.35) gives:

$$\begin{aligned}\mathcal{L}_{A_5,A_6} &\supset \frac{1}{2}(A_5^{(k,l)},A_6^{(k,l)})\cdot\begin{pmatrix}-\partial_\mu^2-\xi k^2-l^2 & -(\xi-1)kl\\ -(\xi-1)kl & -\partial_\mu^2-k^2-\xi l^2\end{pmatrix}\cdot\begin{pmatrix}A_5^{(k,l)}\\ A_6^{(k,l)}\end{pmatrix}\\ &\supset \frac{1}{2}(A_\pi^{(k,l)},A_\varphi^{(k,l)})\cdot\begin{pmatrix}-\partial_\mu^2-\xi(k^2+l^2) & 0\\ 0 & -\partial_\mu^2-(k^2+l^2)\end{pmatrix}\cdot\begin{pmatrix}A_\pi^{(k,l)}\\ A_\varphi^{(k,l)}\end{pmatrix}\end{aligned} \tag{2.43}$$

This implies that those both fields are present and are related to A_5 and A_6 by:

$$A_5^{(k,l)} = \frac{l}{m_{k,l}}A_\varphi^{(k,l)}+\frac{k}{m_{k,l}}A_\pi^{(k,l)}, \tag{2.44}$$

$$A_6^{(k,l)} = -\frac{k}{m_{k,l}}A_\varphi^{(k,l)}+\frac{l}{m_{k,l}}A_\pi^{(k,l)}. \tag{2.45}$$

For $(k,0)$ or $(0,l)$ modes, the physical scalar is only present for k odd if we consider a $(++)$ gauge boson and no vector state is allowed. While for k even, the goldstone is present with the vector field. Note that this last effect cannot be seen in table 2.2 because it gives wavefunctions in unitary gauge. For the zero mode then, only the massless vector part will be allowed.

Ghost

Concerning the ghost part of the Lagrangian, we obtain:

$$\mathcal{L}_{\text{ghost}} = \int_0^{2\pi} dx_5\, dx_6\; \bar{c}^a \left\{ (-\partial_\mu (D^\mu)^{ac} + \xi \partial_5 (D_5)^{ac} + \xi \partial_6 (D_6)^{ac}) \right\} c^c \,, \tag{2.46}$$

where $(D_M)^{ac} = \partial_M \delta^{ac} - ig(t_G^b)^{ac} = \partial_M \delta^{ac} + g f^{abc} A_M^b$. After KK expansion, we see that the ghost behaves like a scalar field with the same parity as the vector component and with a mass proportional to ξ.

2.2.3 Fermions

The action for a 6D Dirac fermion Ψ in Section 2.1.2 leads to the following EOMs for the 4 components:

$$i\bar{\sigma}^\mu \partial_\mu \chi_\pm + (\partial_5 \mp i\partial_6)\bar{\eta}_\pm = 0\,, \tag{2.47}$$
$$i\sigma^\mu \partial_\mu \bar{\eta}_\pm - (\partial_5 \pm i\partial_6)\chi_\pm = 0\,; \tag{2.48}$$

Then we expand each component in a tower of 4D Dirac fermions $(\chi, \bar{\eta})$ satisfying the usual Dirac EOMs:

$$\Psi(p^2, x_5, x_6) = \begin{pmatrix} \chi_+ \\ \bar{\eta}_- \\ \chi_- \\ \bar{\eta}_+ \end{pmatrix} \Longrightarrow \begin{cases} \chi_+(p^2, x_5, x_6) = \sum_{k,l} f_1^{k,l}(x_5, x_6)\chi^{(k,l)}(p^2) \\ \chi_-(p^2, x_5, x_6) = \sum_{k,l} f_2^{k,l}(x_5, x_6)\chi^{(k,l)}(p^2) \\ \bar{\eta}_+(p^2, x_5, x_6) = \sum_{k,l} f_3^{k,l}(x_5, x_6)\bar{\eta}^{(k,l)}(p^2) \\ \bar{\eta}_-(p^2, x_5, x_6) = \sum_{k,l} f_4^{k,l}(x_5, x_6)\bar{\eta}^{(k,l)}(p^2) \end{cases} \tag{2.49}$$

Those first order equations can be decoupled (60), and each component satisfies the same quadratic equation as scalar fields of the previous section. The solutions are usual combinations of sines and cosines, and the first order EOMs relate the coefficients of the two 4D components. Then to determine the form of the solutions we need to assign the parity of the fields. The rotation gives a different parity to the two 4D-chiralities, and a fermion with $p_r = +$ ($p_r = -$) will have a left-handed (right-handed) zero mode. On the other hand, the glide will relate the two 6D chiralities, so that the four wavefunctions are not independent: the value of the parity under the glide does not play any role on the zero mode spectrum and, as we will see, the only requirement is that the SM doublets and singlets have the same glide parity in order to allow Yukawa couplings with the bulk Higgs.

For a left-handed fermion, case $(+, p_g)$, the KK modes are given by:

(k,l)	f_1	f_2	f_3	f_4
$(0,0)$	$\frac{1}{2\sqrt{2}\pi}$	$p_g \frac{1}{2\sqrt{2}\pi}$	0	0
$(0,l)$	$\frac{1}{2\pi}\cos lx_6$	$p_g(-1)^l \frac{1}{2\pi}\cos lx_6$	$-\frac{i}{2\pi}\sin lx_6$	$p_g(-1)^l \frac{i}{2\pi}\sin lx_6$
$(k,0)$	$\frac{1}{2\pi}\cos kx_5$	$p_g(-1)^k \frac{1}{2\pi}\cos kx_5$	$-\frac{1}{2\pi}\sin kx_5$	$-p_g(-1)^k \frac{1}{2\pi}\sin kx_5$

An important feature, we have to emphasize, is the case where both $k, l \neq 0$. Two degenerate orthogonal solutions are present for each level. We write for convenience $\Psi^{(+,p_g)} = \sum_{k,l} \Psi_{k,l}^{(+,p_g)}$ the KK-expanded 6D spinors and the solutions for the (k,l) mode can be parametrized as:

$$\Psi_{k,l}^{(+,p_g)} = \begin{pmatrix} (a\cos kx_5\, \cos lx_6 + b \sin kx_5\, \sin lx_6)\, \chi^{(k,l)} \\ p_g(-1)^{k+l}\, (c \sin kx_5\, \cos lx_6 - d \cos kx_5\, \sin lx_6)\, \bar{\eta}^{(k,l)} \\ p_g(-1)^{k+l}\, (a\cos kx_5\, \cos lx_6 - b \sin kx_5\, \sin lx_6)\, \chi^{(k,l)} \\ (c \sin kx_5\, \cos lx_6 + d \cos kx_5\, \sin lx_6)\, \bar{\eta}^{(k,l)} \end{pmatrix}, \tag{2.50}$$

where we can use the EOMs and normalization condition to fix the coefficients:

$$\begin{array}{ll} a = \frac{\cos\alpha}{\sqrt{2}\pi} & c = -\frac{k\cos\alpha - il\sin\alpha}{\sqrt{2}\pi\sqrt{k^2+l^2}} \\ b = \frac{\sin\alpha}{\sqrt{2}\pi} & d = \frac{k\sin\alpha - il\cos\alpha}{\sqrt{2}\pi\sqrt{k^2+l^2}} \end{array} \tag{2.51}$$

The two orthogonal states can be obtained by choosing $\alpha = \theta$ and $\alpha = \pi/2 + \theta$, where θ is an arbitrary mixing angle. We can keep it free in loop or cross-section calculations and use it as a check because physical observables do not depend on θ. Nevertheless for simplicity, here we take $\theta = 0$ and denote the 4D fields defined with $\alpha = 0$ by the index a and its orthogonal partner with the index b. In this case, the field wavefunction becomes:

$$\Psi_a^{(+p_g)} = \frac{1}{\sqrt{2}\pi}\begin{pmatrix} (\cos kx_5\ \cos lx_6)\,\chi_a^{k,l} \\ p_g(-1)^{k+l}\left(-\frac{k}{\sqrt{k^2+l^2}}\sin kx_5\ \cos lx_6 + \frac{il}{\sqrt{k^2+l^2}}\cos kx_5\ \sin lx_6\right)\bar{\eta}_a^{k,l} \\ p_g(-1)^{k+l}\,(\cos kx_5\ \cos lx_6)\,\chi_a^{k,l} \\ \left(-\frac{k}{\sqrt{k^2+l^2}}\sin kx_5\ \cos lx_6 - \frac{il}{\sqrt{k^2+l^2}}\cos kx_5\ \sin lx_6\right)\bar{\eta}_a^{k,l} \end{pmatrix} \tag{2.52}$$

and

$$\Psi_b^{(+p_g)} = \frac{1}{\sqrt{2}\pi}\begin{pmatrix} (\sin kx_5\ \sin lx_6)\,\chi_b^{k,l} \\ p_g(-1)^{k+l}\left(\frac{il}{\sqrt{k^2+l^2}}\sin kx_5\ \cos lx_6 - \frac{k}{\sqrt{k^2+l^2}}\cos kx_5\ \sin lx_6\right)\bar{\eta}_b^{k,l} \\ p_g(-1)^{k+l}\,(-\sin kx_5\ \sin lx_6)\,\chi_b^{k,l} \\ \left(\frac{il}{\sqrt{k^2+l^2}}\sin kx_5\ \cos lx_6 + \frac{k}{\sqrt{k^2+l^2}}\cos kx_5\ \sin lx_6\right)\bar{\eta}_b^{k,l} \end{pmatrix} \tag{2.53}$$

For a right-handed fermion corresponding to the case $(-, p_g)$, the situation is quite similar:

(k,l)	f_1	f_2	f_3	f_4
$(0,0)$	0	0	$\frac{1}{2\sqrt{2}\pi}$	$p_g\frac{1}{2\sqrt{2}\pi}$
$(0,l)$	$-\frac{i}{2\pi}\sin lx_6$	$p_g(-1)^l\frac{i}{2\pi}\sin lx_6$	$\frac{1}{2\pi}\cos lx_6$	$p_g(-1)^l\frac{1}{2\pi}\cos lx_6$
$(k,0)$	$\frac{1}{2\pi}\sin kx_5$	$p_g(-1)^k\frac{1}{2\pi}\sin kx_5$	$\frac{1}{2\pi}\cos kx_5$	$p_g(-1)^k\frac{1}{2\pi}\cos kx_5$

and, for $k, l \neq 0$:

$$\Psi^{(-g)} = \begin{pmatrix} (a\sin kx_5\ \cos lx_6 + b\cos kx_5\ \sin lx_6)\,f_l \\ p_g(-1)^{k+l}\,(c\cos kx_5\ \cos lx_6 - d\sin kx_5\ \sin lx_6)\,\bar{f}_r \\ p_g(-1)^{k+l}\,(a\sin kx_5\ \cos lx_6 - b\cos kx_5\ \sin lx_6)\,f_l \\ (c\cos kx_5\ \cos lx_6 + d\sin kx_5\ \sin lx_6)\,\bar{f}_r \end{pmatrix} \tag{2.54}$$

with

$$\begin{array}{ll} c = \frac{\cos\alpha}{\sqrt{2}\pi} & a = \frac{k\cos\alpha + il\sin\alpha}{\sqrt{2}\pi\sqrt{k^2+l^2}} \\ d = \frac{\sin\alpha}{\sqrt{2}\pi} & b = -\frac{k\sin\alpha + il\cos\alpha}{\sqrt{2}\pi\sqrt{k^2+l^2}} \end{array} \tag{2.55}$$

A last important remark is the fact that we have fixed the normalization of the wavefunctions in such a way that the mass of each (k,l) KK level is real, i.e. $m_{(k,l)} = \sqrt{k^2+l^2}$.

2.2.4 Tree level spectrum and possible extensions

By now we described the field theory in this peculiar RPP framework. To study phenomenology in this orbifold, we will start with the minimal extension in flat dimensions, which is Universal Extra Dimension (UED). As in 5D, the Standard Model particles will propagate in the bulk. The gauge symmetry will be the usual $G_{SM} = SU(3) \times SU(2) \times U(1)$ and will be broken by the Higgs mechanism. To each chiral fermions will correspond a 6D fermion: two doublet Q and L and three singlets U, D and E (and eventually a right handed neutrino N). For (k, l) KK-modes, the tree level mass spectrum (without taking into account the Higgs vev and the loop induced splittings) is degenerate for all particles and is given by:

$$m_{k,l}^2 = \frac{k^2}{R_5^2} + \frac{l^2}{R_6^2} \tag{2.56}$$

As a summary and a reference, in the table 2.6, we present explicitly for the first tiers, the content of particles of the model focusing on spin and KK-parity of the fields.

This model is obviously the easiest option we have as a model-builder. New work will be done afterwards to see if extension can be built in this framework like Gauge-Higgs Unification which can address more puzzles of the Standard Model in addition to Dark Matter. We can also think of using a non-flat metric in this framework and see how warping can generate new interesting features. In all these studies, we will use the advantage of having possible counter-terms on singular points without breaking KK-parity.

Finally let us mention a new interesting idea which appears recently (70). In our case, we considered a flat space to construct the Real Projective Plane and describe field theory. In this case, all the curvature is concentrated on the singular points of the space. However, it exists another possibility to construct a Real Projective Plane which is based on an orbifolding of the sphere S^2 where the two antipodal points are identified. Then the metric is not flat anymore, the curvature is diluted in the whole space and no singularity seem present. But the price to pay is expensive; the spherical metric will probably make all the discussion we are having more and more challenging.

(k, l)	p_{KK}	masses	gauge vector A^μ	gauge scalar $A^{5,6}$	fermions	higgs
$(0,0)$	$+$	0	★	–	★ chiral	★
$(0,1)-(1,0)$	$-$	1	–	★	★	–
$(1,1)$	$+$	$\sqrt{2}$	★	★	★ × 2	★
$(2,0)-(0,2)$	$+$	2	★	–	★	★
$(2,1)-(1,2)$	$-$	$\sqrt{5}$	★	★	★ × 2	★
(k,l)	$(-1)^{k+l}$	$\sqrt{k^2+l^2}$	★	★	★ × 2	★

Table 2.6: Field content on the RPP in UED model for the first KK-levels. Masses are given for the degenerate case $R_5 = R_6 = 1$ in unit of m_{KK}.

2.3 Different approaches for the calculation of radiative corrections in 6D.

In the beginning of the chapter, we focused on the tree-level spectrum of the Standard Model on the Real Projective Plane, and we have seen that the masses of all the fields of a given tier (k, l) are degenerate. Nevertheless this degeneracy will be removed at loop level and we need in this case to develop an efficient tool box to compute the self-energies of the different fields in this six dimensional framework. In this section, we will present three methods to perform the calculation of the loop corrections to the masses. First, we can use the expansion of the 6D propagator in winding modes (71): in this way it is straightforward to renormalize the 6D kinetic terms, which corresponds to removing the contribution of the zero winding modes (64). However, as we will see, the calculation is challenging in general due to the presence of Bessel functions in the expansion. The second way uses the usual KK expansion (64): in this case a more sophisticated technique is required to renormalize the kinetic term. A third possibility is to expand in KK modes along one direction, and use the resummed 5D propagator (72) along the other: the advantage is clear when computing corrections to $(n, 0)$ modes, where conservation of momentum along the second extra direction simplifies the sum over the KK number in the propagators. Notice that all these three techniques are initially equivalent but as we will see, small differences will appear in the result of divergent loops because of the choice of the regularization schemes.

To illustrate these three techniques, we will detail the explicit calculation of the loop in figure 2.6 for the $A_6 \equiv A_\varphi$ scalar modes $(n, 0)$ with n odd. This loop will be one of the contributions to the self-energy of A_6. In order to extract the contribution to the mass correction of the gauge scalar, we will consider the external fields on-shell (8). This implies that:

$$\delta m^2 = m_n^2 - n^2 = \Pi(p^2 = m_n^2) \approx \Pi(p^2 = n^2) \tag{2.57}$$

where p is the external momentum of the gauge scalar, m_n is the "one-loop" mass of the mode and n, its tree level mass. When we will consider in next section the full set of loop corrections, we will just sum all these self-energy contributions. The results from the other loops in section 2.4 have been calculated using at least two of those techniques.

2.3.1 6D winding mode method

A 6D scalar field propagating in an infinite space satisfies the following equation of motion :

$$\left(-\partial_\mu \partial^\mu + \partial_5^2 + \partial_6^2\right) \phi = 0 \tag{2.58}$$

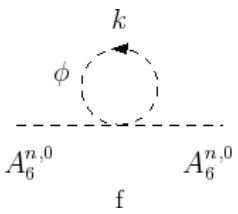

Figure 2.6: One-loop radiative corrections to the gauge scalar self-energy from a scalar field

It is convenient to calculate the propagator in a mixed momentum representation along the uncompactified 4D space and position space along the extra-directions. The propagator is therefore the Green function of the following operator:

$$\left(p^2 + \partial_5^2 + \partial_6^2\right) G_S^{\text{6Dopen}}(p, x_5 - x'_5, x_6 - x'_6) = i\delta(x_5 - x'_5)\delta(x_6 - x'_6) \tag{2.59}$$

The solution to this equation (71), defining $p = \sqrt{p^2}$ and $\overrightarrow{y} = (x_5, x_6)$, is then:

$$G_S^{\text{6Dopen}}(p, \overrightarrow{y} - \overrightarrow{y}') = \frac{1}{4} H_0^{(1)}(p\,|\overrightarrow{y} - \overrightarrow{y}'|) \tag{2.60}$$

where $H_0^{(1)}$ is the zero order Hankel function of first kind. Then we need to translate into the propagator properties, the restriction of the extra-space from $\mathbb{R}^2$ to a compact space. It will be done by using the identification of the orbifold. In a 6D flat geometry, we will have two translations t_5 and t_6 which define periodicity and reduce the open space to a torus. This implies that:

$$|\overrightarrow{y} - \overrightarrow{y}'| \sim |\overrightarrow{y} - \overrightarrow{y}' + \overrightarrow{\Omega}| \tag{2.61}$$

where $\overrightarrow{\Omega} = (2\pi n_1, 2\pi n_2)$ with $(n_1, n_2) \in \mathbb{Z}^2$ which are so-called *winding modes*. The propagator is then given by:

$$G_S^{\text{6D}}(p, \overrightarrow{y} - \overrightarrow{y}') = \sum_{\overrightarrow{\Omega}} \frac{1}{4} H_0^{(1)}(p\,|\overrightarrow{y} - \overrightarrow{y}' + \overrightarrow{\Omega}|) \tag{2.62}$$

Then we will add the whole set of identifications coming from glide and rotation and similarly we get the propagator on the Real Projective Plane (73):

$$\begin{aligned} G_S^{orb}(p, \overrightarrow{y}, \overrightarrow{y}') = \frac{1}{4} \sum_{\overrightarrow{\Omega}} \Big[& G_S^{6D}(p, \overrightarrow{y} - \overrightarrow{y}' + \overrightarrow{\Omega}) + p_g\, G_S^{6D}(p, \overrightarrow{y} - g(\overrightarrow{y}') + \overrightarrow{\Omega}) \\ & + p_r\, G_S^{6D}(p, \overrightarrow{y} - r(\overrightarrow{y}') + \overrightarrow{\Omega}) + p_r\, p_g\, G_S^{6D}(p, \overrightarrow{y} - r \cdot g(\overrightarrow{y}') + \overrightarrow{\Omega}) \Big] \end{aligned} \tag{2.63}$$

where p_r and p_g are the parities of the scalar field under rotation and glide and $f(\overrightarrow{y}')$ are the transformed of the point y' under the transformation f. The coefficient $1/4$ is here to take into account the fact that the RPP space is smaller that the full torus. Moreover we notice that the propagator will depend on $(x_5 + x'_5)$ and $(x_6 + x'_6)$ which breaks the translation invariance along the two extra-dimensions.

The loop correction to the A_6 propagator is given by:

$$\begin{aligned} i\Pi^{66} &= 2ig_6^2 C(r_s) g_{66} \int \frac{d^4k}{(2\pi)^4} \int d\overrightarrow{y}\; G_S^{orb}(k, \overrightarrow{y}, \overrightarrow{y}) f_{A_6}^{(n,0)}(q, \overrightarrow{y}) f_{A_6}^{(n,0)}(q, \overrightarrow{y}) \\ &= iN\,(2\pi)^2 \int d^4k \int d\overrightarrow{y}\; G_S^{orb}(k, \overrightarrow{y}, \overrightarrow{y}) f_{A_6}^{(n,0)}(q, \overrightarrow{y}) f_{A_6}^{(n,0)}(q, \overrightarrow{y}) \end{aligned} \tag{2.64}$$

where $f_{A_6}^{(n,0)}(q, \overrightarrow{y}) = \frac{1}{\sqrt{2\pi}} \sin nx_5$ is the wavefunction of the external field, $g_{66} = -1$ is a metric factor and $g_6^2 = (2\pi)^2 g^2$ is the 6D gauge coupling. In the following, in order to simplify the notation, we will always omit the normalization factor $N = \frac{2g^2 C(r_s) g_{66}}{16\pi^4}$. The correction Π^{66} can

be split into four terms whose signs depend on the parity of the scalar field under the symmetries of the space:

$$\Pi^{66} = \Pi_T + p_g\ \Pi_G + p_r\ \Pi_R + p_g p_r\ \Pi_{G'} \tag{2.65}$$

Π_T is the contribution we would obtain on a torus of same radii and it is finite after the kinetic term renormalization, the other three terms are generated by the symmetries of the orbifold and we do expect a log divergence arising in Π_R due to the fixed points of the rotation.

Torus

The torus contribution is given by the first term in 2.63 plugged in 2.64:

$$\begin{aligned}\Pi_T &= \frac{N}{4}4\pi^2 \int d^4k \sum_{\vec{\Omega}} \frac{1}{4} H_0^{(1)}(k\ |\vec{\Omega}|) \\ &= \frac{N}{4}4\pi^3 \int_0^\infty dk_E \sum_{(n1,n2)\in Z^2} k_E^3\ K_0(2\pi k_E \sqrt{n_1^2+n_2^2})\end{aligned} \tag{2.66}$$

where K_0 is the K-Bessel function of zero order. Here, we have performed the Wick rotation to write the last integral in Euclidean space.

In the UV-limit $p|\vec{\Omega}| \gg 1$, the propagator is exponentially damped:

$$K_0(p|\vec{\Omega}|) \sim e^{-p|\vec{\Omega}|}\sqrt{\frac{\pi}{2p|\vec{\Omega}|}} \tag{2.67}$$

The zero winding mode $(n_1, n_2) = (0, 0)$ contribution is UV divergent, however such divergence is the same we would get in the limit of un-compactified space. Therefore this bulk divergence can be absorbed by a wavefunction renormalization of the 6D field. Removing the $(0, 0)$ mode from the sum and integrating in k

$$\int_0^\infty dk_E\ k_E^3\ K_0(k_E a) = \frac{4}{a^4} \tag{2.68}$$

we obtain:

$$\Pi_T = \frac{N}{4}\ T_6 \quad \text{with} \quad T_6 = \frac{1}{\pi} \sum_{(n1,n2)\neq(0,0)} \frac{1}{(n_1^2+n_2^2)^2} \sim 1.92 \tag{2.69}$$

Glides

From the second term in the propagator 2.63, we get:

$$\Pi_G = \frac{N}{4}4\pi^2 \int d^4k \int d\vec{y} \sum_{\vec{\Omega}} \frac{1}{4} H_0^{(1)}(k\ |\vec{y} - g(\vec{y}) + \vec{\Omega}|) \frac{\sin^2 n x_5}{2\pi^2} \tag{2.70}$$

As the glide does not change sign to the x_5 component, the Hankel function does not depend on x_5 and the integral along this extra-dimension is just given by the normalization of wave functions. After Wick rotating and integrating in k as before we obtain

$$\Pi_G = \frac{N}{4\pi^2} \sum_{(n1,n2)\in\mathbb{Z}^2} \int_0^{2\pi} dx_6 \frac{1}{((n_1 - 1/2)^2 + (x_6/\pi + n_2 - 1/2)^2)^2} \tag{2.71}$$

where we numerically checked that

$$\frac{N}{\pi^2}\sum_{(n1,n2)\in\mathbb{Z}^2}\int_0^\pi dx_5\frac{1}{\left((n_1-1/2)^2+(x_6/\pi+n_2-1/2)^2\right)^2}=7\zeta(3) \tag{2.72}$$

We obtain a similar expression for the other glide $\Pi_{G'}$, now x_6 can be easily integrated out and we are left with:

$$\begin{aligned}\Pi_{G'} &= \frac{N}{4\ \pi^2}\sum_{(n1,n2)\in\mathbb{Z}^2}\int_0^{2\pi} dx_5\frac{1-\cos 2nx_5}{((x_5/\pi+n_1-1/2)^2+(n_2-1/2)^2)^2} \\ &= \frac{N}{4}\left(7\zeta(3)+B_1(n)\right)\end{aligned} \tag{2.73}$$

where we again numerically checked that the n-dependent term corresponds to the function in appendix A.

Rotation

The last contribution is coming from the rotation part: after the Wick rotation

$$\Pi_R=\frac{N}{4}2\pi\int_0^\infty dk\int d\overrightarrow{y}\sum_{\overrightarrow{\Omega}}k^3\ K_0(k\ |2\overrightarrow{y}+\overrightarrow{\Omega}|)\sin^2 nx_5 \tag{2.74}$$

To extract the divergent part, we cut-off the 4D momentum k at a scale Λ, and numerically integrated over the compact space and summed. We can therefore show that the integral is equal to

$$\Pi_R=\frac{N}{4}\quad n^2\pi^2\log\frac{\Lambda^2+n^2}{n^2} \tag{2.75}$$

From the integral form, we can see that the divergences appear when $|2\overrightarrow{y}+\overrightarrow{\Omega}|=0$: those points are indeed the fixed points of the rotation, i.e. the corners of the fundamental square. In this notation, their geometrical origin is clear. Note that this divergence depends on the quantum number of the considered mode, so it cannot be reabsorbed in the renormalization of the bulk 6D fields. These log-divergences will be regularized then by adding localized counter-terms on the singular points as we will discuss in the following of this thesis.

Using this method, the tadpole calculation seems straightforward and the properties of the orbifold appear clearly. Nevertheless, the mathematical complexity will jump significantly when considering loops with two propagators inside. The integrals of Bessel function products will be the most important limitation to perform such calculations.

2.3.2 6D Kaluza-Klein expansion method

This method, the most commonly used one, is based on the 4D KK-mode decomposition, therefore we need to compute loops with usual 4D propagators and then sum over the KK-momenta of the towers. However, the technical difficulties here arise from the computing of all the necessary couplings between modes, and in addition a Fourier transform that goes back to winding modes is necessary for the renormalization of the torus contribution. Nevertheless, this method can be easily applied to any loop structure.

Here we will again focus on our concrete example. The contribution of a scalar field with parities (p_r, p_g) can be still be written as:

$$\Pi_{p_g\ p_r} = \Pi_T + p_g\Pi_G + p_g p_r \Pi_{G'} + p_r \Pi_R \tag{2.76}$$

Therefore if we calculated the contribution of all 4 parity possibilities, we would be able to extract each term:

$$\Pi_T = \frac{1}{4}(\Pi_{++} + \Pi_{+-} + \Pi_{-+} + \Pi_{--}) \tag{2.77}$$

$$\Pi_G = \frac{1}{4}(\Pi_{++} - \Pi_{+-} + \Pi_{-+} - \Pi_{--}) \tag{2.78}$$

$$\Pi_{G'} = \frac{1}{4}(\Pi_{++} - \Pi_{+-} - \Pi_{-+} + \Pi_{--}) \tag{2.79}$$

$$\Pi_R = \frac{1}{4}(\Pi_{++} + \Pi_{+-} - \Pi_{-+} - \Pi_{--}) \tag{2.80}$$

The couplings that enter the loop, $A^6_{(n,0)}A^6_{(n,0)}\phi^\dagger_{(m,l)}\phi_{(m,l)}$ are proportional to $ig^2 g_{66}$ with a coefficient that depends on the wave function integrals. We listed such coefficients in the table 2.7 (here $m, l \neq 0$ are intended). For example, using the previous table, the corrections coming from ϕ_{++}, ϕ_{+-}, ϕ_{+-} and ϕ_{--} running into the loop are:

$$i\Pi_{++} = N\Big(\sum_{(m,l)\geq 1} 2G(m,l) + \sum_{l\geq 1}((-1)^l G(n,l) + 2G(0,2l)) + \sum_{m\geq 1, m\neq n} 2G(2m,0) + 2G(0,0)\Big) \tag{2.81}$$

$$i\Pi_{+-} = N\Big(\sum_{(m,l)\geq 1} 2G(m,l) + \sum_{l\geq 1}(-(-1)^l G(n,l) + 2G(0,2l-1)) + \sum_{m\geq 1, m\neq n} 2G(2m-1,0) + G(n,0)\Big) \tag{2.82}$$

$(p_r\ p_g)$	$(++)$	$(+-)$	$(-+)$	$(--)$
$(0,0)$	2	-	-	-
$(m,0)$ m even	2	-	2	-
$(m,0)$ $m \neq n$ m odd	-	2	-	2
$(n,0)$	-	1	-	3
$(0,l)$ l even	2	-	-	2
$(0,l)$ l odd	-	2	2	-
(m,l) $m \neq n$	2	2	2	2
(n,l) l even	3	1	1	3
(n,l) l odd	1	3	3	1

Table 2.7: Quadrilinear coupling: $A^6_{(n,0)}A^6_{(n,0)}\phi^\dagger_{(m,l)}\phi_{(m,l)}$. The coefficients in this table are multiplied by $ig_6^2 g_{66}$.

$$i\Pi_{-+} = N\Big(\sum_{(m,l)\geq 1} 2G(m,l) + \sum_{l\geq 1}(-(-1)^l G(n,l) + 2G(0,2l-1)) + \sum_{m\geq 1, m\neq n} 2G(2m,0)\Big) \tag{2.83}$$

$$i\Pi_{--} = N\Big(\sum_{(m,l)\geq 1} 2G(m,l) + \sum_{l\geq 1}((-1)^l G(n,l) + 2G(0,2l)) + \sum_{m\geq 1, m\neq n} 2G(2m-1,0) + 3G(n,0)\Big) \tag{2.84}$$

where

$$G(m,l) = \int_0^\infty dk_E \, \frac{k_E^3}{k_E^2 + m^2 + l^2} \tag{2.85}$$

is the integral appearing in the 4D loop.

Torus

For the torus contribution, we reconstruct a sum over all the KK modes on a torus compactification. Then following the usual Fourier expansion in the double sum and removing the zero winding mode contribution, we get:

$$\Pi_T = N\frac{1}{2}\sum_{(m,l)\in\mathbb{Z}^2} G(m,l) = \frac{N}{4}T_6 \tag{2.86}$$

Glides

Following the same procedure, the glide contribution can be written as:

$$\Pi_G = \frac{N}{4}\, 2\sum_{m\in\mathbb{Z}}(-1)^m G(m,0) = \frac{N}{4}\, 7\zeta(3) \tag{2.87}$$

while for the second glide

$$\Pi_{G'} = \frac{N}{4}\, 2\sum_{l\in\mathbb{Z}}(-1)^l (G(n,l) + G(0,l)) = \frac{N}{4}\, (7\zeta(3) + B_1(n)) \tag{2.88}$$

We find in this case, the same result as the one obtained in section 2.3.1.

Rotation

For the rotation contribution, we will follow the same regularization procedure as in the previous section. After cutting-off the 4D momentum at the scale Λ, the loop calculation gives:

$$\begin{aligned}\Pi_R &= \frac{N}{4}\, 2\,(G(0,0) - G(n,0)) = \frac{N}{4}\int_0^\Lambda dk_E \left(k_E - \frac{k_E^3}{k_E^2 + n^2}\right) \\ &= \frac{N}{4}\, n^2\pi^2 \log\frac{\Lambda^2 + n^2}{n^2}\end{aligned} \tag{2.89}$$

2.3.3 6D mixed propagator method

Using the full 6D propagator is complicated because it imposes to deal with Bessel functions and re-sum a double sum. On the other end using directly the double sum from the KK-expansion is challenging from the point of view of coupling calculation. Another original idea is to use a mixed method: 5D propagators can be easily handled, in fact a generic scalar propagator takes the simple form on a S_1 orbifold:

$$G_S^{5D}(\chi_m, y-y') = \frac{i\cos\chi_m(\pi-|y-y'|)}{2\ \chi_m\ \sin\chi_m\pi} \quad \text{where} \quad \chi_m = \sqrt{k^2-m^2} \tag{2.90}$$

and m is the 5D mass of the scalar field. Then we can think of taking advantage of this compact form by expanding in KK modes along one of the extra-dimensions, say x_6, and write the 6D propagator in terms of resummed 5D propagators:

$$G_S^{6D}(k, \overrightarrow{y}-\overrightarrow{y}') = \sum_{l=-\infty}^{\infty} G_S^{5D}(\chi_l, x_5-x'_5)\ f_l^*(x_6)f_l(x'_6) \tag{2.91}$$

where

$$f_l(x_6) = \frac{1}{\sqrt{2\pi}}e^{ix_6 l} \quad \text{and} \quad \chi_l = \sqrt{k^2-l^2} \tag{2.92}$$

The f_l's are the wavefunctions on a circle and l the KK masses for the 5D modes. This method is extremely powerful, especially to calculate corrections for modes like the $(n,0)$: the fact that the external fields do not carry any momentum along x_6, together with the orthonormality of the wavefunctions f_l, allows to easily replace the integral in the coordinate x_6 with a sum. The orbifold propagator and the scalar loop we are considering here are given by the equations (2.63) and (2.64):

$$\begin{aligned} G_S^{orb}(p, \overrightarrow{y}, \overrightarrow{y}') = \frac{1}{4}\sum_{l=-\infty}^{\infty} \big[& G_S^{5D}(\chi_l, x_5-x'_5)\ f_l^*(x_6)f_l(x'_6) \\ & + p_g\, G_S^{5D}(\chi_l, x_5-g(x'_5))\ f_l^*(x_6)f_l(g(x'_6)) + p_r\, G_S^{5D}(\chi_l, x_5-r(x'_5))\ f_l^*(x_6)f_l(r(x'_6)) \\ & + p_r\ p_g\, G_S^{5D}(\chi_l, x_5-rg(x'_5))\ f_l^*(x_6)f_l(rg(x'_6))\big] \end{aligned} \tag{2.93}$$

Contrary to the winding mode method, this one can be extended in a straightforward way to all the other loop diagrams. Finally a last technical and important remark: the orbifolding transformations reduce the fundamental to a subspace of the torus. When we integrate the propagators running in the loop, we have to care that the integration domain is an interval $[0,2\pi)\times[0,2\pi)$, so the transformed points under glides and rotations have also to be in this domain. For instance, we will be careful that:

$$\left\{\begin{array}{l} 0<x_5<\pi:\ g(x_5)=x_5+\pi \\ \pi<x_5<2\pi:\ g(x_5)=x_5-\pi \end{array}\right. , \quad \left\{\begin{array}{l} 0<x_5<\pi:\ rg(x_5)=-x_5+\pi \\ \pi<x_5<2\pi:\ rg(x_5)=-x_5+3\pi \end{array}\right.$$
$$\text{and}\ \ 0<x_5<2\pi:\ rg(x_5)=-x_5+2\pi \tag{2.94}$$

Torus

After integrating over x_5 and x_6, the torus contribution can be written as:

$$\Pi_T = \frac{N}{4} \int d^4k \, \frac{1}{2\pi} \sum_{l=-\infty}^{\infty} \frac{i \cot \chi_l \pi}{2 \, \chi_l} \tag{2.95}$$

To remove the UV divergence, we decided to renormalized it by regularizing each 5D KK-propagators similarly to (72), so that:

$$\Pi_T = \frac{N}{4} \int d^4k \, \frac{1}{2\pi} \sum_{l=-\infty}^{\infty} \frac{i \cot \chi_l \pi - i}{2 \, \chi_l} \tag{2.96}$$

After Wick rotation, separating the $l = 0$ contribution, we get:

$$\begin{aligned} \Pi_T &= \frac{N}{4} \left(\zeta(3) + 4\pi^3 \sum_{l=1}^{\infty} \int_0^{\infty} dk_E \, \frac{k_E^3 \left(\coth \left[\pi \sqrt{k_E^2 + l^2} \, \right] - 1 \right)}{2 \sqrt{k_E^2 + l^2}} \right) \\ &= \frac{N}{4} \, \Delta' \quad \text{with} \quad \Delta' \simeq 1.22 \end{aligned} \tag{2.97}$$

Because of the improper regularization scheme, the finite part is different from the previous correct result. However, the structure is the same, thus providing a powerful way to check the results obtained with the other methods.

Glides

The contribution of the glides is finite, therefore we do not have the same issue with the renormalization which arose for the torus one. Under the glide, x_6 changes sign and therefore:

$$f_l(g(x_6)) = f_l(-x_6 + \pi) = (-1)^l f_{-l}(x_6) \tag{2.98}$$

Due to the orthonormality, the contribution of the $l \neq 0$ modes vanishes, and we are left with

$$\Pi_G = \frac{N}{4} \int d^4k \int_0^{2\pi} dx_5 \, \frac{i \cos \chi_0 (\pi - |x_5 - g(x_5)|)}{2 \, \chi_0 \, \sin \chi_0 \pi} \frac{\sin^2(n x_5)}{2\pi^2} \tag{2.99}$$

After Wick rotation, and integrating in x_5, we obtain:

$$\Pi_G = \frac{N}{4} \, 2\pi^3 \int_0^{\infty} dk_E \, \frac{k_E^3}{k_E \, \sinh \pi k_E} = \frac{N}{4} \, 7\zeta(3) \tag{2.100}$$

That agrees with the result obtained using the winding modes.

Under the second glide

$$f_l(gr(x_6)) = f_l(x_6 + \pi) = (-1)^l f_l(x_6) \tag{2.101}$$

therefore all modes contribute, and a $(-1)^l$ factor appears in the sum:

$$\begin{aligned}
\Pi_{G'} &= \frac{N}{4}\int d^4k \int_0^{2\pi} dx_5 \sum_{l=-\infty}^{\infty} (-1)^l \frac{i\cos\chi_l(\pi - |x_5 - gr(x_5)|)}{2\ \chi_l\ \sin\chi_l\pi} \frac{\sin^2(nx_5)}{2\pi^2} \\
&= \frac{N}{4}\int_0^{\infty} dk_E\ 2\pi^2 k_E^3 \sum_{l=-\infty}^{\infty} (-1)^l \frac{2(k_E^2+l^2)+n^2}{(k_E^2+l^2)\ (k_E^2+l^2+n^2)} \\
&= \frac{N}{4}\int_0^{\infty} dk_E\ \pi^3 \left[\frac{2k_E^2}{\sinh\pi k_E} + \frac{2k_E^3}{\sqrt{n^2+k_E^2}\sinh\left(\pi\sqrt{n^2+k_E^2}\right)}\right] \\
&= \frac{N}{4}\ [7\zeta(3) + B_1(n)]
\end{aligned} \tag{2.102}$$

where

$$B_1(n) = 2\pi^3 \int_0^{\infty} dp\ \frac{p^3}{\sqrt{n^2+p^2}\sinh\left(\pi\sqrt{n^2+p^2}\right)} \tag{2.103}$$

Rotation

Similarly to the glide, for the rotation, only the zero mode contributes:

$$\begin{aligned}
\Pi_R &= \frac{N}{4}\int d^4k \int_0^{2\pi} dx_5\ \frac{i\cos\chi_0(\pi - |x_5 - r(x_5)|)}{2\ \chi_0\ \sin\chi_0\pi} \frac{\sin^2(nx_5)}{2\pi^2} \\
&= \frac{N}{4}\int d^4k\ \frac{in^2}{k^2\ (n^2-k^2)}\,.
\end{aligned} \tag{2.104}$$

After Wick rotation, we regularize the integral by cut off as before:

$$\Pi_R = \frac{N}{4}\int_0^{\Lambda} dk_E\ 2\pi^2 k_E \frac{n^2}{(n^2+k_E^2)} = \frac{N}{4}\quad n^2\pi^2 \log\frac{\Lambda^2+n^2}{n^2}\,. \tag{2.105}$$

2.4 One-loop mass spectrum of $(0,1)$ and $(1,0)$ tiers on the RPP.

2.4.1 Introduction

The degeneracy of each KK level is removed at loop level and in this chapter, we will focus on the modes $(n,0)$ and $(0,n)$ with n odd, because this case covers the lightest tiers, and we will therefore need the mass spectrum of this level to determine the relic density of Dark Matter. As we explain previously and as it will be also detailed in appendix A, the loop contributions (that we generically label Π) can be divided in 4 pieces:

$$\Pi = \Pi_T + \Pi_G + \Pi_{G'} + \Pi_R\ : \tag{2.106}$$

As we already mentioned, the first term Π_T is the contribution we would get from the same fields on a torus and, after renormalization of the bulk kinetic terms, it leaves a finite contribution. The other three terms correspond to the two glides and rotation, in the sense that

their sign depends on the parities (p_r, p_g) of the fields running in the loop. The contribution of the two glides is finite because the glide symmetries do not have any fixed points where a counter-term could be localized. On the other hand, the rotation does generate divergences which can be cut-off by counter-terms localized on the four points left fixed by the rotation, i.e. the two singular points of the orbifold. The singularities will be equally spread on the two points, because of the extended global symmetries of the bulk interactions. In sections 2.4.4 and in chapter 3, we will discuss the generic structure of the counter-terms: for now we will limit ourselves to cutting off the momentum integral in the loop and compute the coefficient on the log divergent term. The estimate of this cut-off scale Λ can be done using a conservative approach which consists in an identification with the lowest scale where the theory starts losing its perturbativity. In extra-dimensional model, this can be done by using a *naive dimensional analysis* and in model with six extra-dimensions, the cut-off scale of the associated effective field theory is pretty low. As a reference, we have chosen to take in this thesis $\Lambda R \sim O(10)$ (74). Finally we have to notice also that bulk interactions respect both KK-parities: p_{KK} and p'_{KK}, therefore there will be no mixing between the states $(n, 0)$ and $(0, n)$: in the following we will compute the diagonal corrections, as the off diagonal ones do generate sub-leading corrections to the spectrum. Mixing between the two states will only be possible through localized interactions if we suppose that p'_{KK} is broken by the UV-completion.

2.4.2 Self-energy of gauge bosons for $(0, n)$ and $(n, 0)$ modes with n odd

The tiers $(0, n)$ and $(n, 0)$ with n odd contain gauge-scalars which correspond to SM gauge bosons. As we explained in equation 2.57, for a generic $SU(N)$ gauge group, this gauge scalars will receive corrections to their mass from the loop diagrams listed in figure 2.7 and expressed in appendix A. The computation of those radiative corrections has be performed using the new method we presented in the previous section and consisting in expanding in KK modes only along one direction and using the re-summed 5D propagator in the sum. The obtained results have been checked in general by using the expansion in 6D KK modes. The winding mode technique could only be used actually for the tadpole computations. The result of the calculation is summarized in table 2.8. The contributions in this table must be multiplied by a normalization factor $\frac{1}{4}\frac{g^2 C(r)}{16\pi^4 R^2}$, where $g = \frac{g_6}{2\pi R}$ is the effective 4D gauge coupling. This relation between g and g_6 is obtained by computing the wavefunction overlapping between two zero-mode

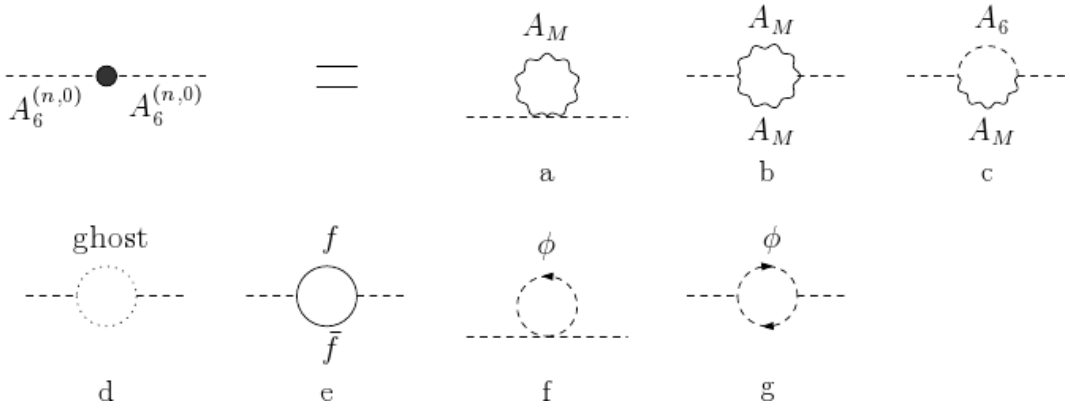

Figure 2.7: One-loop radiative corrections to the gauge scalar self-energy: gauge (a–c), ghost (d), fermion (e) and scalar (f–g) loops.

δm^2 gauge scalars	Π_T	Π_G	$\Pi_{G'}$	Π_R
a	$5T_6$	$5\cdot 7\zeta(3)$	$3\cdot(7\zeta(3)+B_1(n))$	$3n^2\pi^2 L$
b	0	0	$-12B_2(n)$	0
c	$-T_6$	$-3\cdot 7\zeta(3)$	$-(7\zeta(3)+B_3(n))$	$5n^2\pi^2 L$
d	0	0	$+2B_2(n)$	0
e	$-8T_6$	0	0	0
f	T_6	$7\zeta(3)$	$(7\zeta(3)+B_1(n))$	$n^2\pi^2 L$
g	0	0	$-4B_2(n)$	0

Table 2.8: Contribution of gauge, scalar and fermions loops in figure 2.7 to the mass of the gauge scalars in level $(1,0)$-$(0,1)$.

fermions and one zero-mode gauge boson field. $C(r)$ is a gauge group factor and it is defined as $\mathrm{Tr}(t_r^a t_r^b) = C(r)\delta^{a,b}$ for a field in the representation r of a non-abelian group running in the loop. For an abelian $U(1)_Y$, we just replace $C(r)$ by the hypercharge squared Y^2. In the formula, T_6 is the typical sum appearing in the torus compactification (64), we have see in section 2.3.1.

$$T_6 = \frac{1}{\pi}\sum_{(k,l)\neq(0,0)}\frac{1}{(k^2+l^2)^2} \sim 1.92 \tag{2.107}$$

$$L = \log\frac{\Lambda^2R^2+n^2}{n^2} \tag{2.108}$$

L is the log divergence associated with the rotation, and the n-dependent contributions $B_{1,2,3}$ are small corrections listed in the appendix A and coming from heavier modes running in the loop. In this table, we have set to zero the negligible finite contribution coming from the rotation loops and considered only the divergent part.

Summing over the SM fields, the corrections[5] are:

$$\delta m_B^2 = \frac{g'^2}{64\pi^4R^2}\left[-79T_6+14\zeta(3)+\pi^2n^2L+B_1-4B_2\right], \tag{2.109}$$

$$\delta m_W^2 = \frac{g^2}{64\pi^4R^2}\left[-39T_6+70\zeta(3)+17\pi^2n^2L+7B_1-24B_2-2B_3\right], \tag{2.110}$$

$$\delta m_G^2 = \frac{{g_s}^2}{64\pi^4R^2}\left[-36T_6+84\zeta(3)+24\pi^2n^2L+9B_1-30B_2-3B_3\right]. \tag{2.111}$$

Numerically, for n=1, the corrections to the mass $\delta m = \frac{1}{2}\frac{\delta m^2}{m}$ are:

$$\delta m_B R = (-1.4+0.1L)\cdot 10^{-3} = -0.00094\,, \tag{2.112}$$

$$\delta m_W R = (-0.4+5.8L)\cdot 10^{-3} = 0.026\,, \tag{2.113}$$

$$\delta m_G R = (+0.2+28L)\cdot 10^{-3} = 0.13\,; \tag{2.114}$$

where we use $\alpha_s(M_Z)=0.118$, $\alpha(M_Z)=1/127$, $\sin^2\theta_W = 0.23$ and $\Lambda R = 10$ ($L=4.6$).

[5]For instance, the mass correction to $U(1)$ gauge scalar is given by: $\Pi = N_f(2.Y_L^2+Y_E^2+N_c(2.Y_Q^2+Y_U^2+Y_D^2)).(e)+4.Y_h^2((f)+(g))$, where $N_f=3$ is the number of families and $N_c=3$ the number of color. (e),(f) and (g) are the loop contributions extracted from the table 2.8.

2.4.3 Self-energy of fermions for $(0, n)$ and $(n, 0)$ modes with n odd

The corrections to the fermionic Lagrangian, described in figure 2.8 for a generic KK-mode can be written in general as:

$$\delta\mathcal{L} = a_L\bar{\psi}\gamma^\mu p_\mu P_L\psi + a_R\bar{\psi}\gamma^\mu p_\mu P_R\psi - b\bar{\psi}\psi\,. \tag{2.115}$$

The wavefunction renormalization (in general different for the left-handed and the right-handed components) can be re-absorbed by a field renormalization, so that the shift in the mass (at leading order in the corrections) is:

$$\delta m_F = b - m_n\frac{a_L + a_R}{2}\,. \tag{2.116}$$

In table 2.9, we will list the contribution of the gauge and scalar (Higgs) loops to the three terms. The values in this table have to be multiplied by the loop factor $\frac{1}{4}\frac{g^2C_2(r)}{16\pi^4R}$ for the gauge loops (where $C_2(r) = (N^2-1)/2N$ for a fundamental of SU(N), and the charge squared for a U(1)) and $\frac{1}{4}\frac{y_F^2}{16\pi^4R}$ for the Higgs (where y_F is the effective Yukawa coupling).

The n-dependent terms are listed in appendix A and similarly to the gauge boson case, we have set to zero the negligible finite contribution coming from the rotation loops and considered only the divergent part. For a generic fermion in the fundamental representation of SU(2) weak and SU(3) color and with hypercharge Y_F:

$$\delta m_F = \frac{1}{64\pi^4Rn}\left\{\left(21\zeta(3) + 4n^2\pi^2L - F_1 - 6F_2\right)\left(Y_F^2g'^2 + \frac{3}{4}g^2 + \frac{4}{3}g_s^2\right) + \right.$$
$$\left. + \frac{1}{2}\left(21\zeta(3) + n^2\pi^2L - F_1 - 2F_2\right)y_F^2\right\}\,. \tag{2.117}$$

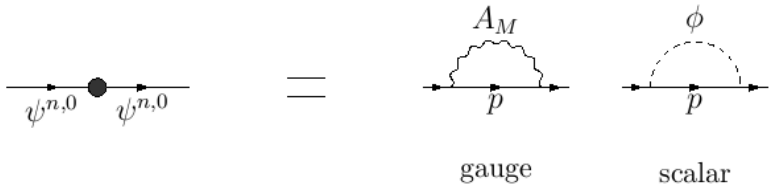

Figure 2.8: One-loop radiative corrections to the fermion self-energy.

fermions	Π_T	Π_G	$\Pi_{G'}$	Π_R
$n^2\,a_L$ gauge	0	$2\cdot 7\zeta(3)$	$2\cdot(-7\zeta(3) + F_1(n) - F_2(n))$	0
$n^2\,a_R$ gauge	0	$2\cdot 7\zeta(3)$	$-2F_2(n)$	0
$n^2\,b$ gauge	0	$4n\cdot 7\zeta(3)$	$-6nF_2(n)$	$4n^3\pi^2L$
$n^2\,a_L$ scalar	0	$7\zeta(3)$	$-7\zeta(3) + F_1(n) - F_2(n)$	$n^2\pi^2L$
$n^2\,a_R$ scalar	0	$7\zeta(3)$	$-F_2(n)$	0
$n^2\,b$ scalar	0	$2n\cdot 7\zeta(3)$	$-nF_2(n)$	$n^3\pi^2L$

Table 2.9: Contributions of gauge and scalar loops to the mass and kinetic renormalization of SM fermions in level $(1,0)$-$(0,1)$.

Numerical values of the mass splittings, at level $n = 1$, for each SM fermion are summarized in table 2.10.

$\delta m_F R$	Q	U	D	L	E	(N)
light gen.s	0.075	0.067	0.065	0.012	0.004	(0)
third gen	0.081	0.072	0.065	0.012	0.004	(0)

Table 2.10: Mass corrections for SM fermions in level $(1,0)$-$(0,1)$. Here we used the same numerical inputs as for the bosons, and $y_{\text{top}} = 1$.

2.4.4 Localized operators

In this section, we will describe another source of mass that can be added to the tree level mass of KK-modes. We have seen that because of the rotation symmetry of the Real Projective Plane, loop corrections to the masses are log-divergent. In this case, to regularize them we need to introduce new counter-terms and they can be written on the singular points of the orbifold. Due to the symmetries of the bulk interactions, we just need that the counter-terms are equal on all the singular points. However, here we will give a more general approach, and add different terms on the two singularities. In this case, one of the residual KK-parity can be broken and we will obtain the most general contribution from localized operators on the Real Projective Plane. In order to keep the glide-invariant form of the Lagrangian, we will introduce two operators:

$$\delta_0 = \frac{1}{2}\left(\delta(x_5)\delta(x_6) + \delta(x_5-\pi)\delta(x_6-\pi)\right) \tag{2.118}$$

$$\delta_\pi = \frac{1}{2}\left(\delta(x_5)\delta(x_6-\pi) + \delta(x_5-\pi)\delta(x_6)\right) \tag{2.119}$$

and label the two singular points with a subscript 0 for the point $(0,0) \sim (\pi,\pi)$, and π for $(0,\pi) \sim (\pi,0)$.

In general the localized interactions must respect only the 4D Lorentz invariance. For a scalar field like the Higgs many terms can be added including a mass term: here we will neglect this case because of the many free parameters and the low phenomenological interest of the Higgs resonances in this model but for few more details about localized interactions for scalar fields, we invite the reader to look at chapter 3.

Concerning gauge fields, the situation is a bit simpler even if the Lagrangian on the singular points does not need to respect the gauge invariance in 6D. However, for our current study of mass corrections of the physical fields, we can choose an arbitrary gauge. Masses of fields being by definition gauge invariant observables every contribution will gather and give gauge invariant results. Therefore we choose the $\xi = -3$ gauge which has the particularity to lead to a gauge invariant form of the counter-terms Lagrangian (68) as we will discuss in chapter 3:

$$\mathcal{L}_i = \frac{\delta_i}{\Lambda^2}\left(-\frac{r_{1i}}{4}F_{\mu\nu}^2 - \frac{r_{2i}}{2}F_{56}^2 + \frac{r_{5i}}{2}F_{5\mu}^2 + \frac{r_{6i}}{2}F_{6\mu}^2 + \frac{r_{56i}}{2}F_{5\mu}F_6^\mu\right) \tag{2.120}$$

where $i = 0, \pi$, and the cut-off suppression compensates for the dimension of the 6D fields (2 for a boson and 5/2 for a spinor). For a Standard Model gauge boson, with parities $(+,+)$, notice that both $A_{5,6}$ and $\partial_{5,6}A_\mu$ vanish on the singular points, therefore $F_{5\mu} = F_{6\mu} = 0$ and $F_{56} = \partial_5 A_6 - \partial_6 A_5$:

$$\mathcal{L}_i = \frac{\delta_i}{\Lambda^2}\left(-\frac{r_{1i}}{4}F_{\mu\nu}^2 - \frac{r_{2i}}{2}(\partial_5 A_6 - \partial_6 A_5)^2\right) . \tag{2.121}$$

The first term is a correction to the kinetic term of the vector bosons, and it also introduces mixing between modes with different (k,l). This will play a crucial role in phenomenology allowing new couplings between levels. Here we will assume those terms to be small, of the same order as the 1-loop corrections: this is a reasonable assumptions because they are in fact counter-terms required by divergences at 1-loop and their coefficient is suppressed by the cut-off of the model. Therefore, most off-diagonal terms will give higher order corrections to the masses: this is not the case, however, for tiers that are degenerate like (k,l) and (l,k). In fact, exchanging the two extra directions is a good symmetry of the Real Projective Plane if we consider the case where the radii $R_5 = R_6$ are degenerate at tree level). When expanding the localized terms in KK modes, the 2×2 blocks will have equal entries, while the loop contributions will be such that the diagonal entries are equal: from this, we see that the block can be diagonalized by the sum and difference of the two states [6]. Therefore, we define

$$(k,l)_\pm = \frac{(k,l) \pm (l,k)}{\sqrt{2}} , \quad \text{with } l > k\,, l, k = 0, 1, \ldots \infty \tag{2.122}$$

and parametrize the correction to the kinetic term as:

$$\mathcal{Z}_{ij} = \delta_{ij} + \frac{z_{ij}}{4\pi^2\Lambda^2} \tag{2.123}$$

The values of the correction from localized terms to gauge vector are given in table 2.11.

Some modes like $(0,2l)_-$, $(2k,2l)_-$, $(2k-1,2l-1)_-$, $(2k,2l-1)_\pm$ and $(2k-1,2l)_\pm$ (with $l>k$) are not affected by those localized counter-terms. Therefore they could have phenomenological interest because of the predictivity of masses and couplings due to finite quantum corrections at one-loop level. However, in the studied case, it seems that most of those levels do not couple to Standard Model particles, but this will have to be explored more deeply.

[6] The situation is more complicated when k and l are part of a Pythagorean triple such that $k^2+l^2=n^2$ or quartet with $k^2+l^2=n^2+m^2$: in this cases 3 or 4 states will be degenerate. However, this situation only happens for relatively large integers, the smallest ones being $(0,5)-(3,4)$ with mass $5\sqrt{2}\sim 7$, which is too close to the cutoff and therefore phenomenologically not interesting: for this reason we will not explore the possibility of Pythagorean triples any further.

z_{ij}	$(0,0)$	$(0,2l)_+$	$(2l,2l)$	$(2k,2l)_+$	$(2l-1,2l-1)$	$(2k-1,2l-1)_+$
$(0,0)$	r_{1+}	$2r_{1+}$	$2r_{1+}$	$2\sqrt{2}r_{1+}$	$2r_{1-}$	$2\sqrt{2}r_{1-}$
$(0,2l')_+$	$2r_{1+}$	$4r_{1+}$	$4r_{1+}$	$4\sqrt{2}r_{1+}$	$4r_{1-}$	$4\sqrt{2}r_{1-}$
$(2l',2l')$	$2r_{1+}$	$4r_{1+}$	$4r_{1+}$	$4\sqrt{2}r_{1+}$	$4r_{1-}$	$4\sqrt{2}r_{1-}$
$(2k',2l')_+$	$2\sqrt{2}r_{1+}$	$4\sqrt{2}r_{1+}$	$4\sqrt{2}r_{1+}$	$8r_{1+}$	$4\sqrt{2}r_{1-}$	$8r_{1-}$
$(2l'-1,2l'-1)$	$2r_{1-}$	$4r_{1-}$	$4r_{1-}$	$4\sqrt{2}r_{1-}$	$4r_{1+}$	$4\sqrt{2}r_{1+}$
$(2k'-1,2l'-1)_+$	$2\sqrt{2}r_{1-}$	$4\sqrt{2}r_{1-}$	$4\sqrt{2}r_{1-}$	$8r_{1-}$	$4\sqrt{2}r_{1+}$	$8r_{1+}$

Table 2.11: Corrections to the kinetic terms of the vector gauge bosons. For convenience we introduce the natural sum-difference basis; then the counter-terms are expressed in terms of $r_{1\pm} = r_{10} \pm r_{1\pi}$).

As expected, the correction to the zero mode renormalizes the gauge coupling:

$$g^2 = \frac{g_6^2}{4\pi^2}\frac{1}{1+\frac{r_{10}+r_{1\pi}}{4\pi^2\Lambda^2}} \sim \frac{g_6^2}{4\pi^2}\left(1-\frac{r_{10}+r_{1\pi}}{4\pi^2\Lambda^2}+\dots\right) \tag{2.124}$$

The diagonal entries of the table 2.11 affect the masses:

$$m^2_{(k,l)} = \sqrt{k^2+l^2}\left(1-\frac{z_{(k,l)}}{4\pi^2\Lambda^2}+\dots\right) \tag{2.125}$$

.

A same analysis can be performed for the scalar components of the gauge fields: note that no further mixing between the vector and scalars is induced, therefore the tree level bulk gauge fixing term is still appropriate. In this case, it is the $(k,l)_{\text{ev.}}$ modes to be unaffected (in unitary gauge), and the correction is a mass term

$$\delta m^2_{i,j} = m_i m_j \frac{\delta_{ij}}{4\pi^2\Lambda^2} \tag{2.126}$$

In the sum-difference basis, we obtain the contributions listed in table 2.12.

For fermions, due to the vanishing of one of the two 4D chiral components, no mass term can be added and only operators of dimension 6 (like in the gauge boson case) are relevant. We will focus later on this case also in chapter 3

2.4.5 Electroweak symmetry breaking effect on the mass splittings

Mass contribution to the heavy states will also appear through the Higgs mechanism. As we already mentioned in this thesis, with UED models we allow the Higgs boson to propagate in the bulk of the extra-dimensions. Like in the Standard Model, the negative mass present in the Higgs potential will generate a vacuum expectation value for the 6D higgs field. This vev is flat along the new extra-dimensions and will not generate mixing between different tiers. This is crucial because it means that the KK-decomposition we used previously can still be used to describe mass eigenstates. By consequence, the (0,0) mode will lead to the well-known Standard Model spectrum and the model will be protected from tree-level mixing between heavier states and SM.

For heavier states, a mixing will be generated between the neutral part of the weak gauge boson W^3 and the hypercharge gauge boson B in a similar way to the Standard Model. The value of the Weinberg angle will be different from to the SM one, because loop effects will correct the masses of W_3 and B as we have seen in the previous section. In the fermion sector it will be similar: we will have a mixing between the doublet and the singlet corresponding respectively to the left-handed and right-handed part of SM field. This effect will be mediated by Yukawa interactions and will be thereby sizable only for the top quark.

δ_{ij}	$(0,2l-1)_+$	$(0,2l-1)_-$	$(2k,2l-1)_+$	$(2k,2l-1)_-$
$(0,2l'-1)_+$	$4r_{2\pi}$	0	0	$4\sqrt{2}r_{2\pi}$
$(0,2l'-1)_-$	0	$4r_{20}$	$4\sqrt{2}r_{20}$	0
$(2k',2l'-1)_+$	0	$4\sqrt{2}r_{20}$	$8r_{20}$	0
$(2k',2l'-1)_-$	$4\sqrt{2}r_{2\pi}$	0	0	$8r_{2\pi}$

Table 2.12: Corrections to the kinetic terms of the scalar gauge bosons in the natural sum-difference basis; then the counter-terms are expressed in terms of $r_{2\pm} = r_{20} \pm r_{2\pi}$).

Gauge bosons: general analysis

The Higgs vev introduces new mixing between the vectors and some scalar components that must be cancelled by a suitable gauge fixing term. For an abelian gauge group, the gauge fixing term in equation 2.31 is replaced by

$$\mathcal{L}_{\xi-\text{gauge}} = -\frac{1}{2\xi}\left(\partial_\mu A^\mu - \xi(\partial_5 A_5 + \partial_6 A_6 - g v_6 \varphi_0)\right)^2 \tag{2.127}$$

if the neutral part of the Higgs boson can be written as:

$$\phi_0 = \frac{1}{\sqrt{2}}\left(v_6 + h + i\varphi_0\right) \tag{2.128}$$

The equations of motion of the vector part are modified simply by the addition of a mass term $m_V^2 = \frac{g_6^2 v_6^2}{4}$. For the scalar sectors, we have now mixing between the three scalars of the theory $A_{5,6}$ and φ_0. The bilinear Lagrangian becomes:

$$\mathcal{L}_{A_5,A_6,\varphi_0} = \int_0^{2\pi} dx_5\, dx_6\, \frac{1}{2}(A_5, A_6, \varphi_0)\cdot \mathcal{D}^2 \cdot \begin{pmatrix} A_5 \\ A_6 \\ \varphi_0 \end{pmatrix}$$

$$\text{where} \quad \mathcal{D}^2 = \begin{pmatrix} -\partial_\mu^2 + \partial_6^2 + \xi\partial_5^2 - m_V^2 & (\xi-1)\partial_5\partial_6 & -(\xi-1)m_V\partial_5 \\ (\xi-1)\partial_5\partial_6 & -\partial_\mu^2 + \partial_5^2 + \xi\partial_6^2 - m_V^2 & -(\xi-1)m_V\partial_6 \\ (\xi-1)m_V\partial_5 & (\xi-1)m_V\partial_6 & -\partial_\mu^2 + \partial_6^2 + \partial_5^2 - \xi m_V^2 \end{pmatrix} \tag{2.129}$$

We can then derive the equations of motion for the scalar sector:

$$(p^2 - m_V^2)A_5 + \partial_6(\partial_6 A_5 - \partial_5 A_6) + m_V\partial_5\varphi_0 + \xi\partial_5(\partial_5 A_5 + \partial_6 A_6 - m_V\varphi_0) = 0 \tag{2.130}$$

$$(p^2 - m_V^2)A_6 + \partial_5(\partial_5 A_6 - \partial_6 A_5) + m_V\partial_6\varphi_0 + \xi\partial_6(\partial_5 A_5 + \partial_6 A_6 - m_V\varphi_0) = 0 \tag{2.131}$$

$$(p^2 + \partial_5^2 + \partial_6^2)\phi_0 - m_V(\partial_5 A_5 + \partial_6 A_6) + \xi m_V(\partial_5 A_5 + \partial_6 A_6 - m_V\varphi_0) = 0 \tag{2.132}$$

In the Feynman-'t Hooft gauge ($\xi = 1$), these equations decouple:

$$(p^2 - m_V^2 + \partial_5^2 + \partial_6^2)\begin{bmatrix} A_5 \\ A_6 \\ \phi_0 \end{bmatrix} = 0 \tag{2.133}$$

and we have three independent towers with masses $m_{(l,k)}^2 = l^2 + k^2 + m_V^2$ but they have different parities under rotation and glide.

In the Unitary gauge, $\xi \to \infty$ and we have to impose the condition:

$$m_V\phi_0 = \partial_5 A_5 + \partial_6 A_6 \tag{2.134}$$

We obtain then the same decoupled equations as in the Feynman-'t Hooft gauge, however the fields are not independent anymore. One combination will be a Goldstone part A_π which disappears, being eaten by the vector part of the gauge boson and it remains two towers of physical

scalars: $A_{\varphi 1}$ and $A_{\varphi 2}$:

$$\begin{aligned} A_5^{(-+)} &= \sum f_5(x_5,x_6)A_{\varphi 1}^{(k,l)} + g_5(x_5,x_6)A_{\varphi 2}^{(k,l)} \\ A_6^{(--)} &= \sum f_6(x_5,x_6)A_{\varphi 1}^{(k,l)} + g_6(x_5,x_6)A_{\varphi 2}^{(k,l)} \\ \varphi_0^{(++)} &= \sum f_0(x_5,x_6)A_{\varphi 1}^{(k,l)} + g_0(x_5,x_6)A_{\varphi 2}^{(k,l)} \end{aligned} \tag{2.135}$$

One solution of the constraint 2.134, for instance $A_{\varphi 1}$, has the form:

$$\partial_5 A_5 + \partial_6 A_6 = 0 \quad \text{and} \quad \phi_0 = 0 \tag{2.136}$$

this solution corresponds to the physical scalar described in the previous sections, the effect of the Higgs VEV only appears in the extra mass contribution m_V^2. The second independent combination of states $A_{\varphi 2}$, satisfying the condition 2.134, is a new physical scalar, mainly consisting of Higgs component: if the gauge symmetry is unbroken by the orbifold. The wavefunctions for this new scalar are given in table 2.13.

Mass of electroweak gauge bosons of level $(1,0)$ and $(0,1)$

If we consider $(n,0)$ and $(0,n)$ levels with n odd, the gauge bosons will be scalars. After neglecting localized term contributions, the masses of the neutral electroweak gauge bosons will be given at one-loop level by the following Lagrangian:

$$\begin{aligned} \mathcal{L} &\supset \begin{pmatrix} W_n^3 & B_n \end{pmatrix} \cdot \begin{pmatrix} \delta m_W^2 + g_w^2 v^2/4 & -g_1 g_w v^2/4 \\ -g_1 g_w v^2/4 & \delta m_B^2 + g_1^2 v^2/4 \end{pmatrix} \cdot \begin{pmatrix} W_n^3 \\ B_n \end{pmatrix} \\ &\supset \begin{pmatrix} W_n^3 & B_n \end{pmatrix} \cdot \begin{pmatrix} \delta m_W^2 + m_W^2 & -\tan\theta_W m_W^2 \\ -\tan\theta_W m_W^2 & \delta m_B^2 + \tan^2\theta_W m_W^2 \end{pmatrix} \cdot \begin{pmatrix} W_n^3 \\ B_n \end{pmatrix} \end{aligned} \tag{2.137}$$

where for instance, W_n represents $W_6^{(n,0)}$ or $W_5^{(0,n)}$. Note again that neither the loop corrections, nor the VEV will mix (n,0) and (0,n) levels with n odd. It will not be the case for n even as we will see in chapter 3. Then like in the Standard Model, the mass matrix can be diagonalized by:

$$\begin{pmatrix} Z_n \\ A_n \end{pmatrix} = \begin{pmatrix} \cos\theta_n & \sin\theta_n \\ -\sin\theta_n & \cos\theta_n \end{pmatrix} \cdot \begin{pmatrix} W_n^3 \\ B_n \end{pmatrix} \tag{2.138}$$

(k,l)	p_{KK}	$g_0^{(++)}$	$g_5^{(-+)}$	$g_6^{(--)}$
$(0,0)$	$+$			
$(0,2l)$	$+$	$\frac{2l}{\sqrt{2}\pi\sqrt{(2l)^2+m_V^2}}\cos 2lx_6$		$\frac{m_V}{\sqrt{2}\pi\sqrt{(2l)^2+m_V^2}}\sin 2lx_6$
$(0,2l-1)$	$-$			
$(2k,0)$	$+$	$\frac{2k}{\sqrt{2}\pi\sqrt{(2k)^2+m_V^2}}\cos 2kx_5$	$\frac{m_V}{\sqrt{2}\pi\sqrt{(2k)^2+m_V^2}}\sin 2kx_5$	
$(2k-1,0)$	$-$			
$(k,l)_{\text{k+l even}}$	$+$	$\frac{k^2+l^2}{\pi N_{k,l}}\cos kx_5\cos lx_6$	$\frac{km_V}{\pi N_{k,l}}\sin kx_5\cos lx_6$	$\frac{lm_V}{\pi N_{k,l}}\cos kx_5\sin lx_6$
$(k,l)_{\text{k+l odd}}$	$-$	$\frac{k^2+l^2}{\pi N_{k,l}}\sin kx_5\sin lx_6$	$-\frac{km_V}{\pi N_{k,l}}\cos kx_5\sin lx_6$	$-\frac{lm_V}{\pi N_{k,l}}\sin kx_5\cos lx_6$

Table 2.13: Normalized wavefunctions for the scalar $A_{\varphi 2}$ sector, where $N_{k,l} = \sqrt{(k^2+l^2)(k^2+l^2+m_V^2)}$. The wavefunctions of the scalar $A_{\varphi 1}$ are : $f_0 = 0$ and f_5 and f_6 are given in table 2.2.

where θ_n is the Weinberg angle of the tiers $(n,0)$ or $(0,n)$ and is defined by:

$$\tan\theta_n = \frac{m_{Z_n}^2 - m_{A_n}^2 + m_Z^2 - 2m_W^2 + \delta m_B^2 - \delta m_W^2}{2m_W m_Z \sin\theta_W}\,. \tag{2.139}$$

The mass eigenstates is finally given by:

$$m_{A_n,Z_n}^2 = \frac{n^2}{R^2} + \frac{1}{2}\Big(m_Z^2 + \delta m_B^2 + \delta m_W^2 \mp \sqrt{(m_Z^2 + \delta m_B^2 - \delta m_W^2)^2 - 4m_W^2(\delta m_B^2 - \delta m_W^2)}\Big) \tag{2.140}$$

We can easily see that the Weinberg angle is not the SM one because $\delta m_B^2 \neq \delta m_W^2$. In the figure 2.9 we show for the lightest tiers how the mixing angle decreases for large m_{KK}, inducing the decoupling of B and W_3 at this scale. We can stress also that this decoupling effect will be more and more sizeable for heavier tiers as the rotation contribution to δm_B^2 and δm_W^2 is proportional to n^2.

Then let us consider the effects of the localized kinetic terms. Because the effects of bulk contributions from loops and Higgs VEV are the same for $(0,n)$ and $(n,0)$ levels, they are also diagonal in the basis $(0,n)_\pm$. The extra-dimension contributions are modified and given by:

$$\begin{aligned} \delta m_{B,W}^2 &\to \delta m_{B,W}^2 + \frac{n^2 r_{2\pi}^{B,W}}{\pi^2\Lambda^2} \quad \text{for} \quad (0,n)_+ \\ \delta m_{B,W}^2 &\to \delta m_{B,W}^2 + \frac{n^2 r_{20}^{B,W}}{\pi^2\Lambda^2} \quad \text{for} \quad (0,n)_- \end{aligned} \tag{2.141}$$

Concerning the charged W's, their masses is given by:

$$m_{W^+}^2 = \frac{n^2}{R^2} + \delta m_W^2 + m_W^2 \tag{2.142}$$

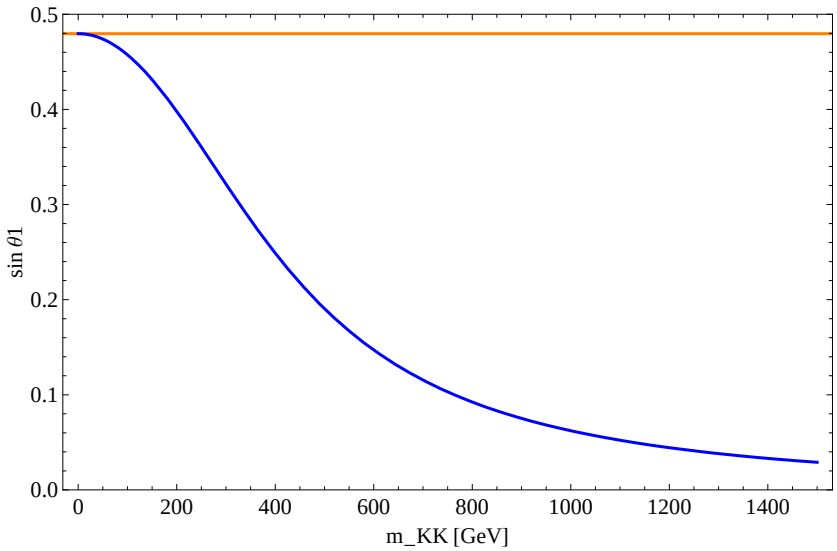

Figure 2.9: Mixing angle $\sin\theta_1$ between the weak gauge scalars as a function of m_{KK}. For zero KK mass we obtain the SM value, for large masses the mixing angle vanishes. The flat line represents the value of the SM $\sin\theta_W$.

and the contribution of the localized terms can be added in the same way as for the neutral gauge bosons. Similar formulas apply for the vector states in the $(n,0)$ and $(0,n)$ tiers, with n even, and to the (k,l) level: however, we need to take into account the loop-induced mixing between the vector and the scalars, therefore the gauge fixing must be redefined at 1-loop.

Fermions of level (1,0) and (0,1)

The Yukawa coupling will also induce a redefinition of eigenstates. As this effect is mostly relevant for the top quark, we will focus on this case and write the Lagrangian of Yukawa interactions as:

$$\begin{aligned} S_{\text{Yukawa}} \supset -\int dx_5 dx_6 \, \frac{Y_6}{\sqrt{2}} \bar{\Psi}_Q h \Psi_U + h.c. = \\ -\int dx_5 dx_6 \, Y_6 \left[\eta_{Q+} h \chi_{U-} + \eta_{Q-} h \chi_{U+} + \bar{\chi}_{Q+} h \bar{\eta}_{U-} + \bar{\chi}_{Q-} h \bar{\eta}_{U+}\right] + h.c. \end{aligned} \tag{2.143}$$

where the Q index is for the doublet field under $SU(2)_W$ and U is for the up-type singlet field. As we discussed in section 1.3.4, this term can be written only if $p_r(Q) = -p_r(U)$ and after expanding in KK-mode those fields, we obtain the mass corrections for each levels. For the Standard Model zero modes:

$$\mathcal{L}_{\text{Yukawa(0,0)}} = -\frac{p_g(Q) + p_g(U)}{2} \frac{Y_6 v_6}{\sqrt{2}} \bar{q}_l^{(0,0)} u_r^{(0,0)} + h.c. \tag{2.144}$$

where $u_{l,r}^{(k,l)}$ and $q_{l/r}^{(k,l)}$ denote respectively the (k,l) 4D-modes of the left- and right-handed components of the singlet and doublet 6D fields. If the fields have the same parity under the glide $p_g(Q) = p_g(U) = p_g$, the mass term is non-vanishing and:

$$m_{\text{top}} = p_g \frac{Y_6 v_6}{\sqrt{2}} \tag{2.145}$$

For $(l,0)$ and $(0,l)$ modes, we obtain:

$$\mathcal{L}_{\text{Yukawa(l,0)}-\text{(0,l)}} = -(-1)^l m_{\text{top}} \left(\bar{q}_l u_r - \bar{q}_r u_l\right) + h.c. \tag{2.146}$$

For the (k,l) modes, the situation is more complicated due to the presence of 2 degenerate states as we discussed in section 2.2: the mass term can be written in general as:

$$\begin{aligned} \mathcal{L}_{\text{Yukawa(k,l)}} = -(-1)^{k+l} m_{\text{top}} (\cos\alpha_Q \cos\alpha_U - \sin\alpha_Q \sin\alpha_U) \\ \left(\bar{q}_l^{(k,l)} u_r^{(k,l)} - \bar{q}_r^{(k,l)} u_l^{(k,l)}\right) + h.c. \end{aligned} \tag{2.147}$$

where the two choices $\alpha_{Q/U} = \theta_{Q/U}, \pi/2 + \theta_{Q/U}$ label the four independent states, and $\theta_{Q/U}$ are arbitrary parameters. If we chose $\theta_Q = -\theta_U$, two sets of states decouple so that there are no off-diagonal mass entries, and the mass matrices reduce to

$$\mathcal{L}_{\text{Yukawa(k,l)}} = -(-1)^{k+l} m_{\text{top}} \left(\bar{q}_l^{(k,l)} u_r^{(k,l)} - \bar{q}_r^{(k,l)} u_l^{(k,l)}\right) + h.c. \tag{2.148}$$

This is therefore a general expression valid for all modes. To find the mass eigenstates, we need to take into account the loop corrections to the Q and U masses. For the $(1,0)$ and $(0,1)$ tiers:

$$\mathcal{L}_{\text{mass}} = -\begin{pmatrix} \bar{q}_l & \bar{u}_l \end{pmatrix} \cdot \begin{pmatrix} \frac{1}{R} + \delta m_Q & -m_{\text{top}} \\ m_{\text{top}} & \frac{1}{R} + \delta m_U \end{pmatrix} \cdot \begin{pmatrix} q_r \\ u_r \end{pmatrix} + h.c. \tag{2.149}$$

This bilinear form will be diagonalized by considering two rotation matrices for the left-handed and right-handed components:

$$\begin{pmatrix} t_{1l} \\ t_{2l} \end{pmatrix} = U_l \begin{pmatrix} q_l \\ u_l \end{pmatrix} \quad \text{and} \quad \begin{pmatrix} t_{1r} \\ t_{2r} \end{pmatrix} = U_r \begin{pmatrix} q_{l,r} \\ u_{l,r} \end{pmatrix} \tag{2.150}$$

where $U_l^\dagger U_l = U_r^\dagger U_r = \mathbf{1}$. We can show easily that U_l and U_r diagonalize the mass-matrix squared $M^\dagger M$:

$$M^\dagger M = \begin{pmatrix} (\frac{1}{R} + \delta m_Q)^2 + m_{\text{top}}^2 & m_{\text{top}}(\delta m_Q - \delta m_U) \\ {}_{\text{top}}(\delta m_Q - \delta m_U) & (\frac{1}{R} + \delta m_U)^2 + m_{\text{top}}^2 \end{pmatrix} \tag{2.151}$$

and

$$U_l M M^\dagger U_l^\dagger = U_r^\dagger M^\dagger M U_r = \begin{pmatrix} m_{t1}^2 & 0 \\ 0 & m_{t2}^2 \end{pmatrix} \tag{2.152}$$

The mass eigenvalues are then given by:

$$m_{t1/2}^2 = \frac{1}{R^2} + m_{\text{top}}^2 + \delta m_Q \left(\frac{1}{R} + \frac{1}{2}\delta m_Q \pm B \right) + \delta m_U \left(\frac{1}{R} + \frac{1}{2}\delta m_U \mp B \right) \tag{2.153}$$

with

$$B = \sqrt{\left(\frac{1}{R} + \frac{\delta m_Q + \delta m_U}{2} \right)^2 + m_{\text{top}}^2} \tag{2.154}$$

and the eigenstates are:

$$\begin{pmatrix} t_{1l} \\ t_{2l} \end{pmatrix} = \begin{pmatrix} \cos\beta_t & +\sin\beta_t \\ -\sin\beta_t & \cos\beta_t \end{pmatrix} \begin{pmatrix} q_l \\ u_l \end{pmatrix} \quad \text{and} \quad \begin{pmatrix} t_{1r} \\ t_{2r} \end{pmatrix} = \begin{pmatrix} \cos\beta_t & -\sin\beta_t \\ +\sin\beta_t & \cos\beta_t \end{pmatrix} \begin{pmatrix} q_{l,r} \\ u_{l,r} \end{pmatrix} \tag{2.155}$$

with the mixing angle $\tan\beta_t$ defined as:

$$\tan\beta_t = \frac{1}{m_{\text{top}}} \left[B - \left(\frac{1}{R} + \frac{\delta m_Q + \delta m_U}{2} \right) \right] \tag{2.156}$$

The figure 2.10 give the m_{KK}-dependence of this angle.

Finally we summarize in figure 2.11, the mass splitting of the gauge bosons and fermions of the first tier. In this plot, we neglect the contributions of the counter-terms due to our poor understanding of the UV-completion of the theory, nevertheless, in some sense, we took some of the order of magnitude of this effect into account through the rotation contribution of the loops. There are two generic features in this plot: first, the loop corrections induce correction of the form K_1/R^2 where K_1 is a generic coefficient coming from peculiarity of quantum effects, then the Higgs mechanism will give a constant correction proportional to the Higgs vev v. For a generic term, we have:

$$m = m_{KK} + \frac{K_1}{R^2} + K_2 v^2 = m_{KK} + K_1 m_{KK}^2 + K_2 v^2 \tag{2.157}$$

which implies:

$$\delta m = m - m_{KK} = \frac{\delta m^2}{2m} \sim \frac{\delta m^2}{2m_{KK}} \begin{cases} \sim \frac{K_1 m_{KK}}{2} & \text{for} \quad m_{KK} \gg v \\ \sim \frac{K_2 v^2}{m_{KK}} & \text{for} \quad v \gg m_{KK} \end{cases} \tag{2.158}$$

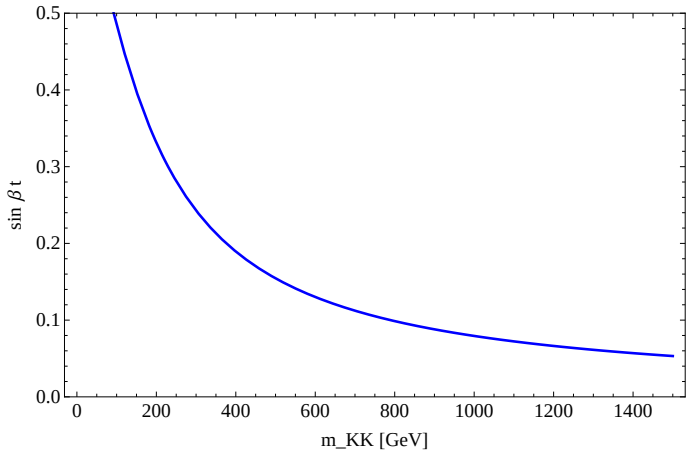

Figure 2.10: Mixing angle $\sin\beta_t$ in the top sector as a function of m_{KK}.

2.5 Extra-dimension radii from Dark Matter constraints

In this last section, we will present the main ideas and details of the calculations which allow us to extract first limits on the extra-dimension radii from cosmological constraints on the Dark Matter relic abundance: this step being essential to understand the motivation to continue the study of such models. Following the prescription proposed in the paper of G. Servant and T.Tait (39), we perform a first analytical estimate of this Dark Matter constraint. Even if the calculation is very sensitive to cosmological parameter, it will help us to find a mass-range of validity for this 6D UED model. Actually, if we can consider that the localized interaction are negligible, extra-dimensional models are interesting because in general only two parameters are relevant to look at Dark Matter constraints: m_{KK}, the characteristic size of the extra-dimensions and m_h, the Higgs mass.

2.5.1 Annihilation of the Dark Scalar Photon

First we have to determine what is the nature of the Dark Matter candidate of our model. If we consider the figure 2.11, for masses $m_{KK} < 200$ GeV, we see that the right-handed electron is the lightest particle. This charged particle cannot play the role of viable Dark Matter candidate, so that it will put a lower bound on the mass-range for the model. Then for masses $m_{KK} > 200$ GeV, the natural Dark Matter candidate is the *scalar photon* which is stable and neutral under the Standard Model gauge group.

As we explained in section 1.2, we can solve then the Boltzmann equations and derive the relic abundance of Dark Matter universe. Therefore, we need to consider the annihilation cross section of $A_5^{0,1}$ or $A_6^{1,0}$ into SM particles. For the first analytical analysis that we proposed, we have decided to neglect the electroweak symmetry breaking effects for the Standard Model particles. This implies that all Standard Model particles will be massless, however the effect of the longitudinal polarization of W and Z are implicitly taken into account through the decay of the scalar photon into the Higgs doublet ϕ. Finally, in our calculation we keep the effect of electroweak symmetry breaking on the Weinberg angle of the first tiers appearing between the heavier gauge bosons and the dark scalar photon. The relevant annihilation processes are then summarized in table 2.14. After expanding for small velocity, the averaged cross-section is then

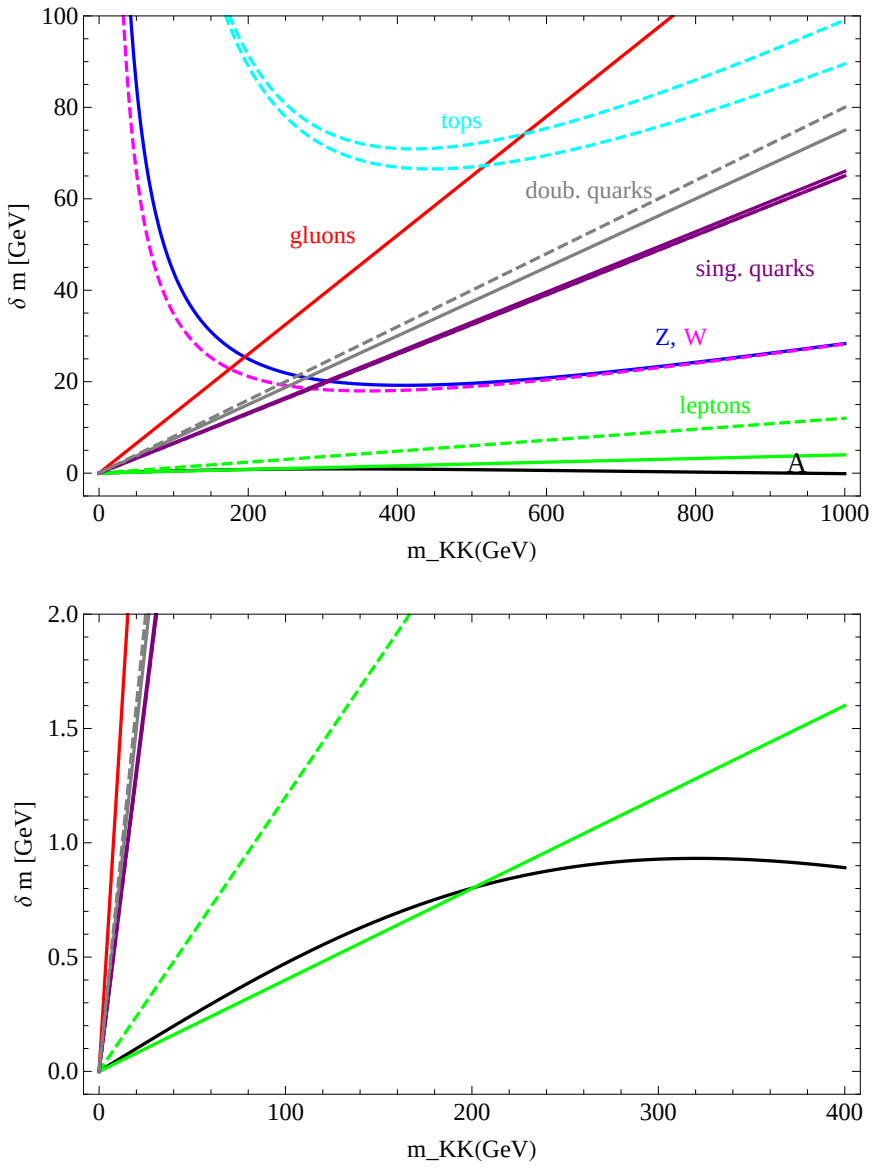

Figure 2.11: Mass splitting between the different states in the tier 1 as a function of m_{KK}: in black the scalar photon (LLP for $m_{KK} > 200$ GeV), in blue the Z, in magenta the W, in solid red the gluon, in green the leptons, in purple the light singlet quarks, in gray the light doublets and in dashed cyan the tops.

given by:

$$\begin{aligned} a =& a_1 + a_2 \\ =& \frac{4\pi\alpha_w^2 \sin\theta_1^4}{m_{KK}^2} + \frac{\pi\alpha_w^2 \sin\theta_1^4}{8m_{KK}^2} \frac{\sin^4(\theta_1+\theta_W) + \sin^4(\theta_1-\theta_W)}{\cos\theta_W^4} \end{aligned} \tag{2.159}$$

$$\begin{aligned} b =& b_1 + b_2 \\ =& -\frac{10\pi\alpha_w^2 \sin\theta_1^4}{3m_{KK}^2} - \frac{\pi\alpha_w^2 \sin\theta_1^4}{16m_{KK}^2} \frac{\sin^4(\theta_1+\theta_W) + \sin^4(\theta_1-\theta_W)}{\cos\theta_W^4} \end{aligned} \tag{2.160}$$

Initial states	Final states	Feynman diagrams	a	b
$A_6^{1,0}$ $A_6^{1,0}$	f $\bar{f}$	$t(f_{1R}, f_{1L})$	0	0
$A_6^{1,0}$ $A_6^{1,0}$	$W+W-$	$t(W), u(W)$, contact	a_1	b_1
$A_6^{1,0}$ $A_6^{1,0}$	ϕ ϕ^*	contact	a_2	b_2

Table 2.14: Relevant Feynman diagrams for $A_6^{1,0}$ annihilations into Standard model particles. t(x),s(x) and u(x) denotes a tree-level diagram with an x-exchange in the s-, t-, u- channel. "contact" is for the four-point interaction and f refers to any fermions and ϕ to the full Higgs doublet.

Here we notice that the average cross-section does not depend on the fermionic degrees of freedom; this feature is due to the spinless nature of the dark photon. The annihilation is mainly dominated by the decay into W^+W^-. This effect is a consequence of the small mass-splittings inside the first tiers. The Weinberg angle of $(1,0)$ and $(0,1)$ is actually not negligible anymore, contrary to the Chiral Square case (75), for instance, where they can assume that the lightest Kaluza-Klein particle is a pure-B gauge boson and where they find a preferred mass range around 200 GeV (for $m_h \ll m_{KK}$). Here, the characteristic spectrum of the RPP model forces us to work with a lightest particle which is a mixture of $U(1)$ and neutral $SU(2)$ gauge bosons. Moreover we see that the relevant parameter of relic density calculation is m_{KK} through cross-sections which drop like $1/m_{KK}^2$. If we focus on the degenerate case where $R_5 = R_6 = R$, we have then two degenerate Dark Matter candidates which do not couple with each other, like in $T^2/\mathbb{Z}_2$ and $T_2/\mathbb{Z}_4$ models. In this case, we can use the formula 1.54 assuming two independent degenerate Dark Matter candidates and the total cross-section is given by: $\sigma_{tot} = \frac{1}{2}\sigma_{(0,1)\text{level}}$ and $g_{tot} = 2$ instead of 1. Finally, in our case, the typical value for the reduced freeze-out temperature is $x_F \sim 25$ and the typical m_{KK} is below 1 TeV: this leads to the chosen value of $g_* = 86.25$ because we are below the W^+W^- threshold of thermal production. Taking all these considerations into account, the figure 2.12 shows the mass range expected for the radii from relic abundance which 290 GeV $< m_{KK} <$ 320 GeV.

2.5.2 Relevance of coannihilation processes

The most relevant feature of the RPP model is the small mass splitting between the different particles in the $(1,0)$ and $(0,1)$ tiers. This peculiarity of the mass spectrum will induce large contributions from coannihilation processes. If we consider the relative mass splitting Δ_E and Δ_L for lepton singlet and doublet, the Boltzmann suppression factor is given by:

$$e^{-\Delta_{E/L} x_F} \sim e^{-0.01\times 25} \sim 0.77 \quad \text{where} \qquad \Delta_x = \frac{m_x - m_A}{m_A} \tag{2.161}$$

In this case, we understand clearly why the contribution of those particles will be relevant. Then, due to the large number of leptonic degrees of freedom, if we compute the relic density only taking into account photon and leptons, we observe a dilution of cross-section. The result is that the allowed mass range is lowered of almost 100 GeV and starts being close to the 200 GeV bound for the degenerate case. This effect has been observed in (75) but as their annihilation cross-section were smaller, it pushed down the typical mass-range for the lightest KK particle around 200 GeV (for $m_h \ll m_{KK}$).

Another difference with the Chiral Square model (75), is that here, the characteristic spectrum of the RPP model forces us to include the contributions of $SU(2)_W$ gauge bosons. Even if the mass splitting is larger for W and Z (see figure 2.11), their annihilation cross sections

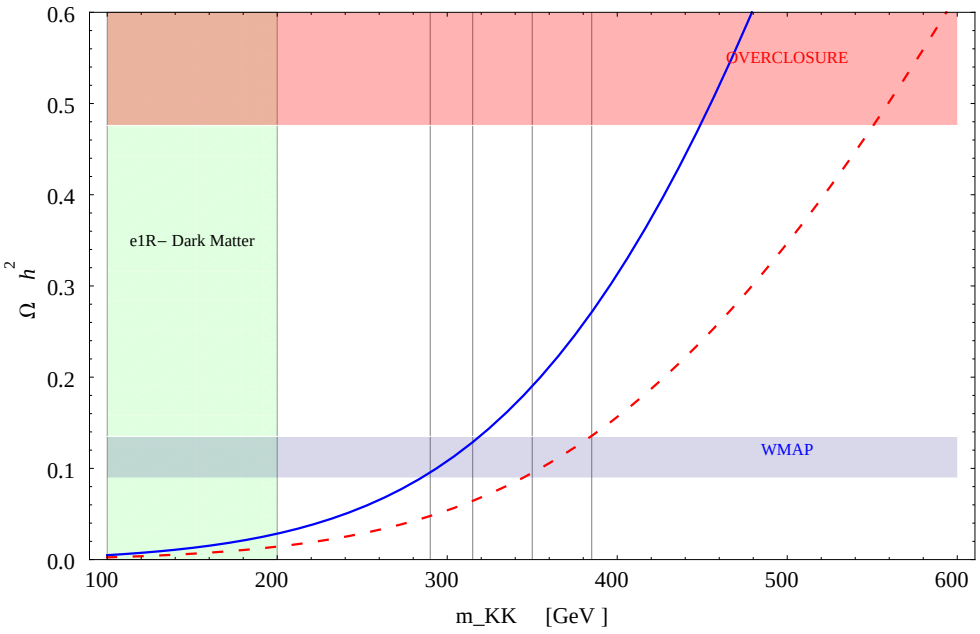

Figure 2.12: Relic density of LKP, including only A_5 and A_6 scalar photon annihilation, as a function of m_{KK} in the RPP model. The solid blue line is for the degenerate case where $R_5 = R_6 = R$ and where (1,0) and (0,1) are both Dark Matter candidate. The red dashed line is for the asymmetric case where for instance $R_5 \gg R_6$ and where $(1,0)$ is the Dark Matter candidate. The light blue band denotes the WMAP preferred region for the relic density: $0.095 < \Omega_{dm}h^2 < 0.13$.

into Standard Model particles and their coannihilations with the scalar photon are actually sizeable. Therefore if we consider naively only the gauge boson coannihilations, as it is shown in figure 2.13, the characteristic KK-mass is pushed up around the TeV scale. Nevertheless, the number of $SU(2)$ gauge boson degrees of freedom is small (only 3) and this number has to compared to the large number of fermionic degrees of freedom. This is the reason why, despite an effect expected to be quite sizeable a priori, the contribution of gauge bosons to the relic density calculation will be rather small.

Finally, after performing the full relic density calculation by including lepton and heavy gauge boson contributions, we found the mass-range from figure 2.14:

$$200 \text{ GeV} < m_{KK} < 250 \text{ GeV} \tag{2.162}$$

In this first approach, we also checked that the gluon and quark effects were not sizeable and they have been neglected in this study. We notice also that for $m_{KK} > 460$ GeV, we reach the Universe overclosure limit. This mass range is still quite low, which is interesting regarding LHC phenomenology that we will develop in chapter 4. On the other hand, let us emphasize again that these limits are strongly dependent on the cosmological model we choose (76) and that they have to be taken more as a first approach to get an order of magnitude of the typical KK-scale than as a precision calculation.

2.5.3 5D limit

Previously, we discussed the limit where $R_5 = R_6 = R$, but another interesting limit is given by the asymmetric radii case. If one radius is $O(5\%)$ smaller compared to the other, one tower

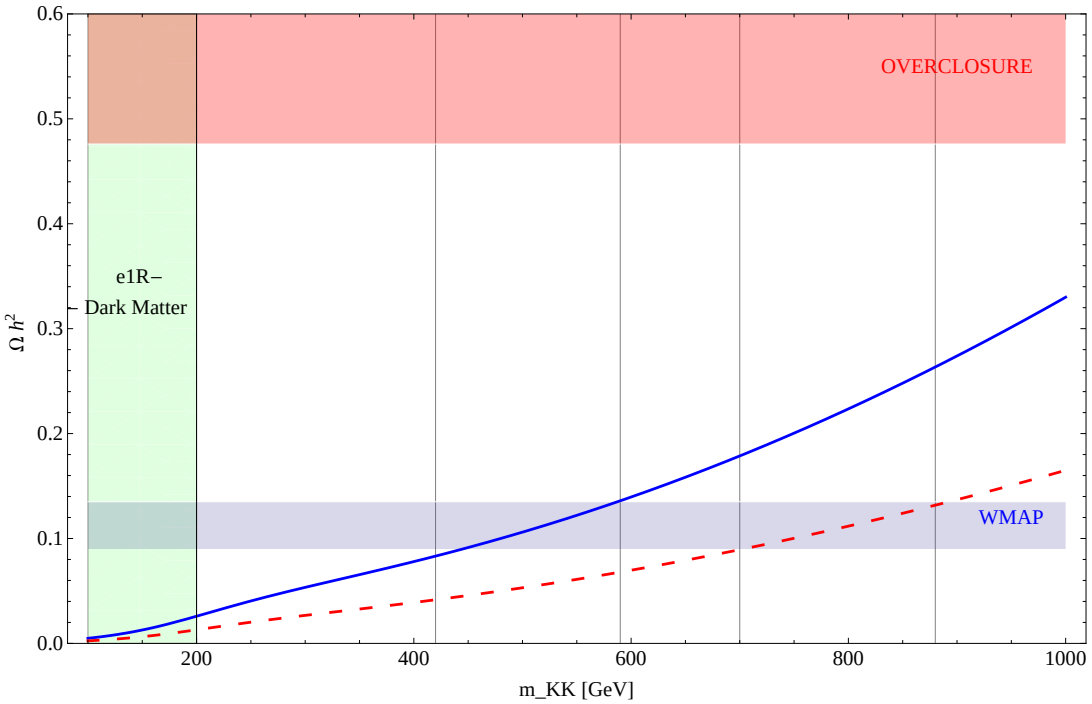

Figure 2.13: Relic density of LKP including only $SU(2) \times U(1)$ gauge boson coannihilation as a function of m_{KK} in the RPP model. The solid blue line is for the degenerate case where $R_5 = R_6 = R$ and where (1,0) and (0,1) are both Dark Matter candidates. The red dashed line is for the asymmetric case where for instance $R_5 \gg R_6$ and where $(1, 0)$ is the Dark Matter candidate. The light blue band denotes the WMAP preferred region for the relic density: $0.095 < \Omega_{dm} h^2 < 0.13$.

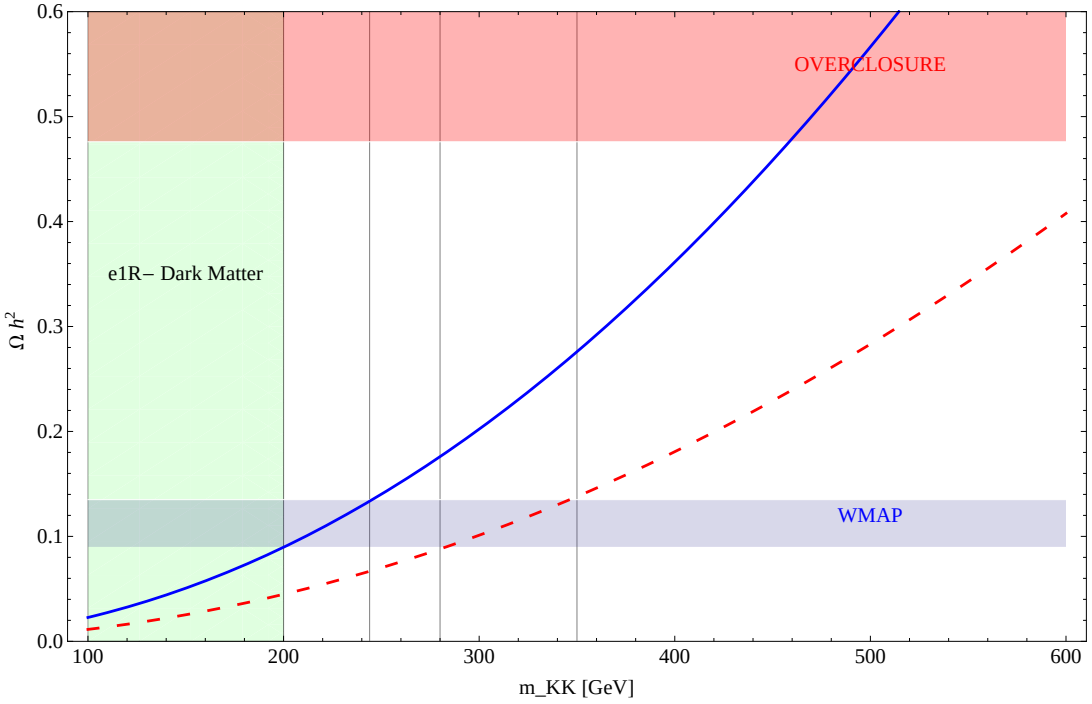

Figure 2.14: Relic density of LKP including $SU(2) \times U(1)$ gauge boson and lepton coannihilations as a function of m_{KK} in the RPP model. The solid blue line is for the degenerate case where $R_5 = R_6 = R$ and where (1,0) and (0,1) are both Dark Matter candidates. The red dashed line is for the asymmetric case where for instance $R_5 \gg R_6$ and where $(1, 0)$ is the Dark Matter candidate. The light blue band denotes the WMAP preferred region for the relic density: $0.095 < \Omega_{dm} h^2 < 0.13$.

"decouples" because of Boltzmann suppression factor and does not contribute anymore to the relic abundance. This order of magnitude is actually determined by the comparison between splitting and freeze-out temperature. This assymetric case is represented by the dashed curves on figures 2.12, 2.13 and 2.14 and we can observe that the typical range is getting heavier:

$$280 \text{ GeV} < m_{KK} < 350 \text{ GeV} \tag{2.163}$$

This is what we expect from previous studies of KK-Dark Matter candidates but because of peculiarity of this 5D limit model, the preferred range is still smaller compared with usual 5D UED model where 500 GeV $< m_{KK} <$ 600 GeV. Moreover this 5D model has still a preserved KK-parity imposed by the 6D completion and because of the space topology, its spectrum is clearly different from usual minimal UED models. This "geometrical" non-decoupling will affect typical phenomenology of the model which will be very similar to the 6D symmetric one except that less states will be present. In the table 2.15, we present the remaining states of this model.

Therefore let us emphasize that the usual minimal 5D UED model is not unique and that its structure and phenomenology will be influenced strongly by the presence of more extra-dimensions. In our future discussion, we will often consider this convenient 5D limit.

2.5.4 Some refinements

The relic abundance analysis we performed, was a first approach but needs to be refined by including some corrections into account which will certainly be relevant. The first effect that will be included soon will be the effect of the SM masses. Tops, Higgs and gauge bosons masses will probably modify slightly the cross-sections, because of the low mass-range of our theory: $m_{KK} \sim 300$ GeV. On another hand, new effects like resonant annihilation via the SM higgs but also via the $(2,0)$-$(0,2)$ levels can be relevant and will probably modify significantly the estimated range as it has been mentioned in 5D in (66; 77). The cross section enhancement through resonant particles in s-channel, can indeed force the typical mass range to be higher then the expected one. However, these heavy tiers, even under KK-parity, decay into SM fields through loop induced couplings so these processes are naturally suppressed. Therefore the balance between these two effects need to be studied in detail as well as the phenomenology of the $(2,0)$-$(0,2)$ tiers. This last part will be one of the motivation of the discussion developed in chapter 3. Finally, the localized kinetic terms effects need also to be taken into account. If those localized terms are significant, the mass of those fields can indeed be lowered and modify the branching fractions into SM particles.

k	p_{KK}	masses	gauge vector A^μ	gauge scalar A^6	fermions	higgs
$0 \equiv (0,0)$	$+$	0	★	–	★ chiral	★
$1 \equiv (1,0)$	–	1	–	★	★	–
$2k \equiv (2k,0)$	$+$	$2k$	★	–	★	★
$2k+1 \equiv (2k+1,0)$	–	$2k+1$	-	★	★	-

Table 2.15: Field content on the RPP in UED model for the first KK-levels. Masses are given for the asymmetric case $R = R_5 \gg R_6$ in unit of m_{KK}.

Chapter 3

Radiative corrections on the 6D Real Projective Plane

3.1 Motivations for one-loop renormalization on the Real Projective Plane

As we discussed in the previous section, the characteristic mass range for new physics is pretty low on the Real Projective Plane framework. Therefore, with numerous new heavy states around the TeV scale, this model can lead to an interesting phenomenology at early stage of LHC with 7 TeV and few fb^{-1} integrated luminosity. Nevertheless to study phenomenology on the Real Projective Plane we need to compute the contributions coming from radiative corrections. In UED model, at tree level all particles are degenerate and possible decays are then on threshold. In general those loop effects are dominated by the logarithmically divergent contribution coming from rotation symmetry and can be estimated using the localized counter-terms written on the singularities. That is the reason why we need a better understanding of the counter-term structure and why we have decided to study more in details the rotation contribution of the 6D loops. The main goal of this chapter, which is based on the publication (78), will be thereby to study the structure of counter-terms and to evaluate them. Then using a limited number of localized terms and the renormalization procedure, we will be able to extract the mass corrections and the effective couplings relevant for phenomenology.

Writing down the full set of allowed counter-terms, imposing gauge and Lorentz invariance, would lead to a quite large number of parameters but it would be feasible and it would allow us to predict the phenomenology of all the heavy states. However, a subtlety arises: corrections coming from loops are not generally gauge invariant meaning that the associated counter-terms are not gauge invariant either. Therefore we cannot use gauge invariance to predict for instance the trilinear coupling corrections directly from the mass ones. In the Standard Model, this behavior is well-known and it is not a limitation. In our case, one-loop calculations in 6D model are getting more and more complex as soon as we increase the number of fields propagating into the loop. In order to predict masses and couplings for phenomenology studies, it is mandatory to predict the 6D divergences from a reasonable amount of loop calculations. This non gauge invariant counter-term issue has already been observed in other extra-dimensional model (68) by using generic ξ-gauge. The authors stressed that for a peculiar gauge choice $\xi = -3$, some cancellations happen and lead to a Lagrangian which seems to be gauge invariant; mass term respects the gauge invariant counter-term and interaction terms can then be deduced using covariant derivatives from the kinetic terms. We will stress in appendix B, that this feature is not peculiar to extra-dimensional model but that it is already present in 4D.

The following study will be done in the context of the RPP in 6D, but this prescription is completely applicable to any compact space. It is based on the idea that in extra-dimension, due to the relic of Lorentz invariance there are sum rules for the quantized momenta along the extra-dimension which control the different couplings present in the theory. Usually we can distinguish three different kinds of couplings in extra-dimensional models:

- Bulk vertices: they arise from the bulk Lagrangian which possesses the 6D Lorentz invariance and therefore they conserve momenta flow. For that, if we consider the trilinear coupling between (k_1, l_1), (k_2, l_2) and (k_3, l_3), we always have a combination of sign which satisfies:

$$k_1 \pm k_2 \pm k_3 = 0 \quad \text{and} \quad l_1 \pm l_2 \pm l_3 = 0 \tag{3.1}$$

- Loop induced vertices: they are generated by the connections between different bulk vertices. They can break Lorentz invariance but on the RPP they will preserve all the residual KK-parities which are coming from the 6D Lorentz invariance.
- Localized interactions: they respect only the fundamental parities of the orbifold and the 4D Lorentz invariance.

In the rest of this thesis, we will focus on the two first kinds. Bulk vertices will be easy to compute and to implement if we want to make phenomenological studies. Loop induced vertices will be obtained by a shrewd calculation, focusing on the effective couplings between the mode $(2k, 2l)$ with $(k, l) \in \mathbb{N}^2$ into zero mode Standard Model particles. This peculiar choice of modes has been motivated by the fact only one type of particle can propagate in the loop linking $(2k, 2l)$ and $(0, 0)$ which are the (k, l) modes. This is imposed by the conservation of momenta on the tree level vertices. Here k and l are fixed which helps to reduce 6D loop calculations with double-sum to 4D loop calculation. In this case, only the rotation contribution remains because it is the only symmetry which violates translation symmetry along the extra-dimensions. If we need more general cases, we will show that they can be inferred from this particular choice. So in the following we will compute one-loop divergent corrections in ξ-gauge on the Real Projective Plane and we will show how, for this "magic gauge" choice $\xi = -3$, gauge invariance in Lagrangian is restored. Next sections are heavily inspired from our paper (78).

3.2 Gauge boson fields

In this section we will discuss the loops generating mixing in the gauge sector between the $(2k, 2l)$ mode and zero modes. We will consider only corrections to the two and three point functions and show that in the $\xi = -3$ gauge the two terms respect gauge invariance in the sense that the effective couplings are related to each other and correspond to a gauge invariant counter-term localized on the two singular points.

3.2.1 Bilinear mixing terms

Here we will consider mixing terms between the vector and two scalar modes in the level $(2k, 2l)$ with the vector zero mode, which corresponds to a SM gauge boson. The results have been computed in the usual 4D dimensional regularization, and they show the expected logarithmic sensitivity to the cut-off of the theory.

Vector mixing: $A_\mu^{2k,2l} - A_\nu^{0,0}$

For gauge loops, the mixing can be parametrized as [1]:

$$i\Pi^{\mu\nu} = \frac{g^2 C_2(G)\delta^{ab}}{16\pi^4}\left[\left(\lambda_1 \frac{i\pi^2}{\epsilon} + \kappa_1 \frac{i\pi^3}{\eta}\right) g^{\mu\nu} + \lambda_2 \frac{i\pi^2}{\epsilon} q^\mu q^\nu\right] \tag{3.2}$$

where $1/\epsilon = \log \Lambda R$ and $1/\eta = 1/4\,\Lambda^2$. We have computed the log divergent parts in the usual 4D dimensional regularization scheme in $d = 4 - \epsilon$ and the quadratic divergence in 2D dimensional regularization with $d = 2 - \eta$. The same results can be obtained with a cutoff regularization, with Λ equal to the UV cutoff of the integrals. For the scalar loop, the same parametrization is valid: the only difference is that the group factor in front is different. For a non Abelian group

[1] We recall the definition of the group theory factor $f^{acd} f^{bcd} = C_2(G)\delta^{ab}$. For SU(N), $C_2(G) = N$.

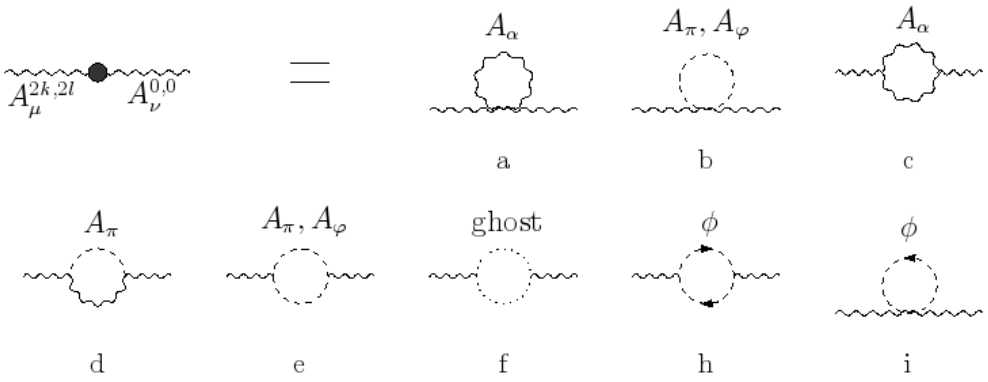

Figure 3.1: $A_\mu^{2k,2l} - A_\nu^{0,0}$ mixing: loops a–f are gauge corrections while h and i are scalar field corrections.

and a scalar in the representation r_ϕ, the coefficient $C_2(G)$ is replaced by $C(r_\phi) = \frac{d(r_\phi)}{d(G)} C_2(r_\phi)$ [2]; while for a U(1), it is replaced by the square of the charge of the scalar field Y_ϕ^2 multiplied by the number of complex components of the scalar. The contribution of each loop to the coefficients λ_1, λ_2 and κ_1 are listed in table 3.1 (for simplicity we define $M = M_{k,l} = \sqrt{k^2 + l^2}\ m_{KK}$).

Note that, as expected, the quadratic divergence vanishes. The total contribution of gauge loops is therefore given by:

$$i\Pi^{\mu\nu}_{\text{gauge}} = \frac{g^2 C_2(G)\delta^{ab}}{16\pi^4} \frac{i\pi^2}{\epsilon} \left[M^2(\xi+3) g^{\mu\nu} - \frac{(\xi-5)}{2}(q^2 g^{\mu\nu} - q^\mu q^\nu) \right] \tag{3.3}$$

The total contribution of scalar loops:

$$i\Pi^{\mu\nu}_{\phi} = \frac{g^2 C(r_\phi)\delta^{ab}}{16\pi^4} \frac{i\pi^2}{\epsilon} \left[-\frac{1}{3}(q^2 g^{\mu\nu} - q^\mu q^\nu) \right] \tag{3.4}$$

[2] $\text{Tr}(t_r^a t_r^b) = C(r)\delta^{ab}$. For a fundamental of SU(N), $C(N) = \frac{1}{2}$.

λ_{1a}	$\frac{1}{4}\left(-3M^2(\xi^2+3)\right)$	κ_{1a}	$2(\xi+1)$	λ_{2a}	0
λ_{1b}	$M^2(\xi+1)$	κ_{1b}	-8	λ_{2b}	0
λ_{1c}	$\frac{1}{12}\left(9M^2(\xi^2+\xi+4)+q^2(25-6\xi)\right)$	κ_{1c}	$-2(\xi+2)$	λ_{2c}	$\frac{1}{6}(3\xi-14)$
λ_{1d}	$\frac{1}{4}\left(3M^2(\xi+3)\right)$	κ_{1d}	0	λ_{2d}	0
λ_{1e}	$\frac{1}{6}\left(-6M^2(\xi+1)+2q^2\right)$	κ_{1e}	8	λ_{2e}	$-\frac{1}{3}$
λ_{1f}	$\frac{1}{12}\left(-6M^2\xi+q^2\right)$	κ_{1f}	2	λ_{2f}	$\frac{1}{6}$
λ_{1gauge}	$\frac{1}{2}\left(2M^2(\xi+3)-q^2(\xi-5)\right)$	κ_{1gauge}	0	λ_{2gauge}	$\frac{1}{2}(\xi-5)$
λ_{1h}	$\frac{1}{3}\left(6M^2-q^2\right)$	κ_{1h}	-8	λ_{2h}	$\frac{1}{3}$
λ_{1i}	$-2M^2$	κ_{1h}	$+8$	λ_{2h}	0
$\lambda_{1scalar}$	$-\frac{1}{3}q^2$	$\kappa_{1scalar}$	0	$\lambda_{2scalar}$	$\frac{1}{3}$

Table 3.1: Contributions of the loops in figure 3.1.

Physical scalar: $A_\varphi^{2k,2l} - A_\mu^{0,0}$

This mixing is absent at 1-loop, because the trilinear coupling with a physical scalar and a gauge boson of level (k, l) vanishes, and similarly for the ghosts.

Goldstone-vector mixing: $A_\pi^{2k,2l} - A_\mu^{0,0}$

The mixing between the Goldstone boson and the zero mode is given by the graphs in figure 3.2: the scalar field does not contribute because the coupling of the Goldstone boson to two scalars in tier (k, l) vanishes. The general structure of the mixing is as follows:

$$i\Pi^\mu = \frac{g^2 C_2(G)\delta^{ab}}{16\pi^4} \frac{i\pi^2}{\epsilon} \lambda \, (-iM)q^\mu \tag{3.5}$$

The contributions of the two diagrams in figure 3.2 to the coefficient λ are given in table 3.2.

All in all, the mixing is given by:

$$i\Pi^\mu = \frac{g^2 C_2(G)\delta^{ab}}{16\pi^4} \frac{i\pi^2}{2\epsilon} [iM(\xi + 3)q^\mu)] \tag{3.6}$$

The presence of this new mixing between Goldstone boson and vector would require a redefinition of the gauge fixing parameter ξ at one loop. Note however that the definition of the Goldstone boson is not modified because there is no mixing generated with the physical scalar A_φ, and also that the mixing vanished in the $\xi = -3$ gauge.

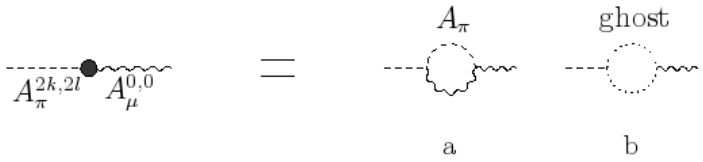

Figure 3.2: $A_\pi^{2k,2l} - A_\mu^{0,0}$ mixing.

λ_a	$-\frac{\xi}{2}$
λ_b	$-\frac{3}{2}$
λ_{tot}	$-\frac{1}{2}(\xi + 3)$

Table 3.2: Contributions to the mixing of the Goldstone boson.

3.2.2 Trilinear couplings

In this section we present the results for the three-point functions with one gauge state from level $(2k, 2l)$ and two vector zero modes.

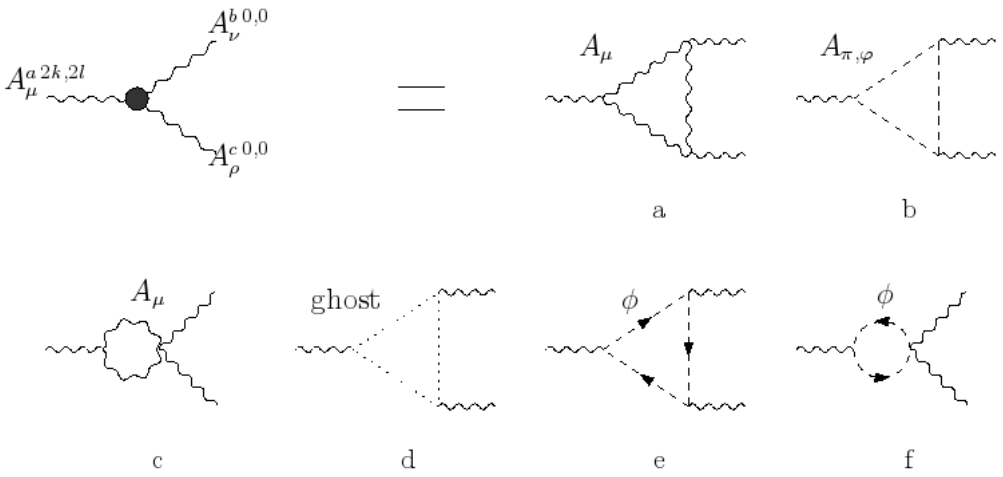

Figure 3.3: $A_\mu^{2k,2l}$ coupling to two SM vectors. In graphs c and f, the sum with the graph with loops on the zero mode legs are included.

Gauge vector trilinear coupling

The effective coupling can be written as:

$$iV^{\mu\nu\rho} = \frac{ig^3 f^{abc} C_2(G)}{16\pi^4} \frac{i\pi^2}{4\epsilon}\ \tau\ \mathcal{O}^{\mu\nu\rho} \tag{3.7}$$

where $\mathcal{O}^{\mu\nu\rho} = (q_2^\mu - q_1^\mu)g^{\nu\rho} - (q_1^\nu + 2q_2^\nu)g^{\mu\rho} + (2q_1^\rho + q_2^\rho)g^{\mu\nu}$ is the usual tensor from tree level trilinear couplings. q_1^ν and q_2^ρ are the momenta of the zero modes and are taken coming out of the vertex. For the scalar loops, the gauge factor $C_2(G)$ is replaced by $C(r_\phi)$ for an SU(N) representation r_ϕ. Note that the vertex vanishes for a U(1) gauge group, because the tensor is antisymmetric. The contributing loops are in figure 3.3, and their individual contribution is listed in table 3.3. The total gauge contribution is therefore given by:

$$iV^{\mu\nu\rho}_{\text{gauge}} = \frac{ig^3 f^{abc} C_2(G)}{16\pi^4} \frac{i\pi^2}{4\epsilon}\ (-3\xi + 7)\mathcal{O}^{\mu\nu\rho} \tag{3.8}$$

For the scalar contribution:

$$iV^{\mu\nu\rho}_{\phi} = \frac{ig^3 f^{abc} C(r_\phi)}{16\pi^4} \left(\frac{-i\pi^2}{3\epsilon}\right) \mathcal{O}^{\mu\nu\rho} \tag{3.9}$$

τ_a	$-\frac{1}{2}(9\xi + 4)$
$\tau_b(A_\pi + A_\varphi)$	$\frac{4}{3}$
τ_c	$\frac{3}{2}(\xi + 5)$
τ_d	$\frac{1}{6}$
τ_{gauge}	$(-3\xi + 7)$
τ_e	$-\frac{4}{3}$
τ_f	0
τ_ϕ	$-\frac{4}{3}$

Table 3.3: Contributions to the trilinear vector coupling.

Goldstone $A_\pi^{2k,2l}$ to two vectors

The coupling of the Goldstone boson with two zero mode vectors is given by the loops in figure 3.4. However, we can show that the loops give a finite result: for loops a and b, the divergent part cancels out after symmetrizing the diagrams with respect to the vector legs, while the ghost loop is finite.

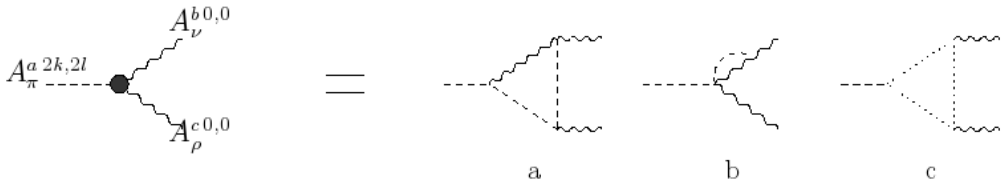

Figure 3.4: $A_\pi^{2k,2l}$ coupling to SM vectors

Scalar $A_\varphi^{2k,2l}$ to SM vectors

Because $A_\varphi^{2k,2l}$ is a physical scalar, the coupling $A_\varphi^{k,l} A_\mu^{k,l} A_\nu^{0,0}$ is forbidden. There is then no way to close the loop by using the new extra physical scalar and this field does not couple to SM model gauge bosons.

3.3 Scalars fields

We will focus here on loops involving the scalar field on the external legs. For simplicity, we will quote the results for a representation r_ϕ of a SU(N) group, and we will specify how to modify them for U(1) gauge fields. We will ignore the potentially large contribution of the scalar quartic coupling due to the poor understanding of the Higgs sector in UED models and also because of our main interest in the gauge dependence of the result. As already mentioned, we also drop the dependency on the scalar bulk mass because we assume that it is of the order of the VEV.

3.3.1 Mixing terms

The mixing between the massive scalar and the zero mode can be parametrized in general as [3]:

$$i\Pi = -\frac{g^2 C_2(r_\phi)}{16\pi^4}\left(\lambda\frac{i\pi^2}{\epsilon} + \kappa\frac{4i\pi^3}{\eta}\right) \tag{3.10}$$

In the case of a U(1), it would be sufficient to replace $C_2(r_\phi) \to Y_\phi^2$.

The contribution of the diagrams in figure 3.5 are listed in table 3.4. Notice that there is no contribution coming from fermion loops.

Summing all the gauge contributions we obtain:

$$i\Pi = -\frac{g^2 C_2(r_\phi)}{16\pi^4}\left((M^2(2\xi+1) - q^2(\xi-3))\frac{i\pi^2}{\epsilon} - \frac{4i\pi^3}{\eta}\right) \tag{3.11}$$

[3] Note that $\sum_a t_r^a t_r^a = C_2(r)\cdot 1$. For a fundamental of SU(N), $C_2(N) = \frac{N^2-1}{2N}$.

Note that in this case the quadratic divergence remains, signaling the presence of a localized counter-term for the mass. This localized mass will add up to the bulk mass for the scalar, in particular for the zero mode which we want to identify with the Higgs boson. The mass of the Higgs is expected to be small compared to the KK-mass scale so we have to consider two possibilities: either the localized contribution is important but there exists a fine-tuning which compensates this contribution, or the localized mass is small, which is also a new source of fine-tuning to the 4D Standard Model case. We have decided to follow the last statement, therefore, we can assume that this term is small, and reabsorb it into the definition of the Higgs VEV. We emphasize also that a large localized mass would significantly modify the flat wave-function of the Higgs boson, and then induce mixing between KK tiers!

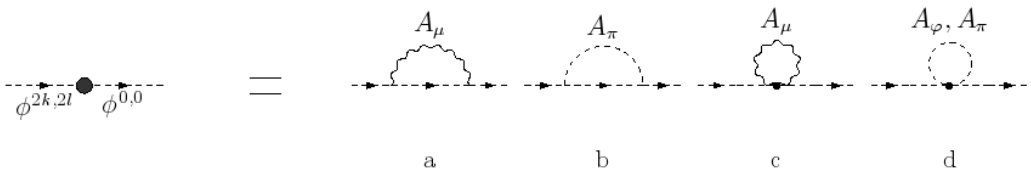

Figure 3.5: Scalar mixings generated by gauge loops.

λ_a	$(M^2\xi(\xi+1) - q^2(\xi-3))$	κ_a	$-\xi$
λ_b	$3M^2$	κ_b	0
λ_c	$-M^2(\xi^2+3)$	κ_c	$\xi+1$
λ_d	$M^2(\xi+1)$	κ_d	-2
λ_{gauge}	$(M^2(2\xi+1) - q^2(\xi-3))$	κ_{gauge}	-1

Table 3.4: Contributions to the scalar mixing.

3.3.2 Gauge couplings

In this section, we calculate the loop contribution to trilinear couplings involving two scalars and a gauge field. There are 2 kinds of couplings: a massive gauge field coupling to two zero mode scalars, and a massive scalar coupling to a zero mode scalar and a massless gauge boson.

Vector $A_\mu^{2k,2l}$ to SM scalars

This coupling can be parametrized as:

$$iV_A^\mu = \frac{g^3}{16\pi^4}\frac{i\pi^2}{\epsilon}\ \tau_A\ (q_1^\mu - q_2^\mu)t^a \tag{3.12}$$

where q_1 and q_2 are the out-coming momenta of the two massless scalars. The loop computations are also done using dimensional regularization, and the diagrams are given in figure. 3.6.

For SU(N) gauge fields, the contributions of the single diagrams are listed in table 3.5. Summing all the contributions, we obtain:

$$iV_A^\mu = -\frac{g^3}{16\pi^4}\frac{i\pi^2}{4\epsilon}\ (4(\xi-3)C_2(r_\phi) + (\xi+3)C_2(G))\ (q_1^\mu - q_2^\mu)t^a \tag{3.13}$$

This result is valid if both the external and internal gauge bosons belong to the same SU(N) gauge group. For U(1) gauge groups, it suffices to replace $C_2(r_\phi) \to Y_\phi^2$, $C_2(G) \to 0$ and $t^a \to Y_\phi$. If the gauge bosons in the external and internal line belong to different gauge groups, then only the diagrams a and b in figure 3.6 contribute: the result is the same as in the table with $C_2(r_\phi) \to C_2(r')$ and $C_2(G) \to 0$, and the total result is

$$iV^\mu_{A'} = -\frac{gg'^2}{16\pi^4}\frac{i\pi^2}{\epsilon}\ (\xi-3)C_2(r')\ (q_1^\mu - q_2^\mu)t^a \tag{3.14}$$

If the external gauge boson is a U(1), $t^a \to Y_\phi$; if the internal one is a U(1), $C_2(r') \to Y_\phi^2$.

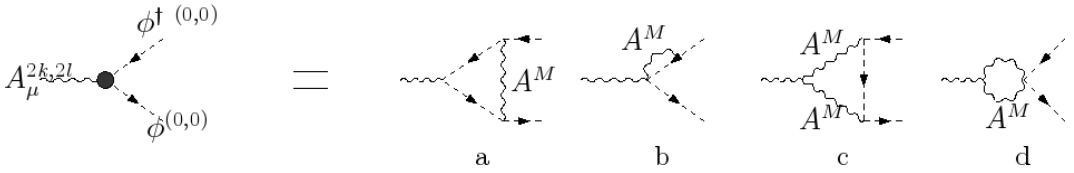

Figure 3.6: Coupling of $A_\mu^{2k,2l}$ with two SM scalars.

τ_{Aa}	$-(C_2(r_\phi) - 1/2C_2(G))\xi$
τ_{Ab}	$\frac{3}{2}(2C_2(r_\phi) - 1/2C_2(G))$
τ_{Ac}	$-\frac{3}{4}C_2(G)\xi$
τ_{Ad}	0
τ_{Atot}	$-\frac{1}{4}(4(\xi-3)C_2(r_\phi) + (\xi+3)C_2(G))$

Table 3.5: Contributions to the coupling of a massive vector to massless scalars.

Gauge scalar and Goldstone $A_{\varphi,\pi}^{2k,2l}$ to SM scalars

Now concerning the coupling of gauge scalars to two SM scalars, we see that for the physical scalar $A_\varphi^{2k,2l}$ no coupling at one loop is possible. For the Goldstone boson $A_\pi^{2k,2l}$, the only loops that can contribute are in figure 3.7. The couplings between A_π and two scalars with the same KK-masses are indeed zero. The divergent contribution of these loops is vanishing because of a cancellation coming from symmetric diagrams ($a1/a2$ and b_1/b_2).

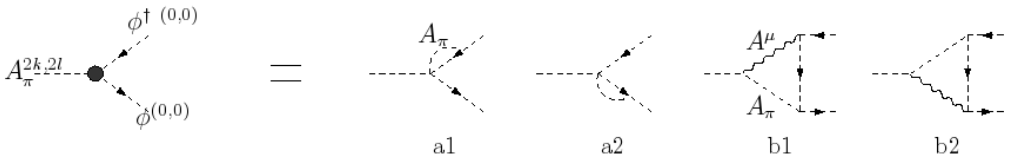

Figure 3.7: $A_\pi^{2k,2l}$ coupling to SM scalars.

Scalar $\phi^{2k,2l}$ to SM gauge boson and massless scalar

We also computed the decay of a heavy scalar into a SM one and a SM gauge boson. It is expected to give similar results as the previous one and that is what we are going to check. The coupling can be written as:

$$iV_\phi^\mu = \frac{g^3}{16\pi^4}\frac{i\pi^2}{\epsilon}\,\tau_\phi\,(-q_1^\mu - 2q_2^\mu)t^a \tag{3.15}$$

where q_1 is the momentum of the gauge boson and q_2 of the massless scalar. The diagrams in figure 3.8 are the same as in figure 3.6 with reversed external legs, and, because the coefficient τ does not depend on the external masses or momenta, we expect the same results to apply here. The q-dependent factor comes from the replacement $q_1 \longrightarrow -q = -q_1 - q_2$. We calculated the diagrams and checked explicitly that the contributions are the same as in the previous table. For U(1) and different gauge groups, the same considerations as above apply.

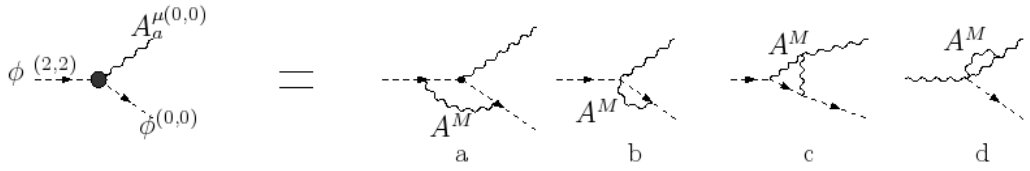

Figure 3.8: $\phi^{2k,2l}$ decay in SM scalar and gauge boson.

3.4 Fermions fields

3.4.1 Mixing terms

In a generic level (k, l) with non-zero integers, there are two degenerate fermions at tree level, labeled $\psi_a^{k,l}$ and $\psi_b^{k,l}$. With our choice of basis, the couplings of the two states are very different: for instance, ψ_a couples to the Goldstone A_π while ψ_b couples to the physical gauge scalar A_φ. The main consequence is that only ψ_a can mix with a zero mode fermion, see figure 3.9, while no loop can be closed for ψ_b. This means that, in general, the states ψ_a couple to the counter-terms and receive divergent contributions from the loops, while corrections for the ψ_b fermions are finite (at one-loop order).

In the following, we will focus on a fermion with left-handed zero modes: results for the right-handed zero modes can be easily obtained from this calculation. The mixing term can be written as:

$$\mathcal{L}_{\text{mix}} = i\bar{\psi}_a^{2k,2l}\, i\Sigma\, P_L\, \psi^{0,0} + \text{h.c.} \tag{3.16}$$

where P_L is the chirality projector on left-handed zero mode and

$$i\Sigma = \frac{g^2 C_2(r_f)}{16\pi^4}\frac{i\pi^2}{\epsilon}\left(\lambda_1 \not{q} + \lambda_2 M\right) \tag{3.17}$$

The contribution of each diagram is given in table 3.6 and the total contribution is therefore

$$i\Sigma_{\text{gauge}} = \frac{g^2 C_2(r_f)}{16\pi^4}\frac{i\pi^2}{\epsilon}\left(-M(\xi+3) + (\xi-1)\not{q}\right) \tag{3.18}$$

For U(1) gauge bosons, it is enough to replace $C_2(r_f) \to Y_f^2$. For fields with right-handed zero modes, it is enough to replace the chirality projector.

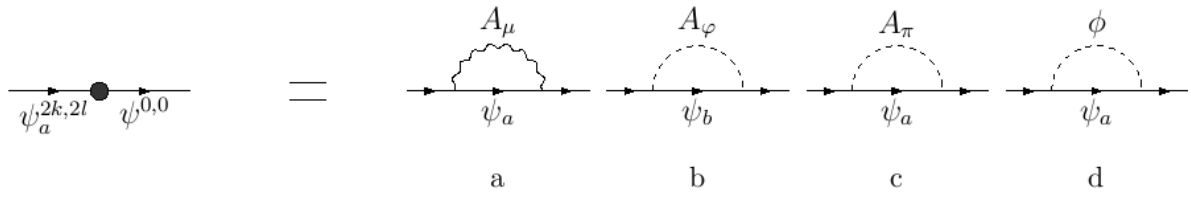

Figure 3.9: Fermion mixing: no one-loop diagram exists for ψ_b.

λ_{1a}	ξ	λ_{2a}	$-(\xi+3)$
λ_{1b}	$-\frac{1}{2}$	λ_{2b}	1
λ_{1c}	$-\frac{1}{2}$	λ_{2c}	-1
$\lambda_{1\,tot}$	$(\xi-1)$	$\lambda_{2\,tot}$	$-(\xi+3)$

Table 3.6: Contributions of gauge loops to the fermion mixing.

Yukawa couplings

In the Standard Model, fermions also couple to the scalar Higgs field through Yukawa interactions. The Higgs loops will only be numerically relevant for the top Yukawa, therefore they affect the third generation doublet (left-handed top and bottom) and the top singlet (right-handed top). This contribution comes through the (d)-loop and, for the left-handed doublet, is given by:

$$i\Sigma^{\mathrm{D}}_{\mathrm{scalar}} = \frac{y_f^2}{16\pi^4}\frac{i\pi^2}{\epsilon}\left(\frac{1}{2}\not{q} - M\right) \tag{3.19}$$

where y_f is the 4D Yukawa of the fermions. Note that the result is the same as the gauge scalar A_φ loop, up to a sign which is the different parity under the rotation symmetry. Here the singlet fermion will be running into the loop. For the top singlet, the same formula applies with a right-handed projector but is multiplied by a factor of 2. In this case, the doublet field is indeed running into the loop and we need to take into account the two components up and down of the $SU(2)$ doublet.

3.4.2 Fermionic couplings

Gauge vector $A_\mu^{2k,2l}$ to two SM fermions

The coupling can be expressed as

$$i\Gamma_A^{a,\mu} = \frac{g^3}{16\pi^4}\frac{i\pi^2}{\epsilon}\tau_A\gamma^\mu P_L t^a \tag{3.20}$$

where t^a is the generator of the SU(N) gauge group.

The contributions from the diagrams in figure 3.10 are listed in table 3.7.

The total contribution is therefore:

$$i\Gamma_A^{a,\mu} = \frac{g^3}{16\pi^4}\frac{i\pi^2}{\epsilon}\left((\xi-1)C_2(r_f) + \frac{\xi+3}{4}C_2(G)\right)\gamma^\mu P_L t^a \tag{3.21}$$

For a U(1) gauge group, only diagrams of type (a) are present, and it would be enough to replace $C_2(r_f) \to Y_f^2$, $C_2(G) \to 0$ and $t^a \to Y_f$. Similarly, if the external gauge boson is different from the internal one, we would have (with the same replacements if one of the two gauge bosons is a U(1)):

$$i\Gamma_{A'}^{\mu} = \frac{gg'^2}{16\pi^4}\frac{i\pi^2}{\epsilon}(\xi-1)C_2(r')\gamma^\mu P_L t^a \tag{3.22}$$

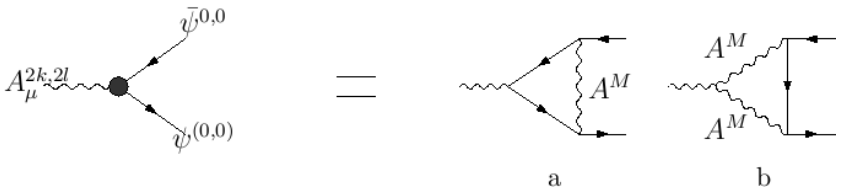

Figure 3.10: $A_\mu^{2k,2l}$ coupling to two SM fermions.

$\tau_{Aa}(A^\mu)$	$\xi(C_2(r_f) - 1/2C_2(G))$
$\tau_{Aa}(A_\varphi + A_\pi)$	$-2\ \frac{1}{2}(C_2(r_f) - 1/2C_2(G))$
$\tau_{Ab}(A^\mu)$	$\frac{3}{4}(\xi+1)C_2(G)$
$\tau_{Ab}(A_\varphi + A_\pi)$	$-2\frac{1}{4}C_2(G)$
$\tau_{A\,tot}$	$\frac{1}{4}(4(\xi-1)C_2(r_f) + (\xi+3)C_2(G))$

Table 3.7: Contributions of non-abelian gauge loops.

Yukawa couplings

As we explained in the previous section, for massive SM fermions, Yukawa interactions can be sizeable. We need in this case to compute also the scalar field effects on the vertex corrections. As we presented in section 2.4.5, the Yukawa coupling will induce a coupling between the doublet ψ_D and singlet ψ_S fields. For down-type Yukawa it will have the following form:

$$\mathcal{L}_{\text{yuk}} \supset y_\psi \bar{\psi}_D \phi \psi_S \tag{3.23}$$

This gauge invariant Lagrangian will impose a peculiar relation between $U(1)$ hypercharges: $Y_D = Y_S + Y_\phi$ for down-type fermions.

Then for up-type Yukawa which will be interesting for studying top physics on the RPP, we have:

$$\mathcal{L}_{\text{yuk}} \supset y_\psi \bar{\psi}_D \phi^\dagger \psi_S \tag{3.24}$$

which implies that we just have to change in the case of $U(1)$ loops, $Y_\phi \to -Y_\phi$.

Now that we remind the structure of the Yukawa coupling, we can express the gauge coupling with scalar exchange as:

$$i\Gamma^\mu_\phi = \frac{g y_\psi^2}{16\pi^4}\frac{i\pi^2}{\epsilon}\tau_\phi \gamma^\mu P_R t^a \tag{3.25}$$

with contributions from the diagrams in figure 3.11. Because of the gauge transformations of the Higgs we need to distinguish different cases which are listed in table 3.8. For U(1) couplings the generator $t^a \to 1$. In the case of a singlet, the diagram (b) picks up a minus sign because it is $\phi^\dagger$ that runs in the loop, therefore the sign of the Yukawa coupling changes.

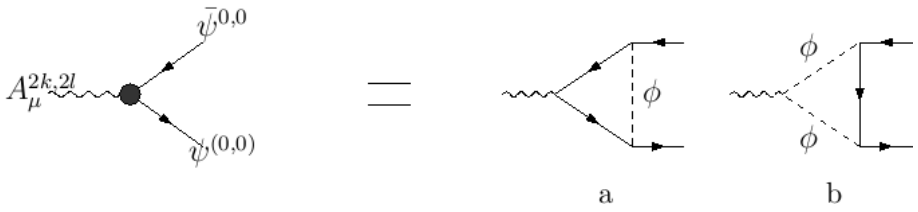

Figure 3.11: $A_\mu^{2k,2l}$ coupling to two SM fermions with scalar exchange.

	U(1) to singlet	U(1) to doublet	SU(2) to singlet	SU(2) to doublet	SU(3)
$\tau_{\phi a}$	Y_D	$1/2Y_S$	0	0	1/2
$\tau_{\phi b}$	$-Y_\phi$	$1/2Y_\phi$	0	1/2	0
τ_ϕ	Y_S	$1/2Y_D$	0	1/2	1/2

Table 3.8: Contributions of Higgs loops. Y_S and Y_D are the hypercharges of the singlet and doublet respectively, while Y_ϕ is the hypercharge of the Higgs. We also used the fact that $Y_D = Y_S + Y_\phi$.

Heavy fermion $\psi_a^{2k,2l}$ coupling to a SM gauge boson and fermion.

Diagrams in figure 3.12 generate the coupling of a heavy fermion $\psi_a^{2k,2l}$ with SM fermion and gauge vector. Very similar to the ones in figure 3.10, the only difference is a change in the momenta and masses of the external legs. However, it can be shown that respective diagrams will lead to the same results, so that the same formulas as above apply.

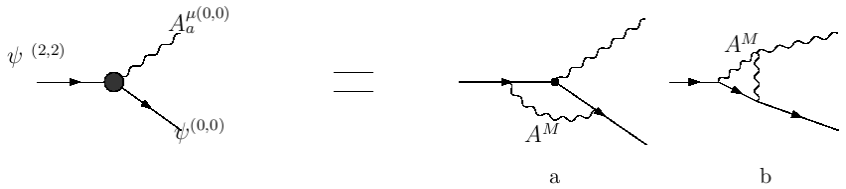

Figure 3.12: $\psi_a^{2k,2l}$ decay in SM fermion and gauge boson.

Gauge scalar $A_{\varphi,\pi}^{2k,2l}$ couplings to SM fermions.

We can show that $A_{\varphi}^{2k,2l}$ cannot couple to SM fermions because the loops cannot be closed, contrary to the Goldstone $A_{\pi}^{2k,2l}$. Nevertheless, all the possible loops, listed in figure 3.13, are finite. The power of the momentum flowing into the loops (a) and (b) is too small, so the loop is finite. The divergent contribution of the loop (c) is vanishing because of a cancellation coming from symmetric diagrams. The proof is analog to the scalar one.

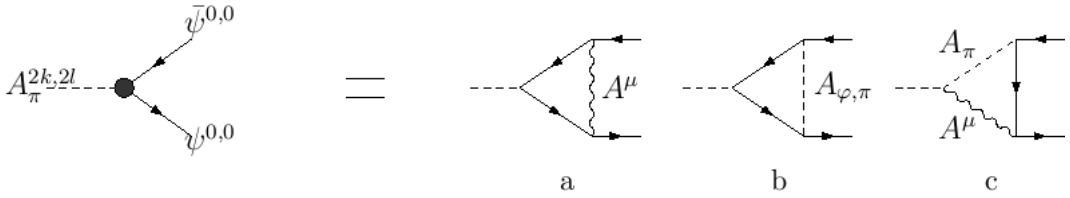

Figure 3.13: $A_{\pi}^{2k,2l}$ coupling to two SM fermions.

Heavy fermion $\psi_a^{2k,2l}$ coupling to a SM Goldstone ϕ and fermion.

The Yukawa coupling will also induce a coupling between the doublet ψ_D and singlet ψ_S fields. We have just seen that the down-type Yukawa Lagrangian can be written as:

$$\mathcal{L}_{\text{yuk}} \supset y_{\psi} \bar{\psi}_D \phi \psi_S \tag{3.26}$$

In this case, the coupling for a heavy ψ_D going into ψ_S can be expressed as:

$$i\Gamma_{\phi} = -\frac{y_{\chi}}{16\pi^4} \frac{i\pi^2}{\epsilon} (g^2 \tau_{\phi} + y_{\psi}^2 \tau'_{\phi}) P_L \tag{3.27}$$

where y_{χ} is the Yukawa of the intermediate fermions from the level (k,l) which couples directly to the SM scalar and y_{ψ} are the Yukawa of the incoming and out-coming fermions. We have to emphasize that the Yukawa interactions mix doublet and singlet components under $SU(2)_W$, which means that we need to be careful that the representation of the incoming and out-coming fermions can be different for the gauge groups.

The contributions from the diagrams in figure 3.14 are listed in table 3.9. Note that $t^a(r_S)$, $t^a(r_D)$ and $t^a(r_{\phi})$ are the generators of the field under the $SU(N)$ gauge group. They can be different by default, the relation $t^a(r) \cdot t^a(r) = C_2(r) \cdot 1$ is valid only if the representation is the same for the different fields. For $U(1)$, we have still the relation between the different hypercharges of the field: $Y_D = Y_S + Y_{\phi}$ for down-type fermions. Finally for up-type Yukawa, we just have to change in the case of $U(1)$ loops, $Y_{\phi} \to -Y_{\phi}$.

3.5 General structure of counter-terms: the "magic gauge" choice

In this section, we show how we can extract from the previous part, the full set of counter-term to regularize the divergences generated by the rotation part of the one-loop contribution. It exists two singularities on the RPP, which are $(0,0) \equiv (\pi R, \pi R)$ and $(0, \pi R) \equiv (\pi R, 0)$. In general the counter-terms on those two points can be different. However as we are considering

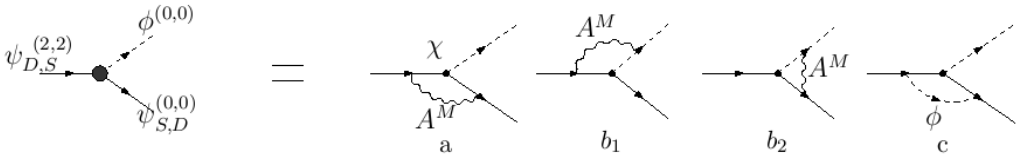

Figure 3.14: $\psi^{2k,2l}$ decay in SM Goldstone ϕ and gauge boson.

$\tau_{\phi a}(A^\mu)$	$(\xi+3)\ t^a(r_D).t^a(r_S)$
$\tau_{\phi a}(A_\varphi + A_\pi)$	0
$\tau_{\phi b}(A^\mu)$	$\xi\ (t^a(r_S).t^a(r_\phi) + t^a(r_D).t^a(r_\phi))$
$\tau_{\phi b}(A_\varphi + A_\pi)$	0
$\tau_{\phi\, tot}$	$(\xi+3)t^a(r_D).t^a(r_S) + \xi(t^a(r_S) + t^a(r_D)).t^a(r_\phi)$
$\tau'_{\phi c}(\phi)$	$+1$

Table 3.9: Contributions of gauge loops and of scalar ϕ, $t^a(r_X)$ is the generator of the field X under the $SU(N)$ gauge group.

divergent loops generated by bulk vertices, symmetries of the orbifold apply on them and assure that the counter-terms on the two points are equal. The counter-term Lagrangian can then be written as:

$$\delta\mathcal{L} = \iint dx_5\ dx_6 \frac{\delta_0 + \delta_\pi}{\Lambda^2}\mathcal{L}_{\mathrm{c-t}} \tag{3.28}$$

where the cut-off Λ shows that we are interested in operators of dimension 6 in $\mathcal{L}_{\mathrm{c-t}}$ and the localization operators [4] are given by:

$$\delta_0 = \frac{1}{2}\left(\delta(x_5)\delta(x_6) + \delta(x_5 - \pi R)\delta(x_6 - \pi R)\right) \tag{3.29}$$

$$\delta_\pi = \frac{1}{2}\left(\delta(x_5)\delta(x_6 - \pi R) + \delta(x_5 - \pi R)\delta(x_6)\right) \tag{3.30}$$

and label the two singular points with a subscript 0 for the point $(0,0) \equiv (\pi R, \pi R)$, and π for $(0,\pi R) \equiv (\pi R, 0)$. It is important to notice that the dimension 6 operators in terms of 6D fields are kinetic terms in the bulk Lagrangian.

Localized interactions have to respect only the 4D gauge invariance and generally they are gauge dependent operators. This observation is not specific to the RPP but is general to all extra-dimensional models however we notice that the localized counter-terms will adopt a 6D gauge invariant form for the specific gauge choice $\xi = -3$. This is also true in 4D as we discussed in appendix B. In extra-dimension, this property is crucial because it will reduce considerably the number of counter-terms, especially the ones involving new gauge scalar fields. This is the reason why in this section, we will use the $\xi = -3$ gauge to present the full set of counter-terms needed at one loop to regularize rotation divergences. They will all be deduced from the previous calculation.

[4] Localization operators have dimension 2 in mass, while $\delta\mathcal{L}$ has dimension 6.

3.5.1 Gauge counter-terms

The general structure of gauge counter-terms is extremely rich and complex. This can be understood by looking at the result of section 3.2. We could think that only 4D gauge invariance can be imposed because only the vector part of the 6D vector A_M is non-zero on the fixed points (both A_5 and A_6 are odd under the rotation symmetry, therefore their wavefunctions vanish on the singular points). However the 6D vector transforms in general as $A_M \to A_M + \partial_M \theta(x^\mu, x_5, x_6)$, where the gauge parameter θ has the same parities $(+,+)$ of the A_μ component. While A_5, for instance, vanishes on the singular points, $\partial_5 A_5$ does not. This generates for instance new type of mixings in $A_\mu \partial^\mu \partial_5 A_5$. The residual gauge transformation $\partial_5 A_5 \to \partial_5 A_5 + \partial_5^2 \theta$ however constrains the possible couplings containing ∂_5. In order to preserve the full gauge invariance, we therefore construct the operators using the energy-stress tensor components $F_{\mu\nu}$, $F_{5\mu}$, $F_{6\mu}$ and F_{56}. The most general gauge-invariant counter-term Lagrangian is (68):

$$\mathcal{L}_{\text{c-t}} = -\frac{r_1}{4} F_{\mu\nu}^2 - \frac{r_2}{2} F_{56}^2 + \frac{r_5}{2} F_{5\mu}^2 + \frac{r_6}{2} F_{6\mu}^2 + \frac{r_{56}}{2} F_{5\mu} F_6^\mu \tag{3.31}$$

for a Standard Model gauge boson, with parities $(+,+)$, both $A_{5,6}$ and $\partial_{5,6} A_\mu$ vanish on the singular points, therefore $F_{5\mu} = F_{6\mu} = 0$ and $F_{56} = \partial_5 A_6 - \partial_6 A_5$. The counter-term Lagrangian reduces to two operators:

$$\mathcal{L}_{\text{c-t}} = -\frac{r_1}{4} F_{\mu\nu}^2 - \frac{r_2}{2} (\partial_5 A_6 - \partial_6 A_5)^2 \tag{3.32}$$

Let us stress that is true only in $\xi = -3$ gauge, because gauge-invariance forbids any new mixing between the gauge scalars and the vector. Moreover scalars only receive a correction to the masses but not to couplings, as we found in the previous section. For a zero mode, the wavefunction is constant and equal [5] to $\frac{1}{2\pi R}$, therefore the counter-term Lagrangian for zero modes is

$$\delta\mathcal{L}|_{(0,0)} = \frac{2 r_1}{4\pi^2 \Lambda^2 R^2} \left\{ -\frac{1}{4} (F_{\mu\nu}^{0,0})^2 \right\} \tag{3.33}$$

where the 4D gauge coupling is defined as $g_4 = g_6/(2\pi R)$. For the mixing of a level $(2k, 2l)$ vector and a zero mode, we have an extra factor of 2 from the different normalization of the wavefunction of the massive state. Therefore, the mixing and trilinear couplings from the counter-term are

$$A_\mu^{2k,2l} A_\mu^{0,0} \quad \to \quad i\Pi_{\mu\nu} = i \frac{r_1}{\pi^2 \Lambda^2 R^2} \left(q^2 g_{\mu\nu} - q_\mu q_\nu \right) \tag{3.34}$$

$$A_\mu^{2k,2l} A_\mu^{0,0} A_\rho^{0,0} \quad \to \quad iV_{\mu\nu\rho} = i \frac{r_1}{\pi^2 \Lambda^2 R^2} g f^{abc} \mathcal{O}_{\mu\nu\rho} \tag{3.35}$$

This result implies that, in the "magic gauge", the coefficient of the vector mixing and trilinear couplings should be the same: this is in fact true for equations 3.3 and 3.8 for $\xi = -3$, and also for the scalar contributions in equations 3.4 and 3.9. Therefore, in the "magic gauge" we can express the counter-term coefficients as

$$\frac{r_1}{\pi^2 \Lambda^2 R^2} = \frac{g^2 C_2(G)}{4\pi^2 \epsilon} = \frac{\alpha C_2(G)}{\pi} \log \Lambda R \tag{3.36}$$

Finally, putting together the contributions of the gauge bosons and the Higgs in the Standard Model, for the three SM gauge groups U(1) (with gauge coupling g_1), SU(2) (g_2) and SU(3)

[5] Here we integrate the 6D Lagrangian on the torus fundamental space, $x_5 \subset [0, 2\pi R)$ and $x_6 \subset [0, 2\pi R)$. This is however equivalent to integrating over the fundamental square $x_5, x_6 \subset [0, \pi R)$.

(g_3), we obtain the three counter-terms:

$$\frac{r_1^{(1)}}{\pi^2\Lambda^2R^2} = -\frac{2Y_\phi^2}{12}\frac{\alpha_1}{\pi}\log\Lambda R = -\frac{1}{24}\frac{\alpha_1}{\pi}\log\Lambda R \tag{3.37}$$

$$\frac{r_1^{(2)}}{\pi^2\Lambda^2R^2} = \left(C_2(G) - \frac{1}{12}C(r_\phi)\right)\frac{\alpha_2}{\pi}\log\Lambda R = \frac{47}{24}\frac{\alpha_2}{\pi}\log\Lambda R \tag{3.38}$$

$$\frac{r_1^{(3)}}{\pi^2\Lambda^2R^2} = C_2(G)\frac{\alpha_3}{\pi}\log\Lambda R = 3\frac{\alpha_3}{\pi}\log\Lambda R \tag{3.39}$$

The value of r_2 should be calculated from the corrections to odd tiers, like $(2m+1,2n)$-$(1,0)$ mixing, because they contain a physical scalar in their spectrum. We did not perform the same calculation to extract r_2 but we preferred to derive it from the mass corrections to the gauge scalars in the levels $(n,0)$ and $(0,n)$ with n odd computed in (63). After comparing the mass corrections with the counter-term we obtain:

$$\frac{r_2^{(1)}}{\pi^2\Lambda^2R^2} = \frac{2Y_\phi^2}{4}\frac{\alpha_1}{\pi}\log\Lambda R = \frac{1}{8}\frac{\alpha_1}{\pi}\log\Lambda R \tag{3.40}$$

$$\frac{r_2^{(2)}}{\pi^2\Lambda^2R^2} = \left(C_2(G) + \frac{1}{4}C(r_\phi)\right)\frac{\alpha_2}{\pi}\log\Lambda R = \frac{17}{8}\frac{\alpha_2}{\pi}\log\Lambda R \tag{3.41}$$

$$\frac{r_2^{(3)}}{\pi^2\Lambda^2R^2} = C_2(G)\frac{\alpha_3}{\pi}\log\Lambda R = 3\frac{\alpha_3}{\pi}\log\Lambda R \tag{3.42}$$

3.5.2 Scalar counter-terms

After imposing gauge symmetry, many counter-terms are allowed for a scalar field:

$$\begin{aligned}\mathcal{L}_{\rm c-t} = c_1\left(D_\mu\phi\right)^\dagger D^\mu\phi - c_5\left(D_5\phi\right)^\dagger D_5\phi - c_6\left(D_6\phi\right)^\dagger D_6\phi - c_{56}\left(\left(D_5\phi\right)^\dagger D_6\phi + \left(D_6\phi\right)^\dagger D_5\phi\right) + \\ c_5'\left(\left(D_5D_5\phi\right)^\dagger\phi + \phi^\dagger\left(D_5D_5\phi\right)\right) + c_6'\left(\left(D_6D_6\phi\right)^\dagger\phi + \phi^\dagger\left(D_6D_6\phi\right)\right) + \\ c_{56}'\left(\left(D_5D_6\phi\right)^\dagger\phi + \phi^\dagger\left(D_5D_6\phi\right)\right) + c_{65}'\left(\left(D_6D_5\phi\right)^\dagger\phi + \phi^\dagger\left(D_6D_5\phi\right)\right) - \delta m^2\phi^\dagger\phi\end{aligned} \tag{3.43}$$

For a SM Higgs, with parities $(+,+)$, $\partial_5\phi = \partial_6\phi = 0$, while terms like $\partial_5\partial_6\phi = 0$ as they are odd under the glide. Therefore, we are left with a much simpler Lagrangian

$$\mathcal{L}_{\rm c-t} = c_1\left(D_\mu\phi\right)^\dagger D^\mu\phi + c_5'\left(\partial_5^2\phi^\dagger\phi + \phi^\dagger\partial_5^2\phi\right) + c_6'\left(\partial_6^2\phi^\dagger\phi + \phi^\dagger\partial_6^2\phi\right) - \delta m^2\phi^\dagger\phi \tag{3.44}$$

Only 4 counter-terms survive, and no gauge couplings involving gauge scalars are left, confirming the result of our loop calculation. From this Lagrangian, we can extract a prediction for mixing and gauge couplings:

$$\phi^{2k,2l}\phi^{0,0} \to i\Pi = \frac{ic_1}{\pi^2\Lambda^2R^2}q^2 - \frac{ic_5'}{\pi^2\Lambda^2R^2}\frac{(2k)^2}{R^2} - \frac{ic_6'}{\pi^2\Lambda^2R^2}\frac{(2l)^2}{R^2} - i\frac{\delta m^2}{\pi^2\Lambda^2R^2} \tag{3.45}$$

$$\phi^{2k,2l}\phi^{0,0}A_\mu^{0,0} \to -iV_\mu = \frac{c_1}{\pi^2\Lambda^2R^2}g(-q_1^\mu - 2q_2^\mu)t^a \tag{3.46}$$

$$A_\mu^{2k,2l}\phi^{0,0}\phi^{0,0} \to -iV_\mu = \frac{c_1}{\pi^2\Lambda^2R^2}g(q_1^\mu - q_2^\mu)t^a \tag{3.47}$$

Once more our loop calculations respect the predictions in the $\xi = -3$ gauge with

$$\frac{c_1}{\pi^2\Lambda^2 R^2} = -\frac{3}{2}C_2(r_\phi)\frac{\alpha}{\pi}\log\Lambda R \tag{3.48}$$

$$\frac{c_5'}{\pi^2\Lambda^2 R^2} = \frac{c_6'}{\pi^2\Lambda^2 R^2} = -\frac{5}{16}C_2(r_\phi)\frac{\alpha}{\pi}\log\Lambda R\,, \tag{3.49}$$

$$\frac{\delta m^2}{\pi^2\Lambda^2 R^2} = C_2(r_\phi)\frac{\alpha}{\pi}\frac{1}{\eta} \tag{3.50}$$

For the SM Higgs doublet, both U(1) and SU(2) gauge bosons contribute (we neglect here the contribution of the quartic Higgs coupling):

$$\begin{aligned}\frac{c_1}{\pi^2\Lambda^2 R^2} &= -\frac{3}{2}\left(Y_\phi^2\frac{\alpha_1}{\pi} + C_2(r_\phi)\frac{\alpha_2}{\pi}\right)\log\Lambda R = \\ &= -\frac{3}{2}\left(\frac{1}{4}\frac{\alpha_1}{\pi} + \frac{3}{4}\frac{\alpha_2}{\pi}\right)\log\Lambda R \end{aligned}\tag{3.51}$$

$$\frac{c_5'}{\pi^2\Lambda^2 R^2} = \frac{c_6'}{\pi^2\Lambda^2 R^2} = -\frac{5}{16}\left(Y_\phi^2\frac{\alpha_1}{\pi} + C_2(r_\phi)\frac{\alpha_2}{\pi}\right)\log\Lambda R \tag{3.52}$$

$$\frac{\delta m^2}{\pi^2\Lambda^2 R^2} = \left(Y_\phi^2\frac{\alpha_1}{\pi} + C_2(r_\phi)\frac{\alpha_2}{\pi}\right)\frac{1}{\eta} \tag{3.53}$$

3.5.3 Fermion counter-terms

For fermions, the number of allowed counter-terms will be important also because we can consider the 4 chiral components of the 8-component 6D field as independent and construct all possible 4D Lorentz invariant operators, without caring about the Lorentz structure in 6D and the 6D chiralities. On the other hand, loops will respect the 6D Lorentz structure, even in the case of the divergent terms that, as we have seen, do correspond to 4D loops. We can therefore safely limit ourselves to operators in terms of the 6D gamma matrices:

$$\begin{aligned}\mathcal{L}_{\rm c-t} = {} & iz_{1\pm}\,\bar\Psi_\pm\Gamma_\mu D^\mu\Psi_\pm - z_{5\pm}\,\left(i\bar\Psi_\pm\Gamma_5 D_5\Psi_\pm + h.c.\right) - z_{6\pm}\,\left(i\bar\Psi_\pm\Gamma_6 D_6\Psi_\pm + h.c.\right) \\ & - z'_{5\pm}\,\left(i\bar\Psi_\pm\Gamma_6 D_5\Psi_\pm + h.c.\right) - z'_{6\pm}\,\left(i\bar\Psi_\pm\Gamma_5 D_6\Psi_\pm + h.c.\right) - \delta m\,\left(\bar\Psi_+\Psi_- + \bar\Psi_-\Psi_+\right)\end{aligned}\tag{3.54}$$

where the subscript $\pm$ refers to the two 6D chiral components. We can focus in the following on the case of a left-handed zero mode, in which case all the right handed components of the fermion vanish on the fixed points (while their derivatives do not); moreover, we can write the counter-term Lagrangian in terms of 4D chiral fields

$$\Psi_+ = \begin{pmatrix}\psi_{L+}\\ \psi_{R+}\end{pmatrix}\,, \qquad \Psi_- = \begin{pmatrix}\psi_{R-}\\ \psi_{L-}\end{pmatrix} \tag{3.55}$$

In this notation,

$$\begin{aligned}\mathcal{L}_{\rm c-t} = {} & iz_{1\pm}\,\bar\psi_{L\pm}\gamma_\mu D^\mu\psi_{L\pm} + z_{5\pm}\,\left(\bar\psi_{L\pm}\gamma_5\partial_5\psi_{R\pm} + h.c.\right) + z_{6\pm}\,\left(\mp i\bar\psi_{L\pm}\gamma_5\partial_6\psi_{R\pm} + h.c.\right) \\ & + z'_{5\pm}\,\left(\mp i\bar\psi_{L\pm}\gamma_5\partial_5\psi_{R\pm} + h.c.\right) + z'_{6\pm}\,\left(\bar\psi_{L\pm}\gamma_5\partial_6\psi_{R\pm} + h.c.\right)\end{aligned}\tag{3.56}$$

Note that gauge couplings only involve the massive vector, and their coefficient is the same as the correction to the kinetic term proportional to momentum: this is confirmed by equations. 3.18 and 3.21 in $\xi = -3$ gauge! For a zero mode, the wavefunctions, evaluated at any of the four fixed points, are given by

$$\psi_{L+} = p_g\psi_{L-} = \frac{1}{2\sqrt{2}\pi R}\psi_L^{0,0}\,, \qquad \psi_{R+} = \psi_{R-} = 0 \tag{3.57}$$

where $\psi^{0,0}$ is the 4D field and p_g is the parity of the fermion under the glide symmetry. The counter-term Lagrangian, therefore, reads for the zero mode

$$\delta\mathcal{L} = \frac{z_{1+}+z_{1-}}{4\pi^2\Lambda^2R^2}\, i\bar{\psi}_L^{0,0}\gamma_\mu D^\mu_{0,0}\psi_L^{0,0} = \frac{z_1}{2\pi^2\Lambda^2R^2}\, i\bar{\psi}_L^{0,0}\gamma_\mu D^\mu_{0,0}\psi_L^{0,0} \tag{3.58}$$

where, for convenience, we have defined $z_1 = \frac{z_{1+}+z_{1-}}{2}$, and $D^\mu_{0,0}$ is the covariant derivative that only contains the zero mode gauge vector. Note that the coupling of $A_\mu^{2k,2l}$ with zero mode fermions will have the same coefficient up to a factor of 2 from the wave function normalization.

Now, let us consider the terms with one fermion from level $(2k, 2l)$ and zero modes: for the state a, the wavefunctions calculated at the fixed points are

$$\psi^a_{L+} = p_g\psi^a_{L-} = \frac{1}{\sqrt{2}\pi R}\psi^{2k,2l}_{aL} \tag{3.59}$$

$$\partial_5\psi^a_{R+} = p_g\partial_5\psi^a_{R-} = -\frac{(2k)^2}{R\sqrt{(2k)^2+(2l)^2}}\frac{1}{\sqrt{2}\pi R}\psi^{2k,2l}_{aR} \tag{3.60}$$

$$\partial_6\psi^a_{R+} = -p_g\partial_6\psi^a_{R-} = i\frac{(2l)^2}{R\sqrt{(2k)^2+(2l)^2}}\frac{1}{\sqrt{2}\pi R}\psi^{2k,2l}_{aR} \tag{3.61}$$

Plugging those solutions in the counter-term Lagrangian, we obtain

$$\delta\mathcal{L}|_a = \frac{z_1}{\pi^2\Lambda^2R^2}\left(i\bar{\psi}_L^{0,0}\gamma_\mu D^\mu_{0,0}\psi^{2k,2l}_{aL} + h.c.\right) - \left[\left(\frac{z_{5+}+z_{5-}}{2\pi^2\Lambda^2R^2} - i\frac{z'_{5+}-z'_{5-}}{2\pi^2\Lambda^2R^2}\right)\frac{2k^2}{R\sqrt{k^2+l^2}} + \left(\frac{z_{6+}+z_{6-}}{2\pi^2\Lambda^2R^2} + i\frac{z'_{6+}-z'_{6-}}{2\pi^2\Lambda^2R^2}\right)\frac{2l^2}{R\sqrt{k^2+l^2}}\right]\left(\bar{\psi}_L^{0,0}\psi^{2k,2l}_{aR} + h.c.\right) \tag{3.62}$$

For a fermion b

$$\psi^b_{L+} = \psi^b_{L-} = 0 \tag{3.63}$$

$$\partial_5\psi^b_{R+} = -p_g\partial_5\psi^b_{R-} = i\frac{(2k)(2l)}{R\sqrt{(2k)^2+(2l)^2}}\frac{1}{\sqrt{2}\pi R}\psi^{2k,2l}_{bR} \tag{3.64}$$

$$\partial_6\psi^b_{R+} = p_g\partial_6\psi^b_{R-} = \frac{(2l)(2k)}{R\sqrt{(2k)^2+(2l)^2}}\frac{1}{\sqrt{2}\pi R}\psi^{2k,2l}_{bR} \tag{3.65}$$

and therefore

$$\delta\mathcal{L}|_b = \left(i\frac{z_{5+}-z_{5-}-z_{6+}+z_{6-}}{2\pi^2\Lambda^2R^2} + \frac{z'_{5+}+z'_{5-}+z'_{6+}+z'_{6-}}{2\pi^2\Lambda^2R^2}\right)\frac{2kl}{R\sqrt{k^2+l^2}}\left(\bar{\psi}_L^{0,0}\psi^{2k,2l}_{bR} + h.c.\right) \tag{3.66}$$

From the kinetic term, we can easily check that in the "magic gauge" the loop calculation agrees with the presence of a unique counter-term, and

$$\frac{z_1}{\pi^2\Lambda^2R^2} = \left(-C_2(r_f)\frac{\alpha}{\pi} + \frac{1}{8}\frac{y_f^2}{4\pi^2}\right)\log\Lambda R \tag{3.67}$$

Note however that we cannot determine if $z_{1+} = z_{1-}$! Regarding the mass terms, from the fact that the fermion b does not receive divergent corrections and that the correction to the fermion a is proportional to $\sqrt{k^2+l^2}$, we can deduce that $z_{5\pm} = z_{6\pm}$ and that $z'_{5+} = z'_{5-} = -z'_{6+} = -z'_{6-} = z'$. Defining $z_2 = \frac{z_{5+}+z_{5-}}{2} = \frac{z_{6+}+z_{6-}}{2}$ and matching with the loop calculation, we have

$$\frac{z_2}{\pi^2\Lambda^2R^2} = \frac{1}{8}\frac{y_f^2}{4\pi^2}\log\Lambda R \tag{3.68}$$

As before, we cannot tell if $z_{5+} = z_{5-}$ or if $z' = 0$. In table 3.10 we list the coefficient for the counter-terms of the SM matter content.

	$\frac{z_1}{\pi^2\Lambda^2R^2}$	$\frac{z_2}{\pi^2\Lambda^2R^2}$
E	$-\frac{\alpha_1}{\pi}+\frac{1}{8}\frac{y_e^2}{4\pi^2}$	$\frac{1}{8}\frac{y_e^2}{4\pi^2}$
L	$-\frac{1}{4}\frac{\alpha_1}{\pi}-\frac{3}{4}\frac{\alpha_2}{\pi}+\frac{1}{8}\frac{y_e^2}{4\pi^2}$	$\frac{1}{8}\frac{y_e^2}{4\pi^2}$
U	$-\frac{4}{9}\frac{\alpha_1}{\pi}-\frac{4}{3}\frac{\alpha_3}{\pi}+\frac{1}{8}\frac{y_u^2}{4\pi^2}$	$\frac{1}{8}\frac{y_u^2}{4\pi^2}$
D	$-\frac{1}{9}\frac{\alpha_1}{\pi}-\frac{4}{3}\frac{\alpha_3}{\pi}+\frac{1}{8}\frac{y_d^2}{4\pi^2}$	$\frac{1}{8}\frac{y_d^2}{4\pi^2}$
Q	$-\frac{1}{36}\frac{\alpha_1}{\pi}-\frac{3}{4}\frac{\alpha_2}{\pi}-\frac{4}{3}\frac{\alpha_3}{\pi}+\frac{1}{8}\frac{y_u^2+y_d^2}{4\pi^2}$	$\frac{1}{8}\frac{y_u^2+y_d^2}{4\pi^2}$

Table 3.10: Coefficients of the fermion counter-terms in the SM.

3.6 Physical observables: effective couplings and decays

In this section we will focus on a set of important effective couplings involving a heavy state $(2k, 2l)$ going into Standard Model particles. There are required to study phenomenology because they control decays and single productions of those heavy states. In the previous section 3.5, we computed actually the corrections to interaction eigenstates and we derived the full set of counter-terms generated on the RPP. But the relevant quantities are the eigenstate of mass to study physical observables. So to obtain the effective couplings of the theory, we need to sum for a process, the whole set of counter-terms with the same order in perturbation field theory. This means summing the correction to the coupling but also mixing term contributions.

We will show that, as expected, they are gauge independent (in the limit of on-shell external particles): this fact has an important consequence. We can use therefore the simple structure of the counter-terms in the "magic gauge" $\xi = -3$ to predict the decay rates and single production cross sections of all KK tiers. This is possible because in all the relevant cases we need the coupling with on-shell particles. The contributions of off-shell particles will be subleading compared to tree-level bulk couplings, therefore gauge dependent contributions can be safely neglected. In the following we consider all the possible decays and explicitly check the gauge invariance of the effective couplings. In the limit of massless Standard Model particles, the decay into heavy gauge bosons (the W and Z) is given, thanks to the equivalence principle, by the decay rate into Higgs boson (ϕ): we will also show in appendix C how we can obtain the same rates from a coupling involving only vector bosons by considering corrections to the effective coupling subleading in the Higgs VEV. This result will be important to obtain these decays in the Unitary gauge.

Figure 3.15: Contributions to the decay from bilinear and trilinear counter-terms.

3.6.1 Heavy gauge boson decays into massless SM particles

Heavy vector to vectors, $A_\mu^{2k,2l} \longrightarrow A_\nu^{0,0} A_\rho^{0,0}$

The effective vertex of one heavy vector to SM vectors is given by the graphs in figure 3.15, where a gray dot stands for a counter-term insertion (either trilinear coupling or mixing term). The mixing terms contribute by converting a massive state in the external leg into a zero mode (while the bulk couplings do preserve KK number). Summing all the contributions for an SU(N) gauge boson, we obtain:

$$iV^{\mu\nu\rho} = \frac{ig^3 f^{abc} C_2(G)}{16\pi^4} \frac{i\pi^2}{\epsilon} \mathcal{T}^{\mu\nu\rho} \tag{3.69}$$

where the gauge dependent tensor $\mathcal{T}^{\mu\nu\rho}$ is given by:

$$\begin{aligned}\mathcal{T}^{\mu\nu\rho} =& \frac{4M^2((\xi-11)\xi+6)(q_1^\nu - q_2^\rho)g^{\mu\rho} + ((\xi-12)\xi+3)(q_2^\mu - q_1^\mu)q_1^\nu q_2^\rho}{16M^2\xi} \\ &+ \frac{(\xi-1)(\xi+1)(\xi+3)(q_1^\mu + q_2^\mu)(q_1^\nu q_1^\rho - q_2^\nu q_2^\rho)}{16M^2\xi}\end{aligned} \tag{3.70}$$

In the limit of massless zero modes, from gauge invariance we would expect this decay to vanish: in fact

$$\mathcal{T}^{\mu\nu\rho}\epsilon^\rho(q_2)\epsilon^\nu(q_1) = 0 \tag{3.71}$$

where $\epsilon^\nu(q_1)$ and $\epsilon^\rho(q_2)$ are the polarization vectors of the two (massless) vectors. Note that the other two contractions

$$\begin{aligned}\mathcal{T}^{\mu\nu\rho}\epsilon^\mu(q)\epsilon^\nu(q_1) &\neq 0 \\ \mathcal{T}^{\mu\nu\rho}\epsilon^\rho(q_2)\epsilon^\mu(q) &\neq 0\end{aligned}$$

do not vanish because $A_\mu^{2k,2l}$ is massive. This means, for instance, that a heavy gluon cannot decay into two SM gluons. On the other hand, the decay into massive gauge bosons, the W and Z, in this limit, is given by the decay into the Higgs components, as discussed below.

Heavy vector to fermions, $A_\mu^{2k,2l} \longrightarrow \bar{f}f$

Fermionic decays of the heavy gauge vector are given by the diagrams in figure 3.16: like in the previous case, we will consider the external particle on-shell; this means that incoming gauge boson is taken with mass $(2M)^2 = q^2$ and that we have $\not{q}_1 = \not{q}_2 = 0$ for the out-coming particles. In this limit, for an SU(N), the effective vertex can be written as:

$$i\Gamma_A^\mu = \frac{g^3}{16\pi^4} \frac{i\pi^2}{\epsilon} \tau_A \gamma^\mu P_L t^a \tag{3.72}$$

where the contribution of the single diagrams are listed in table 3.11.

The total result is, as expected, independent on ξ and given by:

$$i\Gamma^\mu = -\frac{g^3}{16\pi^4} \frac{i\pi^2}{\epsilon} 4(C_2(r_f) - C_2(G))\gamma^\mu P_L t^a \tag{3.73}$$

For a U(1) gauge boson, it is enough to replace $C_2(G) \to 0$, $C_2(r_f) \to Y_f^2$ and $t^a \to Y_f$. If we consider the corrections by a gauge group SU(N') to the decays of an SU(N) gauge boson, in the formula we replace $g^3 \to gg'^2$, $C_2(G) \to 0$ and $C_2(r) \to C_2(r')$. For the Yukawa part, we replace $g^3 \to g{y_\psi}^2$. Recall that for a generic SU(N)[6]: $C_2(G) = N$ et $C_2(N) = \frac{N^2-1}{2N}$.

Finally we quote the effective couplings in the case of the Standard Model on the Real Projective Plane. As more gauge groups contribute to the same effective coupling, we parametrize a generic coupling as

$$i\Gamma_X^\mu = -i\frac{g}{\pi\epsilon}\, C_X \gamma^\mu P_L t^a \tag{3.74}$$

where the various coefficients C_X are listed in table 3.12.

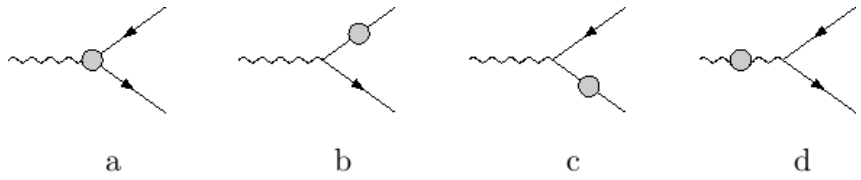

Figure 3.16: Contributions to the decay from bilinear and trilinear counter-terms.

τ_x	R_ξ gauge	$\xi = 1$ Feynman gauge	Higgs	Yukawa
τ_a	$\frac{1}{4}(4(\xi-1)C_2(r_f) + (\xi+3)C_2(G))$	$C_2(G)$	0	1/2
τ_{b+c}	$-2\ \frac{1}{2}(\xi+3)C_2(r_f)$	$-4C_2(r_f)$	0	$-2\ \frac{1}{2}$
τ_d	$\frac{1}{4}(13-\xi)C_2(G)$	$3C_2(G)$	$-\frac{1}{3}C(r_\phi)$	0
τ_{tot}	$4(C_2(G) - C_2(r_f))$	$4C_2(G) - 4C_2(r_f)$	$-\frac{1}{3}C(r_\phi)$	$-\frac{1}{2}$

Table 3.11: Contributions to the effective vertex with two massless fermions. The results in Feynman gauge $\xi = 1$ are also listed to be compared with the direct calculation done in section 3.7. For a singlet, the Yukawa contribution is multiplied by a factor of 2.

Yukawa couplings

In table 3.12, we give the contribution of the Yukawa couplings. Here we will detail the last column of this table. These contributions will be generated by the counter-terms of gauge vertex and fermion propagators, therefore they will contribute to diagrams (a), (b) and (c) in figure 3.16. As singlets and doublets couple differently to the Higgs, we need to distinguish the two cases: the different couplings are summarized in table 3.13.

Note that the contribution to the U(1) gauge boson coupling are always proportional to the fermion hypercharge, as expected. The total contribution is given in table 3.12.

Heavy vector to scalars : $A_\mu^{2k,2l} \longrightarrow \phi^\dagger\phi$

In this section we will focus on the decay into scalars. The incoming gauge boson is taken on-shell with mass $(2M)^2 = q^2$ and also the out-coming particles which means that $q_1^2 = q_2^2 = 0$.

[6]For SU(2): $C_2(2) = \frac{3}{4}$ and $C_2(2) - C_2(G) = -\frac{5}{4}$; while for SU(3): $C_2(3) = \frac{4}{3}$ and $C_2(3) - C_2(G) = -\frac{5}{3}$

U(1)	gauge	Higgs	Yukawa
$B \to E$	α_1	$\frac{1}{24}\alpha_1$	$\frac{1}{2}\frac{y_l^2}{4\pi}$
$B \to L$	$\frac{1}{4}\alpha_1 + \frac{3}{4}\alpha_2$	$\frac{1}{24}\alpha_1$	$\frac{1}{4}\frac{y_l^2}{4\pi}$
$B \to U$	$\frac{4}{9}\alpha_1 + \frac{4}{3}\alpha_3$	$\frac{1}{24}\alpha_1$	$\frac{1}{2}\frac{y_u^2}{4\pi}$
$B \to D$	$\frac{1}{9}\alpha_1 + \frac{4}{3}\alpha_3$	$\frac{1}{24}\alpha_1$	$\frac{1}{2}\frac{y_d^2}{4\pi}$
$B \to Q$	$\frac{1}{36}\alpha_1 + \frac{3}{4}\alpha_2 + \frac{4}{3}\alpha_1$	$\frac{1}{24}\alpha_1$	$\frac{1}{4}\frac{y_u^2+y_d^2}{4\pi}$
SU(2)	gauge	Higgs	Yukawa
$W \to L$	$\frac{1}{4}\alpha_1 - \frac{5}{4}\alpha_2$	$\frac{1}{24}\alpha_2$	$\frac{1}{4}\frac{y_l^2}{4\pi}$
$W \to Q$	$\frac{1}{36}\alpha_1 - \frac{5}{4}\alpha_2 + \frac{4}{3}\alpha_3$	$\frac{1}{24}\alpha_2$	$\frac{1}{4}\frac{y_u^2+y_d^2}{4\pi}$
SU(3)	gauge	Higgs	Yukawa
$G \to U$	$\frac{4}{9}\alpha_1 - \frac{5}{3}\alpha_3$	0	$\frac{1}{2}\frac{y_u^2}{4\pi}$
$G \to D$	$\frac{1}{9}\alpha_1 - \frac{5}{3}\alpha_3$	0	$\frac{1}{2}\frac{y_d^2}{4\pi}$
$G \to Q$	$\frac{1}{36}\alpha_1 + \frac{3}{4}\alpha_2 - \frac{5}{3}\alpha_3$	0	$\frac{1}{4}\frac{y_u^2+y_d^2}{4\pi}$

Table 3.12: Coefficients C_X as defined in equation 3.74 of the effective couplings in the Standard Model in the gauge basis.

	U(1) to singlet	U(1) to doublet	SU(2) to singlet	SU(2) to doublet	SU(3)
a	Y_S	$1/2Y_D$	0	1/2	1/2
$b+c$	Y_S	$1/2Y_D$	0	1/2	1/2
tot	$2Y_S$	Y_D	0	1	1

Table 3.13: Contributions of Higgs loops. Y_S and Y_D are the hypercharges of the singlet and doublet respectively, while Y_ϕ is the hypercharge of the Higgs.

Figure 3.17: Contributions to the decay from bilinear and trilinear counter-terms.

So from this information we can calculate the different contributions given in figure 3.17. For a SU(N) gauge boson, we obtain the following result:

$$iV^\mu = \frac{g^3}{16\pi^4}\left\{\frac{i\pi^2}{\epsilon}\ 4\left(\frac{7}{8}C_2(r_\phi) - C_2(G) + \frac{1}{12}C(r_\phi)\right) - \frac{2i\pi^3}{\eta M^2}C_2(r_\phi)\right\}\ (q_1^\mu - q_2^\mu)t^a \qquad (3.75)$$

In this case the result is gauge independent as expected. In the following we will neglect the quadratically divergent contribution because, as explained before, this contribution is assumed to be of the order of the Higgs mass. As in the fermion case, the previous calculation made for generic SU(N) can be generalized: for a U(1) gauge boson, it is enough to replace $C_2(G) \to 0$, $C_2(r_\phi) \to Y_\phi^2$, $C_(r_\phi) \to 2Y_\phi^2$[7] and $t^a \to Y_\phi$; for corrections of a different gauge group, $C_2(G) \to 0$,

[7]The factor of 2 is here to count the two components of the scalar doublet under $SU(2)$.

$C_2(r) \to C_2(r')$ and $g^3 \to gg'^2$.

The only scalar in the SM is the Higgs, which is a doublet of SU(2) with hypercharge $Y_\phi = 1/2$. Only SU(2) and U(1) gauge fields, therefore, can decay into Higgs fields. Note also that, in the limit of unbroken SU(2)× U(1) that we are considering here, the Higgs doublet contains both the physical Higgs boson h and the Goldstone bosons which are the longitudinal polarizations of the massive zero mode vectors, W and Z. Therefore, we can use the equivalence principle to calculate the decay to Goldstone bosons and identify these partial widths with the ones in massive vectors. We will discuss in more detail the equivalence in appendix C.

The effective coupling of a heavy vector to scalars can be parametrized as:

$$iV^\mu = i\frac{g}{\epsilon}\, C_X\, (q_1^\mu - q_2^\mu) t^a \tag{3.76}$$

The values of the coefficients C_X for SU(2) and U(1) gauge bosons are given in table 3.14.

heavy gauge boson	C_X
$U(1)$	$\alpha_1 \frac{25}{96} + \alpha_2 \frac{21}{32}$
$SU(2)$	$\alpha_1 \frac{7}{32} - \alpha_2 \frac{125}{96}$

Table 3.14: Coefficients of the effective couplings of a heavy vector with scalars.

Gauge scalar decays: $A_\phi^{2k,2l} \longrightarrow \bar{f}f,\ \phi^\dagger\phi$

The gauge scalar can also, in principle, decay into a pair of fermions or scalars via the diagrams in figure 3.18: note that counter-terms of the trilinear coupling and of the mixing of the gauge scalar are absent. However, the sum of the two diagrams vanishes once we take on-shell fermions: in the mixing counter-term, the part proportional to the momentum is equal to zero for on-shell external fermions, while the term proportional to the heavy mass M cancels out between the two diagrams. Therefore, this effective vertex is absent.

Figure 3.18: Contributions to the decay from bilinear and trilinear counter-terms.

3.6.2 Heavy fermion decays

Via a (massless) gauge boson, $\psi^{2k,2l} \to f A_\mu$

Heavy fermions can couple to a light fermion plus a zero mode gauge boson. In this section, we will limit ourselves to the case of exactly massless gauge bosons: the decay to massive ones, like the W and Z, is in this approximation given by the decay to Higgs bosons. The effective vertex is given by the diagrams in figure 3.19: we will always consider on-shell external particles, therefore $\not{q} = 2M$ while the out-coming particles are massless.

In general, the effective vertex is given by the following formula:

$$i\Gamma^{\mu}_{X} = \frac{g^3}{16\pi^4}\frac{i\pi^2}{\epsilon}(\tau_x\gamma^{\mu} + \sigma_x q_1^{\mu})P_L t^a \tag{3.77}$$

The τ-term is a correction to the usual gauge coupling and, from gauge invariance, we would expect it to vanish. To be more concrete, physical decays mediated by a Lagrangian of the form: $\psi^{2k,2l}\gamma^{\mu} f A_{\mu}$ and because of gauge invariance this term would be associated to the non-diagonal kinetic term: $\psi^{2k,2l}\gamma^{\mu}\partial_{\mu} f$. Nevertheless such non-diagonal kinetic term cannot be present anymore because it has been removed by the procedure consisting in summing all the bilinear and trilinear counter-terms.

The second term (where q_1 is the momentum of the gauge boson) is potentially non-zero and will lead to a coupling quite similar to the $b \to s\gamma$ coupling of the Standard Model. However, when calculating the decay width, is must be contracted with the polarization vector of the gauge boson:

$$i\mathcal{M} = i\Gamma^{\mu}\epsilon_{\mu}(q1) \propto q_1^{\mu}.\epsilon_{\mu}(q_1) = 0 \tag{3.78}$$

where the product vanishes because of the masslessness of the gauge boson. Therefore, we expect that the fermion cannot decay into a massless gauge boson.

The contributions of each diagram are listed in table 3.15: all in all we have

$$i\Gamma^{\mu} = \frac{g^3}{16\pi^4}\frac{i\pi^2}{8M\epsilon}(13-\xi)C_2(G)q_1^{\mu}P_L t^a \tag{3.79}$$

We can see that this vertex is gauge dependent, however it does not contribute to the decay width.

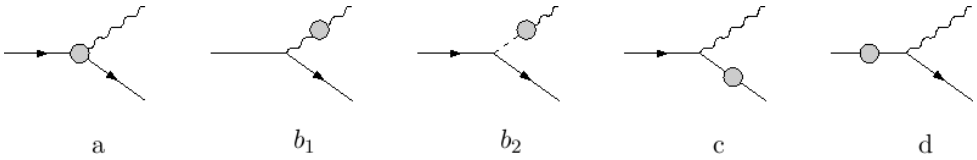

Figure 3.19: Contributions to the decay from bilinear and trilinear counter-terms.

diagram	τ_x	σ_x
a	$\frac{1}{4}(4(\xi-1)C_2(r)+(\xi+3)C_2(G))$	0
b_1+b_2	$-\frac{1}{4}(\xi+3)C_2(G)$	$\frac{1}{8M}(13-\xi)C_2(G)$
c	$-\frac{1}{2}(\xi+3)C_2(r_f)$	0
d	$(-(\xi-1)+\frac{1}{2}(\xi+3))C_2(r_f)$	0
tot	0	$\frac{1}{8M}(13-\xi)C_2(G)$

Table 3.15: Contributions to the effective coupling of heavy fermions with SM fermions and massless gauge bosons.

Via a (massless) Higgs boson, $\psi^{2k,2l} \to f\phi$

Heavy fermions can also couple to a light fermion plus a scalar zero mode through Yukawa couplings. The effective vertex, given by the diagrams in figure 3.20, will describe the coupling

to the Higgs boson and also to the longitudinal polarization of W and Z gauge bosons. We will always consider on-shell external particles, therefore $\not{q} = 2M$ while the out-coming particles are massless.

In general, the effective vertex is given by the following formula:

$$i\Gamma = -\frac{y_\psi}{16\pi^4}\frac{i\pi^2}{\epsilon}(g^2\tau_\phi + y_\psi^2\tau'_\phi)P_{L(R)} \tag{3.80}$$

The τ, τ'-term are corrections to the usual Yukawa coupling and are given in table 3.16. Here we consider the case of the down-type Yukawa where $Y_D = Y_S + Y_\phi$.

While τ'_x is gauge invariant, τ_x may in general depend on the ξ parameter: therefore we need to check case by case that the gauge dependence is canceled. For a U(1) gauge boson, $t^a(r_X) \to Y_X$ and $C_2(r_X) \to Y_X^2$:

$$\tau^D_{U(1)} = \frac{\xi}{2}(Y_D - Y_S - Y_\phi)^2 + 3Y_DY_S - 1/4Y_\phi^2 - 3/2Y_S^2 + 5/2Y_D^2 = \\ 3Y_DY_S - 1/4Y_\phi^2 - 3/2Y_S^2 + 5/2Y_D^2 \tag{3.81}$$

In the case of SU(2), when D and the scalar are doublets and S is a singlet, we have $t^a(r_D).t^a(r_h) = C_2(r_\phi)$ while $t^a(r_S) = 0$ and $C_2(r_S) = 0$; therefore

$$\tau^D_{SU(2)} = \frac{\xi}{2}(2C_2(r_\phi) - C_2(r_\phi) - C_2(r_\phi)) + \left(-\frac{1}{4} + \frac{5}{2}\right)C_2(r_\phi) = \frac{9}{4}C_2(r_\phi) = \frac{27}{16} \tag{3.82}$$

Finally, for SU(3), it is the Higgs that does not couple to gluons, therefore $t^a(r_D).t^a(r_S) = C_2(r_f)$ while $t^a(r_\phi) = 0$ and $C_2(r_\phi) = 0$. The total result is:

$$\tau^D_{SU(3)} = \frac{\xi}{2}(2C_2(r_f) - C_2(r_f) - C_2(r_f)) + \left(3 - \frac{3}{2} + \frac{5}{2}\right)C_2(r_f) = 4C_2(r_f) = \frac{16}{3} \tag{3.83}$$

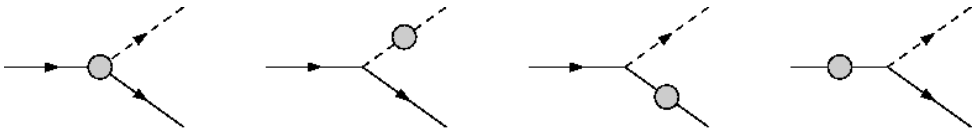

Figure 3.20: Contributions to the decay from bilinear and trilinear counter-terms.

diagram	τ_x	τ'_x
a	$(\xi+3)t^a(r_D).t^a(r_S) + \xi(-t^a(r_S) + t^a(r_D)).t^a(r_h)$	1
b	$-\frac{1}{4}(2\xi+1)C_2(r_h)$	0
c	$-\frac{1}{2}(\xi+3)C_2(r_S)$	$-\frac{1}{2}$
d	$\frac{1}{2}(-\xi+5)C_2(r_D)$	0
tot	$\xi(t^a(r_D).t^a(r_S) - t^a(r_S).t^a(r_h) + t^a(r_D).t^a(r_h)) +$ $-\xi/2(C_2(r_h) + C_2(r_D) + C_2(r_S)) +$ $3t^a(r_D).t^a(r_S) - 1/4C_2(r_h) - 3/2C_2(r_S) + 5/2C_2(r_D)$	$\frac{1}{2}$

Table 3.16: In the case of $SU(2)$ the representation is the same for the Higgs and for the fermion doublets.

For the decay of singlets into doublets, we have up-type Yukawa couplings and in table 3.16, the diagram (c) is proportional to $C(r_S)$, while diagram (d) to $C(r_D)$. The new coefficient in this case are:

$$\tau^S_{U(1)} = 3Y_D Y_S - 1/4 Y_\phi^2 - 3/2 Y_D^2 + 5/2 Y_S^2 \tag{3.84}$$

$$\tau^S_{SU(2)} = \left(-\frac{1}{4} - \frac{3}{2}\right) C_2(r_\phi) = -\frac{7}{4} C_2(r_\phi) = -\frac{21}{16} \tag{3.85}$$

$$\tau^S_{SU(3)} = \tau^D_{SU(3)} \tag{3.86}$$

Furthermore, the contribution of diagram (c) to τ'_X picks a factor of $1/2$ because it applies to the correction to a doublet fermion, and it is proportional to both Yukawa couplings of the doublet (this is relevant in the case of the quarks).

To summarize the results in the case of Standard Model fermions, if we parametrize the effective coupling as

$$i\Gamma = -i\frac{y_f}{\pi\epsilon} C_X P_{L(R)} \tag{3.87}$$

the coefficients are given in table 3.17.

heavy gauge boson	C_X
$C_{L\to E\phi}$	$\frac{9}{64}\alpha_1 + \frac{29}{64}\alpha_2 + \frac{1}{8}\frac{y_l^2}{4\pi}$
$C_{E\to L\phi^\dagger}$	$\frac{57}{64}\alpha_1 - \frac{21}{64}\alpha_2 + \frac{3}{16}\frac{y_l^2}{4\pi}$
$C_{Q\to U\phi^\dagger}$	$-\frac{47}{576}\alpha_1 + \frac{29}{64}\alpha_2 + \frac{4}{3}\alpha_3 + \frac{1}{8}\frac{y_u^2}{4\pi}$
$C_{Q\to D\phi}$	$-\frac{47}{576}\alpha_1 + \frac{29}{64}\alpha_2 + \frac{4}{3}\alpha_3 + \frac{1}{8}\frac{y_d^2}{4\pi}$
$C_{U\to Q\phi}$	$\frac{193}{576}\alpha_1 - \frac{21}{64}\alpha_2 + \frac{4}{3}\alpha_3 + \frac{1}{16}\frac{3y_u^2+2y_d^2}{4\pi}$
$C_{D\to Q\phi^\dagger}$	$\frac{1}{576}\alpha_1 - \frac{21}{64}\alpha_2 + \frac{4}{3}\alpha_3 + \frac{1}{16}\frac{3y_d^2+2y_u^2}{4\pi}$

Table 3.17: Coefficients of the effective couplings of an heavy fermion decaying into SM scalar and fermion.

3.7 Compatibility with "genuine" 6D calculations

In this section, we will present the original computation performed to extract the couplings between the $(2n, 0)$ modes and zero-modes. Interesting from a phenomenological point of view, this study has been considerably simplified by the previous considerations. However, we will show with this full "genuine" 6D calculation the compatibility of both techniques to extract the structure of localized counter-terms. Here we will also obtain in addition the finite part contribution coming from the torus and glides. The 6D calculations were performed in Feynman gauge ($\xi = 1$) and using the 6D mixed propagator we presented in section 2.3. We will focus, for this purpose, on the decay of heavy vectors into massless Standard Model fermions.

3.7.1 Off diagonal mixing between $(2n, 0)$-$(0, 0)$

In order to compute the whole set of counter-terms with the same order in perturbation theory for masses and couplings, we derived the loop corrections to self-energy of gauge bosons and fermions and trilinear vertices.

The mixing between the $(2n,0)$ and $(0,0)$ modes is obtained by computing the same loop as the one mentioned in figure 3.1. The external field $(2n,0)$ with the 4D-momentum q is taken on-shell, which implies $q^2 = 4n^2$. We will consider only the contribution of the $g^{\mu\nu}$ part, the non-relevant $q^\mu q^\nu$ part has not been computed in this study. Following the prescription, we described in chapter 2, we can show that the mixing term Π can be written as $\Pi = \Pi_T + \Pi_G + \Pi_{G'} + \Pi_R$ where

$$\Pi = \frac{1}{3}\left(\Pi^\mu_{\ \mu} - \frac{q^\mu q^\nu}{q^2}\Pi_{\mu\nu}\right) \tag{3.88}$$

Torus and glide contributions are vanishing and the non-zero contributions are compiled in table 3.18. The coefficients of this table need to be multiplied by the factor N' to obtain Π self-energy:

$$N' = \frac{1}{\sqrt{2}}\frac{2g^2C_2(r)}{4\ 16\pi^4} \tag{3.89}$$

where $C_2(r)$ is the quadratic Casimir operator of the r representation under $SU(N)$.

As these calculations are done with dimensional regularization, the log-divergence corresponds to the $1/\epsilon$ pole in $d = 4$. In this framework, we can also show that there is no divergence for a dimension $d = 2$ (no pole in $1/\eta$) as we can expect from gauge boson self-energy. Note that for the loop with scalar fields, a quadratic divergence in the rotation part remains if we use directly the cut-off regularization (8).

3.7.2 6D loop triangle calculation with mixed propagators

When we compute triangle loops with the mixed propagator technique, we also divide the different contributions, which will be label V, into 4 pieces. This property is directly linked to the symmetry of propagators under the RPP isometries. From a technical point of view, the three propagators that will enter into the loop calculation will be the one given in appendix A. So by default we could think of having $4 \times 4 \times 4 = 64$ different parts corresponding to the 64

Π	Π_T	Π_G	Π'_G	Π_R
a+b	0	0	$(-1)^{n+1}\ (-3\Phi_1(n))$	$-\pi^2 n^2 L$
c	0	0	$(-1)^{n+1}\left(-\frac{9\Phi_3(n)}{4} + \Phi_1(n) + 8\Phi_2(n)\right)$	$\pi^2\frac{65}{6}L$
d	0	0	$(-1)^{n+1}\ (4\Phi_2(n) + \Phi_3(n))$	$3\pi^2 n^2 L$
e	0	0	0	$-\frac{2}{3}\pi^2 n^2 L$
f	0	0	$(-1)^{n+1}\ \frac{\Phi_3(n)}{4}$	$-\pi^2\frac{1}{6}n^2 L$
fermions	0	0	0	0
total	0	0	$(-1)^{n+1}\,(-2\Phi_1(n) + 12\Phi_2(n) - \Phi_3(n))$	$12n^2\pi^2 L$
hcomplex	0	0	$(-1)^{n+1}\ (-\Phi_3(n))$	$\frac{2}{3}\pi^2 n^2 L$
icomplex	0	0	$2(-1)^{n+1}\ (-\Phi_1(n))$	$-2\pi^2 n^2 L$

Table 3.18: $A_\mu^{2n,0} - A_\nu^{0,0}$ mixing: loops a–f are gauge corrections while h and i are scalar field corrections. Those loops are drawn in figure 3.1. This calculation has been performed in Feynman gauge ($\xi = 1$) using directly the mixed propagator technique in 6D.

possibilities of combining the various parts of the propagator. Nevertheless by doing appropriate changes of variables, we can prove that there are only four equivalent classes of contributions to the coupling corrections:

$$V = V_T + V_G + V_{G'} + V_R \tag{3.90}$$

the first term V_T is the contribution we would get from the same fields on a torus orbifold. This contribution is finite because we are considering a vertex which violates KK-momentum conservation. In general, we should renormalize the bulk kinetic terms to reabsorb all divergences. The other three terms correspond to the two glides and the rotation, in the sense that their sign depends on the parities (p_r, p_g) of the fields running in the loop. The contribution of the two glides is finite because the glides do not have any fixed points where a counter-term could be localized. On the other hand, the rotation does generate divergences which will be cut-off by counter-terms localized on the four points left fixed by the rotation, i.e. the two singular points of the orbifold. As we have already seen, the singularities will be equally spread on the two points, because of the extended global symmetries of the bulk interactions. As we are considering the example of the heavy gauge boson decay, the triangle loops that are present in our case are represented in figure 3.21. The contribution for the loop a_1 is given by the following expression:

$$\begin{aligned} iV_{a1}^{\mu} =& g_6^3 \cdot C_2(r) t^a \cdot \frac{i^3}{16\pi^4} \sum_{l,l',l''} \int dp \int dx_1 \dots dy_3 \\ & \theta_M^t \; F_{\bar{\Psi}}^{0,0}(x_3, y_3) \Gamma^M \Gamma^A \Gamma^\mu \Gamma^B \Gamma^N F_{\Psi}^{0,0}(x_2, y_2) \\ & i\partial_A G_s(\chi_3^{l''}, x_3, x_1) \; (-g^{MN}) G_s(\chi_2^{l'}, x_2, t(x_3)) \; i\partial_B G_s(\chi_1^{l}, x_1, x_2) \\ & f_l^*(y_1) f_l(y_2) f_{l'}^*(y_2) f_{l'}(t(y_3)) f_{l''}^*(y_3) f_{l''}(y_1) \; f_A^{2n,0}(x_1, y_1) \end{aligned} \tag{3.91}$$

Gauge and fermion propagators are given in appendix A, and $t = id, g, rg, r$ are RPP isometries. Here $f_{A^\mu}^{2n,0}$ is the wavefunction of the heavy gauge boson and $F_{\Psi}^{0,0}$ stands for the vector

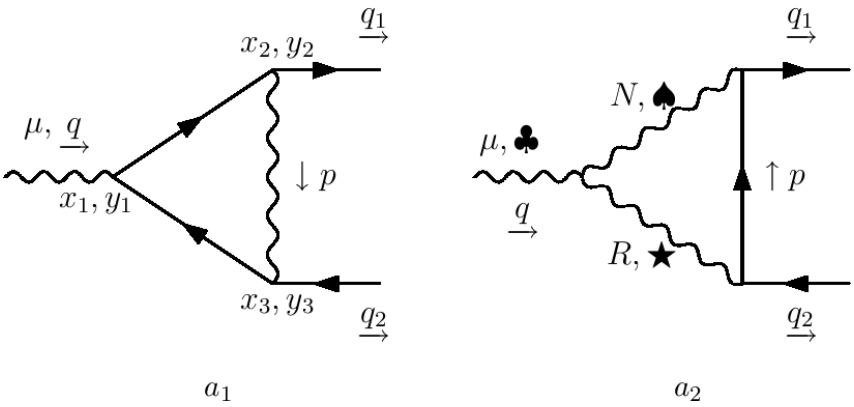

Figure 3.21: $A_\mu^{2n,0}$ coupling to two SM fermions. See the text for a detailed explanation of the notations.

formed by wavefunctions of the $(0,0)$ 4D-fermions:

$$F_{\Psi}^{0,0}(x,y) = \begin{pmatrix} f_{\Psi 1}^{0,0}(x,y) \\ f_{\Psi 2}^{0,0}(x,y) \\ f_{\Psi 3}^{0,0}(x,y) \\ f_{\Psi 4}^{0,0}(x,y) \end{pmatrix} \tag{3.92}$$

x corresponds to x_5 and y to x_6, the Latin indices $M, N, A, B = 0..6$ and the Greek ones $\mu = 0..3$. The parameter θ_M^t is defined as:

$$\theta_M^t = \frac{t(x^M)}{|x^M|} = \pm 1 \tag{3.93}$$

The notation $i\partial^A$ is a compact notation and refers to:

$$i\partial^A G_s(\chi_3^{l''}, x_3, x_1) f_{l''}^*(y_3) f_{l''}(y_1) = \begin{cases} (p-q_2)^\rho \; G_s(\chi_3^{l''}, x_3, x_1) f_{l''}^*(y_3) f_{l''}(y_1) \text{ with } A = \rho \\ i\partial_{x_3}(G_s(\chi_3^{l''}, x_3, x_1)) f_{l''}^*(y_3) f_{l''}(y_1) \text{ with } A = 5 \\ -\frac{l''}{R} G_s(\chi_3^{l''}, x_3, x_1) \; f_{l''}^*(y_3) f_{l''}(y_1) \text{ with } A = 6 \end{cases} \tag{3.94}$$

Finally χ stands for the moduli of the 4D momenta running in the loop:

$$\begin{aligned} \chi_1^l &= \sqrt{(p+q_1)^2 - l^2} \\ \chi_2^{l'} &= \sqrt{p^2 - l'^2} \\ \chi_3^{l''} &= \sqrt{(p-q_2)^2 - l''^2} \end{aligned} \tag{3.95}$$

For the loop a_2, the expression is quite similar but we have to take into account the 6D trilinear coupling between gauge bosons. We will also change for convenience the orientation of the momenta running into the loop as it can be seen in figure 3.21.

$$\begin{aligned} iV_{a2} =& g_6^3 \cdot C_2(G) t^a \frac{i^3}{16\pi^4} \sum_{l,l',l''} \int dp \int dx_1 \dots dy_3 \\ & \theta_R^t \; F_{\tilde{\Psi}}^{0,0}(x_3, y_3) \Gamma^R \Gamma^A \Gamma^N \; F_{\Psi}^{0,0}(x_2, y_2) \\ & \mathcal{T}^{RN\mu} \; i\partial_A G_s(\chi_3^{l''}, x_3, x_2) \; G_s^{\bigstar}(\chi_2^{l'}, x_1, t(x_3)) G_s^{\spadesuit}(\chi_1^l, x_1, x_2) \\ & f_l^*(y_1) f_l(y_2) f_{l'}^*(y_2) f_{l'}(t(y_3)) f_{l''}^*(y_3) f_{l''}(y_1) \; f_A^{\clubsuit, 2n, 0}(x_1, y_1) \end{aligned} \tag{3.96}$$

In this expression, $i\partial_A$ is the derivative operator defined in equation 3.94 and we have for the 6D trilinear gauge coupling:

$$\mathcal{T}^{RN\mu} = i[g^{\mu N}(\partial_{x1,\clubsuit}^R - \partial_{x1,\spadesuit}^R) + g^{NR}(\partial_{x1,\spadesuit}^\mu - \partial_{x1,\bigstar}^\mu) + g^{\mu R}(\partial_{x1,\bigstar}^N - \partial_{x1,\clubsuit}^N)] \tag{3.97}$$

The $\spadesuit$, $\clubsuit$, $\bigstar$ symbols are here to indicate on which propagator or wave-function applies the derivative of $\mathcal{T}^{RN\mu}$ tensor. Finally we give:

$$\begin{aligned} \chi_1^l &= \sqrt{(p-q_1)^2 - l^2} \\ \chi_2^{l'} &= \sqrt{(p+q_2)^2 - l'^2} \\ \chi_3^{l''} &= \sqrt{p^2 - l''^2} \end{aligned} \tag{3.98}$$

Those two tremendous expressions will be split in a peculiar way to make appear the different components of the gauge bosons running into the loops. We will not have the possibility to give all the details of this calculation in this thesis but the results coming from the various pieces will be gathered and the total contribution will be given in table 3.19.

3.7.3 6D corrections to $(2n,0)-(0,0)-(0,0)$ trilinear vertex

Fermionic decay of the heavy gauge vector is mediated by the diagrams compiled in figure 3.22. Using the previous results of mixing and triangle loop calculations in 6D, we will compute the effective vertex and show that it is well-matching with the result we found in section 3.6. For that purpose, we will consider the external particles on-shell; this means that the incoming gauge boson is taken with mass $(2M)^2 = q^2$ and also that for out-coming particles $\not{q}_1 = \not{q}_2 = 0$. In this limit, for a SU(N) gauge group, the effective vertex can be written as:

$$iV_A^\mu = i\,\frac{1}{4}\frac{g^3}{16\pi^4}\frac{1}{2\sqrt{2}n^2}\;\boldsymbol{\alpha}\;\gamma^\mu P_{L(R)}t^a \tag{3.99}$$

where the $\boldsymbol{\alpha}$ contributions are listed in table 3.19. For the mixing terms, the Dirac structure is quite easy to understand. For the triangle, this is more tedious but we can show that the effective Lagrangian term is also proportional to $\bar{\psi}^{(0,0)}t^a\gamma^\mu P_{L(R)}\psi^{(0,0)}A_\mu^{a,(2n,0)}$, after projecting the external legs of the 6D loop on the different KK-modes. Here $g = \frac{g_6}{2\pi R}$.

Here, $L = \log\frac{\Lambda^2R^2+n^2}{n^2}$ is the log divergence associated with the rotation, and the n-dependent contributions $\Phi_{1,2,3,4}$ are small corrections listed in the appendix A and coming from heavier modes running in the loop.

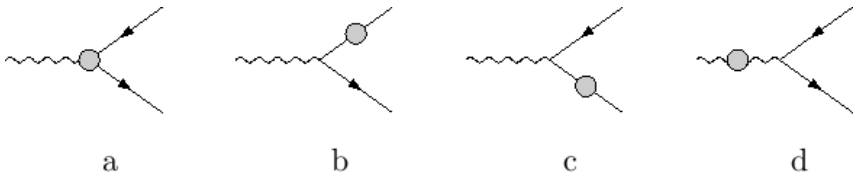

Figure 3.22: Contribution to the decay from bilinear and trilinear counter-terms.

	T	G	G'	R
α_{a1}	0	0	$(-1)^n(\Phi_1(n)+\Phi_3(n)+\Phi_2(n)-\Phi_4(n))\ C_2(r)$	0
$\alpha_{a2}(A_\mu/A_\mu)$	0	0	$(-1)^{n+1}\ (3\Phi_1(n)-8\Phi_2(n)+3\Phi_3(n))\ C_2(G)$	$\pi^2n^2 4L\ C_2(G)$
$\alpha_{a2}(A_5/A_M)$	0	0	$(-1)^{n+1}\ (2\Phi_1(n)+2\Phi_2(n)+2\Phi_3(n)+2\Phi_4(n))\ C_2(G)$	0
$\alpha_{a2}(A_6/A_M)$	0	0	$(-1)^{n+1}\ (6\Phi_2(n)+6\Phi_4(n))\ C_2(G)$	0
$\alpha_{a2}(\text{total})$	0	0	$(-1)^{n+1}\ (5\Phi_1(n)+5\Phi_3(n)+8\Phi_4(n))\ C_2(G)$	$n^2\pi^2 4L\ C_2(G)$
α_b	0	0	$(-1)^{n+1}(12\Phi_2(n))\ C_2(r)$	$-8n^2\pi^2 L\ C_2(r)$
α_c	0	0	$(-1)^{n+1}(12\Phi_2(n))\ C_2(r)$	$-8n^2\pi^2 L\ C_2(r)$
α_d	0	0	$(-1)^{n+1}\,(-2\Phi_1(n)+12\Phi_2(n)-\Phi_3(n))\ C_2(G)$	$n^2\pi^2 12L\ C_2(G)$

Table 3.19: Contributions to the effective vertex $A_\mu^{2n,0} \to f^{0,0}\bar{f}^{0,0}$. The 6D results computed in Feynman gauge $\xi = 1$ listed have to be compared with the 4D counter-term calculation.

The rotation contribution is given by:

$$\begin{aligned} iV_A^\mu &= i\,\frac{1}{4}\frac{g^3}{16\pi^4}\frac{1}{2\sqrt{2}n^2}\;16(C_2(G)-C_2(r))\pi^2 n^2 L\;t^a\gamma^\mu P_{L(R)} \\ &= -\;\frac{g^3}{16\pi^4}\frac{1}{\sqrt{2}}\;4(C_2(r)-C_2(G))\;\frac{i\pi^2}{\epsilon}\;t^a\gamma^\mu P_{L(R)} \end{aligned} \tag{3.100}$$

This result has to be compared to the one obtained in section 3.6 for the decay of a heavy gauge bosons $A_\mu^{2k,2l}$, which was:

$$i\Gamma^\mu = -\frac{g^3}{16\pi^4}\frac{i\pi^2}{\epsilon}\;4(C_2(r)-C_2(G))\gamma^\mu P_{L(R)}t^a\,. \tag{3.101}$$

We find actually that:

$$i\Gamma^\mu = \sqrt{2}\cdot iV^\mu \tag{3.102}$$

This result was expected and can be explained easily by looking at the counter-term Lagrangian in the magic gauge. If we consider the bilinear and trilinear terms presented in section 3.6, we have in general:

$$\mathcal{L}_{\text{c-t}} \;\supset\; iz_{1\pm}\;\bar{\psi}_{L\pm}\gamma_\mu D^\mu\psi_{L\pm} \tag{3.103}$$

This can be expanded in our case for the level $(2k,2l)$ and $(2n,0)$:

$$\begin{aligned} \delta\mathcal{L} \;\supset\; & i\frac{z_1}{\Lambda^2R^2}\frac{1}{4\pi^2}\;\left\{\bar{\psi}_L^{0,0}\gamma_\mu\partial^\mu\psi_{aL}^{2k,2l}+ig\bar{\psi}_L^{0,0}\gamma_\mu A^\mu_{2k,2l}\psi_L^{0,0}\right\} \\ & + i\frac{z_1}{\Lambda^2R^2}\frac{1}{4\sqrt{2}\pi^2}\;\left\{\bar{\psi}_L^{0,0}\gamma_\mu\partial^\mu\psi_L^{2n,0}+ig\bar{\psi}_L^{0,0}\gamma_\mu A^\mu_{2n,0}\psi_L^{0,0}\right\} \end{aligned} \tag{3.104}$$

We see clearly that, for the relevant rotation part, the difference obtained between Γ^μ and V^μ is only linked to the 6D wavefunctions which are determined on the localized point of the RPP. This shows the power of using the counter-term approach and the magic gauge choice which avoids us to perform the full set of triangle calculations.

Chapter 4

Phenomenology on the 6D Real Projective Plane

In this chapter, we will present the first predictions we obtained for phenomenology of the Universal Extra-Dimensional model on the Real Projective Plane. As we mentioned in previous chapters, the low mass range, expected after relic density calculation, leads to a rich phenomenology that could be observed during the first years of LHC running. For the discussions which will follow, we will choose, as a typical benchmark point, a characteristic KK-mass around $m_{KK} = 300$ GeV. We will therefore first discuss briefly the physics of the level $(1,0)$ and $(0,1)$, then we will focus on the level $(2,0)$-$(0,2)$ and present the relevant processes we want to investigate at the LHC.

4.1 General presentation of the first tier phenomenology

The tiers $(1,0)$ and $(0,1)$, associated to the Dark Matter candidate, will provide the lightest new particles of the model. In addition to the WMAP observations which tend to prefer a low m_{KK} range around $m_{KK} \sim 300$ GeV, another peculiarity of this level is the small mass splittings among the particles inside the level.

The typical and dominant phenomenology at the LHC is the production of colored particles from pp-collisions via tree level bulk interactions. Due to the conservation of KK-parity, these heavy states will have to be pair-produced and will chain decay into the lightest particle of the tier, which is the dark scalar photon, after radiating Standard Model particles. This feature seems to be quite similar to the one expected in supersymmetric model or in minimal UED model in 5D. Nevertheless due to the small mass splittings, the energy available for the Standard Model particles is rather small and make this soft activity difficult to trigger on at the LHC.

To be more concrete, let us consider some cases involving $(1,0)$ particles. The heaviest particle of the $(1,0)$ level is the top doublet: the mass difference with the photon $A^{(1,0)}$ at $m_{KK} = 300$ GeV is around 60 GeV. It will decay into $t^{(1,0)} \to bW^{(1,0)}$. The produced $W^{(1,0)}$ will decay into leptons and missing transverse energy (referred later as MET). The final state will be thus: $b\nu l A^{(1,0)}$. If the quarks are lighter then the $W^{(1,0)}$, they may be also a decay into $q\bar{q}A^{(1,0)}$. The second heaviest state is the gluon $G^{(1,0)}$ and the associated mass splitting is around 30 GeV. This state will then decay mainly into quark pairs. Due to conservation of KK parity, we have $G^{(1,0)} \to \bar{q}q^{(1,0)} \to \bar{q}qA^{(1,0)}$ as it can be seen in figure 4.1. In this case, the final state is characterized by 1, 2, or 3 soft jets with energy around $10 - 20$ GeV and an important amount of missing transverse energy. In this case, these events will never pass the trigger of experiments like ATLAS and CMS.

Then the third heaviest particles are $W^{(1,0)}$ and $Z^{(1,0)}$ which will decay into leptons and quarks also. We already discussed the impossibility of triggering on the soft final jets and the situation is quite similar for leptons. Even if CMS and ATLAS trigger on smaller energy for leptons, the smaller splitting of $W^{(1,0)}$ and $Z^{(1,0)}$ will make them escape from detection also. In

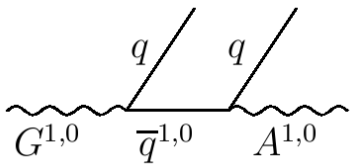

Figure 4.1: Decay chain of the heavy gluon $G^{(1,0)}$.

table 4.1, we summarized all the main decay processes for the first KK-level.

To conclude, in all these situations, even if the production cross-sections are sizeable at the LHC (around few picobarns), the detection of such states will be really challenging. The only opportunity to observe such particles would be to look for boosted particles. We can indeed think that a non negligible part of the heavy partners will not be produced at rest. Thereby the produced "soft" jets or leptons will be boosted and then the events will pass the trigger of generalist experiments like CMS and ATLAS (79). In order for this to happen, the heavy particles should receive a boost of at least 500 GeV in the transerve direction; the calculation of the production cross section, with this cut on the transverse momentum of the heavy particles, shows that the cross section drops to a few fb [1].

Another possibility would be to use the Initial State Radiation (ISR) tagging (80) to trigger on events involving the first tiers. We will have a monojet signature with a lot of missing transverse energy plus soft activity and the characteristic mass of the KK-mode could be inferred from the p_T of the ISR jet. Such signatures will need a detailed and sophisticated study using a full Monte-Carlo simulation of the signal and backgrounds at the LHC which is not available yet and this is reason why we will not develop more the phenomenology of these tiers.

$(1,1)$ level is also an interesting tier which is currently studied by G. Cacciapaglia, L. Panizzi et alii (81). This level is slightly heavier $m_{1,1} = \sqrt{2}m_{KK} \sim 425$ GeV and can be also accessible at the LHC where pair-production cross-sections are also of the order of picobarn. Like for the tiers $(1,0)$ or $(0,1)$, the particles will chain decay until they reach the lightest particle of the tier which is the vector photon $A^{(1,1)}$. If we assume the general case where the accidental KK-parity is broken by localized interactions, this particle will decay directly in Standard Model fields and the characteristic strength of the coupling will be at the order of loop induced couplings. So we can expect at the LHC to observe 4-top production through processes like:

$$pp \to q^{1,1}\bar{q}^{1,1} \to jjA^{1,1}A^{1,1} \to jjt\bar{t}t\bar{t}$$

where j denotes the soft jets coming from the chain decay inside the $(1,1)$ level. The interesting point with 4-top channels is that these processes have a large cross-section associated to a very low Standard Model background. So the constraints on the mass and branching ratio of $A^{1,1}$

[1] Third year project of N. Williams and M. Siddiqi at King's College London, under the supervision of J. Ellis and G. Cacciapaglia.

	$m_X - m_{A^{(1,0)}}$ in GeV	decay mode	final state + MET
$t^{(1,0)}$	$60-70$	$bW^{(1,0)}$	bjj $bl\nu$
$G^{(1,0)}$	26	$qq^{(1,0)}$	jj
$q^{(1,0)}$	$13-18$	$qA^{(1,0)}$	j
$W^{(1,0)}$	17	$l\nu^{(1,0)}$, $\nu l^{(1,0)}$	$l\nu$
$Z^{(1,0)}$	19	$ll^{(1,0)}$	ll
$l^{(1,0)}$	$1-3$	$lA^{(1,0)}$	l
$A^{(1,0)}$	0	-	

Table 4.1: Mass splitting of the first tier for a characteristic $m_{KK} = 300$ GeV and principal decay modes of heavy particles. The missing transverse energy is due to the escape of the stable $A^{(1,0)}$ photon from detection.

will be quite stringent.

The levels $(2,0)$ and $(0,2)$ are also tiers that can have clear signatures at the LHC. Being even under KK-parity, particles from these levels can be pair or singly produced and will have the possibility to decay:

- either in the $(1,0)$ and $(0,1)$ through bulk tree level interactions but the decays will be on threshold because of the small mass-splitting induced by the radiative corrections.
- or directly into Standard Model particles through loop induced couplings. From an experimental point of view, such channels will lead to clear identifiable resonances.

The phenomenology of this tiers will be discussed more in details in the end of this chapter.

Finally, we will focus on the $(2,1)$ and $(1,2)$ levels. These tiers, whose mass is around $\sqrt{5}m_{KK} \sim 670$ GeV, are odd under the KK-parity. Therefore, they can only decay at one-loop into one particle of $(0,1)$ or $(1,0)$ and one Standard Model particle. Even if this coupling is loop suppressed, the final states will contain typically hard jets or leptons with few hundreds GeV of energy and an important part of missing transverse energy. The phenomenology of this level is close to the one we can expect from supersymmetric scenario for instance and could lead to rare and clear signatures such as monojets (82) or single charged electron productions.

All these very different and peculiar signatures should be observable at the LHC within a reasonable amount of time and at relatively low energy. The combination of all these evidences will be a precious tool in order to discriminate between such extra-dimensional models and supersymmetric model for instance. However, as the reader can see, this model will have a rich phenomenology involving all the first KK-tiers so that, in order to make theoretical predictions, we need an efficient tool which allows us to have a description of the important amount of states of our theory. A direct implementation of this model into Monte-Carlo generators would be complex and a source of many mistakes. Therefore we decided to choose a more global approach that we will describe in the next section.

4.2 Numerical implementation of the model

To perform a realistic analysis of the LHC phenomenology on the Real Projective Plane, we need to implement our model into Monte-Carlo codes. In high energy *pp*-collider like LHC, the production cross-section of new particles will be dominated by QCD activity. Signals of new physics and SM backgrounds will involve a large number of jets, leptons and missing transverse energy. In order to disentangling them, we are forced to generate numerical simulations that reproduce as well as possible the data from SM backgrounds and from the eventual signal, both measured by detectors. The first step to study possible deviations from the Standard Model predictions, is to use matrix-element (ME) Monte-Carlo generator to produce both background and signal. Let us mention two of them to which we will refer in this thesis: `CALCHEP` (83) and `MADGRAGH/MADEVENT` (84). They will be used to perform the hard process integration taking into account the Parton Distribution Functions (PDF) of the incoming protons. Nevertheless, to be complete, the analysis of a hadronic collision requires a full modelization of the parton showering and of the hadronization. This can be performed in our framework by using for instance `PYTHIA` (85) code interfaced with `MADGRAGH/MADEVENT` as it is proposed in (81). However introducing our model of new physics into ME generator is quite complex because the number

of new states that could be relevant for phenomenology is quite significant. In this context, we decide to use FEYNRULES code which will ease considerably the implementation of the UED model on the Real Projective Plane.

4.2.1 FEYNRULES implementation

FEYNRULES (86) is a MATHEMATICA package which allows the model builder to implement in a readable and straightforward way, his new physics model by writting the new Lagrangian of his theory as well as the field content and the model parameters in a MATHEMATICA language. Then the package will generate automatically all the interaction vertices of the theory. This will have the advantage for us not to hide the Lagrangian properties into a tremendous number of vertices. In figure 4.2, we summarize schematically the organization of all these different codes. All the needed information of the model are compiled in different text files and a MATHEMATICA notebook will be used to make run the FEYNRULES code. Here we will present the structure of our model files S6UED, inspired from the implementation of the Minimal 5D UED done by P. de Aquino (86) and we will show the possibilities to generate, from the FEYNRULES package, model files that will be useable by ME generators.

The main model file

The main model file, so-called S6ued.fr, is a text file written with MATHEMATICA syntax, which contains the definition of all the indices and the gauge structure of the theory. For instance, in the case of QCD, the gauge class is defined as:

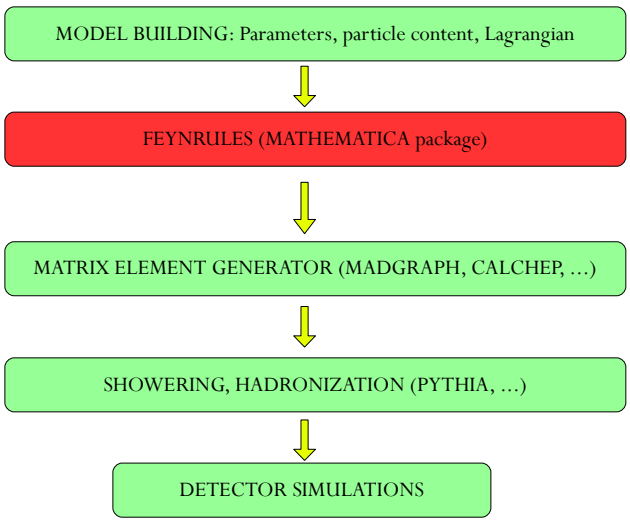

Figure 4.2: Generic organization of the different codes needed to study the phenomenology of a new model at colliders.

```
SU3C == {
Abelian             ->  False,
GaugeBoson          ->  G,
StructureConstant   ->  f,
SymmetricTensor     ->  dSUN,
Representations     ->  {T, Colour},
CouplingConstant    ->  gs}
```

As we will work with a UED model, the gauge structure will be copied from the Standard Model implementation. This file is also used to call all the different definition files for parameters and the field descriptions. Then it will be used to call the various files associated to the Lagrangian of the theory. Finally `S6ued.fr` will permit the user to choose the KK-tiers he wants to consider in his phenomenological study. As we discussed before, all the KK-tiers are not interacting with each other and limit cases are often interesting to make predictions; this will allow us to work with lighter model files easier to handle. To do so tiers are indexed by a number which are compiled in table 4.2 and a list `listLev` will permit to select the levels which will appear in the Lagrangian expansion.

For gauge boson, the procedure is quite easy because there is only one state per tier while for heavy fermions, the two degenerate states of (k, l) level force us to define a special list known as `listFer`. By now, we can use the model until levels $(2,1)$-$(1,2)$ to derive the vertices, however the full implementation of masses and widths is only done until the level $(2,0)$-$(0,2)$. Notice also that the mixing between $(2,0)$-$(0,2)$ has not yet been taken into account in this first version of the model files. For instance, to study the phenomenology of the asymmetrical case where $R_5 \gg R_6$, we consider: `listLev = {1,2,5}`.

1	->	SM
2	->	level (1,0)
3	->	level (0,1)
4	->	level (1,1)
5	->	level (2,0)
6	->	level (0,2)
7	->	level (2,1)
8	->	level (1,2)

Table 4.2: Indices used in `FEYNRULES` to implement the different KK-tiers of the 6D UED model on the RPP.

Field definition files

As we mentioned during this thesis, the 6D fields which propagate into the Real Projective Plane are to be decomposed in terms of 4D fields using the KK-expansion. This step is realized in `FEYNRULES` thanks to the file `FieldExpansion.fr`. A 6D gauge field is defined as a table of 4D fields by:

```
Gm6D := Table[Gn[listLev[[nkk]]], {nkk, 1, NKKmax+1}];
G56D := Table[G5[listLev[[nkk]]], {nkk, 1, NKKmax+1}];
```

Here NKKmax is the length of the list listLev. The wavefunctions of the states will appear only in the overlapping integrals used to compute the Lagrangian. Then for each gauge bosons the elements of the previous tables will be replaced by the 4D KK-modes corresponding the considered fields. As an example, let us detail the case of the 6D gluons:

```
Glum6D[mu_, a_] := Gm6D /.   {Gn[1] -> G[mu, a], Gn[2] ->0 , Gn[3] -> 0 ,
                             Gn[4] -> sm G3[mu, a], Gn[5] -> sm G5[mu, a], ...};
Glu56D[a_] := G56D /.        {G5[1] -> 0, G5[2] -> 0, G5[3] -> sm G62[a],
                             G5[4] -> sm/Sqrt[2] G63[a], G5[5] -> 0,...};
Glu66D[a_] := G56D /.        {G5[1] -> 0, G5[2] -> sm G61[a], G5[3] -> 0,
                             G5[4] -> - sm/Sqrt[2] G63[a], G5[5] -> 0,...};
```

We separate the 6D gauge bosons into a 4D vector Glum6D and two scalar polarizations Glu56D and Glu66D because the structure of the interaction is different for all these three components. The mu index is the Lorentz index and a the SU(3) index. The coefficient sm is equal to 0 when considering only the SM and equal to 1 otherwise. Some fields are vanishing because of the properties of the RPP orbifolding. The identity cards of those 4D fields will be then gather in the different files called KKmodeXX.fr, which contain all the fields present in the KK-level XX. As an example, we give the typical class which defines the gluons:

```
S[7] == {
ClassName        ->  G61,
SelfConjugate    ->  True,
Indices          ->  Index[Gluon],
Mass             ->  MG1, Internal,
Width            ->  WG1, 4.207153,
PropagatorLabel  ->  G61,
ParticleName     ->  "G61",
PropagatorType   ->  C,
PropagatorArrow  ->  None,
PDG              ->  6100021,
FullName         ->  "sGlu-10" },
```

The different classes of particles are defined by their spin: S, F, V for spins 0, 1/2, 1. The ClassName is the name which will be used when extracting the vertices in MATHEMATICA. The SelfConjugate function specifies if the field is real or not. For complex fields, like quarks q, the antiparticle is denoted by qbar. In general, fields possess different indices in addition to the spin index, so they will be specified in the Indices option. Here for gluons, the $SU(3)$ adjoint index is denoted as Index[Gluon] and will be defined in S6ued.fr. For fermions, we will have specific indices like the Generation or Colour ones. Then we will have to define the mass and the width of the particles. This can be done in two different ways: the mass is usually an internal parameter whereas the width is usually given directly for a chosen mass [2]. Then there are other options for declaring the name of the particles which are presented here and detailed in the FEYNRULES manual (86).

[2] Notice that in MADGRAPH, the width of particles, by default, is the one which is entered in the FEYNRULES files, but we can call the DECAY code to make directly this calculation by the ME generator.

For fermions, the situation is slightly more complicated. We will have to treat separately the left and right handed parts in the Lagrangian and to make a distinction between doublet and singlet fields under $SU(2)$. For instance, lepton singlets are defined by:

```
Elsing6D := Fl6D /.  {Fl[1] -> 0 left[l],
                      Fl[2] -> sm left[L1R], Fl[3] -> sm left[L2R],
                      Fl[4] -> sm left[L3R], Fl[5] -> sm left[L4R], ...};
Elsing6Dbar := HC[Elsing6D];
Ersing6D := Fr6D /.  {Fr[1] -> right[l],
                      Fr[2] -> sm right[L1R], Fr[3] -> sm right[L2R],
                      Fr[4] -> sm right[L3R], Fr[5] -> sm right[L4R], ...};
Ersing6Dbar := HC[Ersing6D];
```

where `left[_]` and `right[_]` are the left and right projectors which apply on Dirac fields. The antiparticle is defined here as the Hermitian conjugate of the 6D field by the function `HC`. `Fl6D` and `Fr6D` are tables defined as follows:

```
Fl6D := Table[Fl[listFer[[nkk]]], {nkk, 1, NFKmax+1}];
Fr6D := Table[Fr[listFer[[nkk]]], {nkk, 1, NFKmax+1}];
```

where `NFKmax` is the length of `listFer`.

Interaction and mass eigenstates

In section 2.4.5, we explained that for electroweak gauge bosons and tops, the kinetic terms of the interaction eigenstates were not diagonal. This forces us to diagonalize and redefine the mass eigenstates of the theory. Such effects are to be implemented in the `FEYNRULES` codes if we want to study the phenomenology of the new states. This requires to add to the mass-eigenstates, new particles which will be unphysical and used in the interaction Lagrangian. The diagonalization will be performed automatically by `FEYNRULES` and the vertices will be given in terms of mass-eigenstates. Here we illustrate it by studying the peculiar case of the top sector:

The left-handed and right-handed parts of the two physical tops are $t_{1,l/r}$ and $t_{2,l/r}$: t_1 is mainly a singlet of SU(2) and t_2 is mainly a doublet so, to simplify, in `FEYNRULES`, they will be denoted by $t1S$ and $t1D$.

```
F[8] == {   ClassMembers  ->  {u1S, c1S, t1S} ,
            ClassName     ->  qu1S},
F[12] == {  ClassMembers  ->  {u1D, c1D, t1D},
            ClassName     ->  qU1D },
```

They are related to the unphysical states: $q_{l/r}$ which is the doublet under SU(2) and $u_{l/r}$ which is a singlet by the diagonalization matrix of equation 4.1:

$$\begin{pmatrix} t_{1l} \\ t_{2l} \end{pmatrix} = \begin{pmatrix} \cos\beta_t & +\sin\beta_t \\ -\sin\beta_t & \cos\beta_t \end{pmatrix} \begin{pmatrix} q_l \\ u_l \end{pmatrix} \quad \text{and} \quad \begin{pmatrix} t_{1r} \\ t_{2r} \end{pmatrix} = \begin{pmatrix} \cos\beta_t & -\sin\beta_t \\ +\sin\beta_t & \cos\beta_t \end{pmatrix} \begin{pmatrix} q_{l,r} \\ u_{l,r} \end{pmatrix} \tag{4.1}$$

This can be expressed in the code as follows by introducing 4 new Dirac objects:

```
    F[9] == {   ClassName    ->  qu1SL,
                Definitions  ->  {qu1SL[s_,1,c_] -> qu1S[s,1,c],
                                  qu1SL[s_,2,c_] -> qu1S[s,2,c],
                                  qu1SL[s_,3,c_] -> sat1 qU1D[s,3,c]
                                  + Sqrt[1-sat1^2] qu1S[s,3,c]},
                Unphysical   ->  True },

    F[10] == {  ClassName    ->  qu1SR,
                Unphysical   ->  True,
                Definitions  ->  {qu1SR[s_,1,c_] -> qu1S[s,1,c],
                                  qu1SR[s_,2,c_] -> qu1S[s,2,c],
                                  qu1SR[s_,3,c_] -> - sat1 qU1D[s,3,c]
                                  + Sqrt[1-sat1^2] qu1S[s,3,c]}},

F[13] == {  ClassName    ->  qU1DL,
            Unphysical   ->  True,
            Definitions  ->  {qU1DL[s_,1,c_] -> qU1D[s,1,c],
                              qU1DL[s_,2,c_] -> qU1D[s,2,c],
                              qU1DL[s_,3,c_] -> Sqrt[1-sat1^2] qU1D[s,3,c]
                              - sat1 qu1S[s,3,c]}},

F[14] == {  ClassName    ->  qU1DR,
            Unphysical   ->  True,
            Definitions  ->  {qU1DR[s_,1,c_] -> qU1D[s,1,c],
                              qU1DR[s_,2,c_] -> qU1D[s,2,c],
                              qU1DR[s_,3,c_] -> Sqrt[1-sat1^2] qU1D[s,3,c]
                              + sat1 qu1S[s,3,c]}}
```

where `sat1` refers to $\sin\beta_t$ and is the mixing angle in the top sector of the first tiers. Here we see explicitly that electroweak symmetry breaking effects are only taken into account for the tops, the other flavors staying unaffected because of their small Yukawa couplings. Notice here that we have been obliged to reintroduce explicitly the indices of spin, flavor and color in the definition of the fields.

The parameter files

After we have described the particle classes, we present briefly the implementation of the numerous parameters of the theory. For this purpose, there are different files involved:

- `Param6D.fr` is a file which contains all the needed constants to describe the model. They can be declared as `External` and in this case their value is given explicitly in the definition. With the mode `Internal`, the parameter can be written in terms of other predefined parameters. As an example we can mention the electric charge definition as a function of the hyperfine structure constant:

```
ee == {
TeX               ->  e,
ParameterType     ->  Internal,
Value             ->  Sqrt[4 Pi \[Alpha]EW],
InteractionOrder  ->  {QED, 1},
Description       ->  "Electric coupling constant"},
```

The `InteractionOrder` option will precise the order of the parameter in a specific coupling which will be crucial when requiring a specific order in the cross-section calculation with `MADGRAPH`.

- In `ParamMassesX.fr` files are gathered all the parameters needed to define particle masses of the level `X`. It contains radiative correction contributions and the full expression of masses including electroweak symmetry breaking effects. As an example, we give the definition of the heavy $(1,0)$ gluon mass[3]:

```
demG == {
ParameterType   ->  Internal,
BlockName       ->  MASSCORR,
Value           ->  gmass ^2 c3 (-36 parT6 + 84 parZ3
                    + 24 parL6 + 9 B1n1 - 30 B2n1 - 3 B3n1),
Description     ->  "Correction G boson mass squared"},
MG1 == {
ParameterType   ->  Internal,
BlockName       ->  MASSCORR,
Value           ->  Mkk * Sqrt[1 + demG],
Description     ->  "G1 mass"}
```

- Finally `Paramtriangle.fr` file is a new file added to gather the useful parameters in order to specify the couplings which violate momentum conservation along the extra-dimensions. By now, it contains the $(2,0)-(0,0)-(0,0)$ couplings which have been computed and discussed in chapter 3. As an example, let us consider the coupling of a heavy $B_\mu^{2,0}$ gauge boson with two Standard Model lepton singlets. The coupling has the following form:

$$i\Gamma^{\mu}_{B\to E} = -ig_1\ \mathcal{C}\ \gamma^\mu P_L t^a \tag{4.2}$$

In `FEYNRULES` language, this $\mathcal{C}$ corresponds to `glR`:

```
glR == {
ParameterType   ->  Internal,
BlockName       ->  VERTCORR,
Value           ->  - (ee/cw)^ 2 * tri,
Description     ->  "coupling of U(1) into lepsing"},
```

where `tri` is a parameter which includes the loop coefficient:

$$\texttt{tri} = -4\cdot\sqrt{2}\cdot\frac{1}{64\pi^4}\cdot\pi^2\log(\Lambda R)^2 \tag{4.3}$$

The Lagrangian files

The last category of files are dedicated to the Lagrangian of the theory:

[3] In `FEYNRULES` code, following the prescription given for the 5D UED model implementation, we took the strong coupling `gmass` equal to 1.0236. This strong coupling constant is computed for a typical energy scale in collision center of mass of 1400 GeV.

- `Lagrangian.fr` contains the bulk Lagrangian. As we are working in the framework of UED models, the present interactions are the ones of the Standard Model but written in terms of 6D fields. For example, if we consider the lepton singlet sector of the theory, we have typically for the trilinear term:

```
Llepsing4D  := Llepsing4D =
            - I gw sw/cw y2/2 Sum[intCSSL[[i,j,k]] Bm6D[mu][[i]]
            (Elsing6Dbar[[j]].Ga[mu].Elsing6D[[k]])
            + intCSSR[[i,j,k]] Bm6D[mu][[i]]
            (Ersing6Dbar[[j]].Ga[mu].Ersing6D[[k]]),
            {i,1,NKKmax+1}, {j,1,NKKmax+1}, {k,1,NKKmax+1}]);
```

  6D fields are expended in terms of 4D KK-modes and this explains the sum over i, j, k indices. Here, we just mentioned the part involving couplings with B^μ, the couplings with B^5 and B^6 are similar and involve different wavefunction integrals. `Ga[mu]` refers to the 4×4 Gamma matrices[4].

- `6DIntegral.fr` file is used to compute the integrals of wavefunction overlapping as `intCSSL[[i,j,k]]` and `intCSSR[[i,j,k]]`, that are in the 6D Lagrangian. These integrals over extra-coordinates, as the one presented below, are crucial to get the effective couplings of the theory:

```
intCSSL = Table[2 Pi Integrate[wavefuC[[i]] (wavefuS1bar[[j]] wavefuS1[[k]]
+ wavefuS2bar[[j]] wavefuS2[[k]]), {y,0,2 Pi}, {z,0,2 Pi}]
, {i,1,NKKmax+1}, {j,1,NFKmax+1}, {k,1,NFKmax+1}];
intCSSR = Table[2 Pi Integrate[wavefuC[[i]] (wavefuS3bar[[j]] wavefuS3[[k]]
+ wavefuS4bar[[j]] wavefuS4[[k]]),
{y,0,2 Pi}, {z,0,2 Pi}], {i,1,NKKmax+1}, {j,1,NFKmax+1}, {k,1,NFKmax+1}];
```

  where `wavefuSi[[k]]` with $i = 1..4$ are the combinations of sine and cosine functions we derived in section 2.2.3. The index `S` refers to fermions with right-handed zero-mode and the index `D` to left-handed ones. `wavefuC[[k]]` is the gauge vector wavefunction given in section 2.2.2.

- `Lagrangian200.fr` file is an extra Lagrangian file containing the effective vertices that are loops induced by the rotation symmetry. This effective 4D Lagrangian is written in terms of 4D fields and effective couplings, as it is shown in the following example. Still considering the decay of heavy $B^{2,0}$ gauge boson into two Standard Model lepton singlets, we have:

```
LLeptonS200 := LLeptonS200 =
((ee/cw) glR Bm6D[mu][[3]] Ersing6Dbar[[1]].Ga[mu].Ersing6D[[1]]);
```

  where `glR` is the coupling we introduced in the previous section and the indices in brackets are chosen from table 4.2 to have $(2, 0)$ coupling with SM particles.

[4] `FEYNRULES` package follows the syntax of `FEYNARTS` mathematica package (87)

The MATHEMATICA notebook

- First we can start deriving automatically the Feynman rules of the model by using the function:

  ```
  FeynmanRules[Lagrangian, FlavorExpand -> True, ScreenOutput -> False]
  ```

  FlavorExpand will permit to express the result in terms of the generic fermion classes or in terms of flavor eigenstates. As the Lagrangian is split into different pieces, we can get the vertices gathered by specific sector of the theory. The figure 4.3 shows for instance the typical output of the MATHEMATICA notebook for the Lagrangian part corresponding to LLeptonS200.

  In this output, flavor and spin indices are written explicitly and P+/- represent $P_{R/L}$ projectors.

- Then we can perform some sanity checks to validate the implementation of the model. The first tests we did, were to check the hermiticity of the Lagrangian with the function CheckHermiticity, the tree level masses were also checked with GetMassTerms. We also controlled the charge conservation of the whole set of vertices and that the Standard Model couplings were correctly generated. With another set of tests, we checked the couplings for the first level by a direct analytical calculation of some generic vertices. These final steps have been done by looking directly at the vertices.

- Finally we generated model files for CALCHEP and MADGRAPH Monte Carlo generators with the FEYNRULES interface using the function: WriteCHOutput[LSUED] and WriteMGOutput[LSUED]. The files are automatically added to the main model folder and can then be exported into the model file of the generators.

We produced different versions of the model file which correspond more specifically to the phenomenology we needed to study. The one we used in this thesis is so-called S6UED20 and only includes the modes $(0,0)$, $(1,0)$ and $(2,0)$. In the article dedicated on the $(1,1)$ level study (81), they used another version containing only $(0,0)$ and $(1,1)$ states and so-called S6UED11.

Before focusing on the implementation of our model in CALCHEP and MADGRAPH generators, let us stress the features that are not yet implemented in the S6UED20 files:

$$\left(\begin{pmatrix} \text{A5} & 1 \\ l^\dagger & 2 \\ l & 3 \end{pmatrix} \quad \frac{i\, c_{w5}\; e\, \text{glR}\; \delta_{f_2,f_3} \left(\gamma^{\mu_1}\cdot P_+\right)_{s_2,s_3}}{c_w}\right)$$

$$\left(\begin{pmatrix} \text{Z5} & 1 \\ l^\dagger & 2 \\ l & 3 \end{pmatrix} \quad -\frac{i\, e\, \text{glR}\; s_{w5}\; \delta_{f_2,f_3} \left(\gamma^{\mu_1}\cdot P_+\right)_{s_2,s_3}}{c_w}\right)$$

Figure 4.3: Vertices generated by FEYNRULES from the Lagrangian LLeptonS200 describing the coupling between heavy $B^{2,0}$ and the singlet part of Standard Model leptons. sw5 designates the Weinberg angle of the level $(2,0)$ known as $\sin\theta_2$.

- Usually, by default, FEYNRULES does not handle the 4-point vertices with gluons like $G5\ G5\ G61\ G61$, $G\ G\ G61\ G61$, $G5\ G5\ G5\ G5$ and $G\ G\ G5\ G5$ vertices. For the ME generators like CALCHEP and also MADGRAPH, the color structure needs to be treated using auxiliary fields and has to be added by hand. This can be done easily in CALCHEP by using the manual of the code or the structure proposed in (88), where they made a direct implementation of those vertices. In MADGRAPH, this will be added in later study of LHC phenomenology.
- The heavy Higgs decay from the $(2,0)$ level through momenta violating vertices has not been taken into account due to our poor understanding of the Higgs sector of UED models.
- To simplify also the model file, CKM structure is not considered yet but in order to perform flavor studies this can be added by the user easily by mimicking the Standard Model example given in the FEYNRULES manual (86).

4.2.2 CALCHEP and MADGRAPH implementation

The main advantage of using FEYNRULES is clear now, the time needed to generate the model file for Matrice Element generators is around thirty minutes instead of days of implementation. Moreover, the definition of fields, parameters and Lagrangians of the theory is performed in a readable way with MATHEMATICA language contrary to the complicated and entangled description which is used in those ME generators.

In this thesis, the presented results have been obtained with CALCHEP code which is a parton-level event generator. We will use it to compute decay widths, branching ratios and cross-sections in the framework of our model. We will not detail how this code is working, we invite the reader to refer to (83) for more information, but we want to emphasize what is crucial to make proper computation with the model file generated by FEYNRULES. The FEYNRULES output will give `*.mdl` model files that will be loaded by CALCHEP. Then the user will have to choose the *unitary gauge* mode to make the calculation, because the model has been implemented using this peculiar gauge choice. Processes will be entered in the code directly, the name of particles being the one given in FEYNRULES by the `ParticleName` line. This name is based on the nomenclature given in the previous section and it is summarized in the graphical interface of CALCHEP. Finally for our simulation, we choose the CTEQ6m Parton Distribution Functions (PDF) of the proton (89) and the mass spectrum will be computed automatically using the formula we entered in FEYNRULES.

MADGRAPH is also a parton-level event generator but results for our model using this code are not proposed in this thesis however we already start testing the model S6UED20. In this case the widths and the masses of particles are determined directly during the generation of the model files. So once the KK-mass range has been chosen in the FEYNRULES file, masses are determined and cannot be modified afterwards. The decay widths are not calculated either and need to be implemented explicitly in the `KKmodeXX.fr` file. Then, we will use MADGRAPH to generate signal and background for different processes and PYTHIA interface to produce showering and hadronization. Note that these two codes have to be compiled together once we have picked and added the model in the MADGRAPH model file. Until now we already made small minor modifications in the code core of MADGRAPH like for instance the extension of the number of particles which is by default to small to handle the huge number of states we are considering [5]. Further checks will be needed to use this MC generator for phenomenology but this implementation

[5] `max_particles` in `params.inc` is changed from $2**7-1$ to $2**8-1$

seems to be a efficient and powerful tool for LHC predictions.

4.3 Focus on the $(0,2)-(2,0)$ tier phenomenology

In the beginning of this chapter we presented the reasons why we studied the levels $(0,2)-(2,0)$ whose particles are even under both KK-parities. Those tiers will have a very promising phenomenology at the LHC; for instance, some commun features with the $(1,1)$ level will lead to a signature involving 4-tops. Moreover, with these levels, we will also predict Standard Model leptonic decays as we showed in (78). Therefore, the study of the $(2,0)$ tier will help to add quickly new constraints on the mass range of this model, more stringent and complementary to the one derived from cosmology. Here, we will outline for the reader, the main channels for LHC phenomenology of the $(2,0)$ level and present the new perspective of study that we will be performed soon.

4.3.1 Mass spectrum of $(0,n)-(n,0)$ tiers with n even

Here we will give a brief description of the mass spectrum of level $(0,n)-(n,0)$ tiers with n even. They will be relevant for our calculation of production cross section and branching ratios. Let us stress that up to now and until the end of this section, we will focus only on the asymmetric case where $R = R_5 \gg R_6$.

Radiative corrections to gauge boson masses

The computation of the gauge boson masses is completely similar to the one presented in the chapter 2 and has been performed by G. Cacciapaglia and B. Kubik using the loop calculations presented in appendix A. We checked of the rotation contribution using the counter-terms technique developed in chapter 3 and the 6D mixed propagator technique. In figure 4.4 and in table 4.3 are listed the relevant diagrams, for a generic $SU(N)$ gauge group, and their contributions to the gauge boson self-energy.

The contributions in this table must be multiplied by a normalization factor $\frac{1}{4}\frac{g^2 C(r)}{16\pi^4 R^2}$, where $g = \frac{g_6}{2\pi R}$ is the effective 4D gauge coupling. $C(r)$ is a gauge group factor and it is defined as $\mathrm{Tr}(t_r^a t_r^b) = C(r)\delta^{a,b}$ for a field in the representation r of a non-abelian group running in the loop.

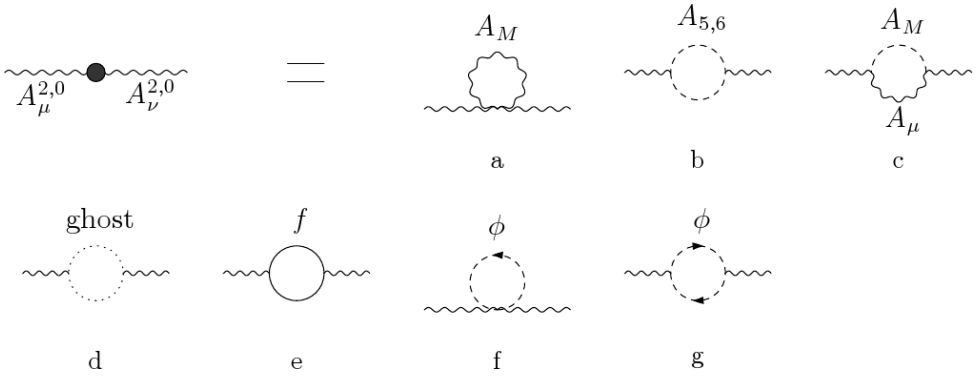

Figure 4.4: One-loop radiative corrections to the gauge scalar self-energy: gauge (a–c), ghost (d), fermion (e) and scalar (f–g) loops.

δm^2 gauge scalars	Π_T	Π_G	$\Pi_{G'}$	Π_R
a	$5T_6$	$3\cdot 7\zeta(3)$	$3\cdot(7\zeta(3)+\Phi_1(n))$	$-n^2\pi^2 L$
b	0	0	0	$-4/3n^2\pi^2 L$
c	$-T_6$	$-7\zeta(3)$	$-7\zeta(3)-8/3\Phi_1(n)$ $-14/3\Phi_2(n)+10/3\Phi_3(n)$	$+32/3n^2\pi^2 L$
d	0	0	$1/3\Phi_1(n)-2/3\Phi_2(n)-2/3\Phi_3(n)$	$-1/3n^2\pi^2 L$
e	$-8T_6$	0	0	0
f	T_6	$7\zeta(3)$	$(7\zeta(3)+\Phi_1(n))$	$-n^2\pi^2 L$
g	0	0	$-2/3\Phi_1(n)+4/3\Phi_2(n)+4/3\Phi_3(n)$	$2/3n^2\pi^2 L$

Table 4.3: Contribution of gauge, scalar and fermion loops in figure 4.4 to the mass of the gauge scalars in level $(n,0)$-$(0,n)$ with n even. *Courtesy to G. Cacciapaglia and B. Kubik.*

For an abelian $U(1)_Y$, we just replace $C(r)$ by the charge squared Y^2. In the formula, like in section 2.4.2, T_6 and L are still defined by:

$$T_6 = \frac{1}{\pi}\sum_{(k,l)\neq(0,0)}\frac{1}{(k^2+l^2)^2}\sim 1.92 \quad \text{and} \quad L=\log\frac{\Lambda^2R^2+n^2}{n^2} \tag{4.4}$$

The n-dependent contributions $\Phi_{1,2,3}$ are small corrections listed in the appendix A. We have set to zero the negligible finite contribution coming from the rotation loops and considered only the log divergent part. Here the calculation of this part has actually been performed using dimensional regularization; the log divergence L corresponds to the $1/\epsilon$ pole divergence in $d=4$.

Summing over the Standard Model fields, the corrections are:

$$\delta m_B^2 = \frac{g'^2}{64\pi^4R^2}\left[-79T_6+14\zeta(3)+\frac{1}{3}\pi^2n^2L+\frac{1}{3}B_1+\frac{4}{3}B_2\right] \tag{4.5}$$

$$\delta m_W^2 = \frac{g^2}{64\pi^4R^2}\left[-39T_6+70\zeta(3)+\frac{47}{3}\pi^2n^2L+\frac{11}{3}B_1+\frac{8}{3}B_2-2B_3\right] \tag{4.6}$$

$$\delta m_G^2 = \frac{{g_s}^2}{64\pi^4R^2}\left[-36T_6+84\zeta(3)+24\pi^2n^2L+5B_1+2B_2-3B_3\right] \tag{4.7}$$

Numerically, for n=2, the corrections to the mass $\delta m=\frac{1}{2}\frac{\delta m^2}{m}$ are:

$$\delta m_B R = (-0.7-0.07L)\cdot 10^{-3} = -0.001 \tag{4.8}$$

$$\delta m_W R = (0.2+11L)\cdot 10^{-3} = 0.049 \tag{4.9}$$

$$\delta m_G R = (2+56L)\cdot 10^{-3} = 0.18 \tag{4.10}$$

where we use $\alpha_s(M_Z)=0.118$, $\alpha(M_Z)=1/127$, $\sin^2\theta_W=0.23$ and $\Lambda R=10$ ($L=4.6$).

Radiative corrections to fermion masses

Like in section 2.4, corrections to the fermionic Lagrangian, for a generic KK mode can be written in general as:

$$\delta\mathcal{L} = a_L\bar{\psi}\gamma^\mu p_\mu P_L\psi + a_R\bar{\psi}\gamma^\mu p_\mu P_R\psi - b\bar{\psi}\psi \tag{4.11}$$

and the shift in the mass (at leading order in the corrections) is:

$$\delta m_F = b - m_n \frac{a_L + a_R}{2} \tag{4.12}$$

Reproducing the calculation performed for the level $(n,0)-(0,n)$ with n-odd, it has been shown by G. Cacciapaglia and B. Kubik that the contribution of the gauge and scalar (Higgs) loops to the three terms a_R, a_L, b are the one listed in table 4.4. The values in this table have to be multiplied by the loop factor $\frac{1}{4}\frac{g^2 C_2(r)}{16\pi^4 R}$ for the gauge loops and $\frac{1}{4}\frac{y_f^2}{16\pi^4 R}$ for the Higgs (where y_f is the effective Yukawa coupling).

The n-dependent terms are listed in appendix A and similarly to the gauge boson case, we have set to zero the negligible finite contribution coming from the rotation loops and considered only the divergent part. For a generic fermion in the fundamental representation of SU(2) weak and SU(3) color and with hypercharge Y_F, the total contribution becomes:

$$\delta m_F = \frac{1}{64\pi^4 R n}\left\{ \left(7\zeta(3) + 4n^2\pi^2 L - F_1 - 6F_2\right)\left(Y_F^2 g'^2 + \frac{3}{4}g^2 + \frac{4}{3}g_s^2\right) + \right.$$
$$\left. + \frac{1}{2}\left(21\zeta(3) + n^2\pi^2 L - F_1 - 2F_2\right) y_f^2 \right\} . \tag{4.13}$$

Numerical values of the mass splittings, at level $n = 2$, for each SM fermion are summarized in table 4.5.

Mass spectrum of the $(2,0) - (0,2)$ levels

After we include electroweak symmetry breaking and radiative corrections, we show in figure 4.5 the mass spectrum of the level $(2,0) - (0,2)$. This plot is quite similar to the one obtained in section 2.4 except that the relative splittings are smaller than the ones of the level $(1,0) - (0,1)$. For our forthcoming phenomenology discussions, we will focus on a benchmark

fermions	Π_T	Π_G	$\Pi_{G'}$	Π_R
$n^2\, a_L$ gauge	0	0	$-2\Phi_2(n)$	0
$n^2\, a_R$ gauge	0	0	$2\cdot(-7\zeta(3) + \Phi_1(n) - \Phi_2(n))$	0
$n^2\, b$ gauge	0	0	$-6nF_2(n)$	$4n^3\pi^2 L$
$n^2\, a_L$ scalar	0	0	$-\Phi_2(n)$	$n^2\pi^2 L$
$n^2\, a_R$ scalar	0	0	$-7\zeta(3) + \Phi_1(n) - \Phi_2(n)$	0
$n^2\, b$ scalar	0	0	$-n\Phi_2(n)$	$n^3\pi^2 L$

Table 4.4: Contribution of gauge and scalar loops to the mass and kinetic renormalization of SM fermions in level $(n,0)$-$(0,n)$ with n even. *Courtesy to G. Cacciapaglia and B. Kubik.*

$\delta m_F R$	Q	U	D	L	E
light gen.s	0.13	0.12	0.12	0.021	0.008
third gen	0.14	0.13	0.12	0.021	0.008

Table 4.5: Mass corrections for SM fermions in level $(2,0)$-$(0,2)$. Here we used the same numerical inputs as for the bosons, and $y_{\rm top} = 1$.

point with characteristic KK-mass range of $m_{KK} \sim 300$ GeV, so we give in table 4.6, the mass of the second tier particles which are around 600 GeV. In both cases, for fermions and gauge bosons, we notice that the rotation contribution starts being dominant when the discrete momentum of the KK-mode increases. This is due to the fact that the rotation contribution is proportional to the square of the tree level mass. So, for heavier modes, we can easily neglect the contribution of torus and glides to the self-energy of the particles. Finally, as we decided to work in the asymmetric case , for our study we do not need to take into account the mixing between the modes $(0,2)$ and $(2,0)$ mediated by the $(1,1)$ levels. Nevertheless this contribution will be included in a more general study of these tiers and will require the diagonalization of the $(0,2)$ and $(2,0)$ states in the $(2,0)_{\pm}$ basis. After implementing those masses in the `S6UED20` file, the `FEYNRULES` model file for the mode $(2,0)$ and $(0,2)$, we started to prepare some predictions for LHC phenomenology. Note that this mass computation will be also useful to study the effect

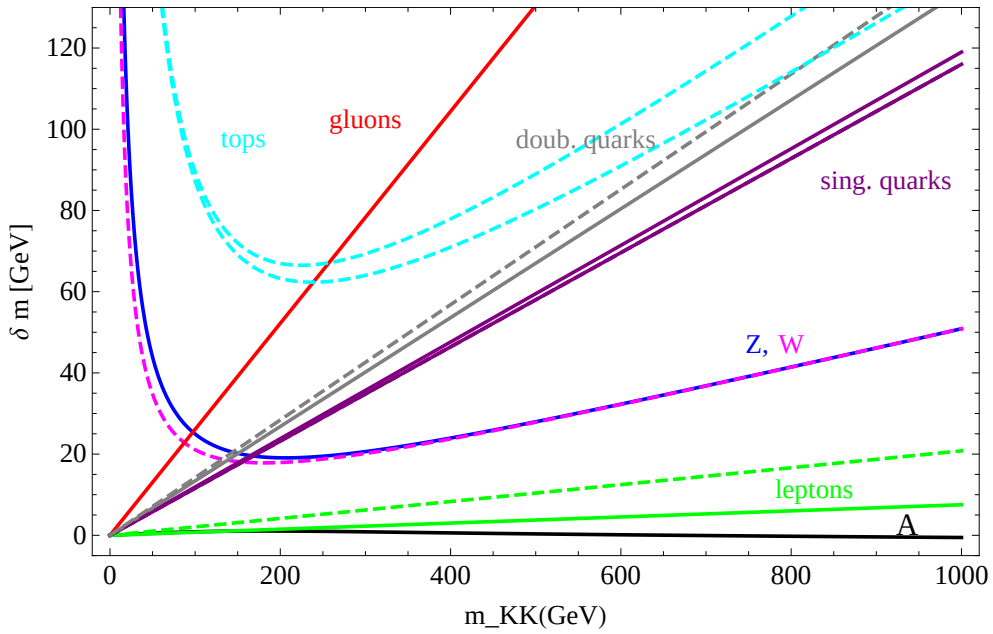

Figure 4.5: Mass splitting between the different states in the tier 2 as a function of m_{KK}: in black the heavy vector photon, in blue the Z, in magenta the W, in solid red the gluon, in green the leptons, in purple the light singlet quarks, in gray the light doublets and in dashed cyan the tops.

particles	masses	particles	masses
$A^{2,0}$	601 GeV	$D^{2,0}$	625 GeV
$E^{2,0}$	602 GeV	$U^{2,0}$	626 GeV
$L^{2,0}$	606 GeV	$Q^{2,0}$	630 GeV
$W^{2,0}$	619.6 GeV	$b_D^{2,0}$	633 GeV
$Z^{2,0}$	620 GeV	$t_S^{2,0}$	652 GeV
$G^{2,0}$	653 GeV	$t_D^{2,0}$	657 GeV

Table 4.6: Characteristic mass spectrum of the level $(2,0)$ for $m_{KK} = 300$ GeV. Q, U and D stand for light quark singlets and doublets, the top and bottom doublets being considered separately because $y_{\text{top}} = 1$. This spectrum has been computed by the `CALCHEP` code.

of the $(2,0)$ resonances on the Dark Matter abundance.

4.3.2 Gauge boson decays

In this section, we will focus on the decay of gauge bosons using our implementation of the UED model on the Real Projective Plane. With `CALCHEP` code, we will produce widths and branching ratios for the second tier in the asymmetric case. Let us recall that in this code, the index `5` denotes the mode $(2,0)$ (see table 4.2).

$G_\mu^{2,0}$ decay

As the heavy gluon can be easily pair-produced or singly produced at the LHC, we will focus here on its main decay channels into $(1,0)$ and Standard Model particles. First, in figure 4.6 and 4.7, we present the width and the branching ratios of $G_\mu^{2,0}$ as a function of $2m_{KK}$ which is the characteristic mass of the $(2,0)$ particles.

On these graphs, we notice that for this mass range the width grows linearly with m_{KK} and that heavy gluons will decay mainly through bulk vertices into either a pair of $(1,0)$ fermions or into a heavy $(2,0)$ fermions plus a Standard Model one. Loop induced vertices lead to a production of SM jets and this contribution is quite important compared to the bulk couplings. The physical reason is the competition between two one-loop effects: the loop induced vertices in one hand and in the other, the fact that bulk decays are on threshold because mass splittings are ruled by radiative corrections.

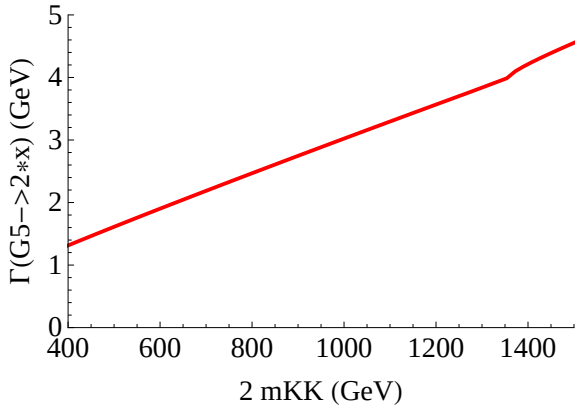

Figure 4.6: Decay width of the heavy $G_\mu^{2,0}$ as a function of 2 m_{KK} in GeV.

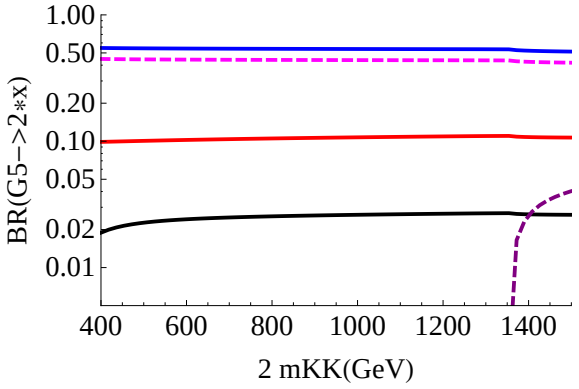

Figure 4.7: Branching ratios of the heavy $G_\mu^{2,0}$ as a function of 2 m_{KK} in GeV: SM jets, SM tops, $f^{2,0}f$, $f^{1,0}f^{1,0}$, $t^{1,0}t^{1,0}$. Here f stands for the light fermions.

$A_\mu^{2,0}$-$W_\mu^{2,0}$-$Z_\mu^{2,0}$ decays

First, let us look at the heavy photon $A_\mu^{2,0}$ decay. Using the vertices obtained in section 3, we include decay modes into fermions and also into the longitudinal parts of SM gauge bosons and the Higgs boson. In figure 4.8 and 4.9, we also plot the total width and branching ratios as function of $2m_{KK}$ which is the characteristic mass of the $(2,0)$ particles. As the photon is the lightest particle of the second tier, we notice that its decay is only generated by loop induced vertices; no phase space being accessible to decay into two first tier particles or into a $(2,0)$ state

and a zero mode. So the decay of such particles, if they are produced almost on-shell, will lead to clear resonances in the invariance mass of the final SM particles.

Due to the QCD loop, the main decay channel generates Standard Model pair of light quarks, so that the observation of such resonance into di-jets is challenging not to say impossible. However, leptonic channels are present at the percent level; if the production cross-section is quite large, this decay channel can become interesting. Another interesting channel is the decay into top pair: the branching ratio into top pair is still sizeable and we will see that a lot of heavier particles will chain-decay until they reach $A_\mu^{2,0}$ so that we can hope to have a cross-section at the LHC which will not be negligible. This discussion will be developed more in detail in section 4.3.4.

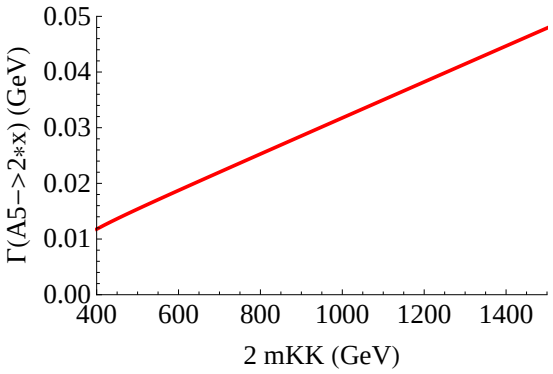

Figure 4.8: Inclusive decay width of the heavy $A_\mu^{2,0}$ as a function of 2 m_{KK} in GeV.

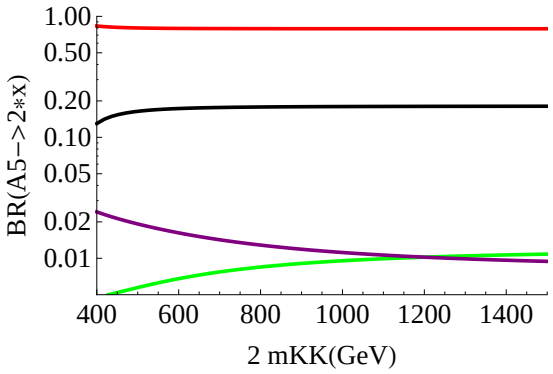

Figure 4.9: Branching ratios of the heavy $A_\mu^{2,0}$ as a function of 2 m_{KK} in GeV: SM jet, SM tops, $l\ \bar{l}$, $\nu\bar{\nu}$. The contributions of $Z_L\ h$ and $W_L^+W_L^-$ channels are smaller than 0.01%.

Finally we looked at the decay of the heavy $Z_\mu^{2,0}$ and $W_\mu^{2,0}$ and we plotted in figures 4.10, 4.11 and 4.12, 4.13 widths and branching ratios as a function of $2m_{KK}$. Note that we summed over the lepton and light quark flavors in these plots. For $Z_\mu^{2,0}$, similarly to the gluons, the decay is dominated by channels involving fermions of the first and second tiers. This has an important consequence: almost half of the branching is into leptons of the first tier which will decay into soft leptons plus a lot of missing transverse energy and around $O(30\%)$ will cascade decay until the heavy photon. We deduce then that more than $O(20\%)$ of the branching ratios involves loop generated vertices, which leads to final states with only Standard Model particles. For the heavy $W_\mu^{2,0}$, the branching into SM particles is larger, around 70%. However this decay is mainly into di-jets, which are hard to detect at the LHC while top and leptonic channels are more suppressed.

Summary

For a gauge boson with a typical mass of $m_{KK} = 300$ GeV, we summarized in table 4.7, the main and most interesting decay channels with their respective branching ratios. The processes which are not indicated in this table are generally subleading and they will not be relevant for LHC phenomenology at low luminosity and low energy. The interest in subleading channels will be increased at linear collider where their signature will be more observable than at the LHC, whose phenomenology is highly driven by QCD.

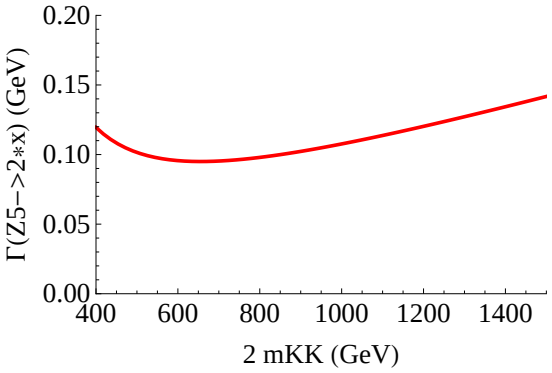

Figure 4.10: Decay width of the heavy $Z_\mu^{2,0}$ as a function of 2 m_{KK}.

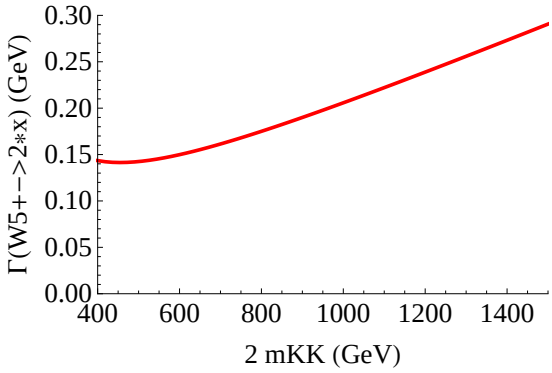

Figure 4.11: Decay width of the heavy $W_\mu^{2,0}$ as a function of 2 m_{KK}.

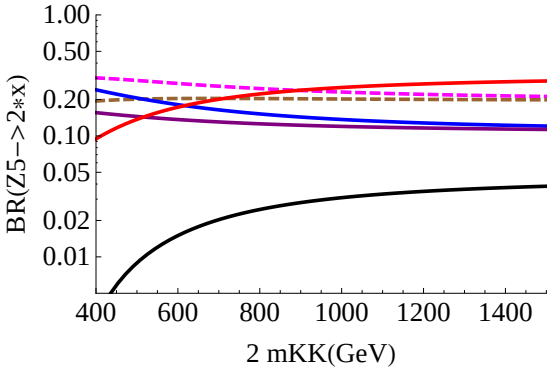

Figure 4.12: Branching ratios of the heavy $Z_\mu^{2,0}$ as a function of 2 m_{KK}: $\nu^{1,0}\bar{\nu}^{1,0}$, $l^{1,0}\bar{l}^{1,0}$, $\nu^{2,0}\bar{\nu}$, $l^{2,0}\bar{l}$, SM jets, SM tops.

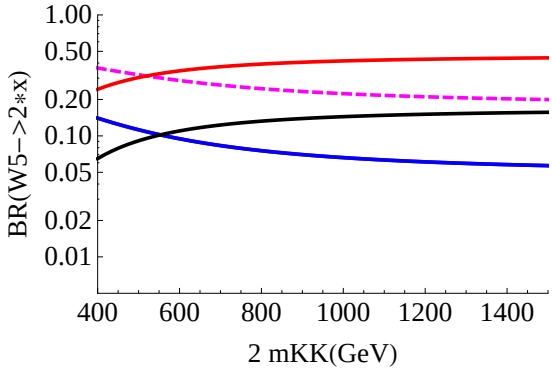

Figure 4.13: Branching ratios of the heavy $W_\mu^{2,0}$ as a function of 2 m_{KK}: $\nu^{1,0}\bar{l}^{1,0}$, $\nu^{2,0}\bar{l}$ and $l^{2,0}\bar{\nu}$, SM jet, t+b.

	width in MeV	decay mode	BR		width in GeV	decay mode	BR
$G^{2,0}$	1900	$f_{S/D}^{2,0} f$	$26\% + 17\%$	$Z^{2,0}$	95	$\nu^{1,0}\bar{\nu}^{1,0}$, $l^{1,0}\bar{l}^{1,0}$	45%
		$f^{1,0} f^{1,0}$	44%			$\nu^{2,0}\bar{\nu}$, $l^{2,0}\bar{l}$	$18\% + 13.7\%$
		SM jets	10%			SM jets	16%
		$t\bar{t}$	2.4%			$t\bar{t}$	1.5%
						$l\bar{l}$, $\nu\bar{\nu}$	$3 \times 0.5\% + 1.8\%$
						$W^+W^- + ZH$	$0.3\% + 0.2\%$
$W^{2,0}$	150	$\nu^{1,0}\bar{l}^{1,0}$	29%	$A^{2,0}$	19	SMjets	80%
		$\nu^{2,0}\bar{l}$, $l^{2,0}\bar{\nu}$	$9.5\% + 9.5\%$			$t\bar{t}$	17%
		SM jets	34%			$\nu\bar{\nu}$	1.6%
		$t\bar{b}$	11%			$l\bar{l}$	$3 \times 0.22\%$
		$\nu\bar{l}$	$3 \times 2.1\%$			ZH	0.26%
		$WZ+WH$	$0.28\% + 0.25\%$				

Table 4.7: Branching ratios for gauge boson decays at $m_{KK} = 300$ GeV. Here we choose $m_h = 120$ GeV.

4.3.3 Fermion decays

In this section, we will describe the decay channels of heavy fermions from the level $(2,0)$. The main feature, here, is the one we developed already in chapter 3. Due to the structure of the gauge coupling, we showed in section 3.6, that there is no loop induced vertex linking one fermion of level $(2,0)$ with a massless gauge boson and a massless fermion. Therefore, the decay of the $(2,0)$ fermions can only happen either inside the level $(2,0)$ with a production of a heavy gauge boson plus a SM fermion or through a pair production of $(1,0)$ particles. Due to the mass spectrum of particles from $(1,0)$ and $(2,0)$ tiers, there is not enough phase space for the decay into another fermion of the $(2,0)$ tier. Finally let us stress that for leptons, labels R/L denote the chirality of the SM fermion zero mode. Another equivalent notation is used for the quark: S/D indices refer to singlet and doublet SM chiral modes and correspond respectively to R/L indices. Note also that all heavy fermion modes are Dirac fields.

First we discuss the case of the heavy lepton singlets and doublets. Due to the smallness of the Yukawa coupling, they can be considered here as degenerate. The plots in figure 4.14 and 4.15 shows the width and the branching ratios of the heavy muon. We see then that leptons mainly decay into a Standard Model lepton and a heavy photon $A_\mu^{2,0}$. Due to the small mass splitting between heavy leptons and the lightest particles of the $(2,0)$ tier, SM leptons will be very soft. The heavy photon will then decay into a pair of visible Standard Model particles. The other decay channel into pairs of particles from the level $(1,0)$ will lead to invisible particles.

All these features will be also similar for heavy quarks, except that they will also decay into heavy $W_\mu^{2,0}$ and $Z_\mu^{2,0}$ because of their bigger mass splitting. In figures 4.17, 4.16 and 4.18, we show that for the quark singlets under $SU(2)_W$, the width is larger due to colored couplings and that the branchings are quite similar to the leptonic ones. For doublets, the situation is different and a bit more complicated; the opening of channels involving heavy $W_\mu^{2,0}$ and $Z_\mu^{2,0}$ influences the width and the branching ratios of the quarks. The main decay channels are actually producing $W_\mu^{2,0}$ and $Z_\mu^{2,0}$ plus soft Standard Model jets. Then we will have to consider the decay chain of heavy $W_\mu^{2,0}$ and $Z_\mu^{2,0}$, which ends quite often into invisible particles as we can see in figure 4.12. Finally, for heavy flavors, a new process will be taken into account: heavy tops or heavy $b_L^{2,0}$ can indeed decay into a Standard Model fermion and the longitudinal part of W and Z through loop induced couplings mediated by the top Yukawa.

To summarize, we give in table 4.8, the main decay channels of heavy fermions with their respective branching ratios for a typical mass range of $m_{KK} \sim 300$ GeV, which is the benchmark point chosen for our phenomenological study.

4.3.4 Production of $(2,0)$ particles at the LHC

In the previous section, we focused on the decays of heavy $(2,0)$ modes but in order to investigate the phenomenology of such level, we also need to know what are the main production channels of $(2,0)$ modes. In the context of this thesis, we will concentrate on predictions for pp-collider like LHC. In such collider, production cross-sections are dominated by QCD processes involving heavy singlet and doublet quarks $q_{S/D}^{2,0}$ and heavy gluons $G_\mu^{2,0}$. The electroweak processes such as Drell-Yann production of heavy photon $A_\mu^{2,0}$, heavy $W_\mu^{2,0}$ and heavy $Z_\mu^{2,0}$ resonances will be actually subleading but interesting at linear e^+e^--colliders. Nevertheless a lot of those particles will be produced during the chain decay of heavy quarks and as the mass splittings inside the second tier are small, heavy gauge bosons will be produced almost at rest

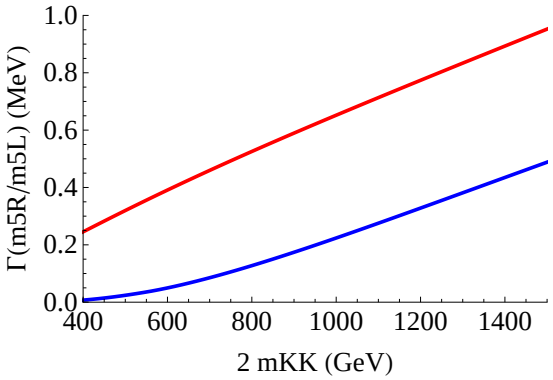

Figure 4.14: Decay widths of the heavy $\mu_R^{2,0}$ and $\mu_L^{2,0}$ as a function of 2 m_{KK}.

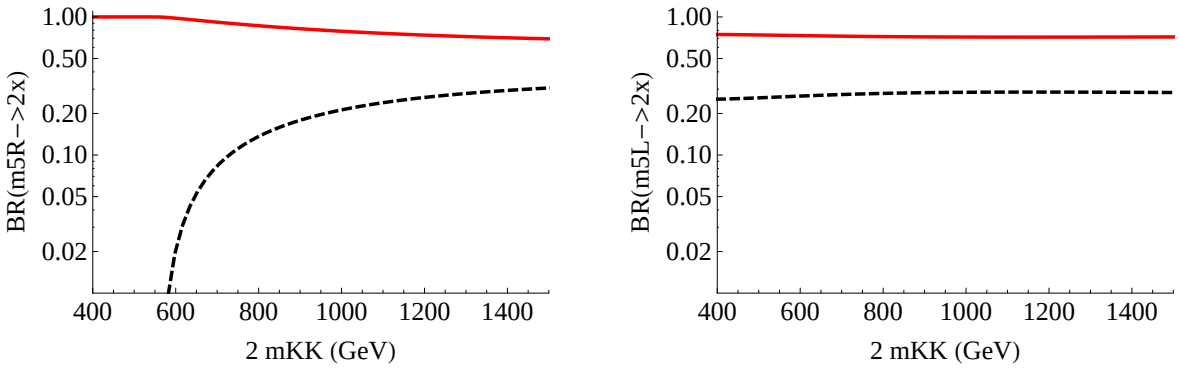

Figure 4.15: Branching ratios of the heavy $\mu^{2,0}$ as a function of 2 m_{KK}: $\mu\ A^{2,0}$, $\mu_{L/R}^{1,0}\ A_6^{1,0}$.

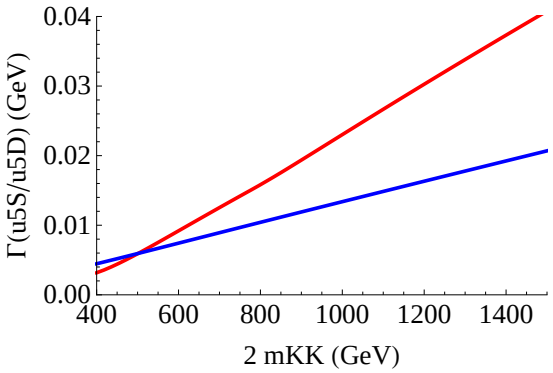

Figure 4.16: Decay widths of the heavy $u_S^{2,0}$ and $u_D^{2,0}$ as a function of 2 m_{KK}.

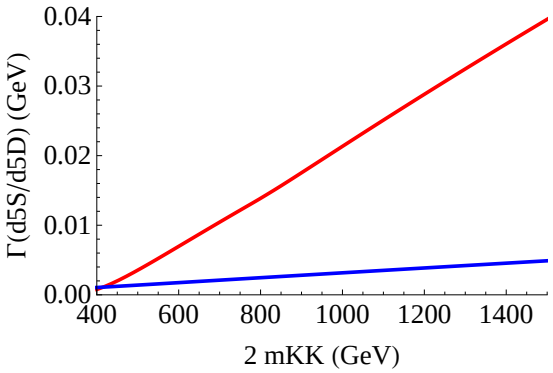

Figure 4.17: Decay widths of the heavy $d_S^{2,0}$ and $d_D^{2,0}$ as a function of 2 m_{KK}.

	width in MeV	decay mode	BR		width in MeV	decay mode	BR
$u_S^{2,0}$	7.4	$A^{2,0}q$ $A_6^{1,0}q^{1,0}$	87% 13%	$l_S^{2,0}$	0.05	$A^{2,0}l$ $A_6^{1,0}l^{1,0}$	98% 2%
$d_S^{2,0}$	1.7	$A^{2,0}q$ $A_6^{1,0}q^{1,0}$	87% 13%				
$\nu^{2,0}$	0.1	$A^{2,0}l$ $A_6^{1,0}l^{1,0}$	94% 6%	$l_D^{2,0}$	0.39	$A^{2,0}l$ $A_6^{1,0}l^{1,0}$	73% 27%
$d_D^{2,0}$	0.007	$W^{2,0}u$ $Z^{2,0}d$ $d^{1,0}A_6^{1,0}$ $A^{2,0}d$	67% 32% 0.8% 0.2%	$u_D^{2,0}$	0.012	$W^{2,0}d$ $uZ^{2,0}$ $uA^{2,0}$ $u^{1,0}A_6^{1,0}$	51% 22% 21% 6%

Table 4.8: Branching ratios for fermion decays at $m_{KK} = 300$ GeV. Here we choose $m_h = 120$ GeV.

and on-shell. In the following, we will first discuss the pair production channels then we will present some examples of heavy gluon single productions.

$q^{2,0}$ quark production

Using `CALCHEP` with our model implementation, we integrated the production cross-section for heavy quarks. Those particles will be pair produced or in association with a heavy gluon; the single production being forbidden by bulk interactions (which conserve momenta along the extra-dimensions) and really suppressed by localized terms because it will be induced by Yukawa couplings. The main contribution to the cross-section is coming from the interaction of up-type partons of the incoming protons and is mediated by the exchange of a heavy gluon in the t- and u-channels. This is due to the fact the heavy ups are valence quarks in the proton.

In the figure 4.19, we present the inclusive production cross-section of heavy quarks at the LHC. This prediction has been done using the `CTEQ6m` Parton Distribution Functions for the proton (89). The range chosen in this plot is the one preferred by the WMAP observations and we see that, in that range, production cross-sections are quite large at 7 TeV LHC, around few picobarns. These cross-sections fall off with the increase of the KK-mass range but this case is disfavored by cosmological constraints. We notice also that productions of pair of heavy quarks and of one heavy quark associated to a heavy gluon are comparable. In table 4.9, we summarized the main cross-sections for the benchmark point we selected at $m_{KK} = 300$ GeV. We did not distinguish between up and down type for the singlet and summed their contribution because their decay modes will be completely similar: the quark singlets will actually decay preferentially into a SM jet and a heavy photon (Figure 4.18). For doublets, as we already mentioned, the phenomenology will be more subtle; new couplings open new dominant decay channels through $Z_\mu^{2,0}$ and $W_\mu^{2,0}$ (Figure 4.12), which will decay afterwards preferentially into invisible particles (Figure 4.13). However these processes can also involve lepton in the final states and this could give signatures which LHC can trigger on. Moreover, in this table, we took also into account s and c quark flavors because at this energy their contributions to the PDF of the proton cannot be neglected anymore. Finally, we did not take into account the eventual QCD enhancement of cross-sections generated by QCD radiative corrections.

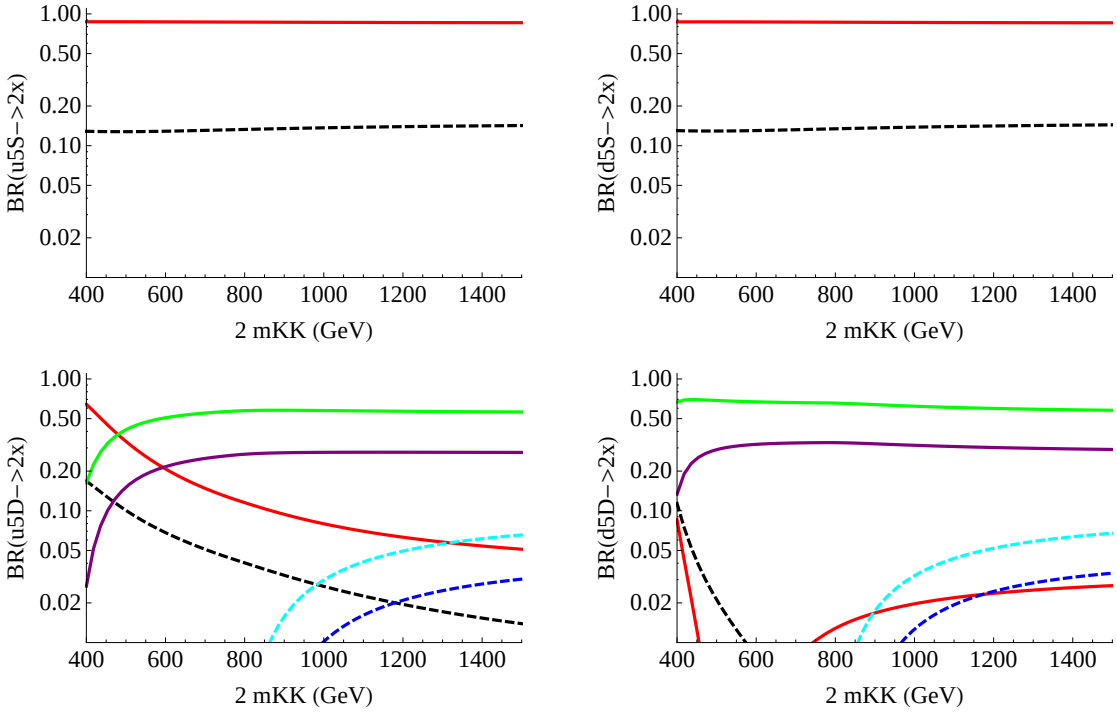

Figure 4.18: Branching ratios of the heavy $q^{2,0}_{S/D}$ as a function of 2 m_{KK}: $qA^{2,0}$, $q^{1,0}_{S/D}$ $A^{1,0}_6$, $q^{1,0}_{S/D}$ $Z^{1,0}_6$, $qZ^{2,0}$, $q'W^{2,0}$, $q'^{1,0}_{S/D}$ $W^{1,0}_6$.

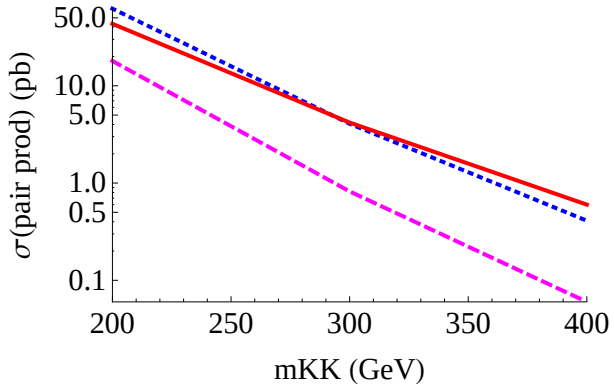

Figure 4.19: Inclusive cross-section productions for pair productions of heavy charged particles at the LHC at 7 TeV: the red line is for the channel with a pair of heavy quarks, in blue a heavy gluon in association with a heavy quark, in magenta a pair of heavy gluons. All cross sections are calculated with `CALCHEP`, using the PDF set `cteq6m`.

Heavy states $(2,0)$	Cross-sections in (fb)
$q_S\ q_S$	1129
$u_D\ q_S$	1086
$d_D\ q_S$	514
$u_D\ u_D$	592
$d_D\ d_D$	166
$u_D\ d_D$	698
$G\ G$	820
$q_S\ G$	2056
$u_D\ G$	1441
$d_D\ G$	573
total	9077

Table 4.9: Inclusive cross-sections for the benchmark point at $m_{KK} = 300$ GeV.

$G_\mu^{2,0}$ production

This vector boson can be generated through processes involving singly or pair produced heavy particles. We already showed, in figure 4.19, that heavy gluons are pair produced in processes involving only bulk vertices which conserve KK-momenta. The production occurs via a quark-antiquark annihilation and is mediated by a Standard Model gluon in s-and t-channel. Another possibility is the associated production with an up or down type quark, mediated with quark in s-and t-channel.

Then, in figure 4.20 and figure 4.21, we detail the results obtained for the single production cross-section of a heavy $(2,0)$ gluon. Single production is allowed for $(2,0)$ gauge bosons and is coming from the loop induced vertices which violate conservation of momenta along the extra-dimensions. In figure 4.20, we present the inclusive production cross section as a function of m_{KK}. The calculation has been realized by considering the annihilation of a pair of quark-antiquark and the production of a heavy gluon in s-channel. To realize the calculation in `CALCHEP`, we choose to use the relation:

$$\sigma_{\text{inclusive}}(q\ \bar{q} \longrightarrow G^{2,0} \to f\bar{f}) = \frac{\sigma(q\ \bar{q} \longrightarrow G^{2,0} \longrightarrow t\bar{t})}{BR(G^{2,0} \to t\bar{t})} \tag{4.14}$$

In figure 4.21, we present another possibility, where $G_\mu^{2,0}$ is produced in association with a quark jet via the exchange of a quark in the t-channel: $\sigma(q\ g \longrightarrow G^{2,0}q)$. Notice that the single production is quite comparable to the associated pair-production.

As a conclusion, we observed that the inclusive production cross-section of heavy partners from the $(2,0)$ level is sizeable, more than 10 pb, if we consider the preferred low mass range for the Dark Matter constraint. This order of magnitude allows the production of thousands of particles after one year of LHC running at 7 TeV with around 1 fb^{-1} luminosity. Now we have to focus on the different means to detect such modes at the LHC.

4.3.5 First prediction for LHC phenomenology

In this section we will put together the predictions we performed for decays and production channels of the $(2,0)$ tier, in order to present some golden processes for early search of this

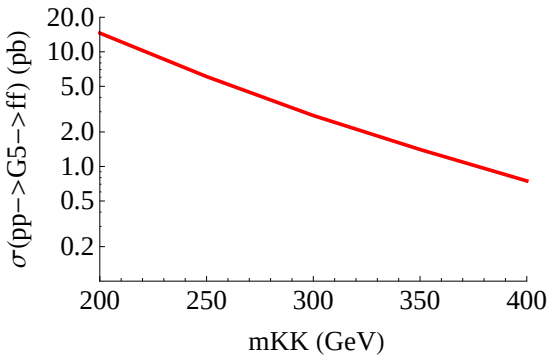

Figure 4.20: $G_\mu^{2,0}$ single production through $q\,\bar{q} \longrightarrow G^{2,0} \longrightarrow f\bar{f}$: 7 TeV cross-section.

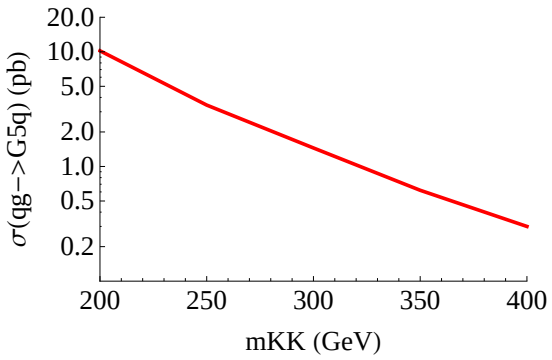

Figure 4.21: $G_\mu^{2,0}$ single production through $q\,g \longrightarrow G^{2,0}\,q$: 7 TeV cross-section.

model at the LHC. Production of heavy gauge bosons directly or through cascade decays of heavy quarks will lead to some final states containing at least a pair of energetic Standard Model fermions. Even if the branching ratios of such states are small, at the LHC due to a very low Standard Model background, these signals will be clean and detectable, like for instance, top or lepton pairs. We identify actually four promising final states to constrain the UED model on the Real Projective Plane: dilepton (e^+e^-, $\mu^+\mu-$), top pairs and 4-tops coming from the decay of heavy $A_\mu^{2,0}$ and $Z_\mu^{2,0}$. The last one consists in one energetic lepton plus missing transverse energy from neutrino ($e^+\nu_e$, $\mu^+\nu_\mu$), coming from the decay of the heavy $W_\mu^{2,0}$.

Final states with tops

Here, we will present our first and preliminary estimate of the production of top pair and 4-top events in this framework. We used the inclusive cross-section from section 4.3.4 and then multiplied them by the branching ratio of the different particles decaying in the chain. Heavy modes are indeed generally produced on-shell and almost at rest in the chain.

For clarity and simplicity reasons, we will present an example of cross-section computation by considering the top coming from the chain decay of heavy singlet pairs (fig. 4.23). This production channel is one of the dominant contribution and will illustrate the procedure we used to perform our analysis.

In figure 4.23, we present the short chain of the singlet which decays directly into an energetic Standard Model pairs from $A_\mu^{2,0}$ and a light quark or into invisible particle and soft activity.

channel	inclusive	di-lepton	lepton	top pair	4 tops
heavy quark pair	4.14 pb	15.5 fb	53 fb	733 fb	42.5 fb
heavy quark + gluon	4.1 pb	11 fb	32 fb	654 fb	30 fb
heavy gluon pair	0.8 pb	1.4 fb	3.5 fb	112 fb	4.3 fb
single prod	4.28 pb	2.4 fb	8.9 fb	291 fb	–
total	13.3 pb	30 fb	98 fb	1.8 pb	77 fb

Table 4.10: Cross sections for the final states di-lepton, single lepton plus neutrino, top pair and 4 tops for the benchmark point $m_{KK} = 300$ GeV.

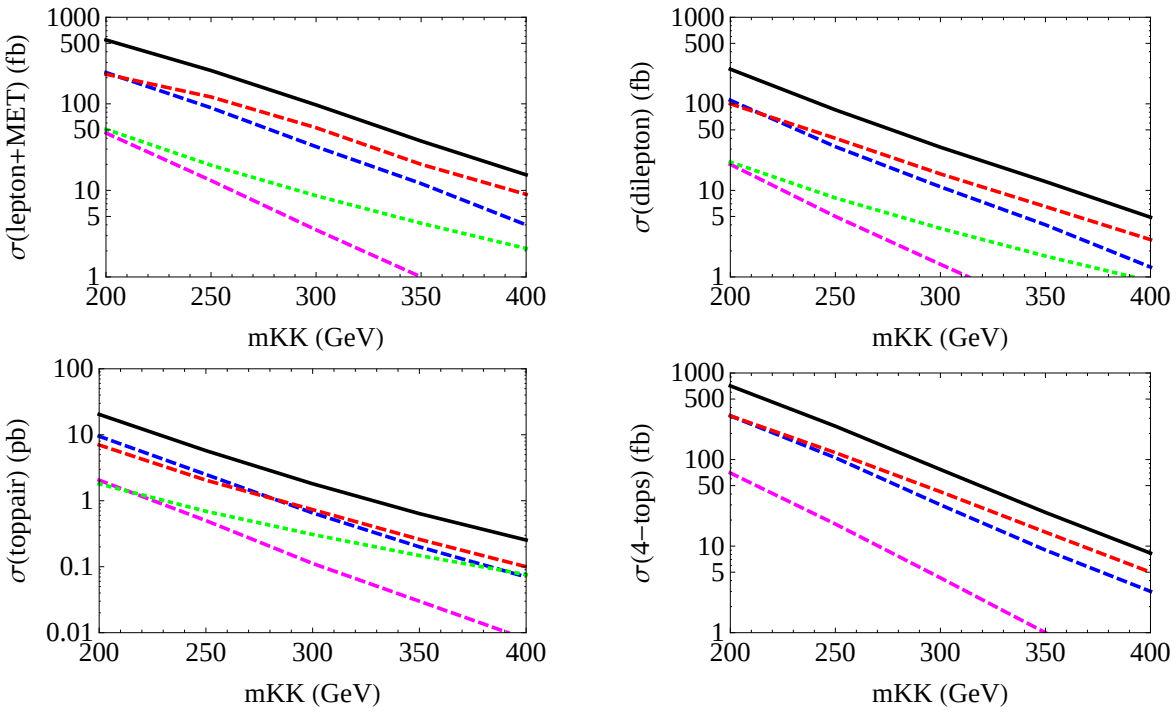

Figure 4.22: Inclusive cross sections for a final state with a single lepton plus neutrino (top-left), di-lepton e^+e^- or $\mu^+\mu^-$ (top-right), top pair $t\bar{t}$ (bottom-left) and 4 tops $t\bar{t}t\bar{t}$ (bottom-right). In all figures, the red line represents the channel with a pair of heavy quarks, in blue a heavy gluon in association with a heavy quark, in magenta a pair of heavy gluons, in green a single production of heavy gluons and in black the total cross sections.

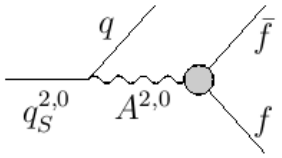

Figure 4.23: $q_S^{2,0}$ decay chain ending in a pair of energetic Standard Model fermions and emitting a soft quark jet.

Note that for doublets, we also took into account decays into $Z_\mu^{2,0}$ and $W_\mu^{2,0}$ plus soft jets. The heavy gauge bosons can cascade decay until they reach $A_\mu^{2,0}$ but they can also produce directly Standard Model particles. For heavy gluons, a small fraction will also decay directly into tops but most of them will chain decay preferentially into jets and a heavy gauge boson. In any case, light jets and leptons produced in the chain will be soft and invisible for the trigger. To do this first analysis we will take the benchmark point at $m_{KK} = 300$ GeV so that the typical mass of heavy modes is in this case around $m_{KK} = 600$ GeV and we will consider a center of mass energy of 7 TeV for the pp-collision at the LHC.

From tables 4.8, we extract branching ratio of $q_S^{2,0}$ into $A^{2,0}$:

$$\mathrm{BR}(q_S^{2,0} \longrightarrow A^{2,0} + X) = 87\% \tag{4.15}$$

where X is for soft quarks produced by the decay chain. Then using table 4.9, we can deduce the heavy quark contribution to $A_\mu^{2,0}$ pair production cross-section:

$$\sigma(pp \longrightarrow q_S^{2,0}\ q_S^{2,0} \longrightarrow A^{2,0}A^{2,0} + X) = 1129 \cdot 0.87^2 = 854 \text{ fb} \tag{4.16}$$
$$\sigma(pp \longrightarrow q_S^{2,0}\ q_S^{2,0} \longrightarrow A^{2,0} + X') = 1129 \cdot 2 \cdot 0.87 \cdot (1 - 0.87) = 255 \text{ fb} \tag{4.17}$$

Then we have to take into account the decay of the heavy photon into Standard Model tops with the following branching ratios:

$$\text{BR}(A^{2,0} \longrightarrow jj) = 80\% \tag{4.18}$$
$$\text{BR}(A^{2,0} \longrightarrow t\bar{t}) = 17\% \tag{4.19}$$

The main challenge here is to trigger on the events without losing all the signal because the exclusive cross-section can still be small. Here we choose to present two relevant final states that can be observed at 7 TeV LHC with $m_{KK} = 300$ GeV and we still focus on events coming from pair production of heavy singlet quarks:

- The first one is the production of a top pair associated with two hard jets and at least 2 soft jets. In order to pass the trigger of CMS and ATLAS experiments, we can ask for the top to have for instance one leptonic decay. Here, if we consider only the heavy singlet quark production, the cross-section is given by:

  $$\sigma(pp \longrightarrow q_S^{2,0}\ q_S^{2,0} \longrightarrow t\bar{t}jj) = 854 \cdot 2 \cdot 0.17 \cdot (1 - 0.17) + 255 \cdot 0.17 = 284 \text{ fb} \tag{4.20}$$
  $$\sigma(pp \longrightarrow q_S^{2,0}\ q_S^{2,0} \longrightarrow t\bar{t}jj \longrightarrow jjjjl\nu jj) = 284 \times (1 - (1 - 0.22)^2) = 111 \text{ fb} \tag{4.21}$$

  Then we can reconstruct the invariant mass of the two heavy photons and use the two resonances to make clear determination of the typical KK-mass range.

- The second process is the 4-top production which will be observable through a multijet final states. We have actually 4 b-jets + 4 W + soft jets and W's will decay preferentially into jets also.

  $$\sigma_{\text{inclusive}}(pp \longrightarrow q_S^{2,0}\ q_S^{2,0} \longrightarrow t\bar{t}t\bar{t}) = 854 \cdot 0.17^2 = 25 \text{ fb} \tag{4.22}$$

Finally, to be complete, after taking into account all the production channels, the full results are summarized in table 4.10 and in figure 4.22. Let us stress that, for $m_{KK} = 300$ GeV, summing all the different production processes make the inclusive contribution sizeable for the top-pair and for the 4-top production:

$$\sigma(pp \longrightarrow t\bar{t}jj) = 1.8 \text{ pb} \tag{4.23}$$
$$\sigma(pp \longrightarrow t\bar{t}t\bar{t}) = 77 \text{ fb} \tag{4.24}$$

This last result has to be compared for instance with the Standard Model background for 4-top process (90):

$$\sigma_{\text{SM inclusive}}(pp \longrightarrow t\bar{t}t\bar{t}) = 0.53 \text{ fb} \tag{4.25}$$

Dilepton final states

Another interesting class of decay is the one involving energetic leptons in the final states. Here there are two relevant possibilities at 7 TeV LHC and for a KK-mass range of $m_{KK} = 300$ GeV:

- The first one is the production of a charged dilepton pair (e^+e^- and $\mu^+\mu^-$) and at least 2 soft jets. Heavy quarks and gluons will chain decay hadronically until they reach $A_\mu^{2,0}$ or $Z_\mu^{2,0}$. Then, one of the heavy electroweak gauge bosons, which are almost on shell, can produce di-lepton pairs. Even if the branching ratio into leptons is small, the total cross-section of heavy quarks and heavy gluons is large enough to produce a sizeable effect:

$$\sigma(pp \longrightarrow e^+e^- \text{ or } \mu^+\mu^- + X) = 30 \text{ fb} \tag{4.26}$$

  Then we can reconstruct the invariant mass of the charged di-lepton resonance and make a clear determination of the typical KK-mass range.

- The other channel involves the production of at least one heavy charged $W_\mu^{2,0}$ in the decay chain of heavy quarks. In this case, this gauge boson can decay in a Standard Model lepton plus neutrino. The neutrino will be missing transverse energy and the isolated lepton will be energetic enough to pass the trigger of CMS and ATLAS. This signature should be quite similar to the one that experimentalists study for W' constraints up to the soft activity coming from the decay chain. Our first estimate is quite large also:

$$\sigma_{\text{inclusive}}(pp \longrightarrow W_5 + X') = 3504 \text{ fb} \tag{4.27}$$
$$\sigma_{\text{inclusive}}(pp \longrightarrow W_5, W_5 + X') = 590 \text{ fb} \tag{4.28}$$
$$\sigma(pp \longrightarrow l\bar{\nu}_l + X) = 590 \cdot 2 \cdot 0.021 \cdot 0.98 + 3504 \cdot 0.021 \sim 98 \text{ fb} \tag{4.29}$$

Those results are also presented in table 4.10 and in figure 4.22. They are given for only one generation of leptons in order to be comparable directly to current experimental data from CMS and ATLAS.

First LHC constraints

To conclude, these preliminary results presented in table 4.10 and in figure 4.22, seem promising for LHC detection. The LHC experiment has already analyzed 40pb^{-1} of data and ATLAS (91) and CMS (51) have already started to look at dilepton resonances and also at single energetic lepton that could have been produced by heavy resonances like Z' and W'. Our model is slightly more complicated because the heavy gauge boson resonances are coming from a long decay chain which produces in addition a lot of soft leptons, soft jets and missing transverse energy.

Nevertheless, without including any experimental efficiency, we can already propose a first estimate of the strongest bounds on our model. We compared our inclusive cross-section with the direct result of ATLAS and CMS.

First, we used ATLAS analysis (91) on Z' gauge bosons decaying to energetic lepton pairs. In the left panel of figure 4.24, we observe that for 400 GeV$\lesssim m_{l^+l^-} \sim 2 \cdot m_{KK} \lesssim$600 GeV, the experimental results tend to exclude cross-sections greater than 100 fb for the production of neutral heavy gauge bosons. For higher range, bounds on $A_\mu^{2,0}$ or $Z_\mu^{2,0}$ are looser. For

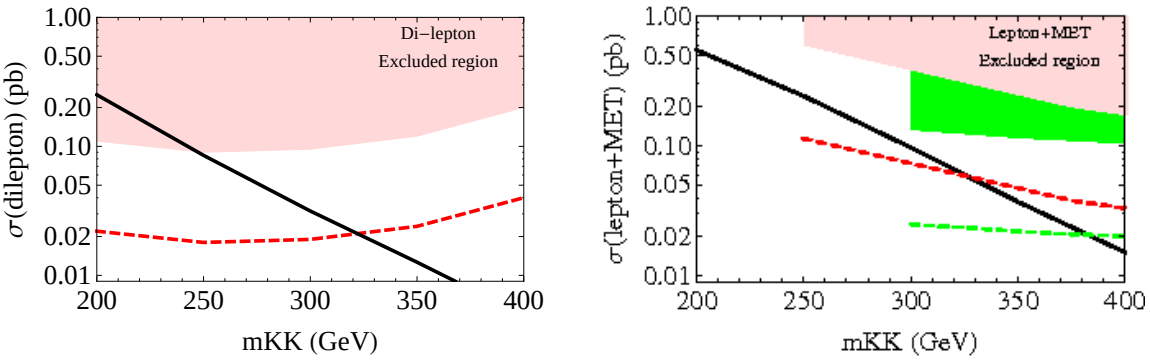

Figure 4.24: ATLAS (red) and CMS (green) bounds on single lepton $\sigma\times$ BR, compared to our inclusive cross sections (black line). The red and green regions are already excluded by the current data. The dashed red and green lines indicate the projected reach for an integrated luminosity of 1 fb^{-1}. These plots have been reproduced from (78).

$m_{l^+l^-} \sim 2 \cdot m_{KK} < 500$ GeV, we see that our model starts to be disfavored by experiment. In the right of figure 4.24, we present also a similar study which has been performed for the $W_\mu^{2,0}$ searches. We looked at the bound put on W' in ATLAS (92) and CMS (93) using single lepton channel above 500 GeV (600 GeV in CMS). In our case, it corresponds to bounds for $m_{KK} > 250 - 300$ GeV and we see that the current data are not yet constraining our model.

As a conclusion, we can say that experimental result will soon give strong constraints on our model. The preferred range by WMAP will be soon explored at the LHC, as we can see on figure 4.24, where the red and green line represent rescaled bounds for 1 fb^{-1} luminosity that should be collected by the end of 2011. This will motivate a detailed study of such processes in order to precisely understand the full event structure and the experimental efficiency of detection.

In a future work, using our implementation with `MADGRAPH`, in a similar way to the work done on the level $(1, 1)$ by the author of this paper (81), we will focus on those 4 channels which will be promising to constrain, validate or rule out such model.

4.4 Discussion on constraints from electroweak precision tests

We could not end our discussion on the 6D Universal Extra Dimensional model on Real Projective Plane without considering the indirect constraints coming from electroweak precision tests. In this paper (74), the authors present the bounds from electroweak data on the size of the extra-dimension accessible to all Standard Model fields. Computing loop contribution to electroweak observables, they focused on the 5D and 6D UED cases. For 5D, they predicted a pretty low compactification scale around ~ 300 GeV. In 6D, they estimated a compactification scale around $400 - 800$ GeV, but above all they showed that the usual S and T parameters, that we presented briefly in chapter 1 and which are used to find bounds on the size of the extra-dimensions, are not finite anymore; they are logarithmically dependent on the cut-off scale. The UV-dependence of the results suggests that S and T are not calculable. The UV-contributions, which can take the form for instance of localized kinetic terms or of bulk higher order operators, will strongly affect S and T parameters.

Here we decided not to pursue precise bounds for the radii of extra-dimensions, but we

preferred to show what is the origin of the logarithmic divergences for the T-parameters. The T-parameter quantifies the custodial symmetry breaking effects and can be defined using the self-energy correction Π to W and Z propagators presented in figure 4.25. Following Peskin notation (15):

$$\alpha T \equiv \frac{e^2}{s_w^2 c_w^2 m_Z^2}[\Pi_{11}(q^2=0) - \Pi_{33}(q^2=0)] \tag{4.30}$$

where q is the momenta of the incoming particle (here W/Z) and the indices 1 ans 3 are for incoming W_1 and W_3 gauge bosons.

Fermionic contribution to gauge boson self-energy Π

The main contribution in the SM to the T-parameter is generated by the large top Yukawa. There is also a contribution from W and Z but their divergences are expected to have the same nature. So we decided to focus on the fermionic part. Using fermionic 6D propagators given in appendix A, we can write the generic loop contribution to the gauge boson self-energy for two massive fermions with masses m_1 and m_2.

$$\begin{aligned}\Pi^{\mu\nu}(q^2) = \sum_{\vec{\Omega}} \int \frac{d^4p}{(2\pi)^4} \int d\vec{x}\, d\vec{x}\,' \\ Tr\left\{ \begin{pmatrix} ig_{6Q}\Gamma^\mu & 0 \\ 0 & ig_{6U}\Gamma^\mu \end{pmatrix} \begin{pmatrix} i\not{\partial}_1 & m_1 I \\ m_1 I & i\not{\partial}_1 \end{pmatrix}_1 \begin{pmatrix} ig_{6Q}\Gamma^\nu & 0 \\ 0 & ig_{6U}\Gamma^\nu \end{pmatrix} \begin{pmatrix} i\not{\partial}_2 & m_2 I \\ m_2 I & i\not{\partial}_2 \end{pmatrix}_2 \right\} \\ G_S^1(p+q, \vec{x} - \vec{x}\,')G_S^2(p, \vec{x}\,' - \vec{x}) f_W^{0,0}(\vec{x}) f_W^{0,0}(\vec{x}\,')\end{aligned} \tag{4.31}$$

where $i\not{\partial}_1 = (p^\mu + q^\mu)\Gamma_\mu - i\partial_{x_5}\Gamma_5 - i\partial_{x_6}\Gamma_6$ and $i\not{\partial}_2 = p^\mu\Gamma_\mu - i\partial_{x'_5}\Gamma_5 - i\partial_{x'_6}\Gamma_6$ act respectively on propagators with the index (1) and (2). The zero mode wavefunction is flat and the normalization constant can be reabsorbed in the definition of the 4D effective couplings. Moreover as we are interested in the $g^{\mu\nu}$ part of the self-energy Π, we traced over μ and ν as in (15) and then we take the $q^2 = 0$ limit.

$$\begin{aligned}\Pi(0) = \int \frac{d^4p}{(2\pi)^4} \int d\vec{x}\, d\vec{x}\,' \ \mathrm{Tr}\left\{(g_Q^2 + g_U^2)\Gamma^\mu \not{\partial}_1 \Gamma^\nu \not{\partial}_2 + 2\ g_Q g_U\ m_1 m_2 \Gamma^\mu \Gamma^\nu\right\} \\ G_S^1(p, \vec{x} - \vec{x}\,')G_S^2(p, \vec{x}\,' - \vec{x})\end{aligned} \tag{4.32}$$

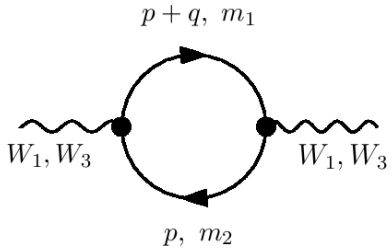

Figure 4.25: Fermionic loop contributions to T parameter.

Focusing on the T-parameter, only doublets are coupling, so we obtain:

$$\Pi(0;m_1,m_2) = i^2 g_Q^2 \int \frac{d^4p}{(2\pi)^4} \int d\overrightarrow{x}\, d\overrightarrow{x}'\ \mathrm{Tr}\left\{\Gamma^\mu \not{\phi}_1 \Gamma^\nu \not{\phi}_2\right\} G_S^1(p,\, \overrightarrow{x} - \overrightarrow{x}') G_S^2(p,\, \overrightarrow{x}' - \overrightarrow{x}) \tag{4.33}$$

We can show then that the T-paramater is proportional to:

$$T \propto (2\ \Pi(0;m_1,m_2) - \Pi(0;m_1,m_1) - \Pi(0;m_2,m_2)) \tag{4.34}$$

To understand the nature of the log-divergences of the T-parameter, we can start looking at the torus contribution.

$$\Pi(0;m_1,m_2) = \frac{i^2 g_Q^2}{4\cdot 16} \sum_{\overrightarrow{\Omega},\overrightarrow{\Omega}'} \int \frac{d^4p}{(2\pi)^4} \int d\overrightarrow{x}\, d\overrightarrow{x}'\ \mathrm{Tr}\left\{\Gamma^\mu \not{\phi}_1 \Gamma^\nu \not{\phi}_2\right\} \tag{4.35}$$

$$H_0^1(\sqrt{p^2-m_1^2}|\overrightarrow{x} - \overrightarrow{x}' - \overrightarrow{\Omega}|) H_0^{(1)}(\sqrt{p^2-m_2^2}|\overrightarrow{x}' - \overrightarrow{x} - \overrightarrow{\Omega}'|) \tag{4.36}$$

where $\overrightarrow{\Omega} = (2\pi n_1, 2\pi n_2)$ with $(n_1,n_2) \in \mathbb{Z}^2$.

After Wick rotation, we can show that the Hankel function becomes K-Bessel function which behaves for large momentum p as:

$$K_0(ap) \sim \sqrt{\frac{\pi}{2ka}} e^{-ap} \tag{4.37}$$

So as long as one of the integrands is not vanishing, the convergence of the T-parameter is fine. The convergence of the integral is indeed coming from the exponential suppression. However, on peculiar lines where distances go to zero, the convergence is not maintained anymore. For the torus contribution, those lines and points where the arguments of the 2 Bessel's vanish are given by the table 4.11.

We can then characterize the type of divergences appearing on those special lines and points: If we call $a = |\overrightarrow{x} - \overrightarrow{x}' - \overrightarrow{\Omega}|$, we can show that for $a \to 0$, at the zeroth order in a, the T-parameter is:

$\Omega = -\Omega'$	conditions	subspaces
(0,0)	$x - x' = 0$	$x = x'$ lines
	$y - y' = 0$	$y = y'$ lines
(0,±1)	$x - x' = 0$	$x = x'$ line
	$y - y' = \pm 2\pi$	$(y,y') = (2\pi,0)$ or $(0,2\pi)$
(±1,±1)	$x - x' = \pm 2\pi$	$(x,x') = (2\pi,0)$ or $(0,2\pi)$
	$y - y' = \pm 2\pi$	$(y,y') = (2\pi,0)$ or $(0,2\pi)$
(±1,0)	$x - x' = \pm 2\pi$	$(x,x') = (2\pi,0)$ or $(0,2\pi)$
	$y - y' = 0$	$y = y'$ line

Table 4.11: Lines and points where the T-parameter contribution is divergent. Here $(x,y),(x',y') \in [0,2\pi] \times [0,2\pi]$.

$$T \supset -\mathcal{N} \int d^4p \frac{1}{2} p^2 \left\{ \log \left(\frac{m_2^2 + p^2}{m_1^2 + p^2} \right) \right\}^2 \tag{4.38}$$

Here we assume that $m_2^2 \gg m_1^2$ which is the case when considering the top/bottom effects. To look at the divergence effect which appears at large-momentum, we can use dimensional regularization, where $d = 4 - \epsilon$ is the dimension of the space:

$$T \supset -\mathcal{N}' \int dp \; p^{4-\epsilon-1} \; \frac{1}{2} p^2 \left(\frac{m_2^2}{p^2} \right)^2 \propto \frac{1}{\epsilon} \tag{4.39}$$

As we have already seen, $1/\epsilon$ pole can be translated into a log-divergent contribution with respect to the UV cut-off of the theory. So on these peculiar subspaces, the T-parameter has divergences similar to the ones obtained with 4D loops. We limited ourselves to the study of the torus contribution of T-parameter coming from top loop, but this feature will also appear with rotation loops of fermions and with gauge boson contributions; the conical singularity effects will also add on this bulk effects. The S-parameter will also have similar divergences as the loop structure is close to the T-parameter one. As the predictability, that we could expect for these electroweak parameters is very low, we did not dig out the precise numerical coefficient $\mathcal{N}'$ to which this log-divergence was proportional.

Conclusion

As it has been shown in (74) using KK-expansion, the density of heavy states in 6D UED model is too important and generates log-divergences. Here we showed where these divergences arise on this orbifold. It is important to notice that the presence of these divergences depends on the implementation of the Higgs sector. In this thesis, using UED model, we have chosen a simple extension of the SM Higgs sector on the RPP 6D background. Therefore, the UV-sensitivity of the precision observables limits the predictivity power of these bounds. This is the reason why we decided not to carry on this calculation but preferred to focus on the direct bounds coming from LHC and Dark Matter abundance. However it is interesting to notice that the situation may be improved in models like Gauge Higgs Unification models. In this case, the corrections to the Higgs boson, including electroweak precision observables, are constrained by the extended gauge symmetry. This might remove the divergences in S and T, at least at one-loop level and allow to give robust bounds on the size of the extra-dimensions.

Chapter 5

Higgs to Gamma Gamma beyond the Standard Model (JHEP publication)

This section is mainly independent of the other sections and will present another study of LHC phenomenology. Contrary to the highly model dependent approach of the first parts of this thesis, in this last chapter we will propose a model independent study of the Higgs sector which will be useful to interpret data obtained from forthcoming collider experiments. Due to the self-consistency of the publication, this section will be based on our original paper published in 2009 in the Journal of High Energy Physics(94). We considered the $H \to \gamma\gamma$ decay process and the gluon fusion production of a light Higgs, and provide a general framework for testing models of new physics beyond the Standard Model. We apply our parametrization to typical models extending the Standard Model in 4 and 5 dimensions, and show how the parametrization can be used to discriminate between different scenarios of new physics at the Large Hadron Collider and at future Linear Colliders.

5.1 Introduction

The decay of the Higgs in two photons is one of the most important discovery channels at the Large Hadron Collider (LHC), and it is certainly the golden mode at low masses, where the decay channels into heavy gauge bosons are closed. Detailed studies, including detector simulations, in the Standard Model (SM) and in its supersymmetric extensions are available (95; 96). This mode is also a powerful probe of the electroweak symmetry breaking sector of the theory, because it is a loop-induced process, therefore it is sensitive to any particle with a large coupling to the Higgs. In the SM it depends primarily on the couplings of the Higgs boson with heavy quarks (the top) and gauge bosons (the W), whose masses are tightly related to the electroweak scale. In any extension of the SM, particles that do couple strongly to the Higgs, and therefore play a role in the breaking of the electroweak symmetry, will also contribute to this loop and modify the SM prediction. For instance, new particles at the TeV scale are required to soften the divergences that appear in the corrections to the Higgs mass generated by top and W-Z loops. Many models in fact predict the existence of partners of the top and W: stops and gauginos in supersymmetry, heavy W's and tops in extra dimensional models and Little Higgs models, and so on. Studying this channel will therefore give an indirect access to the mechanism underlying the electroweak symmetry breaking. At the LHC, we also need to take into account the Higgs production mechanism.

In the SM there are four main production mechanisms : gluon fusion ($gg \to H$), weak vector boson fusion, weak boson associated production (WH, ZH) and top associated production ($t\bar{t}H$). Gluon fusion dominates the inclusive production at LHC energies and it is roughly an order of magnitude larger than vector boson fusion and other processes.

While some of the production channels may have additional leptons, jets or missing energy in their final state, in the photon channel it will be difficult, at least at low luminosity, to take advantage of these different signatures. We shall therefore consider mainly the inclusive $H \to \gamma\gamma$ process. The interest of performing exclusive studies like the production via vector boson fusion, will be also discussed as it allows to better discriminate the kind of new physics that can be tested in the $H \to \gamma\gamma$ mode, especially when large integrated luminosity is available (97). The main production process $gg \to H$ is a loop induced process like the decay $H \to \gamma\gamma$, and it is sensitive to the same particles and physics.

In this paper we study the photon channel with the purpose of performing a model independent analysis, allowing to determine the possibility and the limits for discriminating various scenarios of new physics. In the following we shall propose a model independent parametrization of these loop processes in order to test the possibility of discrimination of various models of new physics. We shall provide a general and simple formalism to easily calculate the contribution of

the new heavy states given their spectrum. We will assume that the new physics only affects those two processes, and corrections to the other production and decay channels are ignored. In the SM it is well known that the contribution of heavy particles to $H \to \gamma\gamma$ and $H \to gg$ processes does not decouple for particle masses much larger than the Higgs boson one. The reason is that these SM masses are uniquely generated by the coupling to the Higgs boson and the mass dependence of their coupling cancels the mass dependence in the loop integral. In general extensions of the SM this is not necessarily the case, as the masses may receive other contributions. The effect on the decay can therefore be sensitive to the mass scale of the new physics. Studying this channel in detail can give some hints about the model of new physics, and this information will be complementary to the direct discovery of new states at the LHC. Finally, the precise determination of the Higgs branching ratios at future Linear Collider will be an even more powerful discrimination tool, even when the new particles are well beyond the direct production threshold at the Linear Collider.

In the next section we settle our notation and define our parametrization of the loop induced processes $H \to \gamma\gamma$ and $H \to gg$. In the sections 5.3 and 5.4 we consider various scenarios of new physics in 4 and 5 dimensions, in section 5.5 we discuss numerical results in various models and how the parametrization we propose can provide a hint to what kind of new physics can be deduced from data both at the LHC and at Linear Colliders. Finally we give our conclusions, and we leave details on the calculation to the appendices.

5.2 Definitions and notations

In order to establish our notations, we will briefly review the decay of the Higgs in photons and gluons (the decay width in gluons is directly related to the gluon-fusion production cross section at hadronic colliders). The decay widths can be written as:

$$\Gamma_{\gamma\gamma} = \frac{G_F \alpha^2 m_H^3}{128\sqrt{2}\pi^3} \left| A_W(\tau_W) + \sum_{\text{fermions}} N_{c,f} Q_f^2 A_F(\tau_f) + \sum_{NP} N_{c,NP} Q_{NP}^2 A_{NP}(\tau_{NP}) \right|^2 , \quad (5.2.1)$$

$$\Gamma_{gg} = \frac{G_F \alpha_s^2 m_H^3}{16\sqrt{2}\pi^3} \left| \frac{1}{2} \sum_{\text{quarks}} A_F(\tau_f) + \sum_{NP} C(r_{NP}) A_{NP}(\tau_{NP}) \right|^2 , \quad (5.2.2)$$

where $\tau_x = \frac{m_H^2}{4m_x^2}$, $N_{c,x}$ is the number of colour states in the colour representation (3 for quarks, 1 for leptons), the constant $C(r)$ is an SU(3) colour factor (defined as $\mathrm{Tr}[t_r^a t_r^b] = C(r)\delta^{ab}$ where t_r^a are the SU(3) generators in the representation r; it is equal to 1/2 for the quarks and 3 for an adjoint), Q_x is the electric charge of the particle in the loop, and the functions $A(\tau)$ depend on the spin and couplings to the Higgs of the particle running in the loop. Note that G_F here is a numerical normalization of the widths, defined in terms of the SM Higgs VEV v_{SM} ($\sqrt{2}G_F = 1/v_{SM}^2$), and not the physical Fermi constant, which may receive corrections from the New Physics.

In the SM, all masses are proportional to the Higgs vacuum expectation value (VEV) v_{SM}, therefore the couplings to the Higgs can be written as

$$y_{h\bar{f}f}^{SM} = \frac{m_f}{v_{SM}} \quad \text{for fermions}\,, \quad (5.2.3)$$

$$g_{h\phi\phi}^{SM} = 2\frac{m_\phi^2}{v_{SM}} \quad \text{for bosons}\,. \quad (5.2.4)$$

Under this assumption, the amplitudes are given by (F stands for spin-1/2 fermions, W for vector bosons and S for scalar bosons) (98)

$$A_F(\tau) = \frac{2}{\tau^2}\left(\tau + (\tau-1)f(\tau)\right), \tag{5.2.5}$$

$$A_W(\tau) = -\frac{1}{\tau^2}\left(2\tau^2 + 3\tau + 3(2\tau-1)f(\tau)\right), \tag{5.2.6}$$

$$A_S(\tau) = -\frac{1}{\tau^2}\left(\tau - f(\tau)\right); \tag{5.2.7}$$

where

$$f(\tau) = \begin{cases} \arcsin^2\sqrt{\tau} & \tau \leq 1 \\ -\frac{1}{4}\left[\log\frac{1+\sqrt{1-\tau^{-1}}}{1-\sqrt{1-\tau^{-1}}} - i\pi\right]^2 & \tau > 1 \end{cases}. \tag{5.2.8}$$

For our study we are particularly interested in the limit of such functions for large mass of the particle in the loop with respect to the Higgs mass, $\tau \ll 1$:

$$A_F(0) = \frac{4}{3}, \quad A_W(0) = -7, \quad A_S(0) = \frac{1}{3}. \tag{5.2.9}$$

Note that the particle in the loop does not decouple for large mass because the (SM) coupling to the Higgs is also proportional to the mass of the particle. As we are interested in Higgs masses below the W threshold and above the LEP limit (where the $\gamma\gamma$ signal is non negligible), the light Higgs approximation is useful for the top and the new physics. For the W, this approximation is not valid, and the function $A_W(\tau_W)$ ranges from -8 for $m_H = 115$ GeV to -9.7 for $m_H = 150$ GeV.

However, the mass of new particles in most models is not proportional to the Higgs VEV v, but receives only a small correction from the electroweak symmetry breaking. Therefore, the amplitude for new physics is given by the same formulas as above up to a factor taking into account the different coupling to the Higgs (which is in general not proportional to the mass). The coupling to the Higgs for a fermion (boson) can be written in general as

$$y_{h\bar{f}f} = \frac{\partial m_f(v)}{\partial v}, \qquad g_{h\bar{\phi}\phi} = \frac{\partial m_\phi^2(v)}{\partial v}. \tag{5.2.10}$$

Therefore we can write the A function for the new physics contribution for fermions (bosons) as

$$A_{NP}^F = \frac{y_{h\bar{f}f}^{NP}}{y_{h\bar{f}f}^{SM}} A_F \quad \text{for fermions}, \tag{5.2.11}$$

$$A_{NP}^{W,S} = \frac{g_{h\phi\phi}^{NP}}{g_{h\phi\phi}^{SM}} A_{W,S} \quad \text{for bosons}; \tag{5.2.12}$$

which can be written without loss of generality, as

$$A_{NP} = \frac{v_{SM}}{m_{NP}} \frac{\partial m_{NP}}{\partial v} A_{F,W,S}. \tag{5.2.13}$$

As the mass can be a generic function of v, this formula allows to treat a wide range of physical situations beyond the standard model, as long as the particle mass is at least partially generated by the Higgs VEV (those formulas are valid for a SM Higgs sector; when the Higgs sector is

extended, and for scalars which do mix with the Higgs doublet, more general formulas apply: see appendix D for details). When the mass of the new physics is not proportional to the Higgs VEV, A_{NP} will decouple for large masses. Examples of such cases will be discussed in detail in sections 5.3, 5.4. Note also that in general $v \neq v_{SM}$, however, as it will be clear in the following, this difference only introduces higher order corrections in an expansion for large new physics scale.

The new physics can be parametrized by two independent parameters describing the contribution of the new particles to the two decay widths, however using the actual amplitude is not a convenient way of treating the new contributions. Here we propose to normalize the new contribution to the top one. The main reason is that the top gives the main contribution to the amplitudes in the SM, and any new physics, which addresses the problem of the Higgs mass naturalness, will have a tight relation with the top. Moreover, as it will soon be clear, those two parameters can give some intuitive information about what kind of new physics runs into the loop. The widths can be rewritten as

$$\Gamma_{\gamma\gamma} = \frac{G_F \alpha^2 m_H^3}{128\sqrt{2}\pi^3} \left| A_W(\tau_W) + 3\left(\frac{2}{3}\right)^2 A_t(\tau_t)\left[1+\kappa_{\gamma\gamma}\right] + \dots \right|^2 , \tag{5.2.14}$$

$$\Gamma_{gg} = \frac{G_F \alpha_s^2 m_H^3}{16\sqrt{2}\pi^3} \left| \frac{1}{2} A_t(\tau_t)\left[1+\kappa_{gg}\right] + \dots \right|^2 , \tag{5.2.15}$$

where the dots stand for the negligible contribution of the light quarks and leptons, and the coefficients κ can be written as:

$$\kappa_{\gamma\gamma} = \sum_{NP} \frac{3}{4} N_{c,NP} Q_{NP}^2 \frac{v_{SM}}{m_{NP}} \frac{\partial m_{NP}}{\partial v} \frac{A_{F,W,S}(m_{NP})}{A_t} , \tag{5.2.16}$$

$$\kappa_{gg} = \sum_{NP} 2C(r_{NP}) \frac{v_{SM}}{m_{NP}} \frac{\partial m_{NP}}{\partial v} \frac{A_{F,W,S}(m_{NP})}{A_t} , \tag{5.2.17}$$

where the ratio of A functions depends on the spin and masses of the new particles (and top). In the light Higgs approximation, however, the ratio only depends on the spin of the new particle:

$$\frac{A_{NP}}{A_t} = \begin{cases} 1 & \text{for fermions} \\ -\frac{21}{4} & \text{for vectors} \\ \frac{1}{4} & \text{for scalars} \end{cases} \tag{5.2.18}$$

An interesting feature of this parametrization is that a particle with the same quantum numbers of the top will give $\kappa_{\gamma\gamma} = \kappa_{gg}$, and a single particle will give a contribution to the two coefficients with the same sign. In this way, if the experimental data allow to point to a specific quadrant in the $\kappa_{\gamma\gamma}$–κ_{gg} parameter space, we can have a hint of the underlying new physics model. This will be illustrated in various examples in the following sections. Note also that positive κ's enhance the top contribution, therefore inducing an enhancement in the gluon channel but a suppression in the photon one, where there is a numerical cancellation between the dominant W contribution and the top one.

The presence of new physics often modifies the tree level relation between the mass of the SM particles and the Higgs VEV. This modification of the SM contribution can also be cast in the κ parameters. For the top it will read:

$$\kappa_{\gamma\gamma}(top) = \kappa_{gg}(top) = \frac{v_{SM}}{m_t} \frac{\partial m_t}{\partial v} - 1 . \tag{5.2.19}$$

For the W:

$$\kappa_{\gamma\gamma}(W) = \frac{3}{4}\left(\frac{v_{SM}}{m_W}\frac{\partial m_W}{\partial v} - 1\right)\frac{A_W(\tau_W)}{A_F(\tau_{top})}, \quad (5.2.20)$$

$$\kappa_{gg}(W) = 0\,. \quad (5.2.21)$$

Here, the difference between the VEVs does introduce relevant corrections and they must be taken into account.

Note that the modification of the SM couplings will also affect the other production channels, and the branching ratio in heavy gauge bosons. Those effects will however have a minor impact on our analysis, and their inclusion will be necessary in a later model-dependent analysis, after (and if) a model is preferred by data

5.2.1 Observables at the LHC and Linear Colliders

The LHC will measure the inclusive $\gamma\gamma$ Higgs decays and the new physics will modify both the total production cross section and the branching fraction in photons. For large masses, close to the W threshold, the decay in two heavy gauge bosons (one is virtual) becomes relevant and will also yield a relatively early measurement. At large luminosities, one may also measure the $\gamma\gamma$ decays in a specific production channel, for instance the vector boson fusion one that can be isolated using two forward jet tagging: in this case one may probe directly the branching ratios.

In the Higgs mass range of interest, between 115 and 150 GeV, the main production channel is gluon fusion with a SM cross section of $40-25$ pb, followed by vector boson fusion ($5-4$ pb) and by other channels (WH, ZH, $\bar{t}tH$) which sum up to $4-2$ pb. Here we will assume that the new physics significantly contributes only to the loop in the gluon fusion channel, while the other cross sections are unaffected. The total production cross section normalized with the SM one, that we denote as $\bar{\sigma}$, can be written as:

$$\bar{\sigma}(H) = \left(\frac{\sigma_{gg}^{NP} + \sigma_{VBF}^{SM} + \sigma_{VH,\bar{t}tH}^{SM}}{\sigma_{gg}^{SM} + \sigma_{VBF}^{SM} + \sigma_{VH,\bar{t}tH}^{SM}}\right) \simeq \left(\frac{(1+\kappa_{gg})^2\sigma_{gg}^{SM} + \sigma_{VBF}^{SM} + \sigma_{VH,\bar{t}tH}^{SM}}{\sigma_{gg}^{SM} + \sigma_{VBF}^{SM} + \sigma_{VH,\bar{t}tH}^{SM}}\right). \quad (5.2.22)$$

In the SM the Higgs branching fraction in photons amounts to $2\cdot 10^{-3}$. In presence of new physics, the branching fraction will also be sensitive to the gluon loop via the total width, as the gluon channel is significant: it amounts to 7% of the total for $m_H = 115$ GeV, decreasing to 3% for $m_H = 150$ GeV. Also in this case, we define a branching ratio normalized to the SM value, $\overline{BR}$

$$\overline{BR}(H\to\gamma\gamma) = \frac{\Gamma_{\gamma\gamma}^{NP}}{\Gamma_{\gamma\gamma}^{SM}}\,\frac{\Gamma_{\rm tot}^{SM}}{\Gamma_{gg}^{NP}+\Gamma_{\gamma\gamma}^{NP}+\Gamma_{\rm others}^{SM}} \simeq \left(1+\frac{\kappa_{\gamma\gamma}}{\frac{9}{16}A_W(\tau_W)+1}\right)^2 \frac{\Gamma_{\rm tot}^{SM}}{(1+\kappa_{gg})^2\Gamma_{gg}^{SM}+(\Gamma_{\rm tot}^{SM}-\Gamma_{gg}^{SM})}\,. \quad (5.2.23)$$

The branching ratio in heavy vectors will depend on κ_{gg} via the total width of the Higgs, therefore the normalized $\overline{BR}$ is

$$\overline{BR}(H\to VV^*) = \frac{\Gamma_{\rm tot}^{SM}}{\Gamma_{gg}^{NP}+\Gamma_{\gamma\gamma}^{NP}+\Gamma_{\rm others}^{SM}} \simeq \frac{\Gamma_{\rm tot}^{SM}}{(1+\kappa_{gg})^2\Gamma_{gg}^{SM}+(\Gamma_{\rm tot}^{SM}-\Gamma_{gg}^{SM})}\,. \quad (5.2.24)$$

For completeness, the normalized gluon branching fraction can be written as

$$\overline{BR}(H \to gg) = \frac{\Gamma^{NP}_{gg}}{\Gamma^{SM}_{gg}} \frac{\Gamma^{SM}_{\rm tot}}{\Gamma^{NP}_{gg} + \Gamma^{NP}_{\gamma\gamma} + \Gamma^{SM}_{\rm others}} \simeq \frac{(1+\kappa_{gg})^2 \Gamma^{SM}_{\rm tot}}{(1+\kappa_{gg})^2 \Gamma^{SM}_{gg} + (\Gamma^{SM}_{\rm tot} - \Gamma^{SM}_{gg})} \,. \quad (5.2.25)$$

The branching ratios will be measured with an accuracy of few % at a TeV e^+e^- Linear Collider.

5.3 Survey of models of New Physics in 4 dimensions

In this section we will summaries the values of the two parameters $\kappa_{\gamma\gamma}$ and κ_{gg} in a variety of models of new physics. It is not intended to be a complete survey, but rather a collection of examples of the usefulness of our proposed parametrization, and of the impact of new physics on the Higgs search. Here, we will briefly discuss a fourth generation, supersymmetry, Little Higgs models, a scalar colour octet and the Lee-Wick SM. As the new particles and mass scales are often heavier than the top, we will use the light Higgs approximation to derive some simple analytical formulas.

5.3.1 A 4$^{\rm th}$ generation

As for SM fermions, the masses of a chiral fourth generation are proportional to the Higgs VEV, and they cannot be arbitrarily large due to the perturbativity of the Yukawa couplings, naively $m_4 < 4\pi v \sim 2$ TeV. It has been shown that the impact of a relatively light 4$^{\rm th}$ generation on the electroweak precision tests can be minimized if the spectrum follows a specific pattern (99): in particular if the splitting between the up and down type quarks is about 50 GeV (and similarly for the leptons). For masses of a few hundred GeV, this is not a severe fine tuning. Finally, let us remind that direct bounds on such new particles are of the order of 190 GeV (for a fourth generation bottom type quark in $p\bar{p}$ collisions (100)) and 100 GeV for a charged lepton.

In the light Higgs approximation, the mass dependence disappears: κ_{gg} simply counts the number of new colour triplet quarks, $\kappa_{gg} = 2$, while $\kappa_{\gamma\gamma}$ depends on the charges

$$\kappa_{\gamma\gamma} = \frac{3}{4}\left[3\left(\frac{2}{3}\right)^2 + 3\left(-\frac{1}{3}\right)^2 + 1\right] = 2\,. \quad (5.3.1)$$

Due to an accident in the charges, therefore, a complete extra generation contributes like two tops. Another accident is that the width in photons is largely suppressed, while the gluon one is enhanced by almost the same amount: overall, the inclusive $\gamma\gamma$ signal will be similar to the SM one (99) (for a light Higgs).

5.3.2 Supersymmetry

The supersymmetric contributions to the $h \to \gamma\gamma$ and $h \to gg$ amplitudes are well studied in supersymmetric extensions of the standard model (see for example (101) for few sample benchmark scenarios). Here we will focus on the common scenario where the heavier Higgses are above the WW threshold, so that the $\gamma\gamma$ decay mode is only relevant for the light Higgs h. However, the parametrization we propose in this paper cannot be used in general for supersymmetric models. In fact, due to the presence of two Higgses which develop a VEV, the tree level couplings of the SM particles to the Higgs are modified at order $\mathcal{O}(1)$ compared to the SM case. If we define $\tan\beta = v_u/v_d$ the ratio of the two VEVs, and α the mixing angle in the neutral

Higgs sector (21), the couplings of W, top (up-type fermions) and bottom (down-type fermions) compared to the SM values are corrected by the following factors:

$$\frac{g_{W^+W^-h}}{g_{SM}} = \sin(\beta-\alpha)\,, \qquad \frac{g_{\bar{t}th}}{g_{SM}} = \frac{\cos\alpha}{\sin\beta}\,, \qquad \frac{g_{\bar{b}bh}}{g_{SM}} = -\frac{\sin\alpha}{\cos\beta}\,. \tag{5.3.2}$$

Those corrections can be large, even for heavy susy masses. In the large $\tan\beta$ case, which is preferred by the top Yukawa perturbativity and experimental constraints, the bottom (and tau) Yukawas are enhanced by a large factor $\sim\tan\beta$: the Higgs width increases and the branching ratio in photons can be easily suppressed by orders of magnitudes, making this channel unobservable. In order to keep the $\gamma\gamma$ channel alive, one needs to compensate the large $\tan\beta$ with a small mixing angle in the Higgs sector: $\alpha\sim\pm(\pi/2-\beta)$. This requirements means that we are close to the decoupling limit in which the behavior of the MSSM Higgs sector is standard model like. Indeed a limit $m_A\gg m_Z$ (where m_A is the mass of the pseudoscalar Higgs) implies that only the standard model like Higgs boson stays light while all the other scalars are heavy and that $\alpha\to(-\pi/2+\beta)$ (for more details concerning this decoupling limit see (102)).

In order to safely use our formalism, we need to make sure that the corrections to the bottom Yukawa (and couplings to the W) are negligible. In the left panel of Figure 5.1 we plotted the region in the α–β parameter space where both the W and bottom couplings deviate by less than 5% from the SM value (up to the overall sign). Note that the region delimited by the solid (red) lines in the left part of the left panel in Figure 5.1 is precisely the one around the line of points where $\alpha=(-\pi/2+\beta)$ which corresponds to the decoupling limit discussed above. We also superimposed the region where corrections to the top Yukawa are smaller than 5%. There is a tiny region where a fine tuning between the two angles allow for our formalism to be used. Note that a larger mixing angle in the Higgs sector will soon enhance the bottom Yukawa and kill the $\gamma\gamma$ signal, so the region is not a negligible part of the parameter space where the signal is observable. On the right panel we used a three level relation between the masses in the Higgs sector and α

$$\frac{\tan 2\alpha}{\tan 2\beta} = \frac{m_A^2+m_Z^2}{m_A^2-m_Z^2}\,, \tag{5.3.3}$$

where m_A is the mass of the pseudoscalar (which also sets the mass scale of the other heavy Higgses), to set a lower bound on the heavy Higgs masses. Therefore, we expect that for masses above 1 TeV, the corrections to the bottom (and tau) Yukawa can be safely neglected. In this region, corrections to the W and top couplings are small too.

For the purpose of illustrating our parametrization, we will focus on some approximate expressions that arise in a simple scenario: the MSSM golden region (103). This scenario is motivated by naturalness in the Higgs mass, minimal fine tuning and precision tests. The main features are large soft masses for the gauginos and for the light generations, and large mixing in the stop sector induced by a large soft trilinear term. A general analysis of the $\gamma\gamma$ channel can be found in Ref. (104). As a numerical example we will consider a variation of the benchmark point in Ref. (103): here, $\tan\beta=10$ and all the soft masses except the stop and Higgs ones are at 1 TeV, $\mu=250$ GeV and the soft trilinear term for the stops A_t is at 1 TeV to induce a large mixing in the stop sector and reduce the fine tuning in the Higgs potential. In this benchmark point, the light Higgs is at 129 GeV. Charginos and neutralinos (mostly higgsinos) are at 250 GeV (set by μ), while the stops are at 400 and 700 GeV. All other masses are above a TeV, and we will neglect the contribution of those sparticles. The only difference is that, in order to avoid the bottom Yukawa problem, we will push the heavy Higgses above 1 TeV: to do that it is enough to increase the H_d soft mass above the TeV scale. This will not introduce a severe

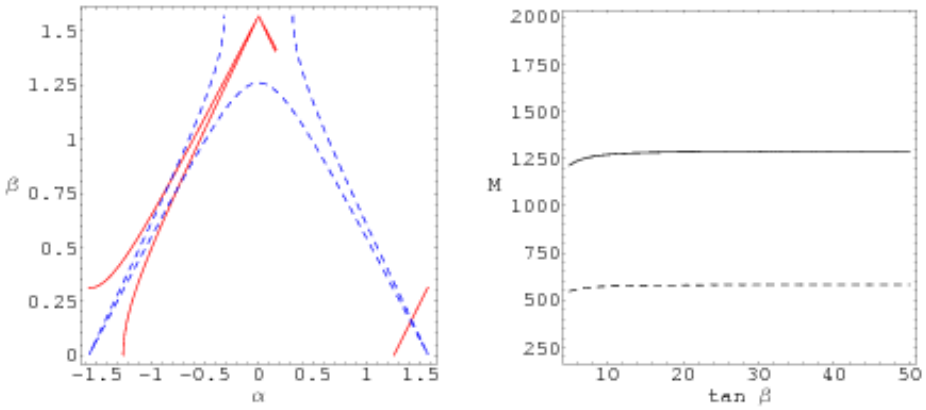

Figure 5.1: Left panel: in solid red the region where the couplings of the W and bottom are both within 5% from the SM values (up to the sign), in dashed blue the same for the top couplings. Right panel: lower bound on the heavy Higgs masses as a function of $\tan\beta$ requiring deviations of 1% (solid) or 5% (dashed).

fine tuning, as the contribution of this mass to the Higgs VEV is also suppressed by the large $\tan\beta$ (21). In this scenario, only the stops contribute to $h \to gg$ and $h \to \gamma\gamma$. We neglect the contribution of charginos because they are mostly higgsinos: the coupling to the Higgs is suppressed by the large gaugino masses. For the stops, assuming that the soft masses for left and right handed scalars are equal (~ 550 GeV at the benchmark point), the contribution to the κ parameters can be expressed as

$$\kappa_{gg}(stops) = \kappa_{\gamma\gamma}(stops) \simeq \frac{m_2^2 + m_1^2}{4m_1^2 m_2^2} m_t^2 - \frac{(m_2^2 - m_1^2)^2}{16 m_1^2 m_2^2} \sim -0.02\,, \tag{5.3.4}$$

where $m_{1,2}$ are the masses of the two eigenstates, and the second term is proportional to the soft trilinear term: $m_2^2 - m_1^2 \simeq 2|A_t| m_t$.

Those formulas are presented here for illustration purpose only, and we will use exact one loop expressions for the numerical analysis, including the contribution of charginos. A more general analysis of the region in the MSSM parameter space is beyond the scope of this paper, and it is postponed to a following publication.

5.3.3 Little Higgs models

We will first derive some very general formulas, and then apply them to explicit examples. In models with only one extra massive gauge boson, W', the cancellation works thanks to the different sign between the couplings of the W and W' (105):

$$g_{hW'W'} = -g_{hWW}\,. \tag{5.3.5}$$

This is a consequence of the fact that $m_W^2 + m_{W'}^2$ does not depend on the Higgs VEV, but it is fixed by the scale f at which the global symmetry is broken. The coupling of the W with the Higgs is also modified

$$g_{hWW} = g_{hWW}^{SM}\,(1 - \delta_W) = \frac{2m_W^2}{v_{SM}}\,(1 - \delta_W)\,, \tag{5.3.6}$$

where δ_W contains corrections in v/f. After recalling that $g_{hWW} = \frac{\partial m_W^2}{\partial v}$, the contribution of the W and W' to the κ parameters is (in the light Higgs approximation) :

$$\kappa_{\gamma\gamma}(W') = \frac{63}{16}\left(\frac{m_W}{m_{W'}}\right)^2(1-\delta_W)\,, \tag{5.3.7}$$

$$\kappa_{\gamma\gamma}(W) = -\frac{9}{16}A_W(\tau_W)\delta_W\,; \tag{5.3.8}$$

while $\kappa_{gg} = 0$.

The precise value of δ_W depends on the symmetry structure of the model: in the Simplest Little Higgs (SLH) model (106), which is based on an SU(3) gauge symmetry,

$$m_W = gf\sin\frac{v}{2f}\,, \tag{5.3.9}$$

$$m_{W'} = gf\cos\frac{v}{2f}\,; \tag{5.3.10}$$

so that

$$\delta_W = 1-\cos\frac{v}{2f} = 1-\frac{m_{W'}}{\sqrt{m_{W'}^2+m_W^2}} \simeq \frac{1}{2}\left(\frac{m_W}{m_{W'}}\right)^2+\dots \tag{5.3.11}$$

At leading order in $m_W/m_{W'} \sim v/f$:

$$\kappa_{\gamma\gamma} \simeq \frac{9}{16}\left(7-\frac{1}{2}A_W(\tau_W)\right)\left(\frac{m_W}{m_{W'}}\right)^2 \sim (6.2\div 6.7)\cdot\left(\frac{m_W}{m_{W'}}\right)^2 \tag{5.3.12}$$

where we have varied the Higgs mass between 115 and 150 GeV.

The top sector is more complicated because doubling of fields is usually required in order to generate a realistic spectrum for the light states. For instance, the simplest way to introduce the top is to embed the SM left-handed doublet in a triplet of SU(3) that couples via the two Higgses to two right-handed singlets. In this case we need to double the right-handed tops in order to give mass both to the top and to its heavy partner T. The symmetry structure of the model implies that $m_t^2+m_T^2$ does not depend on the SM Higgs VEV, therefore the following relation holds between the couplings to the Higgs ($g_{hff} = \frac{\partial m_f}{\partial v}$):

$$g_{hTT} = -\frac{m_t}{m_T}g_{htt}\,. \tag{5.3.13}$$

As in the gauge sector, the coupling of the SM top also receives deviations from the usual Yukawa coupling, which we can parametrize as

$$g_{htt} = \frac{m_t}{v_{SM}}(1-\delta_t)\,. \tag{5.3.14}$$

In terms of this parametrization, the contribution to $\kappa_{\gamma\gamma}$ and κ_{gg} of the top and T are, in the light Higgs approximation:

$$\kappa_{\gamma\gamma}(top) = \kappa_{gg}(top) = -\delta_t\,, \tag{5.3.15}$$

$$\kappa_{\gamma\gamma}(T) = \kappa_{gg}(T) = -\frac{m_t^2}{m_T^2}(1-\delta_t)\,. \tag{5.3.16}$$

In the SLH model, the masses can be written as

$$m^2_{t,T} = \lambda_T^2 f^2 \left(1 \mp \sqrt{1 - \frac{\lambda_t^2}{\lambda_T^2}\sin^2\frac{v}{f}}\right), \tag{5.3.17}$$

where $\lambda_{t,T}$ are related to the Yukawa couplings to the two Higgses $\lambda_{1,2}$:

$$\lambda_T = \sqrt{\frac{\lambda_1^2+\lambda_2^2}{2}}, \qquad \lambda_t = \frac{\lambda_1\lambda_2}{\lambda_T}. \tag{5.3.18}$$

Therefore

$$\delta_t = 1 - \frac{m_T^2}{m_T^2 - m_t^2}\frac{m_{W'}^2 - m_W^2}{m_{W'}\sqrt{m_{W'}^2+m_W^2}} \simeq -\frac{m_t^2}{m_T^2} + \frac{3}{2}\frac{m_W^2}{m_{W'}^2} + \dots \tag{5.3.19}$$

and, at leading order,

$$\kappa_{\gamma\gamma}(top+T) = \kappa_{gg}(top+T) \simeq -\frac{3}{2}\frac{m_W^2}{m_{W'}^2} + \dots \tag{5.3.20}$$

Note that at leading order the result is independent on the heavy top mass, but only depends on the heavy gauge boson W'.

The total contribution is therefore:

$$\kappa_{gg}(SLH) \simeq -\frac{3}{2}\frac{m_W^2}{m_{W'}^2} \sim -0.002\cdot\left(\frac{2\text{TeV}}{m_{W'}}\right)^2, \tag{5.3.21}$$

$$\kappa_{\gamma\gamma}(SLH) \simeq \left(\frac{141}{32} - \frac{9}{32}(7+A_W)\right)\frac{m_W^2}{m_{W'}^2} \sim 0.007\cdot\left(\frac{2\text{TeV}}{m_{W'}}\right)^2; \tag{5.3.22}$$

the Higgs mass dependence in A_W is very mild due to the small coefficient. In the numerical values we have chosen a W' mass of 2 TeV, which is roughly the one required by electroweak precision measurements (107). Note however that the implementation of a T parity (23) would reduce the bound by almost an order of magnitude.

Another simple model using the Little Higgs mechanism was proposed in Ref. (108) and dubbed Littlest Higgs. Here a global SU(5) is spontaneously broken down to SO(5), and a subgroup SU(2)$^2\times$ U(1)^2 is gauged. The mechanism acts thanks to the presence of two copies of the SM gauge group, which are broken to the diagonal by the spontaneous breaking of SU(5). The Higgs again is a pseudo-Goldstone boson of the global symmetry breaking. The model, together with a heavy W (W_H) and top (T) also contains a heavy charged scalar Φ from a triplet of SU(2) that develops a VEV (v'). The model therefore contains more parameters that the SLH, and its contribution to $H\to\gamma\gamma$ and $H\to gg$ has been computed in Ref. (109). Here we will simply translate those results in our notation: the contribution of the W and heavy gauge states is (expressed in terms of the masses at leading order in the Higgs VEV v):

$$\kappa_{\gamma\gamma}(W) \simeq \frac{9}{16}\left(\frac{m_W^2}{m_{W_H}^2} - \frac{5-x^2}{8}\frac{v^2}{f^2}\right)A_W(\tau_W), \tag{5.3.23}$$

$$\kappa_{\gamma\gamma}(W_H) \simeq \frac{63}{16}\frac{m_W^2}{m_{W_H}^2}, \tag{5.3.24}$$

$$\kappa_{\gamma\gamma}(\Phi) \simeq -\frac{4-3x^2}{64}\frac{v^2}{f^2}; \tag{5.3.25}$$

$$\kappa_{gg}(W, W_H, \Phi) = 0. \tag{5.3.26}$$

Here x is proportional to the ratio between the triplet and doublet VEVs ($0 \leq x < 1$). Note that in the limit where the Higgs is much lighter than the W-threshold, the contributions proportional to the W mass tend to cancel, while the ones proportional to v^2 do not. The top and heavy top contributions are

$$\kappa_{\gamma\gamma}(top) = \kappa_{gg}(top) \simeq \frac{m_t^2}{m_T^2} - \frac{7-4x+x^2}{8}\frac{v^2}{f^2}\,, \tag{5.3.27}$$

$$\kappa_{\gamma\gamma}(T) = \kappa_{gg}(T) \simeq -\frac{m_t^2}{m_T^2}\,. \tag{5.3.28}$$

Note that as in the SLH, the contribution proportional to the top mass cancels out. Therefore, the main corrections in this model are proportional to the Higgs VEV and suppressed by the global symmetry breaking f:

$$\kappa_{gg}(LH) \simeq -\frac{7-4x+x^2}{8}\frac{v^2}{f^2}\,, \tag{5.3.29}$$

$$\kappa_{\gamma\gamma}(LH) \simeq \left(\frac{195}{64}+x-\frac{73}{64}x^2\right)\frac{1}{2}\frac{v^2}{f^2} + \\ +\frac{9}{16}(7+A_W)\left(\frac{m_W^2}{m_{W_H}^2} - \frac{5-x^2}{8}\frac{v^2}{f^2}\right)\,. \tag{5.3.30}$$

Note that the second term in $\kappa_{\gamma\gamma}$, which depends on the W_H mass, is negligible due to a small coefficient, therefore the result only depends on f and the triplet VEV x.

The bound from precision measurements on the scale f is around 5 TeV (107), which correspond roughly to masses of order 2 TeV. To give a numerical example, if x is negligible

$$\kappa_{gg}(LH) \simeq -\frac{7}{8}\frac{v^2}{f^2} \sim -0.002\cdot\left(\frac{5\,\text{TeV}}{f}\right)^2\,, \tag{5.3.31}$$

$$\kappa_{\gamma\gamma}(LH) \simeq \frac{195}{128}\frac{v^2}{f^2} \sim 0.0036\cdot\left(\frac{5\,\text{TeV}}{f}\right)^2\,. \tag{5.3.32}$$

Not that when a T parity is implemented on this model (23), the bound on f is lowered to 500 GeV (110), therefore the contribution to the κ parameters is 100 times bigger.

5.3.4 Extended scalar sector: colour octet

The scalar sector is experimentally the least tested part of the Standard Model and may be more complicated than the minimal content of the SM. It has been shown (111) that in order to avoid tree level flavor changing neutral currents, the extra scalar should be either a copy of the SM one (leading to the two Higgs model) or a colour octet with the same weak quantum numbers as the SM Higgs. Here we will focus on the latter possibility (111). The most general potential contains 3 terms that are bilinear in both the Higgs H and the colour octet S:

$$\mathcal{L} = \lambda_1 H^{\dagger i} H_i S^{\dagger j} S_j + \lambda_2 H^{\dagger i} H_j S^{\dagger j} S_i + \left[\lambda_3 H^{\dagger i} H^{\dagger j} S_i S_j + h.c.\right] + \dots \tag{5.3.33}$$

where i and j are SU(2) indices and we have left implicit the colour contractions. Note that imposing custodial symmetry would require $\lambda_2 = 2\lambda_3$. After the Higgs develops a VEV $\langle H\rangle =$

$v/\sqrt{2}$, the spectrum contains one charged and two neutral scalar octets with masses

$$m^2_{S^\pm} = m^2_S + \lambda_1 \frac{v^2}{4} = m^2_S\,(1 + X_1)\,, \tag{5.3.34}$$

$$m^2_{S^0_{1,2}} = m^2_S + (\lambda_1 + \lambda_2 \pm 2\lambda_3)\frac{v^2}{4} = m^2_S\,(1 + X_1 + X_2 \pm 2X_3)\,; \tag{5.3.35}$$

where $X_i = \lambda_i v^2/4$. At loop level, the octet will contribute to the electroweak precision tests (111): the corrections can be encoded in the S and ρ parameters, and for small $v \ll m_S$:

$$S \simeq \frac{2}{3\pi} X_2\,, \tag{5.3.36}$$

$$\Delta\rho \simeq \frac{\sin^2\theta_W\, m_W^2}{96\alpha\pi^3\, m_S^2}(\lambda_2^2 - 4\lambda_3^3)\,. \tag{5.3.37}$$

The corrections to the ρ parameter can be minimized by imposing (approximate) custodial symmetry, while S will give a direct constraint on X_2. Note that X_1 is not strongly constrained.

Using the formalism developed in the previous section we can compute the contribution of the scalar octet to the κ parameters (for $v \ll m_S$):

$$\kappa_{\gamma\gamma}(S) \simeq \frac{3}{2}\frac{\lambda_1 v^2}{4m^2_{S^\pm}} \sim \frac{3}{2} X_1\,, \tag{5.3.38}$$

$$\begin{aligned}\kappa_{gg}(S) &\simeq \frac{C(8)}{2}\left(\frac{\lambda_1 v^2}{4m^2_{S^\pm}} + \frac{1}{2}\frac{(\lambda_1+\lambda_2+2\lambda_3)v^2}{4m^2_{S^0_1}} + \frac{1}{2}\frac{(\lambda_1+\lambda_2-2\lambda_3)v^2}{4m^2_{S^0_2}}\right)\\ &\sim \frac{3}{2}(2X_1 + X_2)\,;\end{aligned} \tag{5.3.39}$$

where $C(8) = 3$. As a numerical example, we will use $\lambda_1 = 4$, $\lambda_2 = 1$ and $m_S = 750$ GeV. In this case, $X_1 \sim 1/9$ and $X_2 \sim 1/36$, therefore $\kappa_{\gamma\gamma} \sim 0.17$ and $\kappa_{gg} \sim 0.37$.

5.3.5 Lee-Wick Standard Model

Lee and Wick (LW) proposed a modification of the particle propagators in QED by means of higher derivative terms in order to improve the ultraviolet convergence of the theory and make loop corrections finite. This modification of the propagator can also be parametrized by the presence of a new degree of freedom with large mass and negative kinetic term, so that the corrected propagator looks like a Pauli-Villars regularized one, where the Pauli-Villars cutoff scale is replaced by the mass scale of such new degree of freedom. This idea has recently been extended to the full SM (112): in this case the loops are not finite, however the softening of the divergences is enough to address the hierarchy problem in the Higgs mass.

Notwithstanding the theoretical issues arisen by this formulation, the contribution of the LW degrees of freedom to the $H \to gg$ and $H \to \gamma\gamma$ amplitudes has been computed (113): here we will sketch the calculation, making use of the general formulas given in Section 5.2, and give some simple results in the large LW mass approximation.

In this model, to each SM particle, a new LW degree of freedom is associated (2 for each chiral fermion). For more details of the construction we refer the reader to the Refs. (112; 113). The Higgs VEV will generate a mixing between the standard and LW particles, which has been studied in detail in (113): in the following we will review just the results needed to complete our calculation.

In the Higgs sector, the SM Higgs h and the LW scalar $\tilde{h}$ mix via the Higgs VEV: the mixing can be described by a symplectic rotation

$$\begin{pmatrix} \cosh\theta & \sinh\theta \\ \sinh\theta & \cosh\theta \end{pmatrix}, \qquad \text{with} \quad \tanh 2\theta = -2\frac{m_h^2\tilde{m}_h^2}{m_h^4+\tilde{m}_h^4}\,. \tag{5.3.40}$$

A very similar mixing takes place in the gauge sector, between the W and the LW $\tilde{W}$. The two mass eigenstates are

$$m_W^2 = \frac{1}{2}\left(M_2^2 - \sqrt{M_2^4 - g^2v^2M_2^2}\right), \tag{5.3.41}$$

$$\tilde{m}_W^2 = \frac{1}{2}\left(M_2^2 + \sqrt{M_2^4 - g^2v^2M_2^2}\right); \tag{5.3.42}$$

where M_2 is the mass of the LW partner of the SU(2) gauge bosons. Note that there is no trilinear coupling between the W and the LW Higgs $\tilde{h}$, therefore (using the formulas in Appendix D):

$$\frac{v_{SM}}{m_W}\frac{\partial m_W}{\partial v} \to \cosh\theta\,\frac{gv}{2m_W}\frac{M_2^2}{\sqrt{M_2^4-g^2v^2M_2^2}} = \frac{\tilde{m}_h^2}{\sqrt{m_h^4+\tilde{m}_h^4}}\frac{\tilde{m}_W\sqrt{\tilde{m}_W^2+m_W^2}}{\tilde{m}_W^2-m_W^2} \simeq 1+\frac{3}{2}\frac{m_W^2}{\tilde{m}_W^2}\,. \tag{5.3.43}$$

For the $\tilde{W}$, the coupling to the Higgs is given by $-\frac{\partial\tilde{m}_W^2}{\partial v}$: the minus sign comes from the negative sign of the kinetic term. This can be proved by an explicit calculation, and it is true for all the LW fields (for fermions, the coupling to the Higgs is $-\frac{\partial\tilde{m}_f}{\partial v}$). However, another minus sign comes from the loops: compared to the SM ones, propagators and couplings to the gauge bosons (photons and gluons) have a minus sign from the negative kinetic term of the LW fields. All in all, a minus sign form the loop compensates the minus sign in the Higgs coupling and we can safely use the formulas in Section 5.2:

$$\frac{v_{SM}}{\tilde{m}_W}\frac{\partial\tilde{m}_W}{\partial v} \to -\cosh\theta\,\frac{gvm_W}{2\tilde{m}_W^2}\frac{M_2^2}{\sqrt{M_2^4-g^2v^2M_2^2}} \simeq -\frac{m_W^2}{\tilde{m}_W^2}\,. \tag{5.3.44}$$

Putting the two results together, and expanding for $m \ll \tilde{m}$:

$$\kappa_{\gamma\gamma}(W+\tilde{W}) \simeq \frac{27}{32}\frac{m_W^2}{\tilde{m}_W^2}\left(7+A_W(\tau_W)\right) - \frac{63}{32}\frac{m_W^2}{\tilde{m}_W^2}\,. \tag{5.3.45}$$

This result is numerically small [1], and the contribution of the W and its LW partner partially cancel each other in the light Higgs limit.

The spectrum also contains a LW charged scalar: in fact the LW Higgs does not develop a VEV and its charged component $\tilde{h}^+$ is not eaten up. The mass of such scalar is simply given by the Higgs LW mass $\tilde{m}_{h^\pm}^2 = M_H^2$. Nevertheless, as it happens in the SM with the Goldstone boson in the Higgs, the Lagrangian contains a coupling between $\tilde{h}^+$ and the Higgs field which

[1] The authors of Ref. (113) find that the contribution of the W is proportional to the SM amplitude by a factor $s_{(A+\tilde{A})^2} = \frac{\tilde{m}_W^2+m_W^2}{\tilde{m}_W^2-m_W^2}$. In fact, the coupling of the W with the Higgs can be written as $\cosh\theta\, s_{(A+\tilde{A})^2}\,\frac{g^2v}{2}$; however $\frac{gv}{2} = \frac{m_W\tilde{m}_W}{\tilde{m}_W^2+m_W^2} \neq m_W$.

can be calculated explicitly and enters the formulas in section 5.2 as (we are using here the same notation as in Ref.s (112; 113))

$$\frac{v_{SM}}{\tilde{m}_{h^\pm}}\frac{\partial \tilde{m}_{h^\pm}}{\partial v} \to -\frac{v_{SM}}{2\tilde{m}^2_{h^\pm}}(\cosh\theta - \sinh\theta)\frac{\lambda v}{2} = \\ -\frac{1}{2}\frac{\sqrt{\tilde{m}^2_W + m^2_W}}{\tilde{m}_W}\frac{m^2_h + \tilde{m}^2_h}{\sqrt{m^4_h + \tilde{m}^4_h}}\frac{m^2_h \tilde{m}^2_h}{\tilde{m}^2_{h^\pm}(m^2_h + \tilde{m}^2_h)} \simeq -\frac{1}{2}\frac{m^2_h}{\tilde{m}^2_{h^\pm}}\,, \quad (5.3.46)$$

where an extra minus sign comes from the propagators in the loop. Therefore

$$\kappa_{\gamma\gamma}(\tilde{h}^\pm) \simeq -\frac{3}{32}\frac{m^2_h}{\tilde{m}^2_{h^\pm}}\,. \quad (5.3.47)$$

This result is also different from the result in Ref. (113), where the contribution of the charged LW Higgs vanishes at this order [2].

The top sector is more complicated because for each chiral SM fermion one needs to add a massive Dirac fermion (with negative kinetic term). The Yukawa couplings, however, have a simple form: in particular they have the same structure as the SM Yukawas, and they are functions of the field combination $H - \tilde{H} = 1/\sqrt{2}(v + h - \tilde{h} + \dots)$: the presence of a LW Higgs will only manifest itself in the fact that the couplings to the standard Higgs are proportional to $\cosh\theta - \sinh\theta$. The spectrum can be calculated as a series for large LW top mass M_t (assuming the same mass for the LW partners of the left- and right-handed tops):

$$m_t = M_t\epsilon\left(1 + \epsilon^2 + \dots\right)\,, \quad (5.3.48)$$

$$\tilde{m}_{t1,2} = M_t\left(1 \mp \frac{1}{2}\epsilon - \frac{3}{8}\epsilon^2 + \dots\right)\,; \quad (5.3.49)$$

where $\epsilon = \frac{y_t v}{\sqrt{2}M_t}$. The contribution of the top (and partners) is therefore:

$$\kappa_{gg}(\text{tops}) = \kappa_{\gamma\gamma}(\text{tops}) = \left((\cosh\theta - \sinh\theta)\frac{2m_W}{gv}\frac{\epsilon}{m_t}\frac{\partial m_t}{\partial \epsilon} - 1\right) + \\ (\cosh\theta - \sinh\theta)\left(\frac{\epsilon}{\tilde{m}_{t1}}\frac{\partial \tilde{m}_{t1}}{\partial \epsilon} + \frac{\epsilon}{\tilde{m}_{t2}}\frac{\partial \tilde{m}_{t2}}{\partial \epsilon}\right) \simeq \frac{m^2_h}{\tilde{m}^2_h} + \frac{1}{2}\frac{m^2_W}{\tilde{m}^2_W} + \dots\,. \quad (5.3.50)$$

The ϵ dependence cancels out between the top and LW tops contributions, at the end the result only depends on the LW Higgs mass.

In total (at this order $\tilde{m}_{h^\pm} = \tilde{m}_h$):

$$\kappa_{gg} \simeq \frac{m^2_h}{\tilde{m}^2_h} + \frac{1}{2}\frac{m^2_W}{\tilde{m}^2_W} \sim 0.015 \cdot \left(\frac{m_h}{120\,\text{GeV}}\frac{1\,\text{TeV}}{\tilde{m}_h}\right)^2\,, \quad (5.3.51)$$

$$\kappa_{\gamma\gamma} \simeq \frac{29}{32}\frac{m^2_h}{\tilde{m}^2_h} - \frac{47}{32}\frac{m^2_W}{\tilde{m}^2_W} + \frac{9}{16}\frac{m^2_W}{\tilde{m}^2_W}(7 + A_W(\tau_W)) \sim 0.017 \cdot \left(\frac{m_h}{120\,\text{GeV}}\frac{1\,\text{TeV}}{\tilde{m}_h}\right)^2 \quad (5.3.52)$$

where in the numerical example we neglected the contribution proportional to the W mass because of the higher bound on $\tilde{m}_W$ from electroweak precision tests ($\tilde{m}_W \gg 3$ TeV) (114).

[2] In Ref. (113), the authors include the contribution of the charged LW Higgs using the amplitude of the SM Goldstone boson in the Feynman gauge rescaled by the ratio $\frac{m^2_W}{\tilde{m}^2_{h^\pm}}$. However the coupling of a Goldstone boson (which is the same as $\tilde{h}^+$) is not proportional to its mass. See Appendix D.3 for more details.

5.4 Survey of models of New Physics in extra dimensions

In this section we will focus on models of new physics in one extra dimension, in particular on the different ways one can employ the Higgs mechanism in this context. Most models can be divided in 3 main categories: bulk Higgs (BH), brane Higgs (bH) and Gauge Higgs (GH). In the first case, the Higgs is just a 5D scalar field in the bulk, which picks up a VEV due to a potential, which may be localized on one brane. In this class of models we find Universal Extra Dimensions (115; 116; 74) and gaugephobic Higgs models (117) in warped space, as an example. In brane Higgs models, the Higgs is a 4 dimensional field localized on one brane or end-point of the compact space: the advantage of these models is that there is no tower of massive scalars and, if the brane where the Higgs is localized plays a special role like the TeV brane in warped space, the model may address the little hierarchy problem. A model of this kind was proposed by Randall-Sundrum (50; 118). Finally, a new possibility allowed only in extra dimensional models is that the Higgs is part of a gauge group (119): in fact the 5^{th} component of a bulk gauge vector is a scalar from the 4D point of view. The interactions and potential of such particle are however constrained by 5D Lorentz and gauge invariance: in particular, the Higgs potential (including its mass) is finite and insensitive to the physics at the cutoff. The limit of this mechanism is that the model is only valid below an effective scale of few TeV (few Kaluza-Klein modes). In this class we can find examples both in flat (120; 121; 122) and warped space (36; 123; 124; 125). It is interesting to note that the sign of the Higgs couplings, which are also related to the cancellation of the UV sensitivity of the Higgs mass, determines the sign of the contribution to the loop decays. For instance, in models of Gauge-Higgs unification we expect a reduction of the gluon coupling due to negative interference, contrary to what happens in models of Universal Extra dimensions (see for instance (122)).

Extra dimensional models are by nature non normalizable: from the 4D point of view, they are an effective description of the physics below a cutoff scale where some of the bulk interactions become strong. Such scale lies typically above a few tens of Kaluza-Klein (KK) modes. In general, if the symmetries allow so, we can add a tree level higher order operator which describes the coupling between the Higgs and the massless gauge bosons: in this way, the decay widths would be non-calculable. Adding such operator is actually necessary in order to act as a counter-term to the divergences that will arise at loop level. However, the loops we are interested in are effectively a box diagram if one considers a VEV insertion in the loop, therefore the one loop calculation turns out to be finite in all 5 dimension models. The counter-term will only be required at higher loops, and we will take the finite one loop result as a good approximation. In some cases, like in the Barbieri-Hall-Nomura model (), the operator is actually forbidden by an extra symmetry (supersymmetry in this case). Models of Gauge Higgs are special: the Higgs interactions are constrained not only by gauge symmetry, but by 5D Lorentz invariance as well. This is enough to forbid a tree level potential for the Higgs, and also tree level contributions to the decay widths. Therefore, in this models the Higgs mass is really protected by symmetry and our calculation can be trusted as UV insensitive (126).

As we want to keep the discussion here as model independent as possible, we will express the spectra as a function of a dimensionless parameter α that is proportional to the Higgs VEV. Its precise definition depends on the specific model, and it will be specified case by case. In general, we will write:

$$\frac{v_{SM}}{m_{NP}}\frac{\partial m_{NP}}{\partial v} = \frac{v_{SM}}{v}\cdot\frac{\alpha}{m_{NP}}\frac{\partial m_{NP}}{\partial \alpha}\,. \tag{5.4.1}$$

The factor $v_{SM}/v = 1-\delta_v$ contains eventual deviations in the numerical value of the Higgs VEV, and its effect is only relevant for the W and top contributions. We will present some

general results on two different geometries: a flat extra dimension compactified on an interval (which is equivalent to an orbifold) and a warped extra dimension.

5.4.1 Gauge bosons in a flat extra dimension

In the flat case, the metric is an extended Minkowski, where the extra coordinate y lies on an interval $[0, \pi L]$. The notation is such that typically the mass of the first Kaluza-Klein state is $m_{KK} = 1/L$: this will be our reference mass scale in the following. Note that this is the only mass scale introduced by the extra space structure. This scale should be much larger than the W mass due to direct and indirect constraints: the electroweak precision tests usually push it above $\sim$ 2 TeV (see for example (120; 121)). It is possible to relax this bound by adding symmetries: as a typical number in this scenario we will use $m_{KK} \sim 500$ GeV. This is the case, for example, in Universal Extra dimensions due to a Kaluza-Klein parity or the model.

Gauge Higgs

One of the peculiarities of this models is the presence of a tower of charged vectors, H^+_μ, associated with the charged component of the Higgs. They will necessarily mix with the W_μ via the Higgs VEV. Here we will focus on the simplest example, a $SU(3)$ gauge symmetry in the bulk, broken to $SU(2) \times U(1)$ at both endpoints. The value of the Higgs VEV can be expressed in terms of a dimensionless parameter α, which is indeed proportional to the field expectation value. We postpone all details of the calculation of the spectrum and the precise definition of α in the Appendix E.1.1. The spectrum for the W and its KK tower is simply given, in terms of α, as

$$m_n^2 = \frac{(n+\alpha)^2}{L^2}\,, \quad n = 0, \pm 1, \pm 2 \ldots \tag{5.4.2}$$

where $n = 0$ corresponds to the W mass:

$$m_W = \frac{\alpha}{L}\,. \tag{5.4.3}$$

For the purpose of this section, this can be considered as the definition of $\alpha = m_W L = m_W/m_{KK}$: it is typically a small number because we want the mass of the first KK mode to be much larger than the W mass in order to avoid direct and indirect bounds. The W mass is proportional to the Higgs VEV, so that its contribution to the loop is equal to the SM one and one finds $\delta_v(\text{GHflat}) = 0$. The KK tower contribution to the κ's is proportional to

$$\sum_n \frac{\alpha}{m_n}\frac{\partial m_n}{\partial \alpha} = \alpha \sum_{n=1}^{\infty}\left(\frac{1}{n+\alpha} - \frac{1}{n-\alpha}\right) = \pi\alpha\cot\pi\alpha - 1 = -\frac{\pi^2\alpha^2}{3} + \mathcal{O}(\alpha^4)\,. \tag{5.4.4}$$

We can use the definition of α to express the result in terms of the W mass and the mass of the first KK mode $m_{KK} = 1/L$:

$$\begin{aligned}\kappa_{\gamma\gamma}(W_{KK}) &= -\frac{63}{16}\left(\pi\frac{m_W}{m_{KK}}\cot\left(\pi\frac{m_W}{m_{KK}}\right) - 1\right) \\ &\simeq \frac{63}{16}\frac{\pi^2}{3}\frac{m_W^2}{m_{KK}^2} \sim 0.021 \cdot \left(\frac{2\,\text{TeV}}{m_{KK}}\right)^2\,;\end{aligned} \tag{5.4.5}$$

and $\kappa_{gg} = 0$. Note that the contribution has an opposite sign compared to the W.

Models with a gauge group larger than $SU(3)$ may also contain gauge bosons with different boundary conditions on the two endpoints. Those fields consist only of a tower of massive vector bosons, and they do not give rise to any massless vector of scalar modes. Also, they cannot mix with the W due to the flatness of the Higgs profile, therefore their presence will not affect the previous result. If they do couple to the Higgs, their spectrum is given by

$$m_n^2 = \frac{(n+1/2+c\alpha)^2}{L^2}\,, \quad n = 0, \pm 1, \pm 2 \ldots \tag{5.4.6}$$

where c is a coefficient determined by gauge group factors. Their contribution to $\kappa_{\gamma\gamma}$ is proportional to the sum of all modes. The sum can be rewritten in terms of a sum from zero to infinity

$$c\alpha \sum_{n=0}^{\infty} \left(\frac{1}{n+1/2+c\alpha} - \frac{1}{n+1/2-c\alpha} \right) = -\pi c\alpha \tan \pi c\alpha = -\pi^2 c^2 \alpha^2 + \mathcal{O}(\alpha^4)\,; \tag{5.4.7}$$

where therefore (Q_X being the charge of the extra gauge boson)

$$\kappa_{\gamma\gamma}(X) \simeq -\frac{63}{16}\pi^2 Q_X^2 c^2 \frac{m_W^2}{m_{KK}^2} \sim -0.063\, Q_X^2 c^2 \cdot \left(\frac{2\,\text{TeV}}{m_{KK}} \right)^2 . \tag{5.4.8}$$

Note that it has an opposite sign compared to the W tower contribution, and that it tends to be larger by a factor of 3.

Brane Higgs

Let us first consider a bulk $SU(2) \times U(1)$ gauge symmetry, so that there is a single W tower. The spectrum is determined by the zeros of the equation (for more details, see the appendix E.1.2)

$$f(m, \alpha) = \pi L m \tan \pi L m \; - \pi^2 \alpha^2 = 0\,, \tag{5.4.9}$$

where α is again a dimensionless quantity proportional to the Higgs VEV. The spectrum can be computed in an expansion for small α:

$$m_W^2 L^2 = \alpha^2 \left(1 - \frac{\pi^2}{3}\alpha^2 + \mathcal{O}(\alpha^4) \right), \tag{5.4.10}$$

$$m_n^2 L^2 = n^2 + 2\alpha^2 + \mathcal{O}(\alpha^4)\,. \tag{5.4.11}$$

In first approximation, $\alpha \sim m_W L = m_W/m_{KK}$: however higher order corrections in α will modify the couplings of the W to the Higgs, and they must be taken into account. The VEV is modified compared to the SM one, and in appendix E.1.2 we calculated

$$\delta_v(\text{bHflat}) \simeq \frac{\pi^2}{6}\alpha^2\,. \tag{5.4.12}$$

Even though the spectrum cannot be calculated analytically, in the appendix we showed that

$$1 - \frac{\alpha}{m_W}\frac{\partial m_W}{\partial \alpha} = \sum_{n=1}^{\infty} \frac{\alpha}{m_n}\frac{\partial m_n}{\partial \alpha} = 1 - \frac{2\sin(2\pi L m_W)}{2\pi L m_W + \sin(2\pi L m_W)}$$
$$= \frac{\pi^2}{3} m_W^2 L^2 + \mathcal{O}(m_W^4 L^4)\,. \tag{5.4.13}$$

The contribution to κ can be therefore written as:

$$\kappa_{\gamma\gamma}(W) = -\frac{9}{16}\left(7 + A_W(\tau_W)\right)\left(1 - \frac{2\sin(2\pi L m_W)}{2\pi L m_W + \sin(2\pi L m_W)}\right)(1-\delta_v) - \frac{9}{16}\delta_v A_W(\tau_W)\,. \quad (5.4.14)$$

Expanding for small L:

$$\kappa_{\gamma\gamma}(W) \simeq -\frac{9}{32}\pi^2\left(7 + A_W(\tau_W)\right)(m_W L)^2 + \frac{21}{32}\pi^2(m_W L)^2 \sim (0.015 \div 0.022)\cdot\left(\frac{2\,\text{TeV}}{m_{KK}}\right)^2 \quad (5.4.15)$$

where we have varied the H mass from 115 to 150 GeV. Note that the contribution of the KK tower is the same as in the Gauge Higgs case (up to a sign): however, the total contribution is suppressed by a partial cancellation between the KK tower and the W.

We can also consider the case of a bulk custodial symmetry, which will contain a W_R gauge boson which mixes with the W. In order to make it massive, one can impose Dirichlet boundary conditions on $y = 0$, the opposite brane to where the Higgs is localized. The spectrum is very similar, the only difference is to replace $L \to 2L$ in all the equations. However, this effect is compensated by the fact that the lightest KK mode from the W_R tower has mass $1/(2L)$ instead of $1/L$, therefore the result is the same as a function of the lowest KK mass.

Bulk Higgs

When the Higgs is in the bulk, it will generate a bulk mass for the gauge bosons. The VEV therefore will shift the spectrum

$$m_n^2 = \frac{n^2 + \alpha^2}{L^2}\,. \quad (5.4.16)$$

In this case, the W mass ($n = 0$) is proportional to the Higgs VEV (α), so that no corrections will come from the ordinary W ($\delta_v(\text{BHflat}) = 0$). We postpone details of the precise definition of α in the Appendix E.1.1. The contribution of the tower is proportional to the sum

$$\sum_{n=1}^{\infty}\frac{m_W^2 L^2}{n^2 + m_W^2 L^2} = \frac{\pi m_W L\coth\pi m_W L - 1}{2} = \frac{\pi^2}{6}m_W^2 L^2 + \mathcal{O}(m_W^4)\,. \quad (5.4.17)$$

The contribution to $\kappa_{\gamma\gamma}$ is therefore:

$$\kappa_{\gamma\gamma}(W) \simeq -\frac{63}{16}\frac{\pi^2}{6}m_W^2 L^2 \sim -0.01\left(\frac{2\,\text{TeV}}{m_{KK}}\right)^2\,. \quad (5.4.18)$$

Note that the sign is different from the previous two cases, so that this contribution tends to sum up with the ordinary W one.

5.4.2 Gauge bosons in a warped extra dimension

A warped extra dimension is characterized by a non-trivial metric that, in the covariant coordinates that we will be using in this paper, can be written as

$$ds^2 = \left(\frac{R}{z}\right)^2\left(\eta_{\mu\nu}dx^\mu dx^\nu - dz^2\right), \quad (5.4.19)$$

where R is the curvature of the space. Moving along the extra coordinate z, the unit length in 4D is rescaled, so that the natural energy scale of the model depends on the position along the warped extra coordinate. Now, z spans over an interval, but the two endpoints have a very different meaning: the brane at small $z = \epsilon$ is called the UltraViolet (UV) brane, and its typical scale represents the ultimate UV cutoff of the theory, $1/\epsilon = \Lambda$. One can imagine that this scale is very large, say the Planck scale M_{Pl}. On the other hand, at large $z = R'$ one places an InfraRed (IR) brane: its energy scale is directly related to the mass of the KK modes, so that $m_{KK} \sim 1/R'$ of order TeV. The proportionality factor depends on the particle we are considering: for a gauge boson like the W, the first KK mode is at $2.4\, m_{KK}$.

The large splitting between the UV and IR scale, beyond explaining the weakness of gravitational interactions, also introduces a gap between the W mass and the KK mass scale

$$m_{KK} \simeq m_W \sqrt{\log \Lambda R'} \sim 6\ m_W \tag{5.4.20}$$

for $\Lambda = M_{Pl}$ and $R' = 1\ \text{TeV}^{-1}$. This feature makes those models much more attractive than the flat cases, because the Higgs VEV can be closer to the IR scale. Finally, indirect bounds will usually require $m_{KK} \geq 1$ TeV, which corresponds to a W' above 2 TeV (127; 36; 123), similar to the flat case.

Here we will show some features of those models, and use a numerical evaluation of the κ's in generic models. We focus on Gauge Higgs and IR brane Higgs models, as generic bulk Higgs models are much more complicated to deal with, both analytically and numerically (117).

Gauge Higgs

The spectrum of gauge bosons is determined by a complicated equation involving Bessel functions of order 1 and 0 (more details in the appendix E.1.1). If we expand for large UV scale, we can get a very good approximate spectrum which depends only logarithmically on Λ. For the W, assuming that it is much lighter than the KK mass, we can expand for small $m_W R' \ll 1$:

$$m_W^2 R'^2 \simeq \frac{2}{\log \Lambda R'} \sin^2 \pi\alpha \simeq \frac{2\pi^2}{\log \Lambda R'} \alpha^2 \,, \tag{5.4.21}$$

where we have neglected higher order corrections in the log. The first KK mode will be given by the zeros of Bessel functions and one finds $m_{W'} \sim 2.4/R'$. Note also that this expression fixes α as a function of the KK scale R'. Contrary to the flat case, the W mass is not linear in the Higgs VEV, so that there will be corrections coming from the deviations from the SM coupling to the Higgs. We found (see appendix E.1.1):

$$\delta_v(\text{GHwarped}) \simeq 1 - \frac{\sin \pi\alpha}{\pi\alpha} \,, \tag{5.4.22}$$

and the total correction is therefore proportional to

$$(1-\delta_v)\frac{\alpha}{m_W}\frac{\partial m_W}{\partial \alpha} - 1 \simeq \cos \pi\alpha\ - 1 \simeq -\frac{m_W^2 R'^2}{4} \log \Lambda R' \sim -0.055 \left(\frac{1/R'}{1\text{TeV}}\right)^2 . \tag{5.4.23}$$

Note that one can use the same trick that we used in the flat brane Higgs (see appendix E.1.2) to calculate this quantity exactly: however, for our purpose, this approximate result is more than sufficient, and we can check that sub-leading terms will be suppressed by a log compared to this result:

$$\frac{\alpha}{m_W}\frac{\partial m_W}{\partial \alpha} - 1 = -\frac{m_W^2 R'^2}{6} \log \Lambda R' \left(1 - \frac{9}{4}\frac{1}{\log \Lambda R'} + \frac{3}{2}\frac{1}{\log^2 \Lambda R'}\right) + \mathcal{O}(m_W^4 R'^4) \,. \tag{5.4.24}$$

The contribution to $\kappa_{\gamma\gamma}$ is

$$\kappa_{\gamma\gamma}(W) \sim \frac{9}{16}(-0.055)A_W(\tau_W) \sim (0.25 \div 0.30) \cdot \left(\frac{1/R'}{1\text{TeV}}\right)^2 \tag{5.4.25}$$

where $m_H = 115 \div 150$ GeV.

One can also numerically compute the KK tower contribution to the κ's and find (for a W tower):

$$\kappa_{\gamma\gamma}(W_{KK}) \sim 0.009 \cdot \left(\frac{1\,\text{TeV}}{1/R'}\right)^2 \tag{5.4.26}$$

for $\Lambda = M_{Pl}$. This contribution is much smaller that the contribution of the W.

Brane Higgs

Expanding for large Λ and small $m_W R' \ll 1$, the mass of the W is (for more details, see the appendix E.1.2):

$$m_W^2 R'^2 = \frac{\alpha^2}{(1+\alpha^2/2)\log \Lambda R'} + \dots \tag{5.4.27}$$

and

$$\delta_v(\text{bHwarped}) \simeq \frac{\alpha^2}{4} \simeq \frac{m_W^2 R'^2}{4} \log \Lambda R' \,. \tag{5.4.28}$$

Similarly to the Gauge Higgs case, the coupling of the W to the Higgs will receive corrections, and the contribution to the κ will be proportional to

$$\frac{\alpha}{m_W}\frac{\partial m_W}{\partial \alpha} - 1 = -\frac{m_W^2 R'^2}{2}\log \Lambda R' \left(1 - 2\frac{1}{\log \Lambda R'} + \frac{1}{\log^2 \Lambda R'}\right) + \mathcal{O}(m_W^4 R'^4) \,. \tag{5.4.29}$$

We also numerically computed the contribution of the KK tower, and, as in the flat case, the following relation holds:

$$\sum_{n=1}^{\infty} \frac{\alpha}{m_n}\frac{\partial m_n}{\partial \alpha} = 1 - \frac{\alpha}{m_W}\frac{\partial m_W}{\partial \alpha} \,. \tag{5.4.30}$$

Numerically:

$$\kappa_{\gamma\gamma}(W) \sim -\frac{9}{16}(0.12)\,(7 + A_W(\tau_W)) - \frac{9}{16}(0.06)A_W(\tau_W) \sim (0.34 \div 0.51) \cdot \left(\frac{1/R'}{1\text{TeV}}\right)^2 \tag{5.4.31}$$

where $m_H = 115 \div 150$ GeV.

5.4.3 Bulk fermions in a flat extra dimension

Bulk fermions are easier to analyze because the basic structure is common to all kind of Higgs models: we always need two bulk fermions, a doublet and a singlet of SU(2), that couple via the Higgs (either in the bulk or on the brane). In Gauge Higgs, those fields are in the same representation of the extended bulk gauge symmetry, while in other models they can be independent fields. Both in Gauge Higgs and in the brane Higgs case, the Higgs appears in the

boundary conditions, which have the same form in the two cases: the reason is that one can use a gauge transformation to remove the Gauge Higgs VEV from the bulk equations of motion, as explained in more detail in the appendix E.2. The only difference is that the boundary conditions depend differently on the Higgs VEV. In the following we will use the notation of the Gauge Higgs models, where the Higgs VEV enters via trigonometric functions of a dimensionless parameter β. Note that the β parameter is different in general from the one for the gauge bosons α, due to either gauge group factors or Yukawa couplings. In Gauge Higgs, both β and α are proportional to the Higgs VEV. In the brane Higgs case, we can also define a fictitious β parameter that is related to the actual brane Higgs VEV V (see the appendix E.2 for more details) as

$$\tan \pi\beta = yV \,, \tag{5.4.32}$$

where y is an effective Yukawa coupling. The spectrum will be the same in the two cases, as a function of β, however the couplings to the Higgs are different. The results in the brane Higgs case are equal to the Gauge Higgs case, up to a correction factor

$$\frac{V}{\beta}\frac{\partial\beta}{\partial V} = \frac{\sin\pi\beta\ \cos\pi\beta}{\pi\beta} \,. \tag{5.4.33}$$

This factor takes into account the non linear relation between β and the brane Higgs VEV V. Like in the gauge case, we will use eq. (5.4.1) (with α replaced by β), and take into account the contribution of δ_v on the top one. For simplicity, we will leave this effect implicit through this section.

In the Bulk Higgs case, the spectrum is different: the calculation is more complicated in the case of a generic Higgs profile, and we will only study the case of a constant Higgs VEV in a flat extra dimension, which is relevant for the UED model.

Bulk fermions

The first spectrum we will consider is the following:

$$m_n^2 = M^2 + \frac{(n+\beta)^2}{L^2} \,, \quad n = 0, \pm1, \pm2 \ldots \tag{5.4.34}$$

This spectrum can arise in many scenarios: in Gauge Higgs models, one can generate the masses of light fermions by using two copies of bulk fermions with opposite boundary conditions, and connected by a bulk mass term M (59). The light fermions are localized degrees of freedom that can mix with the massive bulk fields via localized mass terms: the electroweak symmetry breaking is mediated to the localized fields by the massive ones, like in the Froggatt-Nielsen model. In this case, the smallness of the light mass can be achieved either by a small mixing, or by a large bulk mass M.

For $M = 0$

$$m_n^2 = \frac{(n+\beta)^2}{L^2} \,, \quad n = 0, \pm1, \pm2 \ldots \tag{5.4.35}$$

and we have a light mode with mass

$$m_f = \frac{\beta}{L} \,. \tag{5.4.36}$$

In Gauge Higgs models, this can be identified with the top, whose mass is of order the electroweak scale: a $m_{top} \neq m_W$ can be obtain by using a large representation for the field containing the

top (120), or by an explicit breaking of Lorentz invariance (121). As we will shortly see, warped geometry automatically solves this problem. In brane Higgs models, all fermion masses can be generated in this way, because the relation between β and the Higgs VEV depends on Yukawa couplings and each field will feel a different effective β parameter. Finally, this spectrum will be generated also by a Bulk Higgs with a flat profile, where β is proportional to the Higgs VEV. For more detail about the spectra, see the appendix E.2.

The κ's will be proportional to the sum

$$\begin{aligned}\sum_n \frac{\beta}{m_n}\frac{\partial m_n}{\partial \beta} &= \frac{\beta^2}{(ML)^2+\beta^2} + \beta\sum_{n=1}^{\infty}\frac{n+\beta}{(ML)^2+(n+\beta)^2} - \frac{n-\beta}{(ML)^2+(n-\beta)^2} = \\ &= \frac{\pi\beta\sin(2\pi\beta)}{\cosh(2\pi ML)-\cos(2\pi\beta)}\,,\end{aligned} \tag{5.4.37}$$

with the proportionality coefficient determined by the quantum numbers of the 5D field (charge and colour), and a correction factor in the brane Higgs case. For large ML, this contribution is exponentially suppressed: the mass of the localized fermions is also suppressed by $\exp(-\pi ML)$, therefore we find

$$\kappa \sim \frac{m_f^2}{m_{KK}^2}\,. \tag{5.4.38}$$

In this class of models, one can safely neglect the contribution of the light fermion towers.

For the top in Gauge Higgs, or in the case of brane Higgs and Bulk Higgs models ($M=0$), $\beta = m_f L$ and

$$\sum_n \frac{\beta}{m_n}\frac{\partial m_n}{\partial \beta} = \pi\beta\cot\pi\beta\,. \tag{5.4.39}$$

The contribution of the top tower is:

$$\kappa_{\gamma\gamma} = \kappa_{gg} = \left(\pi\frac{m_t}{m_{KK}}\cot\left(\pi\frac{m_t}{m_{KK}}\right)-1\right) \simeq -\frac{\pi^2}{3}\frac{m_t^2}{m_{KK}^2} \sim -0.025\left(\frac{2\,\text{TeV}}{m_{KK}}\right)^2\,, \tag{5.4.40}$$

where we have subtracted the top contribution. In the brane Higgs case:

$$\begin{aligned}\kappa_{\gamma\gamma} = \kappa_{gg} &= \left((1-\delta_v)\cos^2\left(\pi\frac{m_t}{m_{KK}}\right)-1\right) \\ &\simeq -\pi^2\frac{m_t^2}{m_{KK}^2} - \frac{\pi^2}{6}\frac{m_W^2}{m_{KK}^2} \sim -0.076\left(\frac{2\,\text{TeV}}{m_{KK}}\right)^2\,.\end{aligned} \tag{5.4.41}$$

The contribution from other light fermion towers are negligible, as they will be proportional to the light fermion mass squared.

For completeness, let us also report the contribution from a tower of states with twisted boundary conditions, which may be present in models with large bulk representation and have a spectrum

$$m_n^2 = M^2 + \frac{(n+1/2+\beta)^2}{L^2}\,, \quad n = 0, \pm1, \pm2\ldots \tag{5.4.42}$$

In this case:

$$\sum_n \frac{\beta}{m_n}\frac{\partial m_n}{\partial \beta} = \beta\sum_{n=0}^{\infty}\frac{n+1/2+\beta}{(ML)^2+(n+1/2+\beta)^2}-\frac{n+1/2-\beta}{(ML)^2+(n+1/2-\beta)^2} = \\ = -\frac{\pi\beta\sin(2\pi\beta)}{\cosh(2\pi ML)+\cos(2\pi\beta)}\,. \tag{5.4.43}$$

This contribution is also suppressed for large bulk masses. In the $M \to 0$ limit we get:

$$\sum_n \frac{\beta}{m_n}\frac{\partial m_n}{\partial \beta} = -\pi\beta\tan\pi\beta \simeq -\pi^2\beta^2\,. \tag{5.4.44}$$

The contribution to the κ's is

$$\kappa_{gg}(\text{twisted}) = -\left\{\begin{array}{c}\pi\beta\tan\pi\beta\\(1-\delta_v)\sin^2\pi\beta\end{array}\right\} \sim -0.075\,\frac{m_f^2}{m_t^2}\left(\frac{2\,\text{TeV}}{m_{KK}}\right)^2, \tag{5.4.45}$$

$$\kappa_{\gamma\gamma}(\text{twisted}) = \frac{9}{4}Q_f^2\,\kappa_{gg}\,, \tag{5.4.46}$$

for a colour-triplet with $m_f L = \beta$. The two results in the brackets correspond to GH/BH (up) and bH (down), and they give the same contribution in the small β limit.

Bulk fermion in UED models

In this case the spectrum is (similarly to the gauge case)

$$m_n^2 = \frac{n^2+\beta^2}{L^2}\,, \quad n = 0,1,2\ldots \tag{5.4.47}$$

with β proportional to the Higgs VEV via the bulk Yukawa coupling: for any SM fermion, $\beta = m_f L$, therefore only the top quark is relevant. The contribution to the amplitude is the same as for the gauge bosons, so that the top KK tower gives

$$\kappa_{\gamma\gamma}(top) = \kappa_{gg}(top) \simeq \frac{\pi^2}{6}m_t^2L^2 \sim 0.01\left(\frac{2\text{TeV}}{m_{KK}}\right)^2. \tag{5.4.48}$$

Note that this contribution has an opposite sign compared to the GH/bH cases, and, in $\kappa_{\gamma\gamma}$, it tends to cancel the contribution of the W tower.

Odd bulk masses: fermions in models of flavor

Lorentz invariance in 5D allows to write down a mass term for a single 5D fermion $\tilde{M}$: this mass term is however forbidden in orbifold models, because the two components of the 5D fermions have opposite parities (unless the mass has an odd profile). A model defined on an interval is less constrained as it allows for the presence of such masses. Those odd masses have a very important phenomenological feature (128): the zero mode of the 5D fermion is chiral, therefore $\tilde{M}$ cannot give it a mass! Its effect is to exponentially localize the zero mode, and therefore modify the overlap with other fields, in particular with the Higgs (either bulk or localized). This feature can be used in a variety of models to generate the hierarchies in the fermion masses using order 1 Yukawas and bulk masses for all fermion fields! This is an alternative mechanism to generate light fermions in GH models, where the Yukawa couplings are equal due to gauge invariance, but it can also be used in bH and BH models. There is

however a crucial difference between the two: in GH models the bulk masses are the same for the two SM fields that couple to the Higgs, because they come from the same bulk multiplet, while in bH/BH models they can be different. As we will see, this has dramatic consequences for the Higgs phenomenology.

Here we will focus on the GH and bH cases: the Higgs VEV enters via a dimensionless parameter β, and we will define

$$m_f = \beta/L\,. \tag{5.4.49}$$

As a reference, we will assume $m_f = m_{top}$, but this may not be the case in all models. The equation determining the spectrum is more complicated than in the previous case, therefore we will limit ourselves to an expansion for small β. In the GH case, the odd masses are the same for the two bulk fields, $\tilde{M}$. Expanding for $mL \ll \tilde{M}L$, we can calculate the mass of the light mode, which would be identified with the SM fermion:

$$m_l^2 = \frac{2\tilde{M}^2 \sin^2\pi\beta}{\cosh(2\pi\tilde{M}L) - \cos(2\pi\beta)} \simeq \frac{2\tilde{M}^2L^2\pi^2}{\sinh^2\pi\tilde{M}L} m_f^2\,. \tag{5.4.50}$$

It is clear from this formula that the light mode mass is suppressed by $\exp(-\pi\tilde{M}L)$ compared to the Higgs VEV β. Therefore, a $\tilde{M}L \sim \mathcal{O}(1)$ can explain the lightness of the fermions in the SM. The spectrum of the heavy modes, $m_n > \tilde{M}$, is more complicated:

$$m_n^2L^2 = \tilde{M}^2L^2 + n^2 \pm \frac{2n^2}{\sqrt{n^2+\tilde{M}^2L^2}}\beta + \frac{n^4+3\tilde{M}^2L^2n^2}{(n^2+\tilde{M}^2L^2)^2}\beta^2 + \mathcal{O}(\beta^3)\,. \tag{5.4.51}$$

The couplings of each mode to the Higgs are large, however like in the previous case the modes have a different sign in the coupling. The sum, therefore, gives at leading order in β:

$$\sum_n \frac{\beta}{m_n}\frac{\partial m_n}{\partial\beta} = -2\beta^2\sum_{n=1}^{\infty}\frac{n^4-3\tilde{M}^2L^2n^2}{(n^2+\tilde{M}^2L^2)^2} = \\ -\frac{\pi^2\beta^2}{\sinh^2\pi\tilde{M}L}\left(\frac{\pi\tilde{M}L}{\tanh\pi\tilde{M}L}-1\right) \simeq -\frac{m_l^2}{2\tilde{M}^2}\left(\frac{\pi\tilde{M}L}{\tanh\pi\tilde{M}L}-1\right)\,. \tag{5.4.52}$$

We find again that the tower of light modes does not contribute significantly to the widths: the only contribution will come from the top tower ($\tilde{M} \to 0$) which is approximate by the result in the previous subsection. Note again that this exponential suppression comes from a non trivial cancellation between modes.

In models with brane Yukawa couplings, the fields containing the SU(2) doublet and singlet are not necessarily the same, so they can have different bulk masses, $\tilde{M}_L$ and $\tilde{M}_R$. In this case, the spectra of the two bulk fermions are different, the two KK towers are not degenerate in the $\beta \to 0$ limit and there are no cancellations between modes. As we will see, the spectra are degenerate if $\tilde{M}_R = -\tilde{M}_L$, however, even in this case, the cancellation between modes that we observe in the GH case does not occur. In conclusion, in models of this kind, the contribution of the KK tower of light modes can be large, as it is proportional to the 5D Yukawa coupling and not to the effective light-mode Yukawa (light fermion mass). As an example, we can study the latter case $\tilde{M}_L = -\tilde{M}_R = \tilde{M}$, where some simple analytical results can be obtained. The zero mode mass is, at leading order,

$$m_l \simeq 4\tilde{M}e^{-2\pi\tilde{M}L}\sin\pi\beta\,, \tag{5.4.53}$$

suppressed by $\exp(-2\pi\tilde{M}L)$. As before, we can compute the approximate KK spectrum for small β

$$m_n^2 L^2 = \tilde{M}^2 L^2 + n^2 \pm \frac{2n^2}{\sqrt{n^2+\tilde{M}^2L^2}}\beta + \frac{(1-2\pi\tilde{M}L)n^4 + (3-2\pi\tilde{M}L)\tilde{M}^2L^2n^2}{(n^2+\tilde{M}^2L^2)^2}\beta^2 + \mathcal{O}(\beta^3)\,, \quad (5.4.54)$$

which differs to the $\tilde{M}_L = \tilde{M}_R$ case only at order β^2, and the sum over the massive modes (the SM fermion is not included)

$$\sum_n \frac{\beta}{m_n}\frac{\partial m_n}{\partial\beta} = -2\beta^2 \sum_{n=1}^{\infty} \frac{(1+2\pi\tilde{M}L)n^4 - (3-2\pi\tilde{M}L)\tilde{M}^2L^2n^2}{(n^2+\tilde{M}^2L^2)^2} = - \frac{\pi^2\beta^2}{4\sinh^3\pi\tilde{M}L}\Big(\cosh(3\pi\tilde{M}L) + (4\pi\tilde{M}L-1)\cosh(\pi\tilde{M}L) - 4(\pi\tilde{M}L+1)\sinh(\pi\tilde{M}L)\Big) \simeq -\pi^2\beta^2 \sim -0.075\left(\frac{2\text{TeV}}{m_{KK}}\right)^2\left(\frac{m_f}{m_{top}}\right)^2 . \quad (5.4.55)$$

The result is not very sensitive to the precise value of the bulk masses, even in the case of $\tilde{M}_L \neq \tilde{M}_R$ (we checked this numerically). Moreover, corrections from the non-linear relation between β and the Higgs VEV (the same multiplicative factor as in the previous section) will only affect this result at higher orders in β, while the light mode is negligible. The contribution of the top tower will be the same as in the massless case and, at leading order, it also gives $-\pi^2\beta^2$. For a model with this flavor structure, contributions of the light fermion and top towers are:

$$\kappa_{\gamma\gamma} = \kappa_{gg} \simeq 6(-\pi^2\beta^2) - \frac{\pi^2\alpha^2}{6} \sim -0.45\left(\frac{2\text{TeV}}{m_{KK}}\right)^2 , \quad (5.4.56)$$

where the factor of 6 takes into account 3 complete SM generations, and we assumed that all the Yukawa couplings are of the same order (as the top one).

5.4.4 Fermions in a warped extra dimension

The localization mechanism in warped extra dimension is much more effective than in the flat case: the reason is that the localization is exponential with the large number $\Lambda R'$. The geometry itself generates two hierarchical mass scales: the UV cutoff Λ on the UV brane and the KK scale $1/R'$ on the IR brane. Here we will use the usual notation to call c the odd bulk mass in units of the curvature, $c = \tilde{M}R$. A left-handed (right-handed) zero mode is localized on the UV brane for $c > 1/2$ ($c < -1/2$) and IR brane for $c < 1/2$ ($c > -1/2$) (129; 130).

GH models are characterized by the same odd mass c for the two fields that couple to the Higgs, because they are part of the same bulk multiplet. Like in the gauge boson case, we can expand for large UV cutoff, however in the fermionic case the expansion is more complicate and depends on the value of the bulk mass c. For $-1/2 < c < 1/2$ (when both zero modes are localized on the IR brane), the mass of the light mode is

$$m_f R' \simeq \sqrt{1-4c^2}\,\pi\beta\left(1 - \frac{3+4c^2}{9-4c^2}\pi^2\beta^2 + \mathcal{O}(\beta^4)\right) . \quad (5.4.57)$$

The mass is not suppressed compared to the Higgs VEV β; notice also that the log suppression between the W mass and β is not present here, therefore one can fit the top mass without using a large representation (therefore, $\beta = \alpha$ is acceptable)! The mass does not depend linearly on β, thus the coupling with the Higgs receives corrections compared to the SM value, that will contribute to the κ's. For a fermion with the same quantum numbers of the top (and in the light-Higgs approximation):

$$\kappa_{\gamma\gamma}(t) = \kappa_{gg}(t) = (1-\delta_v)\frac{\beta}{m_f}\frac{\partial m_f}{\partial \beta} - 1 \simeq -\frac{32}{3}\frac{c^2}{(9-4c^2)(1-4c^2)} m_f^2 R' - \delta_v \,. \tag{5.4.58}$$

We also calculated this contribution exactly, and verified that this approximation is good for $|c| < 0.4$ at a few percent level. The κ's vanish for $c \to 0$: in fact, in this limit the Bessel functions reduce to sines and cosines and we recover the flat case result where the light fermion mass is linear in the Higgs VEV. The coupling of the Higgs to the KK modes is also large. In summary, for $-1/2 < c < 1/2$, the light mass is un-suppressed compared to the Higgs VEV and the contribution of the tower to the κ's is sizable. Numerically we found

$$\kappa_{\gamma\gamma}(t_{KK}) = \kappa_{gg}(t_{KK}) \sim -\frac{1}{3} m_f^2 R'^2 \tag{5.4.59}$$

for a fermion tower with the same quantum numbers of the top. This contribution will sum with the one coming from the top; notice that it is very similar to the flat case result (factor of 1/3). For the top quark in GH (with $1/R = 1$ TeV, and $\beta = \alpha$ fixed by the W mass), we need $c \sim 0.43$: numerically

$$\kappa_{\gamma\gamma}(top) = \kappa_{gg}(top) \sim (-0.029 - 0.018) + (-0.011) = -0.06 \cdot \left(\frac{1\text{TeV}}{1/R}\right)^2 . \tag{5.4.60}$$

Note finally that this result can also be generalized to the brane-Higgs case with equal masses, taking into account the correction mentioned in the previous section, which is the same independently on the geometry.

For $c > 1/2$ and $c < -1/2$ the two zero modes are localized on different endpoints, and the light mass is suppressed:

$$m_f R' \simeq \left(\frac{1}{\Lambda R'}\right)^{|c|-\frac{1}{2}} \sqrt{4c^2-1}\, \sin \pi\beta \,. \tag{5.4.61}$$

In this case the coupling of the KK modes to the Higgs is also suppressed by:

$$\left(\frac{1}{2\Lambda R'}\right)^{2|c|-1} \sim \frac{m_f^2}{m_{KK}^2} \,. \tag{5.4.62}$$

The contribution of a light fermion KK tower is negligible [3], however, contrary to the flat case, there is no cancellation involved and each KK mode coupling is suppressed by the light fermion mass. In figure 5.2 we computed numerically the contribution of a bulk fermion as a function of the bulk mass c ($\beta = \alpha$ fits the W mass and $1/R' = 1$ TeV). The contribution of the light fermion is the deviation from a SM fermion of the same mass: it vanishes for $c = 0$, grows towards $c = 1/2$ reaching the value calculated for the W, and then goes down due to the decrease in the SM amplitude for a light fermion. The contribution of the KK modes, on the other hand,

[3] This result agrees with Ref. (125).

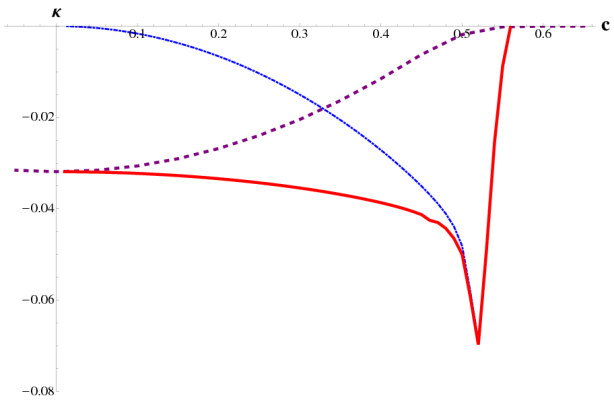

Figure 5.2: Contribution to κ from a bulk fermion in GHU as a function of the bulk mass c, $1/R = 1$ TeV, and $m_H = 130$ GeV. The dotted line represents the contribution of the light mode (deviation from the SM one), the dashed line is for the KK tower and the thick one corresponds to the sum of both.

decreases for large c. The total contribution is almost constant for $c < 1/2$, then reaches a peak when the light fermion is at the Higgs decay threshold (in the plot, $m_H = 130$ GeV), and then goes rapidly to zero.

It is straightforward to understand the suppression if we analyze in detail the structure of the wave functions: let us consider first the doublet, which contains a left-handed zero mode. The wave functions, after applying the UV boundary conditions, are

$$\chi_L = A_L z^{5/2}\left[J_{-c+\frac{1}{2}}(p/\Lambda)J_{c+\frac{1}{2}}(pz) + J_{c-\frac{1}{2}}(p/\Lambda)J_{-c-\frac{1}{2}}(pz)\right] \quad (5.4.63)$$

$$\psi_L = A_L z^{5/2}\left[J_{-c+\frac{1}{2}}(p/\Lambda)J_{c-\frac{1}{2}}(pz) - J_{c-\frac{1}{2}}(p/\Lambda)J_{-c+\frac{1}{2}}(pz)\right] \quad (5.4.64)$$

where χ (ψ) is the left-handed (right-handed) wave function component. The expansion for small p/Λ depends on the value of c ($J_\nu(x) \sim x^\nu$ for small x):

$$\chi_L \simeq \begin{cases} J_{c+\frac{1}{2}}(pz) & \text{for } c > 1/2 \\ J_{-c-\frac{1}{2}}(pz) & \text{for } c < 1/2 \end{cases} \qquad \psi_L \simeq \begin{cases} J_{c-\frac{1}{2}}(pz) & \text{for } c > 1/2 \\ J_{-c+\frac{1}{2}}(pz) & \text{for } c < 1/2 \end{cases} \quad (5.4.65)$$

plus corrections suppressed by $\left(\frac{p}{\Lambda}\right)^{|2c-1|}$. For the singlet field, that contains the right-handed zero mode

$$\chi_R \simeq \begin{cases} J_{c+\frac{1}{2}}(pz) & \text{for } c > -1/2 \\ J_{-c-\frac{1}{2}}(pz) & \text{for } c < -1/2 \end{cases} \qquad \psi_R \simeq \begin{cases} J_{c-\frac{1}{2}}(pz) & \text{for } c > -1/2 \\ J_{-c+\frac{1}{2}}(pz) & \text{for } c < -1/2 \end{cases} \quad (5.4.66)$$

plus corrections suppressed by $\left(\frac{p}{\Lambda}\right)^{|2c+1|}$. The IR boundary conditions are:

$$\psi_L \cos\pi\beta + i\psi_R \sin\pi\beta = 0\,, \quad (5.4.67)$$

$$\chi_R \cos\pi\beta + i\chi_L \sin\pi\beta = 0\,. \quad (5.4.68)$$

It is clear that if the wave functions are proportional to each other, $\psi_L \propto \psi_R$ and $\chi_L \propto \chi_R$, the β dependence drops out from the equations: this is indeed the case at leading order for $c > 1/2$ and $c < -1/2$. In this case the Higgs VEV will affect the spectrum only via a suppressed contribution.

We can apply the same discussion to the generic brane localized Higgs: in this case, there are two different bulk masses c_L and c_R. Unless $c_L = c_R$, the wave functions are different and

cannot be proportional to each other, therefore the coupling of the Higgs will be sizable even though the zero mode mass is suppressed due to the localization of its wave functions. As in the flat case, the towers of light modes will give a large contribution to the κ's. It can be calculated numerically and we found that for $c_L > 1/2$ and $c_R < -1/2$ it can be approximated by

$$\kappa_{\gamma\gamma} = \kappa_{gg} \simeq -\pi^2\beta^2 \sim -0.12 \cdot \left(\frac{1\,\text{TeV}}{1/R'}\right)^2 \tag{5.4.69}$$

for a fermion tower with the same quantum numbers of the top, $\Lambda = M_{Pl}$ and using $\beta = \alpha$ that fits the W mass. Like in the flat case, the contribution of the KK towers of the light fermions is very large. To conclude, we can quote the number for a realistic quark and lepton spectrum. We use $c_L^{top} = 0.37$, $c_R^{top} = 0$, $c_R^{bot} = -0.55$:

$$\kappa_{\gamma\gamma}(\text{fermions}) \simeq \kappa_{gg}(\text{fermions}) \sim -0.71 \cdot \left(\frac{1\,\text{TeV}}{1/R'}\right)^2 . \tag{5.4.70}$$

5.5 Numerical results

In this section we present exact numerical results for the models we considered in the previous two sections: in all cases, the analytic formulas are a very good approximation. We considered the following models:

- [♦] a fourth generation (the result is independent on the masses and Yukawa couplings);
- [♣] supersymmetry in the MSSM golden region: we only included the contribution of the stops with the spectrum given by the benchmark point in (103). In this case the result is very sensitive to the parameters in the superpotential and in the susy breaking terms, therefore the general MSSM will cover a region of the parameter space;
- [▲] Simplest Little Higgs, the result scales with the W' mass (in the plots, $m_{W'} = 2$ TeV);
- [$*$] Littlest Higgs, the result scales with the symmetry breaking scale f and has a mild dependence on the triplet VEV x (we set $x = 0$): for a model with T-parity we use $f = 500$ GeV, without T parity $f = 5$ TeV;
- [■] colour octet model, the result depends on 2 free parameters: for illustration we use in the plots $X_1 = 1/9$ and $X_2 = 1/36$ (see Section 5.3.4);
- [▶] Lee-Wick Standard Model, the result scales with the LW Higgs mass: in the plots we set it to 1 TeV for illustration;
- [⊗] Universal Extra Dimension model (74), where only the top and W resonances contribute and the result scales with the size of the extra dimension: here we set $m_{KK} = 500$ GeV close to the experimental bound;
- [★] the model of Gauge Higgs unification in flat space in Ref. (121), where only the W and top towers contribute ($\beta = m_t L$), with the first W resonance at 2 TeV;
- [•] the Minimal Composite Higgs (36; 123) (Gauge Higgs unification in warped space) with the IR brane at $1/R' = 1$ TeV: only W and top towers contribute significantly. The point only depends on the overall scale of the KK masses, as the other parameters are fixed by the W and top masses;

- [▼] a flat (W' at 2 TeV) and [♠] warped ($1/R'$ at 1 TeV) version of brane Higgs models, in both cases the hierarchy in the fermionic spectrum is explained by the localization, and all light fermion towers contribute. Notwithstanding the many parameters in the fermion sector, the result only depends on the overall scale of the KK masses.

In the numerical results, the value of the mass of the new particles is at or around the lower bound given by precision electroweak tests; for larger masses, the contribution scales like the inverse squared mass (with the exception of the fourth generation). Note that in many cases, the result only depends on one mass scale, and is insensitive to other free parameters present in the model: for example, in extra dimensional models with flavor, the final result does not depend on the precise localization pattern of the bulk fields. Therefore, changing the parameters of the model can only move the point towards the origin by increasing such mass scale (except for supersymmetry and the colour octet model, where a wide region of the parameter space may be covered). The models are displayed in Figures 5.3 and 5.4: different classes of models point in different quadrants of the parameter space. Therefore, if we could measure experimentally the two parameters, depending on the accuracy of the measurements, we may be able to distinguish between models and have an hint of what kind of mechanism lies behind the breaking of the electroweak symmetry. The direct discovery of the new particles would then be a confirmation of the model. The complementarity between the two measurements is crucial, because this indirect probe is sensitive to the quantum numbers and couplings to the Higgs of the new particles. This information is hardly accessible at the LHC, except in some special cases: most of the models analyzed here predict new states above 1 TeV, at which mass scale one can only probe states produced by strong interactions, and their couplings to the Higgs and weak bosons will generally not play any significant role. It is crucial to understand the reach and discrimination power of the LHC in this parameter space.

The LHC will surely be able to measure the inclusive cross section $\sigma(pp \to H \to \gamma\gamma)$, as this is one of the golden channels for the discovery of a light Higgs. For an integrated luminosity of 10 fb^{-1} we can expect a 10% accuracy with respect to the Standard Model one (131). We plotted the inclusive cross section normalized by the SM value in the $\kappa_{\gamma\gamma}$–κ_{gg} parameter space for a light Higgs ($m_H = 120$ GeV) in Figure 5.3 and for a Higgs near the VV-threshold ($m_H = 150$ GeV) in Figure 5.4: many models lie very far from such line, and a 10% measurement would allow to probe new physics masses up to few TeV in some cases. Note that many of the models we studied predict a reduction of the inclusive signal: the measurement of an enhancement at the LHC may be a sign of unexpected new physics. Note also that some very different models can give the same prediction, like the fourth generation case where a suppression in the $\gamma\gamma$ decay is accidentally compensated by an enhancement in the gluon fusion cross section. Therefore, we need to measure another observable at the LHC in order to distinguish such models. For the light Higgs case, in Figure 5.3 we plotted the vector boson fusion channel, which is sensitive to the $\gamma\gamma$ branching fraction directly. This channel is orthogonal to the inclusive one, and therefore offers the best discrimination power. Experimentally, this channel is very promising even at low luminosity, for the observation of the Higgs Boson in the $H \to \gamma\gamma$ decay mode (132). However a detailed study of this channel, as required for the precise determination of the κ parameters demands a high luminosity (133). A precise study requires a detailed simulation and will not be given here. For a heavier Higgs, in Figure 5.4, the decay in massive gauge bosons $H \to V^*V$ (with one virtual) becomes relevant and offers another discovery channel. This channel, sensitive to the total cross section, will allow for a discrimination for Higgs masses near the WW threshold.

The Linear Collider will have a much better chance to discriminate between models than the LHC. In fact, an experiment at a linear collider will be able to measure directly the branching fractions into gluons and photons. After 100 fb^{-1} of data, in the photon channel an accuracy

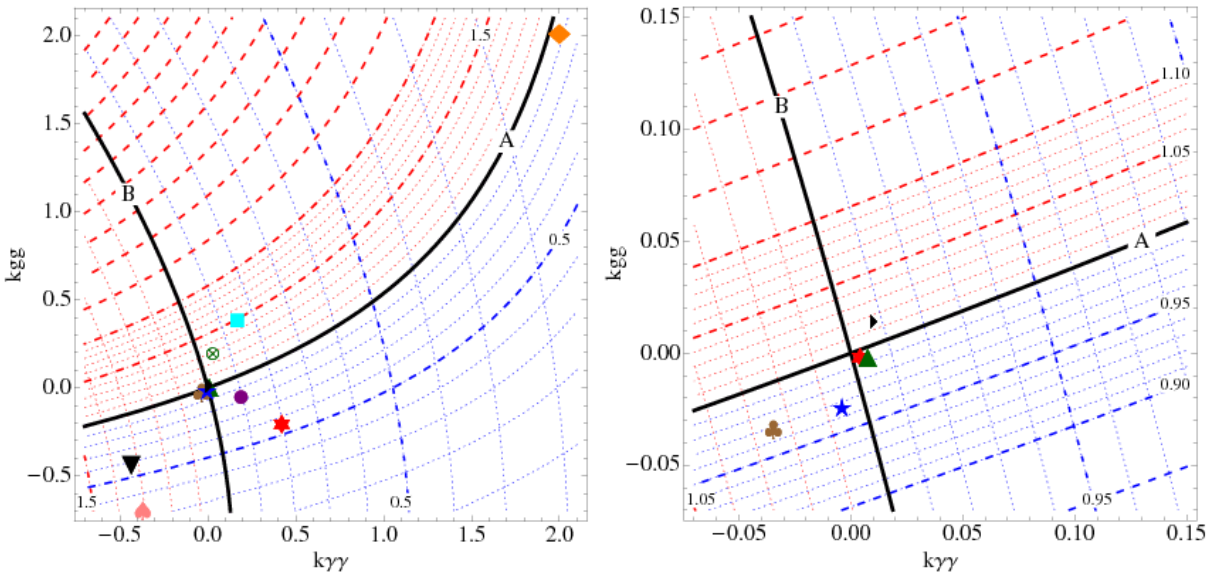

Figure 5.3: $\kappa_{\gamma\gamma}$ and κ_{gg} at the LHC for a light Higgs ($m_H = 120$ GeV). The two solid lines correspond to the SM values of the inclusive $\gamma\gamma$ channel (**A**), and the vector boson fusion production channel (**B**). On the left panel, the dashed lines are spaced by 0.5, while the dotted ones by 0.1. On the right, we zoomed near the SM point.

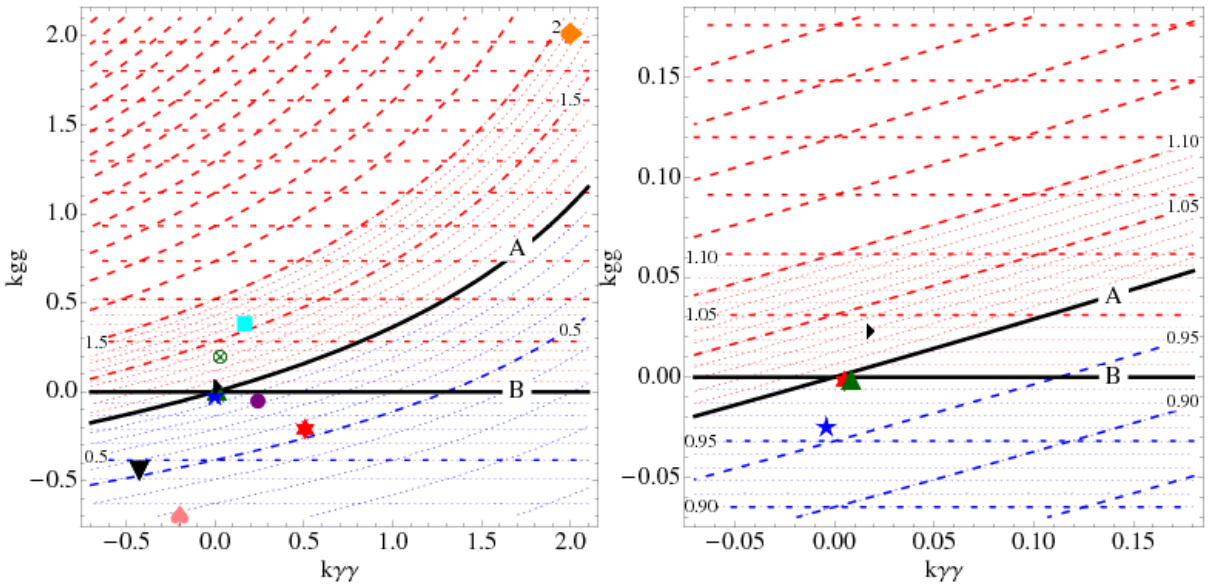

Figure 5.4: $\kappa_{\gamma\gamma}$ and κ_{gg} at the LHC for a Higgs near the WW threshold ($m_H = 150$ GeV). The two solid lines correspond to the SM values of the inclusive $\gamma\gamma$ channel (**A**), and the inclusive V^*V channel ($V = W, Z$) (**B**). On the left panel, the dashed lines are spaced by 0.5, while the dotted ones by 0.1. On the right, we zoomed near the SM point.

of 5–7 % is expected (reduced to 2–3 % with the $\gamma\gamma$ collider option), while the gluon channel offers a 2 % accuracy (assuming SM values) (134). We compared the models with the ILC measurements in Figure 5.5.

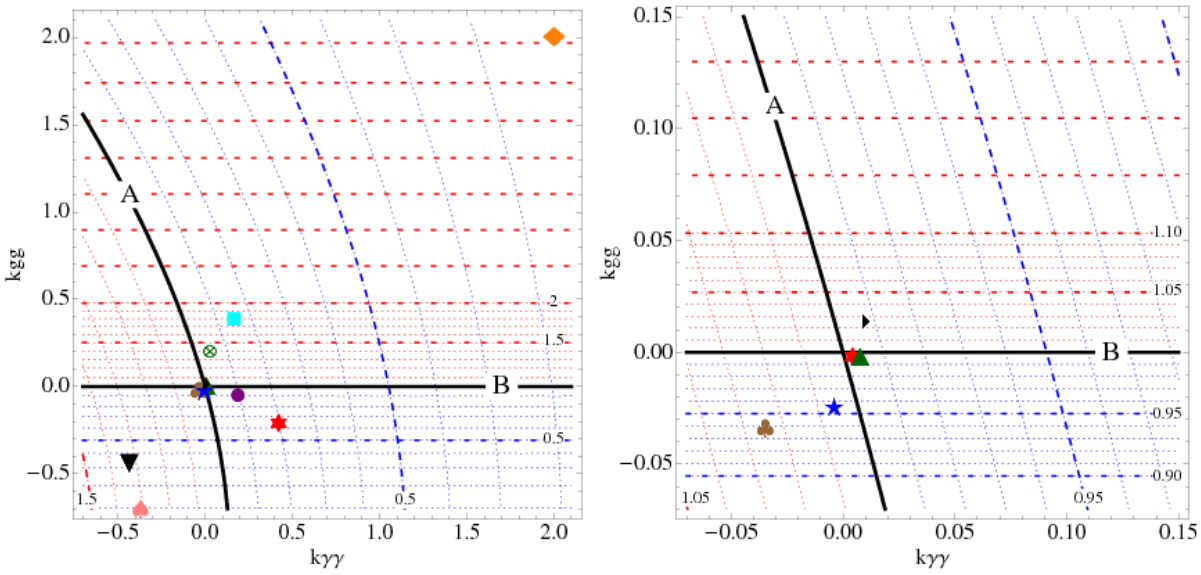

Figure 5.5: $\kappa_{\gamma\gamma}$ and κ_{gg} at the ILC ($m_H = 120$ GeV). The two solid lines correspond to the SM values of the $\gamma\gamma$ (**A**) and gluon (**B**) branching ratios. On the left panel, the dashed lines are spaced by 0.5, while the dotted ones by 0.1. On the right, we zoomed near the SM point.

5.6 Conclusions

The decay in a pair of photons is the golden channel for the discovery of the Higgs boson at the LHC for an intermediate mass, below the WW threshold, where the dominant decay mode would be $\bar{b}b$. This decay occurs via a loop diagram, where the heaviest particles in the SM (W and top) contribute the most. Furthermore, the production cross section at the LHC is dominated by a similar loop diagram that mediates the coupling of the Higgs to a pair of gluons. This situation offers a precious handle on new physics: in fact, new particles that may be present at the TeV scale will also contribute to those loops, therefore modifying the SM predictions for the Higgs production and decay rates.

One of the main motivations to expect new physics at the TeV scale is the naturalness of the Higgs mass (electroweak scale): the new particles, partners of the gauge bosons and of the top, will cancel or soften the divergences in the loop corrections to the Higgs mass. If this is the case, the new particles will have a significant coupling to the Higgs and therefore contribute significantly to the loop couplings of the Higgs. The LHC will be able to discover such new particles, with masses up to few TeV for particles with strong interactions and 1 TeV for weakly interacting ones. However, little information on the couplings will be directly accessible: the discovery of new states will not tell us if they play any role in the Higgs physics. Measuring deviations in the $H \to \gamma\gamma$ and $H \to gg$ couplings at later times will give us an important hint to understand the nature of the new states and of the underlying model of electroweak symmetry breaking.

In this paper, we studied the contribution of new physics to the $H \to \gamma\gamma$ and $H \to gg$ decay widths (the latter is proportional to the production cross section). We propose a convenient parametrization of the new contributions, by introducing two independent parameters $\kappa_{\gamma\gamma}$ and κ_{gg}. Such a simple parametrization neglects contributions to the tree level processes, such as production channels other than gluon fusion and decays, that are generically present in models

of new physics. This parametrization is especially useful in models where such effects are small. They could be taken into account in a later model-dependent analysis once a specific model or class of models is preferred by data. On more general grounds, more parameters can be introduced and the analysis extended in a similar fashion: for instance, in supersymmetry, a parameter describing the variation of the total width of the Higgs due to the bottom Yukawa coupling can be used. We avoided doing so as many models do have small corrections and in order to keep the parametrization as simple as possible.

Simple new physics scenarios give rise to simple correlations in this parameter space: for instance, a top partner will have $\kappa_{\gamma\gamma} = \kappa_{gg}$, while a single new particle will generate same-sign κ's. In order to illustrate the power of a model independent measurement at the LHC (and at future Linear Colliders) we compiled a necessarily incomplete survey of models of new physics both in 4 and 5 dimensions. Our results show that there are classes of models pointing in different quadrants of the parameter space, and that the deviations from the SM predictions can be as large as 50%. Moreover, in most cases those results do not depend on the details of the model and they are sensitive to just one mass scale of the new physics. Therefore, a cross section measurement at the LHC will allow to discriminate models even with new particle masses at the TeV scale. At the Linear Collider, the few percent level measurement of the Higgs branching ratios will allow an even better discrimination. Note also that most of the models in our survey populate the $\kappa_{\gamma\gamma} < \kappa_{gg}$ region, where we generically expect a suppression of the inclusive cross section. In this parametrization it would be easy to discover hints of unconventional or unexpected new physics, independently on direct and/or indirect signals in other channels.

Conclusion & perspectives

As the reader can have found out throughout this thesis, the philosophy of our work has been oriented towards the possibility of new physics discovery at the Large Hadron Collider. During these three years of PhD, I focused mainly on two different topics and approaches which help me to have a very large overview of the physics beyond the Standard Model that should be observed soon at LHC.

Firstly, we performed a model-independent study of the Higgs decay into photons. This golden channel at the LHC is really sensitive to new physics through radiative corrections. Therefore we concentrated on the effective descriptions of this process that can be used by experimentalists to interpret their measurements in terms of eventual deviations from the Standard Model predictions. This has been realized by introducing only two parameters which characterize the modifications of the Higgs production by gluon fusion and of the Higgs decay into photons. We have also shown how theorists can use this method to constrain their models with the future LHC and Linear Collider observations. In the short-term, Monte-Carlo simulations have already been performed by experimentalists working on the Higgs detection in CMS and within few months or years, they will be able to test this parametrization directly on their data. In a further future, for precision measurements with Linear Collider, this technique will be a great tool to understand the eventual link between the new heavy physical states that could be detected at the LHC and the nature of the electroweak symmetry breaking sector.

Later, we decided to focus on a peculiar kind of effective field theory based on extra-dimensions. In general, the new symmetries imposed by the presence of the new extra-space will give rise to new features that can be interesting for addressing Standard Model puzzles. Here we have chosen to present a six-dimensional model where the discrete symmetry generating the Dark Matter candidate is not imposed by hand but is a genuine geometrical consequence of the compactification topology. In our work we showed why the Real Projective Plane is the unique 6D orbifold where we can reproduce the Standard Model chiral fermions without any fixed points/lines. The absence of such fixed points/lines will preserve the KK-parity, which is a relic of 6D Lorentz invariance. In order to study the properties of such original orbifold, we choose to investigate the case of an Universal Extra-Dimensional model. The topology of the (flat) Real Projective Plane affects the loop corrections and as a consequence, it strongly influences the mass-spectrum, the couplings and the structure of localized operators of the model. In order to understand better the phenomenology of this model we developed techniques in six dimensions to perform one-loop calculations for the first Kaluza-Klein levels. Starting with the lightest tiers $(1,0)$ and $(0,1)$, we have found that the Dark Matter candidate is a scalar photon. Then with a first analytical calculation, we estimate that the relic abundance constraints lead to a mass-range $200 < m_{KK} < 250$ GeV ($280 < m_{KK} < 350$ GeV in the asymmetric case). In the short-term, this analytical analysis will be refined using numerical calculation in order to give

a more stringent and accurate cosmological bound on the mass-range expected for our model. We decided then to use this first mass-range prediction to study the LHC phenomenology of our UED model on the Real Projective Plane. We showed that, in this range, the splittings inside the lightest tiers are so small that the observation of the particles will be really challenging at the LHC as the SM decay products are too soft. Therefore we focused on the phenomenology of higher levels which can be easier to observe, as they could decay into SM particles without missing energy and so we choose to work with the level $(2,0)$ (or $(0,2)$). To simplify our study, we considered the limit case where one of the two dimensions is much smaller that the other. This limit is really interesting because the model has one extra-dimension with an unbroken KK-parity imposed by the 6D completion and its phenomenology is very different from the usual 5D case because the particle content and the mass splittings are very different. For instance, the Dark Matter candidate is a scalar instead of a vector massive photon.

This phenomenological study of the level $(2,0)$ motivates then our discussion on the general one-loop structure of masses and couplings on the Real Projective Plane. We found a great simplification to study the localized counter-terms on the RPP and more generally in extra-dimension by performing our calculation in the special gauge $\xi = -3$. In this case, the loop corrections require gauge invariant counter-terms which allow to correlate directly mass corrections to loop induced couplings. We detailed then the phenomenology of the $(2,0)$ and $(0,2)$ tiers. These states mainly cascade decay within the same tier to the lightest state of this tier or decay in pairs of $(1,0)$ or $(0,1)$ modes. Nevertheless, the mass-splittings for level $(1,0)$, $(0,1)$, $(2,0)$ or $(0,2)$ are generated by loop corrections so the phase space available for those particles to decay is really small. Therefore those channels are suppressed and are in competition with the direct loop induced decays into Standard Model particles. This last possibility is really exciting for LHC searches. Using our model implementation into `FEYNRULES` and `CALCHEP`, we have shown that these decays can produce signatures with Standard Model resonances. We presented our first analysis on channels involving di-lepton (e^+e^- and $\mu^+\mu^-$), single lepton plus neutrino, top-pair and 4-tops, coming from the decays of the gauge vectors $A_\mu^{2,0}$, $Z_\mu^{2,0}$ and $W_\mu^{2,0}$. We emphasized also that 7 TeV LHC data already start to put limits on our model and how they will soon allow to explore all the preferred range by WMAP data. This will strongly constrain the available KK-mass range and will potentially help to confirm or rule out this simplest UED model on the Real Projective Plane.

To conclude let us stress that the Real Projective Plane can present a really promising framework for the study of extra-dimensional models. In our Universal Extra-Dimensional version, the model does not address all the Standard Model puzzles but, using the protection of the KK-parity by the Real Projective Plane background we can foresee to refine this model either by changing the metric of the extra-dimensions or by using Gauge Higgs Unification model.

Appendix A

Useful tools for 6D loop calculations

A.1 n-dependent integrals over 4D momentum

The functions of n appearing in the loop corrections can be expressed in terms of the four following integrals:

$$\Phi_1(n) = 2\pi^3 \int_0^\infty dk \, \frac{k^3}{\sqrt{k^2+n^2}\sinh \pi\sqrt{k^2+n^2}} \tag{A.1.1}$$

$$\Phi_2(n) = 2\pi^3 \int_0^\infty dk \, \frac{kn(\sqrt{k^2+n^2}-n)}{\sqrt{k^2+n^2}\sinh \pi\sqrt{k^2+n^2}} \tag{A.1.2}$$

$$\Phi_3(n) = 2\pi^3 \int_0^\infty dk \, \frac{k^3(\sqrt{k^2+n^2}-n)}{n\sqrt{k^2+n^2}\sinh \pi\sqrt{k^2+n^2}} \tag{A.1.3}$$

$$\Phi_4(n) = 2\pi^3 \int_0^\infty dk \, \frac{kn^2}{\sqrt{k^2+n^2}\sinh \pi\sqrt{k^2+n^2}} \tag{A.1.4}$$

Numerically the integrals are suppressed for large n:

	$n=1$	$n=2$	$n=3$
Φ_1	1.43	0.109	0.0067
Φ_2	0.54	0.047	0.0030
Φ_3	1.02	0.037	0.0015
Φ_4	1.71	0.294	0.0286

The functions appearing in the loop corrections are (where we report the numerical value for $n=1$):

$$B_1 = \Phi_1 \sim 1.43 \tag{A.1.5}$$

$$B_2 = \Phi_1 - \Phi_2 \sim 0.89 \tag{A.1.6}$$

$$B_3 = \Phi_1 + \frac{9}{2}\Phi_2 - 2\Phi_3 \sim 2.64 \tag{A.1.7}$$

$$F_1 = \Phi_1 - 2\Phi_2 \sim 0.35 \tag{A.1.8}$$

$$F_2 = \Phi_2 \sim 0.54 \tag{A.1.9}$$

A.2 6D mixed propagators

In this section, in order to complete the discussion of chapter 2, we summarized the expression of the 6D propagators expressed with the mixed momentum-position representation. We also present the propagator for massive fields which get their mass from the electroweak symmetry breaking. This will be interesting to understand the issues arising in electroweak observables, we discussed in section 4.4.

Scalar fields

We already presented the case of the massless scalar in section 2.3. If the field is massive the equations of motion are modified and include a new mass term. In this case, by working with the pure winding mode decomposition, the propagator is modified in such a way that:

$$G_S^{6D}(k, \overrightarrow{y} - \overrightarrow{y}') = \frac{1}{4} \sum_{\Omega=(n1,n2)\in Z_2} H_0^{(1)}(\chi|\overrightarrow{y} - \overrightarrow{y}' + \overrightarrow{\Omega}|) \tag{A.2.10}$$

where

$$\chi = \sqrt{k^2} \longrightarrow \sqrt{k^2 - M(v)^2}\,. \tag{A.2.11}$$

If we choose to use the mixed propagator with winding mode along one direction and KK-decomposition along the other, the idea is similar and we have:

$$G_S^{6D}(k, \overrightarrow{y} - \overrightarrow{y}') = \sum_{l=-\infty}^{\infty} G_S^{5D}(\chi_l, x_5 - x'_5)\ f_l^*(x_6) f_l(x'_6) \tag{A.2.12}$$

where

$$\chi_l = \sqrt{k^2 - l^2} \longrightarrow \sqrt{k^2 - l^2 - M(v)^2} \tag{A.2.13}$$

Here $M(v)$ is the mass given by the electroweak symmetry breaking through the Higgs mechanism. This is the only modification compared to the massless case. Then, in order to take into account the orbifolding of the two extra dimensions, we need to impose the parity conditions on this propagator. By splitting the contribution of each symmetry of the space, we can write the propagator of the field from $\overrightarrow{y}'$ to $\overrightarrow{y}$:

$$\begin{aligned} G_S^{orb}(k, \overrightarrow{y} - \overrightarrow{y}') = \frac{1}{4}(G_S^{6D}(k, \overrightarrow{y} - \overrightarrow{y}') + p_g G_S^{6D}(k, \overrightarrow{y} - g(\overrightarrow{y}')) \\ + p_r G_S^{6D}(k, \overrightarrow{y} - r(\overrightarrow{y}')) + p_g p_r G_S^{6D}(k, \overrightarrow{y} - gr(\overrightarrow{y}'))) \end{aligned} \tag{A.2.14}$$

For simplicity reason, we will write G_S^{6D} as G_s.

Gauge Bosons

We can define the vector boson propagator from $\overrightarrow{y}'$ to $\overrightarrow{y}$ using the scalar propagator. So we obtain the following propagator in the Feynman gauge:

$$D_{MN}^{6D}(k, \overrightarrow{y} - \overrightarrow{y}') = -g_{MN} G_s(k, \overrightarrow{y} - \overrightarrow{y}') \tag{A.2.15}$$

and here we also replace $k^2 \longrightarrow k^2 - M(v)^2$. As we choose the $\xi = 1$ gauge, we have not to forget the Goldstone boson which picked also a mass from the symmetry breaking: $M^2(v) = \frac{g^2 v^2}{4}$. To get the full propagator on the orbifold, we have to implement the effects of the orbifold symmetries as it is presented in (73):

$$\begin{aligned} D_{MN}^{orb}(k, \overrightarrow{y} - \overrightarrow{y}') = -g_{MN}\frac{1}{4}\Big(G_S^{6D}(k, \overrightarrow{y} - \overrightarrow{y}') + p_g \theta_N^g G_S^{6D}(k, \overrightarrow{y} - g(\overrightarrow{y}')) \\ + p_r \theta_N^r G_S^{6D}(k, \overrightarrow{y} - r(\overrightarrow{y}')) + p_g p_r \theta_N^{rg} G_S^{6D}(k, \overrightarrow{y} - gr(\overrightarrow{y}'))\Big) \end{aligned} \tag{A.2.16}$$

where

$$\theta_M^t = \frac{t(x^M)}{|x^M|} = \pm 1 \tag{A.2.17}$$

Fermions

We can also define the propagator from $\overrightarrow{y}'$ to $\overrightarrow{y}$ of fermionic fields using the scalar propagator. Here because of the Lagrangian structure, the definition is a bit more subtle. Let us remind the fermionic Lagrangian including Yukawa interactions between doublets (Q) and singlets (U) of $SU(2)$:

$$\mathcal{L} \supset \int dx_5 \int dx_6 \, i\Big\{\bar{\Psi}_{Q,U}\Gamma^\alpha\partial_\alpha\Psi_{Q,U} - y_f\bar{\Psi}_Q H\Psi_U - y_f\bar{\Psi}_U H^\dagger\Psi_Q\Big\} \tag{A.2.18}$$

The coupled equations of motion of the doublet and singlet fields will have the following form with $m(v) = \frac{y_f v}{\sqrt{2}}$:

$$\begin{pmatrix} i\Gamma^\alpha\partial_\alpha & -m\ \mathbf{1} \\ -m\ \mathbf{1} & i\Gamma^\alpha\partial_\alpha \end{pmatrix}\begin{pmatrix} \Psi_Q \\ \Psi_U \end{pmatrix} = 0 \tag{A.2.19}$$

We can deduce thereby the following propagator for the fermionic fields:

$$S^{6D}_{\alpha\beta}(k, \overrightarrow{y} - \overrightarrow{y}') = \begin{pmatrix} (p^\mu\Gamma_\mu - i\partial_{x_5}\Gamma_5 - i\partial_{x_6}\Gamma_6)_{\alpha\beta} & m\ \mathbf{1}_{\alpha\beta} \\ m\ \mathbf{1}_{\alpha\beta} & (p^\mu\Gamma_\mu - i\partial_{x_5}\Gamma_5 - i\partial_{x_6}\Gamma_6)_{\alpha\beta} \end{pmatrix} G_s(k, \overrightarrow{y} - \overrightarrow{y}') \tag{A.2.20}$$

In the massless case, the result simplifies and for both fields we get:

$$S^{6D}_{\alpha\beta}(k, \overrightarrow{y} - \overrightarrow{y}') = (p^\mu\Gamma_\mu - i\partial_{x_5}\Gamma_5 - i\partial_{x_6}\Gamma_6)_{\alpha\beta}\, G_s(k, \overrightarrow{y} - \overrightarrow{y}') \tag{A.2.21}$$

Like in the gauge boson case, if we want to express the full propagator on the orbifold, we have to include the effects of the RPP symmetries. The game is slightly more tricky for fermions but we can show, as it is suggested in (73) that $S^{orb}_{\alpha\beta}$ can be written as:

$$\begin{aligned} S^{orb}_{\alpha\beta}(k, \overrightarrow{y} - \overrightarrow{y}') = \frac{1}{4}(p^\mu\Gamma_\mu - i\partial_{x_5}\Gamma_5 - i\partial_{x_6}\Gamma_6) \cdot \Big(&G^{6D}_S(k, \overrightarrow{y} - \overrightarrow{y}') + p_g\overline{\Gamma}^g G^{6D}_S(k, \overrightarrow{y} - g(\overrightarrow{y}')) \\ &+ p_r\overline{\Gamma}^r G^{6D}_S(k, \overrightarrow{y} - r(\overrightarrow{y}')) + p_g p_r\overline{\Gamma}^{rg} G^{6D}_S(k, \overrightarrow{y} - gr(\overrightarrow{y}'))\Big) \end{aligned} \tag{A.2.22}$$

A.3 Starting a 6D loop calculation

In section 2.3, we developed the calculation of the scalar tadpole correction to the $(n, 0)$ gauge boson mass. As a complement to this section, here we will give to the reader an overview of the complete calculation we performed to obtain the full set of radiative corrections to $(n, 0)$-$(0, n)$ levels. This appendix will be a usefull tool, if we need to derive 6D loop calculations for other modes and also for other extradimensional model in 6D. The results of the following integrals are the one compiled in section 2.4 and 4.3.1. In all this discussion, x corresponds to x_5 and y to x_6, the Latin indices $M, N, A, B = 0..6$ and the Greek ones $\mu, \nu = 0..3$. The momenta running into the loop are given by:

$$\begin{aligned} \chi_1^l &= \sqrt{p^2 - l^2} \\ \chi_2^{l'} &= \sqrt{(p-q)^2 - l'^2} \end{aligned} \tag{A.3.23}$$

and when needed, we will use a simplified notation with $i\partial_A \to p^\mu$ when $A = \mu = 0..3$, where p is the momentum of the considered propagator.

A.3.1 Gauge boson self-energy

The radiative corrections we have to compute, are represented by the loop diagrams given in Figure 2.7. Here we present the generic result for the n both even and odd.

Scalar contribution $(f-g)$

The (f)-tadpole case has already been discussed in chapter 2.3. Here we will study the (g)-loop:

$$\begin{aligned} i\Pi^{g}_{MN} =& p_t^{\clubsuit}\frac{1}{4}\frac{i^2 g_6^2}{16\pi^4}C_2(r)\sum_{l,l'}\int dp\int dx_1\dots dy_2 \quad f^{n,0}_{A_M}(x_1,y_1)f^{n,0}_{A_N}(x_2,y_2)\\ & \mathcal{O}_{MN}\; G_s^{\bigstar}(\chi_1^l,x_1,x_2)\; G_s^{\clubsuit}(\chi_2^{l'},x_2,t(x_1))f_l^*(y_1)f_l(y_2)f_{l'}^*(y_2)f_{l'}(t(y_1)) \end{aligned} \tag{A.3.24}$$

where $\mathcal{O}^{MN}=i^2(\partial^M_{x_1,\bigstar}-\partial^M_{x_1,\clubsuit})(\partial^N_{x_2,\clubsuit}-\partial^N_{x_2,\bigstar})$. We choose, for the vertices, incoming momenta convention. $f^{n,0}_{A_M}$ is the wavefunction of the outcoming legs, because we are looking at the self-energy correction to a given 4D KK-mode. The symbol $\bigstar$ and $\clubsuit$ show on which propagator or wavefunction apply the derivative operators. $p_t^{\clubsuit}$ is the parity under the t symmetry of the field propagating in the loop with the propagator $G_s^{\clubsuit}$.

Gauge contribution $(a-d)$

We present here the case of the (b,c) loops:

$$\begin{aligned} i\Pi^{b,c}_{MN} =& \frac{1}{4}C_2(G)\frac{i^2 g_6^2}{16\pi^4}\sum_{l,l'}\int dp\int dx_1\dots dy_2 \quad p_t^{\clubsuit}\theta_R^t\mathcal{T}_{MPR}\mathcal{T}_{NQS}f^{\spadesuit,n,0}_{A_M}(x_1,y_1)f^{\blacktriangle,n,0}_{A_N}(x_2,y_2)\\ & g^{PQ}G_s^{\bigstar}(\chi_1^l,x_1,x_2)\; f_l^*(y_1)f_l(y_2)\; g^{RS}G_s^{\clubsuit}(\chi_2^{l'},x_2,t(x_1))f_{l'}^*(y_2)f_{l'}(t(y_1)) \end{aligned} \tag{A.3.25}$$

where

$$\begin{aligned} \mathcal{T}^{MPR} &= i[g^{MP}(\partial^R_{x1,\spadesuit}-\partial^R_{x1,\bigstar})+g^{PR}(\partial^M_{x1,\bigstar}-\partial^M_{x1,\clubsuit})+g^{RM}(\partial^P_{x1,\clubsuit}-\partial^P_{x1,\spadesuit})]\\ \mathcal{T}^{NQS} &= i[g^{NQ}(\partial^S_{x2,\blacktriangle}-\partial^S_{x2,\bigstar})+g^{QS}(\partial^N_{x2,\bigstar}-\partial^N_{x2,\clubsuit})+g^{SN}(\partial^Q_{x2,\clubsuit}-\partial^Q_{x2,\blacktriangle})] \end{aligned} \tag{A.3.26}$$

Even if this formula looks really complex, once we choose if n is odd or even, some modes vanish and the expression can be simplified. It will allow us afterwards to make the distinction between (b) and (c) loops.
The ghost loop (d) can be inferred from the (g)-loop; due to couplings and the anticommutation rule of ghost fields, we can show that:

$$i\Pi^{d}_{MN} = -\frac{1}{2}\; i\Pi^{g}_{MN} \tag{A.3.27}$$

For the gauge tadpole (a), the result is very similar to the scalar tadpole (f):

$$\begin{aligned} i\Pi^{a}_{MN} =& \frac{1}{4}C_2(G)\frac{-ig_6^2}{16\pi^4}\sum_{l}\int dp\int dx_1dy_1 \quad p_t^{\clubsuit}\theta_R^t\mathcal{Q}_{MNPQ}f^{n,0}_{A_M}(q,x_1,y_1)f^{n,0}_{A_N}(q,x_2,y_2)\\ & g^{PQ}G_s^{\clubsuit}(\chi_1^l,x_1,t(x_1))\; f_l^*(y_1)f_l(t(y_1)) \end{aligned} \tag{A.3.28}$$

where

$$\mathcal{Q}^{MNPQ} = 2[g^{MN}g^{PQ}-g^{MP}g^{NQ}] \tag{A.3.29}$$

Fermion contribution

The fermion loop (e) is then given by:

$$i\Pi^{e}_{MN} = \frac{1}{4}C_2(G)\frac{i^2 g_6^2}{16\pi^4}\sum_{l,l'}\int dp \int dx_1 \dots dy_2 \;\; p_t^{\clubsuit}\;\mathrm{Tr}[\Gamma^M\Gamma^A\Gamma^N\Gamma^B\overline{\Gamma}^t]\; A^{n,0}_M(q,x_1,y_1)A^{n,0}_N(q,x_2,y_2)$$
$$i\partial_A G_s(\chi_1^l,x_1,x_2)\; f_l^*(y_1)f_l(y_2)\; i\partial_B G_s^{\clubsuit}(\chi_2^{l'},x_2,t(x_1))f_{l'}^*(y_2)f_{l'}(t(y_1)) \tag{A.3.30}$$

A.3.2 Fermion self-energy

The radiative corrections, we have to compute are represented by the loop diagrams given in figure 2.8. Here we presented the generic result for the n both even and odd.

Gauge contribution

The contribution from gauge field is given by:

$$i\Sigma_A = \frac{1}{4}\frac{i^2 g_6^2}{16\pi^4}\sum_{l,l'}\int dp \int dx_1 \dots dy_2\; p_t^{\clubsuit}\theta_M^t\; F^{n,0}_{\bar{\Psi}}(x_1,y_1)\Gamma^M\Gamma^A\Gamma^N F^{n,0}_{\Psi}(x_2,y_2)$$
$$(-g^{MN})\; i\partial_A G_s(\chi_1^l,x_1,x_2)\; G_s^{\clubsuit}(\chi_2^{l'},x_2,t(x_1))f_l^*(y_1)f_l(y_2)f_{l'}^*(y_2)f_{l'}(t(y_1)) \tag{A.3.31}$$

Here $F^{n,0}_{\Psi}$ stands for the vector formed by wavefunctions of the $(n,0)$ 4D-fermions:

$$F^{n,0}_{\Psi}(x,y) = \begin{pmatrix} f^{n,0}_{\Psi_1}(x,y) \\ f^{n,0}_{\Psi_2}(x,y) \\ f^{n,0}_{\Psi_3}(x,y) \\ f^{n,0}_{\Psi_4}(x,y) \end{pmatrix} \tag{A.3.32}$$

Scalar contribution

The scalar contribution is quite similar to the boson one and for a Yukawa coupling, y_6, we have:

$$i\Sigma_\phi = \frac{1}{4}\frac{i^2 y_6^2}{16\pi^4}\sum_{l,l'}\int dp \int dx_1 \dots dy_2\; p_t^{\clubsuit}\; F^{n,0}_{\bar{\Psi}}(x_1,y_1)\Gamma^A F^{n,0}_{\Psi}(x_2,y_2)$$
$$i\partial_A G_s(\chi_1^l,x_1,x_2)\; G_s^{\clubsuit}(\chi_2^{l'},x_2,t(x_1))f_l^*(y_1)f_l(y_2)f_{l'}^*(y_2)f_{l'}(t(y_1)) \tag{A.3.33}$$

The peculiar structure of the Γ matrices, applied on $F^{n,0}_{\Psi}$ wavefunction vector, will generate the kinetic and the mass contributions of the heavy fermion self-energy.

Appendix B

General structure of the counter-terms

The main purpose of this appendix is to help the reader to make the link between the well-known 4D renormalization procedure and the counter-term structure that has been studied in chapter 3 in the context of 6D extra-dimensional models.

B.1 4D renormalization reminder

For simplicity we will consider a $SU(N)$-gauge theory, coupling with a fermion and a scalar field. At one loop, the renormalized Lagrangian can be written in the generic form in 4D as (8):

$$\mathcal{L}_{bare} = \mathcal{L}_{ren} + \mathcal{L}_{c.t.} \tag{B.1.1}$$

$\mathcal{L}_{bare}$ is the bare Lagrangian in which the field will be denoted by the subscript 0 and which represents the tree level Lagrangian. It is equal to the sum of the renormalized Lagrangian which describes the physical quantities and of the counter-term Lagrangian which will "contain" the divergences of the bare variables.

$$\begin{aligned}\mathcal{L}_{ren} = &-\frac{1}{4}F^a_{\alpha\beta}F^{a\alpha\beta} - \frac{1}{2\xi}\left(\partial_\mu A^{a,\mu}\right)^2 - \bar{c}^a\partial^2_\mu c^a - g f^{abc}\ \bar{c}^a\partial^\mu(A^b_\mu\ c^c)\\ &+ \bar{\Psi}(i\not{D} - m_f)\Psi + (D^\mu\phi)^\dagger(D_\mu\phi) - m^2_\phi\ \phi^\dagger\phi\end{aligned} \tag{B.1.2}$$

where A is a $SU(N)$ gauge boson, Ψ is a fermion with mass m_f and ϕ a complex scalar with mass m_ϕ. $D_M = \partial_M - igA^a_M t^a_r$ and $F^a_{\alpha\beta} = \partial_\alpha A^a_\beta - \partial_\beta A^a_\alpha + g f^{abc}A^b_\alpha A^c_\beta$.

Note that $\mathcal{L}_{bare}$ can be deduced from $\mathcal{L}_{ren}$ by adding the subscript 0 to all couplings, masses and fields similarly to the example presented in 1.1.1.

$$\mathcal{L}_{bare} = \mathcal{L}_{ren} \text{ where } A \to A_o, c \to c_o, \phi \to \phi_o, \psi \to \psi_o, g \to g_o, \xi \to \xi_o, \cdots \tag{B.1.3}$$

Finally the 4D counter-term Lagrangian is given by:

$$\begin{aligned}\mathcal{L}_{c.t.} = &-\frac{1}{4}\delta Z_3(\partial_\alpha A^a_\beta - \partial_\beta A^a)^2 - \frac{1}{2\xi}\left(\partial_\mu A^{a,\mu}\right)^2 - \delta Z'_2\bar{c}^a\partial^2_\mu c^a + \bar{\Psi}(i\delta Z_2\not{\partial} - \delta_m)\Psi + \delta Z_\phi(\partial^\mu\phi)^\dagger(\partial_\mu\phi)\\ &- g\delta c_1\ f^{abc}\partial_\mu A^a_\nu\ A^{b,\mu}A^{c,\nu} - g^2\delta c_4\ (f^{abc}A^b_\mu A^c_\nu)(f^{ade}A^{d,\mu}A^{e,\nu}) - g\delta c'_1 f^{abc}\bar{c}^a\partial^\mu(A^b_\mu\ c^c)\\ &+ g\delta c_{1f}\bar{\Psi}(t^a_r)\not{A}_a\Psi - ig\delta c_{1\phi}(\partial^\mu\phi^\dagger t^a_r\phi - \phi^\dagger t^a_r\partial_\mu\phi)A^a_\mu + g^2\delta c_{4\phi}\ \phi^\dagger\{t^a_r, t^b_r\}\phi\ A^a_\mu A^{b,\mu} - \delta m^2_\phi\ \phi^\dagger\phi\end{aligned}$$

Here the counter-terms δZ_i, δc_i and δm_i are associated to the renormalization of wavefunctions, couplings and masses.

The counter-term contributions are here to cancel the divergent contributions coming from the one-loop divergences. They can be deduced from radiative corrections. Moreover due to the gauge symmetry of the Lagrangian, all these coefficients are not independent. So at one loop, we should have for instance (8):

$$\mathcal{A}(\xi) = \delta c_{1\phi} - \delta Z_\phi = \delta c_{1f} - \delta Z_2 = \delta c_1 - \delta Z_3 = \frac{1}{2}(\delta c_4 - \delta Z_3) = \delta c_1' - \delta Z_2' \tag{B.1.4}$$

From this discussion, we notice easily that the counter-term Lagrangian is not gauge invariant anymore. Because of the renormalizability of this Lagrangian, the absence of gauge invariance is not a big issue for the calculation. Nevertheless, with a peculiar gauge choice, can this Lagragian find a gauge invariant form? Actually this will be the case if $\mathcal{A}(\xi) = 0$. Using the one-loop Standard Model calculation in generic ξ-gauge (135), we can show that:

$$\mathcal{A}(\xi) \propto \frac{g^2}{(4\pi)^2}\frac{(\xi+3)C_2(G)}{4\epsilon} \tag{B.1.5}$$

So we want to emphasize here that the same curiosity arises in 4D and in 6D. It seems that the $\xi = -3$ gauge choice is quite general to obtain a gauge invariant counter-term Lagrangian at one-loop level.

B.2 6D renormalization

When renormalizing an extra-dimensional quantum field theory, counter-term Lagrangians will also come to compensate the divergences of the theory. On the Real Projective Plane in 6D, we will have two sources of divergences which will have to be regularized. The first ones come from the torus contribution and will be similar to the open space divergences. They correspond technically to the 4D one we just mentioned in the previous section. We will not take those counter-terms into account in this discussion even if they will contribute to the 6D wavefunction renormalization. The second source is a set of log-divergences generated by the rotation contribution in the loops, directly linked to the singular points of the orbifold. The new counter-terms Lagrangian $\mathcal{L}_{c.t.}$, which regularizes the theory, is actually an effective 4D Lagrangian containing interactions localized on the singular points of the orbifold (63). As we already mentioned, this 4D Lagrangian will not respect necessarely the 6D Lorentz and gauge invariance. Therefore, in order to compensate the loop divergences, some new terms have to be added. For instance, mass counter-terms for the gauge bosons will be generated at loop level and they will not be 6D gauge invariant. There are not coming from $(F^{\mu 5})^2$ and $(F^{\mu 6})^2$ because these are vanishing on the fixed points. Considering the previous toy model, we can write the generic Lagrangian:

$$\begin{aligned}\mathcal{L}_{i\ c.t.} \supset \iint_0^{2\pi} dx\ dy\ \delta_i\Big\{ & -\frac{1}{4}\delta Z_3(\partial_\alpha A^a_\beta - \partial_\beta A^a)^2 - \frac{1}{2\xi}(\partial_\mu A^{a,\mu})^2 + \frac{1}{2}\delta m_A^2 A^{a,\mu}(\partial_5^2+\partial_6^2)A^a_\mu \\ & + \frac{1}{2}\delta Z_{mix}(\partial_5 A^{a,\mu}\partial_\mu A^a_5 + \partial_6 A^{a,\mu}\partial_\mu A^a_6) \\ & + \bar\Psi(i\delta Z_2 \not\partial - \delta_m)\Psi + \delta Z_\phi(\partial^\mu\phi)^\dagger(\partial_\mu\phi) + \delta Z_{\phi 5,6}(\partial^2_{5,6}\phi^\dagger\phi + \phi^\dagger\partial^2_{5,6}\phi) \\ & - g_6\delta c_1\ f^{abc}\partial_\mu A^a_\nu\ A^{b,\mu}A^{c,\nu} - g_6^2\delta c_4\ (f^{abc}A^b_\mu A^c_\nu)(f^{ade}A^{d,\mu}A^{e,\nu}) \\ & + g_6\delta c_{1f}\bar\Psi(t^a_r)\not{A}_a\Psi - ig_6\delta c_{1\phi}(\partial^\mu\phi^\dagger t^a_r\phi - \phi^\dagger t^a_r\partial_\mu\phi)A^a_\mu \\ & + g_6^2\delta c_{4\phi}\ \phi^\dagger\{t^a_r,t^b_r\}\phi\ A^a_\mu A^{b,\mu} - \delta m^2_\phi\ \phi^\dagger\phi \\ & + \{\text{terms with } A_\varphi \text{ and } A_\pi\}\Big\}\end{aligned} \tag{B.2.6}$$

where δ_0 and δ_π are combinations of Dirac function.

$$\delta_0 = \frac{1}{2}\left(\delta(x_5)\delta(x_6) + \delta(x_5-\pi)\delta(x_6-\pi)\right), \tag{B.2.7}$$

$$\delta_\pi = \frac{1}{2}\left(\delta(x_5)\delta(x_6-\pi) + \delta(x_5-\pi)\delta(x_6)\right), \tag{B.2.8}$$

In our case from the loop calculation performed in chapter 3, we can deduce the following deltas:

δZ_ϕ	$\frac{g^2C_2(r_\phi)}{(4\pi)^2}\frac{\xi-3}{\epsilon}$
δZ_2	$\frac{g^2C_2(r_f)}{(4\pi)^2}\frac{(\xi-1)}{\epsilon}$
δZ_3	$\frac{g^2}{(4\pi)^2}\left(\frac{(5-\xi)C_2(G)}{2\epsilon} - \frac{C(r_\phi)}{3\epsilon}\right)$
$\delta c_{1\phi}$	$\frac{g^2}{(4\pi)^2}\left(\frac{4(\xi-3)C_2(r_\phi)}{4\epsilon} + \frac{(\xi+3)C_2(G)}{4\epsilon}\right)$
δc_{1f}	$\frac{g^2}{(4\pi)^2}\left(\frac{4(\xi-1)C_2(r_f)}{4\epsilon} + \frac{(\xi+3)C_2(G)}{4\epsilon}\right)$
δc_1	$\frac{g^2}{(4\pi)^2}\left(\frac{(-3\xi+7)C_2(G)}{4\epsilon} - \frac{C(r_\phi)}{3\epsilon}\right)$

$$\delta c_{1\phi} - \delta Z_\phi = \delta c_{1f} - \delta Z_2 = \delta c_1 - \delta Z_3 = \frac{g^2}{(4\pi)^2}\frac{(\xi+3)C_2(G)}{4\epsilon} \tag{B.2.9}$$

Then the mass term generated by the non gauge invariant term gives:

$$\delta m_A^2 \propto \frac{g^2}{(4\pi)^2}\frac{(\xi+3)C_2(G)}{\epsilon} \tag{B.2.10}$$

The mixing term between A_μ and the Goldstone A_π gives also:

$$\delta Z_{mix} \propto \frac{g^2}{(4\pi)^2}\frac{(\xi+3)C_2(G)}{\epsilon} \tag{B.2.11}$$

So we can see clearly that in such gauge $\xi = -3$, the counter-term structure is given by the gauge invariance. This means that the counter-term Lagrangian takes the following form:

$$\begin{aligned}\mathcal{L}_{c.t.}(\xi=-3) = & -\frac{1}{4}\delta Z_3(F^a_{\alpha\beta})^2 - \frac{1}{2\xi}(\partial_\mu A^{a,\mu})^2 + \bar\Psi(i\delta Z_2\not\partial - \delta_m)\Psi + \delta Z_\phi(D^\mu\phi)^\dagger(D_\mu\phi) \\ & - \delta m^2_\phi\ \phi^\dagger\phi + \delta Z_{\phi 5,6}(\partial^2_{5,6}\phi^\dagger\phi + \phi^\dagger\partial^2_{5,6}\phi) + \{\text{terms with } A_\varphi \text{ and } A_\pi\}\end{aligned} \tag{B.2.12}$$

It is obvious now to see the identification between these numbers used in the usual 4D description and the one we defined in section 3.5:

$$\begin{aligned} r_1 &= \delta Z_3 \\ z_1 &= \frac{z_{1+} + z_{1-}}{2} = \delta Z_2 \\ c_1 &= \delta Z_\phi \\ c_5' &= \delta Z_{\phi 5} \quad \text{and} \quad c_6' = \delta Z_{\phi 6} \end{aligned} \tag{B.2.13}$$

We limited the example to a small subset of counter-terms but this can be obviously extended to the full Lagrangian of the SM on the Real Projective Plane.

Appendix C

The equivalence principle at work

In this section, we will introduce a discussion on the equivalence theorem on the Real Projective Plane which is a useful tool to check and compute the coupling of heavy gauge bosons decaying into SM heavy gauge bosons. This technique has been used for instance to implement the couplings of $A_\mu^{2,0}$, $W_\mu^{2,0}$ and $Z_\mu^{2,0}$ with the longitudinal polarization of heavy gauge bosons and the Higgs.

C.1 Decay of $A_\mu^{2k,2l}$ into massive SM gauge fields: effective vertices

In the Standard Model, the electroweak symmetry breaking gives a mass to the $W^\pm$ and Z. This effect needs to be included in the width calculation of the heavy partners. We can understand then that the effective 3-gauge vertex, presented in section 3.6.1, will not vanish anymore. The decay will be indeed allowed through the longitudinal polarization of the SM fields. So we will use the same procedure of adding counter-terms to extract the effective vertices between heavy and SM eigenstates. However this time we will allow the counter-terms coming from the Higgs field Lagrangian.

Using the "magic gauge" ($\xi = -3$) with the equations 3.11 and 3.13, we derive the counter-term Lagrangian of the Higgs sector. The covariant derivative is $D^\mu = \partial^\mu - ig_1 Y_\phi B^\mu - ig_w W^{\mu,a} t^a$.

$$\begin{aligned}\mathcal{L}_{c.t.}(\xi=-3) \supset & -\frac{r_1^{(1)}}{4}(B_{\alpha\beta})^2 - \frac{r_1^{(2)}}{4}(W^a_{\alpha\beta})^2 + c_1(D^\mu\phi)^\dagger(D_\mu\phi) + c_5'(\partial_5^2\phi^\dagger\phi + \phi^\dagger\partial_5^2\phi) \\ & + c_6'(\partial_6^2\phi^\dagger\phi + \phi^\dagger\partial_6^2\phi)\end{aligned} \tag{C.1.1}$$

Extracted from the loop corrections computed in section 3.3.1, we recall that:

$$\frac{c_1}{\pi^2\Lambda^2R^2} = -\frac{3}{2}C_2(r_\phi)\frac{\alpha}{\pi}\frac{1}{\epsilon} \tag{C.1.2}$$

$$\frac{c_5'}{\pi^2\Lambda^2R^2} = \frac{c_6'}{\pi^2\Lambda^2R^2} = -\frac{5}{16}C_2(r_\phi)\frac{\alpha}{\pi}\frac{1}{\epsilon} \tag{C.1.3}$$

where is given by:

$$C_2(r_\phi)\frac{\alpha}{\pi} = \frac{1}{4}\frac{\alpha_1}{\pi} + \frac{3}{4}\frac{\alpha_2}{\pi} \tag{C.1.4}$$

From the kinetic term of the Higgs fields (ϕ), we can obtain the new set of mixing terms. Those terms appear when the Higgs gets a non vanishing vacuum expection value (v). The value of the effective vertex (a) in figure C.1 is given by:

$$i\Pi_a^{\mu\nu} = ig^2 g_w v^2 \frac{-3}{2} C_2(r_\phi) \frac{\alpha}{\pi} \frac{1}{\epsilon} g^{\mu\nu} \tag{C.1.5}$$

The precise value of g^2 will be detailled in a following table. At the same order in v^2, we have also a contribution coming from the mass mixing term between $(2k, 2l)$ modes and zero modes. This term is generated by the c_5' and c_6' mass counter-term and induces a mixing for the vev. As it is shown in figure C.2, we have a new vertex (b) which has to be added to the previous contribution and which takes the value:

$$i\Pi_b^{\mu\nu} = ig^2 g_w v^2 \; 2 \cdot \frac{5}{16} C_2(r_\phi) \frac{\alpha}{\pi} \frac{1}{\epsilon} g^{\mu\nu} \tag{C.1.6}$$

We can add those two contributions and give the effective mass mixing vertex. The following table presents the value of g^2 for the different gauge field combinations:

$$i\Pi_{a+b}^{\mu\nu} = -ig^2 g_w v^2 \frac{7}{8} C_2(r_\phi) \frac{\alpha}{\pi} \frac{1}{\epsilon} g^{\mu\nu} \tag{C.1.7}$$

Mixings	g^2
$B_\mu(2k,2l)/B_\nu(0,0)$	$\frac{g_1^2}{4}$
$W_\mu^3(2k,2l)/B_\nu(0,0)$	$-\frac{g_1 g_w}{4}$
$W_\mu^3(2k,2l)/W_\nu^3(0,0)$	$\frac{g_w^2}{4}$
$W_\mu^\pm(2k,2l)/W_\nu^\pm(0,0)$	$\frac{g_w^2}{4}$

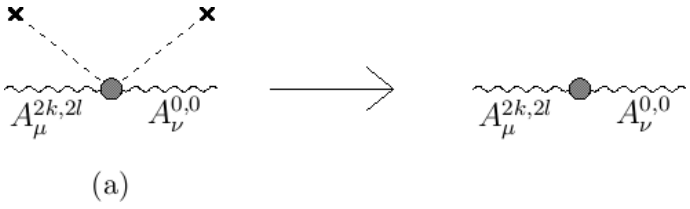

(a)

Figure C.1: $A_\mu^{2k,2l} - A_\nu^{0,0}$ mixing from the quadrilinear vertex of the Higgs kinetic part. The cross represents the vev insertions and the big gray dot, the scalar counter-term vertex.

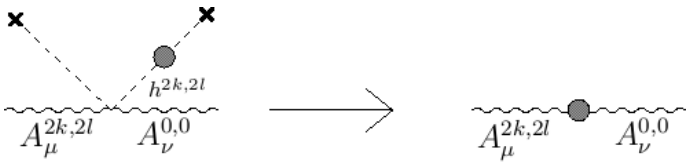

(b)

Figure C.2: $A_\mu^{2k,2l} - A_\nu^{0,0}$ mixing from the Higgs mass term.

C.1.1 Decays into W^+W^-

To obtain the effective vertex with 3-gauge bosons, we have to add together these new counterterms (fig.C.3). They will give a contribution proportional to m_W^2 which will compensate the $1/m_W^2$ contribution coming from the longitudinal polarization of the W's.

The tensor structure of the effective vertex is given by the following formula:

$$iV^{\mu\nu\rho} = c^{(0)}\mathcal{T}^{\mu\nu\rho} + c^{(2)}\frac{m_W^2}{M^2}\mathcal{S}^{\mu\nu\rho} + ... \tag{C.1.8}$$

The tensor $\mathcal{T}^{\mu\nu\rho}$ is the one introduced in section 3.6.1 and it satisfies $\mathcal{T}^{\mu\nu\rho}\epsilon^\rho(q_2)\epsilon^\nu(q_1) = 0$. $c^{(0)}$ is the prefactor in front of $\mathcal{T}^{\mu\nu\rho}$ which could be obtained from section 3.6.1. $c^{(2)}$ contains the contribution coming from the Higgs counter-terms and is given by:

$$c^{(2)}_{a+b} = i\frac{g^2 g_w v^2}{m_W^2}\frac{7}{8}\frac{\alpha}{\pi}\frac{1}{\epsilon} \tag{C.1.9}$$

The effective vertex generated by the Higgs counter-term Lagrangian is finally:

$$iV^{\mu\nu\rho}_{a+b} = c^{(2)}_{a+b}\frac{m_W^2}{M^2}\mathcal{S}^{\mu\nu\rho} \tag{C.1.10}$$

The tensor $\mathcal{S}^{\mu\nu\rho}$ satisfies $\mathcal{S}^{\mu\nu\rho}\epsilon^\rho(q_2)\epsilon^\nu(q_1) \neq 0$. Its expression is different if we consider the decay of $B^{2k,2l}$ or of $W^{2k,2l}$. It is obtained by summing the new set of counterterms in $\xi = -3$ gauge.

$$\begin{aligned}
\mathcal{S}^{\mu\nu\rho}_{(B\to WW)} &= -\frac{1}{4}\left\{(q_2^\mu - q_1^\mu)g^{\nu\rho} - (q_1^\nu + 2q_2^\nu)g^{\mu\rho} + (2q_1^\rho + q_2^\rho)g^{\mu\nu} - \frac{(q_2^\mu + q_1^\mu)(q_1^\nu q_1^\rho - q_2^\nu q_2^\rho)}{M^2}\right\} \\
&= -\frac{1}{4}\left\{\mathcal{O}^{\mu\nu\rho} - \frac{(q_2^\mu + q_1^\mu)(q_1^\nu q_1^\rho - q_2^\nu q_2^\rho)}{M^2}\right\} \\
\mathcal{S}^{\mu\nu\rho}_{(W\to WW)} &= \frac{1}{4}\left\{\mathcal{O}^{\mu\nu\rho} - \frac{M^2(q_2^\rho g^{\mu\nu} - q_1^\nu g^{\rho\nu}) - 2(q_2^\mu + q_1^\mu)(q_1^\nu q_1^\rho - q_2^\nu q_2^\rho) + q_1^\nu q_2^\rho(q_2^\mu - q_1^\mu)}{3M^2}\right\}
\end{aligned} \tag{C.1.11}$$

There is also a third contribution in $c_c^{(2)}$ which will lead to a vertex proportional to m_W^2. This part is directly generated by the gauge boson kinetic term r_1.

After resumming all these diagrams, presented in figure C.4, we show that the additional contribution to the effective vertex (C.1.10) is:

$$\begin{aligned}
iV^{\mu\nu\rho}_{c,\ (B\to WW)} &= -i\frac{g_w\alpha_1 m_W^2}{4M^2\pi\epsilon}\frac{1}{12}C(r_\phi)\left\{\mathcal{O}^{\mu\nu\rho} - \frac{(q_2^\rho g^{\mu\nu} - q_1^\nu g^{\rho\nu})}{4M^2}\right\} \\
iV^{\mu\nu\rho}_{c,\ (W\to WW)} &= -i\frac{g_w\alpha_2 m_W^2}{4M^2\pi\epsilon}(C_2(G) - \frac{1}{12}C(r_\phi))\left\{\mathcal{O}^{\mu\nu\rho} - \frac{(q_2^\rho g^{\mu\nu} - q_1^\nu g^{\rho\nu})}{4M^2}\right\}
\end{aligned} \tag{C.1.12}$$

Figure C.3: New contributions to the decay from bilinear counterterms.

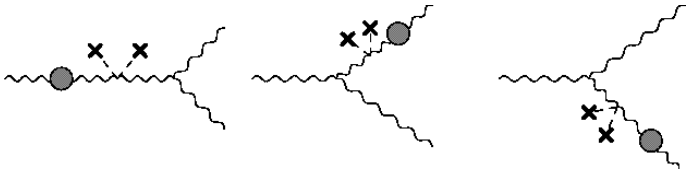

Figure C.4: Contributions to the decay of gauge bosons coming from the kinetic counter-term of gauge bosons.

As an example, for the decay of $B_\mu(2k,2l) \longrightarrow W_\mu^\pm(0,0)W_\mu^\mp(0,0)$, the effective vertex can be written as:

$$iV^{\mu\nu\rho}_{(B\to WW)} = -ig_1 Y_h[\frac{7}{4}\frac{\alpha}{\pi} + \frac{1}{6}C(r_\phi)]\frac{1}{\epsilon}\mathcal{S}^{\mu\nu\rho} \tag{C.1.13}$$

Note that the part of the tensor in $1/M^2$ will generate gauge dependent higher order corrections, and therefore they do not need to be taken into account in our later calculation.

To conclude, this situation will lead to a new effective vertex proportional to the W mass, which will allow the decay into two gauge bosons. For implementations of the decay of heavy B or W, discussed in section 4.2, these new trilinear effective couplings will be taken into account. They will ensure the decay of heavy gauge fields into massive gauge bosons through their longitudinal polarization.

C.1.2 Decays into h Z

In a similar way, we will consider the decay of $B^{2k,2l}$ and $W_3^{2k,2l}$ into $h^{0,0}$ and $Z^{0,0}$. The following table summarizes the effective vertices (fig.C.5) which are involved into the decay in h Z[1].

decays	iV_{higgs}
$B_\mu(2k,2l) \longrightarrow Z_\mu(0,0)h(0,0)$	$-2ig_1Y_h m_Z \frac{1}{\pi\epsilon}[\frac{7}{8}(\frac{1}{4}\frac{\alpha_1}{\pi} + \frac{3}{4}\frac{\alpha_2}{\pi}) - \frac{\alpha_1}{12}C(r_\phi)]g^{\mu\nu}$
$W_\mu^3(2k,2l) \longrightarrow Z_\mu(0,0)h(0,0)$	$+ig_w m_Z \frac{1}{\pi\epsilon}[\frac{7}{8}(\frac{1}{4}\frac{\alpha_1}{\pi} + \frac{3}{4}\frac{\alpha_2}{\pi}) + \frac{\alpha_2}{\pi}C_2(G) - \frac{\alpha_2}{12}C(r_\phi)]g^{\mu\nu}$

C.1.3 Decay of heavy eigenstates

$B_\mu^{(2k,2l)}$ and $W_{3,\mu}^{(2k,2l)}$, as it is the case in the Standard Model, are not mass eigenstates anymore after the electroweak symmetry breaking. As we are interested in the decay of heavy $A_\mu^{(2k,2l)}$ and $Z_\mu^{(2k,2l)}$, we have to consider the eigenstates given by the following expression (63):

$$\begin{cases} A_\mu^{(2k,2l)} = \cos\theta_2\ B_\mu^{(2k,2l)} + \sin\theta_2\ W_{3,\mu}^{(2k,2l)} \\ Z_\mu^{(2k,2l)} = \cos\theta_2\ W_{3,\mu}^{(2k,2l)} - \sin\theta_2\ B_\mu^{(2k,2l)} \end{cases} \tag{C.1.14}$$

where

$$\tan\theta_2 = \frac{m^2_{Z_{(2k,2l)}} - m^2_{A_{(2k,2l)}} + m_Z^2 - 2m_W^2 + \delta m_B^2 - \delta m_W^2}{2m_W m_Z \sin\theta_W}. \tag{C.1.15}$$

[1]When summing all the counter-terms, a sign problem appears in the contribution of the Higgs and of the non-abelian part of the decay into hZ. We expect like in formula 3.75 to have a vertex proportional to $\frac{7}{8}\frac{\alpha}{\pi}C_2(r_\phi) - \frac{\alpha_2}{\pi}C_2(G)$ instead of $\frac{7}{8}\frac{\alpha}{\pi}C_2(r_\phi) + \frac{\alpha_2}{\pi}C_2(G)$. The understanding of this last point is still in progress.

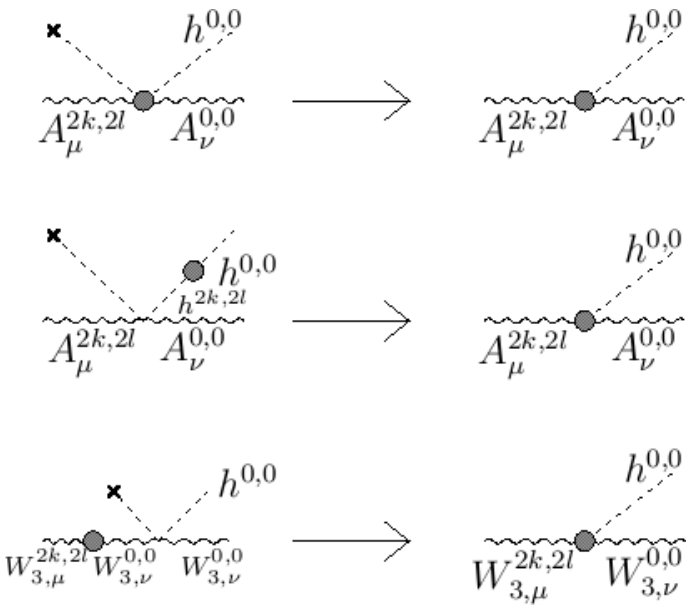

Figure C.5: Different contributions to $A_\mu^{2k,2l} - A_\nu^{0,0} - h^{0,0}$ trilinear vertex.

C.2 Decay widths and equivalence theorem

In this section we propose to establish the partial decay width of heavy gauge bosons going into SM massive gauge fields. And we will use the equivalence theorem to show the consistency of the obtained results.

As an example, we decide to study the case of $B_\mu^{2k,2l} \longrightarrow W_\mu^{\pm(0,0)} W_\mu^{\mp(0,0)}$. The other decay widths can be derived easily with similar calculations. Using the effective vertex from the previous section, we can get the decay width in zeroth order in m_W^2.

$$\begin{aligned}
\Gamma &= \frac{1}{3}|\mathcal{M}|^2 \frac{1}{8\pi}\frac{1}{4M}\sqrt{1-\frac{m_W^2}{2M^2}} \\
\Gamma &= \frac{1}{3}\frac{1}{8\pi}\frac{1}{4M}\left(\frac{g_1 Y_h}{\pi\epsilon}\right)^2\left(\frac{7}{4}(\frac{1}{4}\frac{\alpha_1}{\pi}+\frac{3}{4}\frac{\alpha_2}{\pi})+\frac{\alpha_1}{6}C(r_\phi)\right)^2\cdot \\
&\frac{m_W^4}{M^4}\mathcal{S}^{\mu\nu\rho}\mathcal{S}^{\alpha\beta\gamma}\left(g^{\alpha\mu}-\frac{q^\alpha q^\mu}{4M^2}\right)\left(g^{\beta\nu}-\frac{q_1^\beta q_1^\nu}{m_W^2}\right)\left(g^{\gamma\rho}-\frac{q_2^\gamma q_2^\rho}{m_W^2}\right) \\
\Gamma &\sim \frac{1}{96\pi}\left(\frac{g_1 Y_h}{\pi\epsilon}\right)^2\left(\frac{7}{4}(\frac{1}{4}\frac{\alpha_1}{\pi}+\frac{3}{4}\frac{\alpha_2}{\pi})+\frac{\alpha_1}{6}C(r_\phi)\right)^2 M
\end{aligned} \tag{C.2.16}$$

The last thing we did, was to compare this width (C.2.16) with the one we can compute using the equivalence theorem: $B_\mu^{2k,2l} \longrightarrow \phi^{\pm(0,0)}\phi^{\mp(0,0)}$. $\phi^\pm$ are the Goldstone bosons which will be eaten by the W's to become their longitudinal components in the unitary gauge. From the formula (3.76), we can deduce the vertex for the gauge field decaying into SM scalars. In $\xi = -3$ gauge, the coefficient coming from loops is the same as the one we used before. It is generated actually by the same counter-terms. So the coupling is given by:

$$iV^{\mu}_{(B\to\phi^{\pm}\phi^{\mp})} = i\frac{g_1 Y_h}{\pi\epsilon}\left(\frac{7}{8}(\frac{1}{4}\frac{\alpha_1}{\pi}+\frac{3}{4}\frac{\alpha_2}{\pi})+\frac{\alpha_1}{12}C(r_\phi)\right)^2(q_2^\mu - q_1^\mu) \tag{C.2.17}$$

At the zeroth order in m_W^2, we get the partial decay width of $B_\mu^{2k,2l}$:

$$\begin{aligned}
\Gamma &= \frac{1}{3}|\mathcal{M}|^2\frac{1}{8\pi}\frac{1}{4M}\sqrt{1-\frac{m_W^2}{2M^2}} \\
\Gamma &\sim \frac{1}{3}\left(\frac{g_1 Y_h}{\pi\epsilon}\right)^2\left(\frac{7}{8}(\frac{1}{4}\frac{\alpha_1}{\pi}+\frac{3}{4}\frac{\alpha_2}{\pi})+\frac{\alpha_1}{12}C(r_\phi)\right)^2(q_2^\mu - q_1^\mu)(q_2^\alpha - q_1^\alpha)\left(g^{\alpha\mu}-\frac{q^\alpha q^\mu}{4M^2}\right)\frac{1}{8\pi}\frac{1}{4M} \\
\Gamma &\sim \frac{1}{96\pi}\left(\frac{g_1 Y_h}{\pi\epsilon}\right)^2\left(\frac{7}{4}(\frac{1}{4}\frac{\alpha_1}{\pi}+\frac{3}{4}\frac{\alpha_2}{\pi})+\frac{\alpha_1}{6}C(r_\phi)\right)^2\frac{1}{4}4M
\end{aligned} \tag{C.2.18}$$

Through this calculation, we showed that the computation of the partial width of heavy gauge bosons into SM massive ones can be inferred by using the equivalence theorem which can simplify the calculation. The decay of heavy gauge bosons is actually mediated by the longitudinal polarization of the SU(2) gauge bosons and only ruled by the electroweak symmetry breaking. In our `FEYNRULES` code, we implemented the gauge structure directly however we use the equivalence theorem to check the branching ratios obtained with the `CALCHEP` code by looking at the matching of the two descriptions for high KK-mass limit. Here we focus on the case of the heavy $B^{2k,2l}$ but similar results can be shown for the decay of the $W^\pm$ and W^3. To study the decay of the heavy photon or heavy Z eigenstates, we just need to diagonalize the vertices using the proper Weinberg angle related to the $(2k, 2l)$ level in our case, it will be done automatically by the `FEYNRULES` software.

Appendix D

Higgs couplings in extended Higgs sectors

D.1 Multiple Higgs

The Higgs sector may contain multiple scalar fields which develop a VEV, like for instance in supersymmetry where two Higgs doublets are required in order to allow up and down type Yukawa interactions. Let us imagine that there are n such Higgs multiplets ϕ_i, such that

$$\phi_i = \frac{1}{\sqrt{2}}\left(v_i + c_i h + \dots\right) , \tag{D.1.1}$$

where h is the lightest mass eigenstate (that we would identify with the SM Higgs), and dots represent the other (heavier) scalar mass eigenstates. The VEVs are all non zero $v_i \neq 0$. In this case, in the formulas in Section 5.2, one needs to replace:

$$\frac{v_{SM}}{m}\frac{\partial m}{\partial v} \to \frac{v_{SM}}{m}\sum_i \frac{\partial m}{\partial v_i} c_i \, . \tag{D.1.2}$$

For example, in the case of supersymmetry, there are two Higgs doublets, $H_{u,d}$ with $H_u = 1/\sqrt{2}(v_u + h\cos\alpha + \sin\alpha H)$ and $H_d = 1/\sqrt{2}(v_d - h\sin\alpha + \cos\alpha H)$, and $v_{SM}^2 = v_u^2 + v_d^2$ ($\tan\beta = v_u/v_d$). The W mass is given by $m_W^2 = g^2/4(v_u^2 + v_d^2)$, so that:

$$\frac{v_{SM}}{m_W}\frac{\partial m_W}{\partial v} \to \frac{v_{SM}}{m_W}\left(\frac{m_W}{v_{SM}}\sin\beta\cos\alpha - \frac{m_W}{v_{SM}}\cos\beta\sin\alpha\right) = \sin(\beta-\alpha) \, . \tag{D.1.3}$$

For the top, $m_t = y v_u$:

$$\frac{v_{SM}}{m_t}\frac{\partial m_t}{\partial v} \to \frac{v_{SM}}{m_t} y\cos\alpha = \frac{\cos\alpha}{\sin\beta} \, . \tag{D.1.4}$$

D.2 Higgs mixing

Another interesting case is when the Higgs mixes with additional scalars that do not develop a VEV. This situation may be realized in multiple Higgs models, or in the Lee-Wick SM. We will call S_j those inert scalars, which contain the light Higgs field h:

$$S_j = s_j h + \dots \tag{D.2.5}$$

As before, we are assuming that the other mass eigenstates are heavier than the h, which we want to identify with the SM Higgs. The scalars S_j may couple to a particle p with coupling

$$g_{S_j}\, S_j\, \bar{p}p\,, \tag{D.2.6}$$

which will contribute to the coupling of p to the Higgs h via the mixing. In this case, one can use the formulas in Section 5.2 with

$$\frac{v_{SM}}{m}\frac{\partial m}{\partial v} \to \frac{v_{SM}}{m}\left(\sum_i \frac{\partial m}{\partial v_i}c_i + \sum_j g_{S_j} s_j\right)\,. \tag{D.2.7}$$

D.3 Charged Higgs couplings

Another situation where the coupling to the Higgs does not come via the v-dependence of the mass, is when the particle in question does couple with the Higgs potential. In fact, the Higgs potential implicitly contains the VEV, and this fact may lead to cancellations in the particle mass. One may calculate the mass of the particle as a function of the Higgs field VEV $\langle H\rangle$ and v (which are numerically equal), derive in $\langle H\rangle$ and then impose $\langle H\rangle = v$. In most cases it is easier to compute the coupling directly from the Higgs potential: here we will summarize three cases that are useful for the calculations in this paper.

The most trivial example is the charged Goldstone boson in the SM, which is eaten by the W in the Unitary gauge. In Feynman gauge, the charged component of the Higgs doublet remains in the spectrum and its mass is $m_{\phi^\pm} = m_W$. This may lead to the wrong conclusion that its couplings to the Higgs are the same as the W. The Higgs potential can be written as

$$V(H) = \frac{\lambda}{4}\left(H^\dagger H - \frac{v^2}{2}\right)^2\,; \tag{D.3.8}$$

after expanding the Higgs field as $H = \begin{pmatrix} \phi^+ \\ \frac{v+h+i\phi}{\sqrt{2}} \end{pmatrix}$, it does not generate any mass for the Goldstone bosons ϕ, because of a cancellation between the mass term $-\lambda v^2/4$ and a contribution from the quartic coupling (the mass is given by the gauge fixing term). However, the quartic coupling does generate a trilinear coupling with the Higgs h:

$$\frac{\lambda v}{2}\phi^+\phi^- h = \frac{m_h^2}{v}\phi^+\phi^- h\,. \tag{D.3.9}$$

The coupling to the Higgs is therefore proportional to the Higgs mass. The amplitude generated by the Goldstone boson can be computed starting from the amplitude of a standard scalar

$$A_{\phi^\pm}(\tau_W) = \frac{v}{2m_W^2}\frac{m_h^2}{v}A_S(\tau_W) = 2\tau_W A_S(\tau_W)\,, \tag{D.3.10}$$

where $\tau_W = \frac{m_h^2}{4m_W^2}$.

A similar situation happens in the Lee-Wick SM: together with the standard Higgs field H, there exists a LW scalar $\tilde{H}$ with negative kinetic term. The potential is:

$$V_{LW}(H,\tilde{H}) = V(H-\tilde{H}) - M_H^2\tilde{H}^\dagger\tilde{H}\,. \tag{D.3.11}$$

Only the standard Higgs develops a VEV, while the LW Higgs does not thanks to its large LW mass M_H. The charged component of the Higgs is eaten by the massive W; the charged component of the LW field $\tilde{h}^+$ is a physical degree of freedom with mass given simply by the LW mass: the v dependence cancels out like for the Goldstone bosons. Nevertheless, a trilinear coupling $\tilde{h}^+\tilde{h}^- h$ is present with coefficient proportional to $\lambda v/2$ (the proportionality coefficient depends on the mixing in the neutral sector, and it is discussed in Section 5.3). The amplitude for the LW field can be written as:

$$A_{\tilde{h}^\pm}(\tilde{\tau}_{h^\pm}) = \frac{v_{SM}}{2\tilde{m}^2_{h^\pm}}\frac{\lambda v}{2} A_S(\tilde{\tau}_h) = \frac{\lambda v v_{SM}}{2m_h^2}\, 2\tilde{\tau}_h A_S(\tilde{\tau}_h)\,; \tag{D.3.12}$$

where $\tilde{\tau}_h = \frac{m_h^2}{4\tilde{m}^2_{h^\pm}}$. This formula is different from the one used in Ref. (113).

Finally, let us discuss the case of the charged Higgs in the MSSM: the model contains two Higgs doublets $H_{u,d}$ with opposite hypercharge to generate up- and down-type Yukawas. The potential contains two quartic couplings (21):

$$\begin{aligned} V_{MSSM}(H_u, H_d) &= \frac{g^2+g'^2}{8}\left(|H_u|^2 - |H_d|^2\right)^2 + \frac{g^2}{2}\left|H_u H_d^\dagger\right|^2 + \dots \\ &= \frac{g^2+g'^2}{8}\left(|H_u^0|^2 - |H_d^0|^2 + H_u^- H_u^+ - H_d^+ H_d^-\right)^2 + \frac{g^2}{2}\left|H_u^+ (H_d^0)^* + H_u^0 H_d^+\right|^2 + \dots \end{aligned} \tag{D.3.13}$$

where the dots stand for quadratic terms. The two neutral components develop a VEV: $\sqrt{2}\langle H_u^0\rangle = v_u = v_{SM}\sin\beta$ and $\sqrt{2}\langle H_d^0\rangle = v_d = v_{SM}\cos\beta$. However, only one combination actually acquires a VEV: we can define $H_1 = \sin\beta\, H_u - \cos\beta\, H_d^\dagger$ and $H_2 = \cos\beta\, H_u + \sin\beta\, H_d^\dagger$ such that $\sqrt{2}\langle H_1\rangle = v_{SM}$ and $\sqrt{2}\langle H_2\rangle = 0$. The charged component of H_1 is eaten by the W, while the charged component of H_2 is the physical charged Higgs: $H_u^+ = \cos\beta\, H^+$ and $H_d^+ = \sin\beta\, H^+$. Plugging those solutions in the potential, and expanding around the VEV $\sqrt{2}\langle H_u^0\rangle = v_u + \cos\alpha\, h + \sin\alpha H$ and $\sqrt{2}\langle H_d^0\rangle = v_d - \sin\alpha\, h + \cos\alpha H$, we find that

$$m^2_{H^\pm} = m_A^2 + m_W^2\,, \tag{D.3.14}$$

$$g_{H^+H^-h} = \frac{2m_W^2}{v_{SM}}\sin(\beta-\alpha) + \frac{m_Z^2}{v_{SM}}\cos(2\beta)\sin(\beta+\alpha)\,, \tag{D.3.15}$$

where m_A is a mass term independent on the VEVs. The coupling to the light Higgs has a term proportional to the W mass square, coming from the second term in the potential (this is what we would obtain from the mass formula), and a term proportional to the Z mass square, from the first quartic term in the potential: the latter cancels out in the mass formula but does contribute to the Higgs couplings.

Appendix E

Higgs sector in 5D models

E.1 Gauge bosons in 5D

In this appendix, we propose a more detailed description of the models that we consider in section 5.4, we sketch how to extract the spectra of masses for gauge bosons for different choices of geometry and compactification of the fifth dimension [1].

E.1.1 Gauge Higgs Unification Models

A zero mode for the A_5 component of the gauge field is a physical scalar in the spectrum because it is not eaten up in the Unitary gauge. However, it is a special scalar because its potential is constrained by Lorentz and gauge invariance: in 5D no potential is allowed at tree level, therefore it is generated at loop level and it is finite. This property makes the A_5 an ideal candidate to play the role of the Higgs boson. In order to obtain a zero mode, we need to enlarge the SM gauge group such that a doublet of SU(2) is part of the gauge fields, and break the gauge directions of this doublet on both end points by imposing Dirichlet boundary conditions on the vectors (and therefore Neumann boundary conditions on the A_5 component).

For simplicity, we work on the minimal model where the gauge symmetry is enlarged to $SU(3)$, broken to the electroweak $SU(2) \times U(1)$ at the boundaries. The bulk fields can be written as:

$$A_\mu = \begin{bmatrix} \boldsymbol{W_\mu^{(3)}} + \boldsymbol{1/\sqrt{3} B_\mu^{(8)}} & \boldsymbol{W_\mu^+} & D_\mu^+ \\ \boldsymbol{W_\mu^-} & -\boldsymbol{W_\mu^{(3)}} + \boldsymbol{1/\sqrt{3} B_\mu^{(8)}} & D_\mu^0 \\ D_\mu^- & D_\mu^{0\dagger} & \boldsymbol{2/\sqrt{3} B_\mu^{(8)}} \end{bmatrix} \text{ and } A_5 = \begin{bmatrix} 0 & 0 & \boldsymbol{H^+} \\ 0 & 0 & \boldsymbol{H^0} \\ \boldsymbol{H^-} & \boldsymbol{H^{0\dagger}} & 0 \end{bmatrix} \tag{E.1.1}$$

where W and B are towers with a zero mode, D are massive gauge bosons and H is the Higgs field (only the zero mode). We assume that the radiative potential will generate a VEV for the Higgs

$$\langle H^0 \rangle = \frac{V}{\sqrt{2}} \frac{1}{w(y)}\,, \tag{E.1.2}$$

where V is a constant and the y dependence is encoded in the metric factor w. The presence of this VEV will affect the bulk equation of motions for all fields: however, being H part of gauge

[1] If needed, notations and equation of motion can be found in section 1.3.

fields, we can use an SU(3) gauge transformation to remove the VEV from the bulk equation of motions, and cast it into the boundary conditions (56). For the gauge bosons, we can define:

$$\tilde{A}_M = \Omega(y) A_M \Omega^\dagger(y) - \frac{i}{g_5}\Omega(y)\partial_M \Omega^\dagger(y)$$
$$\text{so that} \quad \langle \tilde{A}_5 \rangle = \Omega(y)\langle A_5 \rangle \Omega^\dagger(y) - \frac{i}{g_5}\Omega(y)\partial_y \Omega^\dagger(y) = 0\,. \tag{E.1.3}$$

The gauge transformation that does this job can be written as:

$$\Omega(y) = \exp\left[i g_5 v/2 \int_{y_1}^{y} dy' \frac{1}{w(y')} \lambda_7 \right], \tag{E.1.4}$$

where λ_7 is the generator of SU(3) aligned with H^0. Note that we fixed the gauge transformation such that it only affects one brane: in fact $\Omega(y_1) = 1$, and

$$\Omega(y_2) = \exp\left[i\pi\alpha\lambda_7\right] = \begin{pmatrix} 1 & 0 & 0 \\ 0 & \cos\pi\alpha & i\,\sin\pi\alpha \\ 0 & i\,\sin\pi\alpha & \cos\pi\alpha \end{pmatrix}, \tag{E.1.5}$$

where

$$\alpha = \frac{g_5 V}{2} \int_{y_1}^{y_2} \frac{dy}{\pi} \frac{1}{w(y)} \tag{E.1.6}$$

is a dimensionless parameter proportional to the Higgs VEV V. The equations of motion of the new fields do not depend on the Higgs VEV, however the boundary conditions on one end will be affected. For example, for the charged gauge bosons, the gauge transformation will mix W^+ and D^+, which have respectively Neumann and Dirichlet boundary conditions on both endpoints: in the new basis

$$\begin{cases} D_\mu^+(y_1) = \tilde{D}_\mu^+(y_1) = 0 \\ \partial_5 W_\mu^+(y_1) = \partial_5 \tilde{W}_\mu^+(y_1) = 0 \end{cases} \quad \text{and} \quad \begin{cases} D_\mu^+(y_2) = \cos\pi\alpha\, \tilde{D}_\mu^+ + i \sin\pi\alpha\, \tilde{D}_\mu^+ = 0 \\ \partial_5 W_\mu^+(y_2) = \cos\pi\alpha\, \partial_5 \tilde{W}_\mu^+ + i \sin\pi\alpha\, \partial_5 \tilde{D}_\mu^+ = 0 \end{cases}$$

Eq.(E.1.6) can be used to calculate δ_v, however we need to first identify the 4-dimensional VEV v. The physical Higgs field has, with a good approximation, the same profile as the 5D VEV V, therefore the couplings of the Higgs can be calculated by replacing $V \to V + h/N$, where N is the normalization of the Higgs wave function:

$$N^2 = \int_{y_1}^{y_2} dy\; w(y) \cdot \frac{1}{w(y)^2}\,, \tag{E.1.7}$$

and $v = VN$. Therefore, α can be written in terms of the 4-dimensional VEV v as:

$$\alpha = \frac{g_5 v N}{2\pi} = \frac{g_4 v}{2\pi} N\sqrt{\mathcal{V}}\,, \quad \text{where} \quad \mathcal{V} = \int_{y_1}^{y_2} dy\; w(y) \tag{E.1.8}$$

is the volume of the extra dimension, and g_4 is the 4-dimensional gauge coupling (equal to the SM one up to electroweak precision corrections). Therefore:

$$\frac{v_{SM}}{v} = 1 - \delta_v = \frac{g_4 v_{SM}}{2\pi\alpha} N\sqrt{\mathcal{V}} = \frac{m_W N\sqrt{\mathcal{V}}}{\pi\alpha}\,. \tag{E.1.9}$$

The specific form of the spectrum depends on the metric: in the flat case

$$\alpha = \frac{g_5 V}{2} \int_0^{\pi L} \frac{dy}{\pi} = \frac{g_5 L}{2} V \,, \tag{E.1.10}$$

and

$$\left\{ \begin{array}{c} \tilde{W}(x,y) \\ \tilde{D}(x,y) \end{array} \right\} = \sum_n \left\{ \begin{array}{c} (A_n \cos m_n y + B_n \sin m_n y) \\ (C_n \cos m_n y + D_n \sin m_n y) \end{array} \right\} W_n(x) \,. \tag{E.1.11}$$

Applying the boundary conditions to such wave functions, we obtain that the spectrum is determined by the solutions of the following equation:

$$\sin \pi \left(m_n L \pm \alpha \right) = 0 \,. \tag{E.1.12}$$

Given $m_W L = \alpha$, and $N^2 = \mathcal{V} = \pi L$:

$$\delta_v = 1 - \frac{\pi m_W L}{\pi \alpha} = 0 \,. \tag{E.1.13}$$

The warped case is more complicated because the solutions of the equations of motion are Bessel functions of the first and second kind of order 1:

$$\alpha = \frac{g_5 V}{2} \int_{1/\Lambda}^{R'} \frac{dy}{\pi} \frac{y}{R} = \frac{g_5 R'^2}{4\pi R} V \left(1 - \frac{1}{(\Lambda R')^2} \right) \,, \tag{E.1.14}$$

and

$$\left\{ \begin{array}{c} \tilde{W}(x,y) \\ \tilde{D}(x,y) \end{array} \right\} = \sum_n \left\{ \begin{array}{c} y(A_n J_1(m_n y) + B_n Y_1(m_n y)) \\ y(C_n J_1(m_n y) + D_n Y_1(m_n y)) \end{array} \right\} W_n(x) \,. \tag{E.1.15}$$

Finally

$$1 - \delta_v = \frac{m_W R'}{\pi \alpha} \sqrt{\frac{\log \Lambda R'}{2}} \simeq \frac{\sin \pi \alpha}{\pi \alpha} \,, \tag{E.1.16}$$

where we used that $N \simeq R'/\sqrt{2R}$, $\mathcal{V} = R \log \Lambda R'$ and

$$m_W R' \simeq \sqrt{\frac{2}{\log \lambda R'}} \sin \pi \alpha \,. \tag{E.1.17}$$

E.1.2 Brane Higgs Models

In these models, the Higgs boson is a 4D field which couples with the 5D gauge bulk field only on a boundary, so that the Higgs VEV only enters in the boundary conditions. We will first focus on the case where the bulk gauge symmetry is the same as in the SM, without extra fields that mix with the W: the action in the bulk is the same as in (1.85) and the 5D field can be KK decomposed as we have done before. The boundary conditions on the two endpoints can be written as (here we assume the Higgs localized on y_2, but the results do not depend on this choice)

$$\left\{ \begin{array}{c} \partial_5 W_\mu^+(y_1) = 0 \\ \partial_5 W_\mu^+(y_2) - \frac{g_5^2 v^2}{4 w(y_2)} \, W_\mu^+(y_2) = 0 \end{array} \right. \tag{E.1.18}$$

where v is the Higgs VEV and g_5 the 5D gauge coupling. If we decompose the 5D fields as usual

$$W^+(y,x) = \sum_n f_n(m_n y)\; W_n(x)^+ \,, \tag{E.1.19}$$

the second boundary condition determines the spectrum as the solutions of the equation

$$m_n \frac{f'(m_n y_2)}{f(m_n y_2)} - \frac{g_5^2 v^2}{4w(y_2)} = 0 \,. \tag{E.1.20}$$

The precise form of the function f depends on the geometry after imposing the boundary condition on the other endpoint. The Higgs VEV can be written in terms of the SM one as:

$$\frac{v_{SM}}{v} = 1 - \delta_v = \frac{g_5 v_{SM}}{2\sqrt{w(y_2)}} \sqrt{\frac{f(m_W y_2)}{m_W f'(m_W y_2)}} = \sqrt{\frac{m_W \mathcal{V}}{w(y_2)}} \sqrt{\frac{f(m_W y_2)}{f'(m_W y_2)}} \,. \tag{E.1.21}$$

In the flat case

$$f(m_n y) = \cos(m_n y) \Rightarrow \pi L m_n \tan \pi L m_n - \pi^2 \alpha^2 = 0 \,, \tag{E.1.22}$$

where we have defined for convenience

$$\alpha = \sqrt{\frac{L}{\pi}} \frac{g_5 V}{2} \,. \tag{E.1.23}$$

Eq.(E.1.21) gives

$$\delta_v = 1 - \sqrt{m_W \pi L \cot(m_W \pi L)} \simeq \frac{\pi^2}{6} (m_W L)^2 \,. \tag{E.1.24}$$

In the warped case

$$f(m_n y) = y(Y_0(m_n R) J_1(m_n y) - J_0(m_n R) Y_1(m_n y)) \,, \tag{E.1.25}$$

and

$$\alpha = \frac{g_5 v R'}{2\sqrt{R}} \,. \tag{E.1.26}$$

Expanding eq.(E.1.21) we obtain

$$\delta_v \simeq \frac{\alpha^2}{4} \,. \tag{E.1.27}$$

Note finally that the simple form of eq. (E.1.20) allows us to calculate the couplings of the n-th mode to the Higgs as a function of the mass, even though the mass cannot be explicitly calculated: in fact, taking the total derivative with respect to V and eliminating V by using eq. (E.1.20), we obtain

$$\frac{v}{m_n} \frac{\partial m_n}{\partial v} = \frac{2\frac{f'}{f}}{\frac{f'}{f} + m_n y_2 \left(\frac{f''}{f} - \left(\frac{f'}{f} \right)^2 \right)} \,. \tag{E.1.28}$$

By studying this expression numerically or in an expansion for small α, we found that the sum rule

$$\sum_n \frac{v}{m_n} \frac{\partial m_n}{\partial v} = 1 \,, \tag{E.1.29}$$

where we are summing over all the mass eigenstates, is respected both in the flat and warped case.

E.2 Fermionic fields

In this appendix, we propose as we did before, a more detailed description of the models that we consider in section 5.4, and we describe how to extract the mass spectra for fermions for different choices of geometry and compactification of the fifth dimension [2]. We remind in this section that we have to consider models with chiral SM fermions. This is achieved by taking boundary conditions for the Dirac fields which allow light chiral zero modes:

$$\begin{array}{c}\text{Left-handed}\\ \text{fermion}\end{array} \rightarrow \psi\,|_{y_1,y_2}= 0 \quad \Big\| \quad \begin{array}{c}\text{Right-handed}\\ \text{fermion}\end{array} \rightarrow \chi\,|_{y_1,y_2}= 0 \tag{E.2.1}$$

To complete the description of fermions and to relate it to SM phenomenology, we need to introduce two bulk fields, a singlet Ψ_R with a right-handed zero mode and a doublet of $SU(2)$ Ψ_L with a left-handed zero mode, and their couplings with the Higgs boson. From here, we need to specify some properties of the 5D models.

E.2.1 Gauge Higgs Unification Models

In this case, the singlet Ψ_R and the doublet Ψ_L are embedded in the same bulk field, a representation of the larger bulk gauge symmetry. Consequently the odd bulk mass $\tilde{M}$ is the same for the doublet and the singlet components. The interaction with the Higgs boson appears in the covariant derivative of Ψ in the kinetic term. This additional term in the action is given by $-ig_5\bar{\Psi}\Gamma^5 A_5\Psi$ in the bulk: the bulk Yukawa coupling is therefore proportional to the gauge coupling g_5 and the proportionality factor depends on the specific representation of Ψ. This term will modify the bulk equations of motion: however, as in the gauge boson case, we can use a gauge transformation to remove the Higgs VEV, and recast its effects on one of the boundary conditions.

Here we will focus on the SU(3) case described in the text for simplicity. The gauge transformed fields on the y_2 brane are

$$\tilde{\Psi}(y_2) = \Omega_f(y_2)\Psi(y_2) \qquad \text{where} \quad \Omega_f(y_2) = \exp\left[i\,\pi\alpha\tilde{\lambda}_7\right]\,, \tag{E.2.2}$$

where $\tilde{\lambda}_7$ is the SU(3) generator in the representation of Ψ. The matrix Ω_f will mix the singlet and the component of the doublet which picks up a mass (for simplicity we will denote it with Ψ_L). The mixing angle however, is not α in general: in fact it will depend on the representation of the bulk field, and the proportionality factor can be calculated by explicitly computing the generator $\tilde{\lambda}_7$ for the bulk fermion representation. In general, we will define a new parameter β to describe the mixing. Note that in the case of a bulk fundamental, Ω is the same as the one used for the gauge bosons in the previous section, therefore $\beta(\mathbf{3}) = \alpha$. The new boundary conditions for the transformed fields are

$$\begin{cases} \psi_L(y_2) = \cos\pi\beta\,\tilde{\psi}_L(y_2) - i\sin\pi\beta\,\tilde{\psi}_R(y_2) = 0 \\ \chi_R(y_2) = \cos\pi\beta\,\tilde{\chi}_R(y_2) - i\sin\pi\beta\,\tilde{\chi}_L(y_2) = 0 \end{cases} \tag{E.2.3}$$

This boundary conditions will determine the spectrum: for instance, the spectrum m_n in the flat case is given by the solutions of

$$-\cos 2\pi L\sqrt{-\tilde{M}^2 + m_n^2} + \cos 2\pi\beta + 2\frac{\tilde{M}^2}{m_n^2}\sin^2\pi\beta = 0\,. \tag{E.2.4}$$

[2] Notations and equation of motion can be found in section 1.3.5.

E.2.2 Brane Yukawas

Fermionic masses can also be generated by Yukawa couplings localized on an endpoint of the extra dimension: this is possible both in the bulk Higgs model and in the localized Higgs case. Like in the Gauge Higgs case, the Higgs VEV only enters in the boundary conditions. However, boundary conditions for fermions are more tricky than for bosons, due to the fact that the equations of motion are first order differential equations: therefore how the VEV enters the boundary conditions depends crucially on the localization mechanism for the Higgs field or for the Yukawa couplings (see Ref. (60)). Here we will consider the simplest possibility: that the boundary conditions are linear in the Higgs VEV:

$$\begin{cases} \psi_L - yvL\psi_R = 0 \\ \chi_R + yvL\chi_L = 0 \end{cases} \tag{E.2.5}$$

Those boundary conditions are the same as in the gauge Higgs case if we identify $\tan \pi\beta = yvL$ (and removing the i with a phase redefinition of the fields). The only difference is that β is not proportional to the Higgs VEV, therefore additional corrections to the couplings will arise. Another novelty is that the singlet and doublet fields are part of different bulk fields, therefore they can have different bulk masses $\tilde{M_L}$ and $\tilde{M_R}$.

References

[1] A. V. Manohar, "Effective field theories," arXiv:hep-ph/9606222. 4

[2] W. Skiba, "TASI Lectures on Effective Field Theory and Precision Electroweak Measurements," arXiv:1006.2142 [hep-ph]. 6, 8

[3] S. L. Glashow, "Partial-symmetries of weak interactions," *Nuclear Physics* **22** no. 4, (1961) 579 – 588. http://www.sciencedirect.com/science/article/B73DR-470FCCY-3/2/73adaafe245cc26ee7aa3aa7215f18e1. 9

[4] A. Salam, "N. svartholm. ed. elementary particle physics: Relativistic groups and analyticity. eighth nobel symposium.," *Stockholm: Almquvist and Wiksell. pp. 367.* **pp. 367.** (1968) . 9

[5] S. Weinberg, "A model of leptons," *Phys. Rev. Lett.* **19** no. 21, (Nov, 1967) 1264–1266. 9

[6] P. W. Higgs, "Broken Symmetries and the Masses of Gauge Bosons," *Physical Review Letters* **13** (Oct., 1964) 508–509. 9

[7] F. Englert and R. Brout, "Broken Symmetry and the Mass of Gauge Vector Mesons," *Physical Review Letters* **13** (Aug., 1964) 321–323. 9

[8] M. E. Peskin and D. V. Schroeder, "An Introduction to quantum field theory,". Reading, USA: Addison-Wesley (1995) 842 p. 11, 38, 51, 63, 116, 197, 198

[9] A. Abashian *et al.*, "The Belle Detector," *Nucl. Instrum. Meth.* **A479** (2002) 117–232. 13

[10] **BABAR** Collaboration, B. Aubert *et al.*, "The BaBar detector," *Nucl. Instrum. Meth.* **A479** (2002) 1–116, arXiv:hep-ex/0105044. 13

[11] **Particle Data Group** Collaboration, C. Amsler *et al.*, "Review of particle physics," *Phys. Lett.* **B667** (2008) 1–1340. 14, 15

[12] **LEP Working Group for Higgs boson searches** Collaboration, R. Barate *et al.*, "Search for the standard model Higgs boson at LEP," *Phys. Lett.* **B565** (2003) 61–75, arXiv:hep-ex/0306033. 14

[13] **CDF and D0** Collaboration, T. Aaltonen *et al.*, "Combined CDF and D0 Upper Limits on Standard Model Higgs Boson Production with up to 8.2 fb-1 of Data," arXiv:1103.3233 [hep-ex]. 14

[14] http://lepewwg.web.cern.ch/LEPEWWG/. 14

[15] M. E. Peskin and T. Takeuchi, "Estimation of oblique electroweak corrections," *Phys. Rev.* **D46** (1992) 381–409. 15, 151

[16] **CDF** Collaboration, T. Aaltonen *et al.*, "Evidence for a Mass Dependent Forward-Backward Asymmetry in Top Quark Pair Production," arXiv:1101.0034 [hep-ex]. 16

[17] M. Milgrom, "MOND–a pedagogical review," *Acta Phys. Polon.* **B32** (2001) 3613, arXiv:astro-ph/0112069. 16

[18] **MACHO** Collaboration, C. Alcock *et al.*, "The MACHO Project LMC Microlensing Results from the First Two Years and the Nature of the Galactic Dark Halo," *Astrophys. J.* **486** (1997) 697–726, arXiv:astro-ph/9606165. 16

[19] P. Minkowski, "mu → e gamma at a Rate of One Out of 1-Billion Muon Decays?," *Phys. Lett.* **B67** (1977) 421. 16

[20] C. Grojean, "New theories for the Fermi scale," *PoS* **EPS-HEP2009** (2009) 008, arXiv:0910.4976 [hep-ph]. 17

[21] S. P. Martin, "A Supersymmetry Primer," arXiv:hep-ph/9709356. 19, 162, 163, 209

[22] N. Arkani-Hamed, A. G. Cohen, and H. Georgi, "Electroweak symmetry breaking from dimensional deconstruction," *Phys. Lett.* **B513** (2001) 232–240, arXiv:hep-ph/0105239. 20

[23] I. Low, "T parity and the littlest Higgs," *JHEP* **10** (2004) 067, arXiv:hep-ph/0409025. 21, 165, 166

[24] **ATLAS** Collaboration, J. E. Garcia, "Little Higgs searches at LHC," arXiv:hep-ph/0405156. 21

[25] K. Lane, "Two lectures on technicolor," arXiv:hep-ph/0202255. 21

[26] G. F. Giudice, C. Grojean, A. Pomarol, and R. Rattazzi, "The Strongly-Interacting Light Higgs," *JHEP* **06** (2007) 045, arXiv:hep-ph/0703164. 21

[27] J. M. Maldacena, "The large N limit of superconformal field theories and supergravity," *Adv. Theor. Math. Phys.* **2** (1998) 231–252, arXiv:hep-th/9711200. 21, 31

[28] T. Appelquist, G. T. Fleming, and E. T. Neil, "Lattice Study of the Conformal Window in QCD-like Theories," *Phys. Rev. Lett.* **100** (2008) 171607, arXiv:0712.0609 [hep-ph]. 21

[29] A. A. Penzias and R. W. Wilson, "A Measurement of excess antenna temperature at 4080- Mc/s," *Astrophys. J.* **142** (1965) 419–421. 23

[30] K. G. Begeman, A. H. Broeils, and R. H. Sanders, "Extended rotation curves of spiral galaxies: Dark haloes and modified dynamics," *Mon. Not. Roy. Astron. Soc.* **249** (1991) 523. 23, 24

[31] D. Clowe *et al.*, "A direct empirical proof of the existence of dark matter," *Astrophys. J.* **648** (2006) L109–L113, arXiv:astro-ph/0608407. 24

[32] **SDSS** Collaboration, E. S. Sheldon *et al.*, "Cross-correlation Weak Lensing of SDSS Galaxy Clusters III: Mass-to-light Ratios," *Astrophys. J.* **703** (2009) 2232–2248, arXiv:0709.1162 [astro-ph]. 24

[33] **Supernova Cosmology Project** Collaboration, M. Kowalski *et al.*, "Improved Cosmological Constraints from New, Old and Combined Supernova Datasets," *Astrophys. J.* **686** (2008) 749–778, arXiv:0804.4142 [astro-ph]. 24, 25

[34] **WMAP** Collaboration, E. Komatsu *et al.*, "Seven-Year Wilkinson Microwave Anisotropy Probe (WMAP) Observations: Cosmological Interpretation," *Astrophys. J. Suppl.* **192** (2011) 18, arXiv:1001.4538 [astro-ph.CO]. 25

[35] "Official wmap webpage." http://map.gsfc.nasa.gov/. 25

[36] K. Agashe, R. Contino, and A. Pomarol, "The Minimal Composite Higgs Model," *Nucl. Phys.* **B719** (2005) 165–187, arXiv:hep-ph/0412089. 25, 170, 174, 183

[37] **SDSS** Collaboration, B. A. Reid *et al.*, "Baryon Acoustic Oscillations in the Sloan Digital Sky Survey Data Release 7 Galaxy Sample," *Mon. Not. Roy. Astron. Soc.* **401** (2010) 2148–2168, arXiv:0907.1660 [astro-ph.CO]. 25

[38] N. Jarosik *et al.*, "Seven-Year Wilkinson Microwave Anisotropy Probe (WMAP) Observations: Sky Maps, Systematic Errors, and Basic Results," *Astrophys. J. Suppl.* **192** (2011) 14, arXiv:1001.4744 [astro-ph.CO]. 26

[39] G. Servant and T. M. P. Tait, "Is the lightest Kaluza-Klein particle a viable dark matter candidate?," *Nucl. Phys.* **B650** (2003) 391–419, arXiv:hep-ph/0206071. 26, 28, 29, 44, 83

[40] K. Griest and D. Seckel, "Three exceptions in the calculation of relic abundances," *Phys. Rev.* **D43** (1991) 3191–3203. 26, 28

[41] E. W. Kolb and M. S. Turner, "The Early universe," *Front. Phys.* **69** (1990) 1–547. 27

[42] A. B. Lahanas, D. V. Nanopoulos, and V. C. Spanos, "Neutralino relic density in a Universe with a non- vanishing cosmological constant," *Phys. Rev.* **D62** (2000) 023515, arXiv:hep-ph/9909497. 28

[43] K. Kong and K. T. Matchev, "Precise calculation of the relic density of Kaluza-Klein dark matter in universal extra dimensions," *JHEP* **01** (2006) 038, arXiv:hep-ph/0509119. 29, 44

[44] G. Belanger, F. Boudjema, A. Pukhov, and A. Semenov, "micrOMEGAs2.0: A program to calculate the relic density of dark matter in a generic model," *Comput. Phys. Commun.* **176** (2007) 367–382, arXiv:hep-ph/0607059. 29

[45] T. Kaluza, "On the Problem of Unity in Physics," *Sitzungsber. Preuss. Akad. Wiss. Berlin (Math. Phys.)* **1921** (1921) 966–972. 30

[46] O. Klein, "Quantum theory and five-dimensional theory of relativity," *Z. Phys.* **37** (1926) 895–906. 30

[47] I. Antoniadis, "A Possible new dimension at a few TeV," *Phys. Lett.* **B246** (1990) 377–384. 30

[48] I. Antoniadis, N. Arkani-Hamed, S. Dimopoulos, and G. R. Dvali, "New dimensions at a millimeter to a Fermi and superstrings at a TeV," *Phys. Lett.* **B436** (1998) 257–263, arXiv:hep-ph/9804398. 30

[49] R. Franceschini, G. F. Giudice, P. P. Giardino, P. Lodone, and A. Strumia, "LHC bounds on large extra dimensions," arXiv:1101.4919 [hep-ph]. 31

[50] L. Randall and R. Sundrum, "A large mass hierarchy from a small extra dimension," *Phys. Rev. Lett.* **83** (1999) 3370–3373, arXiv:hep-ph/9905221. 31, 170

[51] **CMS** Collaboration, S. Chatrchyan *et al.*, "Search for Resonances in the Dilepton Mass Distribution in pp Collisions at sqrt(s) = 7 TeV," arXiv:1103.0981 [hep-ex]. 31, 149

[52] C. Csaki, J. Hubisz, and P. Meade, "Electroweak symmetry breaking from extra dimensions," arXiv:hep-ph/0510275. 32, 34, 38, 41

[53] G. D. Kribs, "Phenomenology of extra dimensions," arXiv:hep-ph/0605325. 32

[54] G. Burdman, "New solutions to the hierarchy problem," *Braz. J. Phys.* **37** (2007) 506–513, arXiv:hep-ph/0703194. 32

[55] H.-C. Cheng, "2009 TASI Lecture – Introduction to Extra Dimensions," arXiv:1003.1162 [hep-ph]. 32

[56] N. Haba, M. Harada, Y. Hosotani, and Y. Kawamura, "Dynamical rearrangement of gauge symmetry on the orbifold S(1)/Z(2)," *Nucl. Phys.* **B657** (2003) 169–213, arXiv:hep-ph/0212035. 37, 212

[57] C. Csaki, C. Grojean, H. Murayama, L. Pilo, and J. Terning, "Gauge theories on an interval: Unitarity without a Higgs," *Phys. Rev.* **D69** (2004) 055006, arXiv:hep-ph/0305237. 37

[58] C. Csaki, C. Grojean, L. Pilo, and J. Terning, "Towards a realistic model of Higgsless electroweak symmetry breaking," *Phys. Rev. Lett.* **92** (2004) 101802, arXiv:hep-ph/0308038. 37

[59] C. A. Scrucca, M. Serone, L. Silvestrini, and A. Wulzer, "Gauge-Higgs Unification in Orbifold Models," *JHEP* **02** (2004) 049, arXiv:hep-th/0312267. 37, 176

[60] C. Csaki, C. Grojean, J. Hubisz, Y. Shirman, and J. Terning, "Fermions on an interval: Quark and lepton masses without a Higgs," *Phys. Rev.* **D70** (2004) 015012, arXiv:hep-ph/0310355. 42, 60, 216

[61] C. Csaki, C. Grojean, and H. Murayama, "Standard Model Higgs from Higher Dimensional Gauge Fields," *Phys. Rev.* **D67** (2003) 085012, arXiv:hep-ph/0210133. 42

[62] B. A. Dobrescu and E. Ponton, "Chiral compactification on a square," *JHEP* **03** (2004) 071, arXiv:hep-th/0401032. 42, 51, 54

[63] G. Cacciapaglia, A. Deandrea, and J. Llodra-Perez, "A Dark Matter candidate from Lorentz Invariance in 6 Dimensions," *JHEP* **03** (2010) 083, arXiv:0907.4993 [hep-ph]. 42, 48, 105, 198, 204

[64] H.-C. Cheng, K. T. Matchev, and M. Schmaltz, "Radiative corrections to Kaluza-Klein masses," *Phys. Rev.* **D66** (2002) 036005, arXiv:hep-ph/0204342. 44, 45, 48, 63, 73

[65] J. Bagger, K. T. Matchev, and D. Pierce, "Precise predictions for masses and couplings in the minimal supersymmetric standard model," arXiv:hep-ph/9503422. 44

[66] G. Belanger, M. Kakizaki, and A. Pukhov, "Dark matter in UED : the role of the second KK level," arXiv:1012.2577 [hep-ph]. 44, 88

[67] L. Nilse, "Classification of 1D and 2D orbifolds," arXiv:hep-ph/0601015. 48, 50

[68] E. Ponton and L. Wang, "Radiative effects on the chiral square," *JHEP* **11** (2006) 018, arXiv:hep-ph/0512304. 51, 75, 90, 104

[69] J. Polchinski, "String theory. Vol. 2: Superstring theory and beyond,". Cambridge, UK: Univ. Pr. (1998) 531 p. 51

[70] H. Dohi and K. ya Oda, "Universal Extra Dimensions on Real Projective Plane," *Phys. Lett.* **B692** (2010) 114–120, arXiv:1004.3722 [hep-ph]. 62

[71] L. Da Rold, "Radiative corrections in 5D and 6D expanding in winding modes," *Phys. Rev.* **D69** (2004) 105015, arXiv:hep-th/0311063. 63, 64

[72] M. Puchwein and Z. Kunszt, "Radiative corrections with 5D mixed position- / momentum- space propagators," *Annals Phys.* **311** (2004) 288–313, arXiv:hep-th/0309069. 63, 70

[73] H. Georgi, A. K. Grant, and G. Hailu, "Brane couplings from bulk loops," *Phys. Lett.* **B506** (2001) 207–214, arXiv:hep-ph/0012379. 64, 193, 194

[74] T. Appelquist, H.-C. Cheng, and B. A. Dobrescu, "Bounds on universal extra dimensions," *Phys. Rev.* **D64** (2001) 035002, arXiv:hep-ph/0012100. 72, 150, 153, 170, 183

[75] B. A. Dobrescu, D. Hooper, K. Kong, and R. Mahbubani, "Spinless photon dark matter from two universal extra dimensions," *JCAP* **0710** (2007) 012, arXiv:0706.3409 [hep-ph]. 85

[76] A. Arbey, A. Deandrea, and A. Tarhini, "Anomaly mediated SUSY breaking scenarios in the light of cosmology and in the dark (matter)," arXiv:1103.3244 [hep-ph]. 86

[77] M. Kakizaki, S. Matsumoto, Y. Sato, and M. Senami, "Relic abundance of LKP dark matter in UED model including effects of second KK resonances," *Nucl. Phys.* **B735** (2006) 84–95, arXiv:hep-ph/0508283. 88

[78] G. Cacciapaglia, A. Deandrea, and J. Llodra-Perez, "The Universal Real Projective Plane: LHC phenomenology at one Loop," arXiv:1104.3800 [hep-ph]. 90, 91, 134, 150

[79] A. Abdesselam *et al.*, "Boosted objects: a probe of beyond the Standard Model physics," arXiv:1012.5412 [hep-ph]. 123

[80] D. Krohn, L. Randall, and L.-T. Wang, "On the Feasibility and Utility of ISR Tagging," arXiv:1101.0810 [hep-ph]. 123

[81] G. Cacciapaglia, R. Chierici, A. Deandrea, L. Panizzi, S. Perries, and S. Tosi, "...." to appear soon. 123, 124, 132, 150

[82] J. Alwall, M.-P. Le, M. Lisanti, and J. G. Wacker, "Model-Independent Jets plus Missing Energy Searches," *Phys. Rev.* **D79** (2009) 015005, arXiv:0809.3264 [hep-ph]. 124

[83] A.Pukhov, "Calchep-calculator for high energy physics- a package for evaluation of feynman diagrams, integration over multi-particle phase space, and event generation.," *not published* (2005) . http://theory.sinp.msu.ru/~pukhov/calchep.html. 124, 133

[84] F. Maltoni and T. Stelzer, "MadEvent: Automatic event generation with MadGraph," *JHEP* **02** (2003) 027, arXiv:hep-ph/0208156. http://madgraph.hep.uiuc.edu/. 124

[85] T. Sjostrand, S. Mrenna, and P. Z. Skands, "A Brief Introduction to PYTHIA 8.1," *Comput. Phys. Commun.* **178** (2008) 852–867, arXiv:0710.3820 [hep-ph]. http://home.thep.lu.se/~torbjorn/Pythia.html. 124

[86] N. D. Christensen and C. Duhr, "FeynRules - Feynman rules made easy," *Comput. Phys. Commun.* **180** (2009) 1614–1641, arXiv:0806.4194 [hep-ph]. http://feynrules.phys.ucl.ac.be/. 125, 127, 133

[87] T. Hahn, "Generating Feynman diagrams and amplitudes with FeynArts 3," *Comput. Phys. Commun.* **140** (2001) 418–431, arXiv:hep-ph/0012260. 131

[88] A. Datta, K. Kong, and K. T. Matchev, "Minimal Universal Extra Dimensions in CalcHEP/CompHEP," *New J. Phys.* **12** (2010) 075017, arXiv:1002.4624 [hep-ph]. http://theory.sinp.msu.ru/~pukhov/calchep.html. 133

[89] S. Kretzer, H. L. Lai, F. I. Olness, and W. K. Tung, "CTEQ6 parton distributions with heavy quark mass effects," *Phys. Rev.* **D69** (2004) 114005, arXiv:hep-ph/0307022. 133, 143

[90] V. Barger, W.-Y. Keung, and B. Yencho, "Triple-Top Signal of New Physics at the LHC," *Phys. Lett.* **B687** (2010) 70–74, arXiv:1001.0221 [hep-ph]. 148

[91] **ATLAS** Collaboration, G. Aad *et al.*, "Search for high mass dilepton resonances in pp collisions at sqrts=7 TeV with the ATLAS experiment," arXiv:1103.6218 [hep-ex]. 149

[92] **ATLAS** Collaboration, G. Aad *et al.*, "Search for high-mass states with one lepton plus missing transverse momentum in proton-proton collisions at sqrt(s) = 7 TeV with the ATLAS detector," arXiv:1103.1391 [hep-ex]. 150

[93] **CMS** Collaboration, S. Chatrchyan *et al.*, "Search for a W' boson decaying to a muon and a neutrino in pp collisions at sqrt(s) = 7 TeV," arXiv:1103.0030 [hep-ex]. 150

[94] G. Cacciapaglia, A. Deandrea, and J. Llodra-Perez, "Higgs to Gamma Gamma beyond the Standard Model," *JHEP* **06** (2009) 054, arXiv:0901.0927 [hep-ph]. 156

[95] M. Pieri *et al.*, "Inclusive search for the Higgs boson in the H –> gamma gamma channel,". CERN-CMS-NOTE-2006-112. 156

[96] **ATLAS** Collaboration, L. Carminati, "Search for a standard model Higgs boson in the H → gamma gamma channel with the ATLAS detector," *Acta Phys. Polon.* **B38** (2007) 747–754. 156

[97] M. Duhrssen *et al.*, "Extracting Higgs boson couplings from LHC data," *Phys. Rev.* **D70** (2004) 113009, arXiv:hep-ph/0406323. 156

[98] M. Spira, A. Djouadi, D. Graudenz, and P. M. Zerwas, "Higgs boson production at the LHC," *Nucl. Phys.* **B453** (1995) 17–82, arXiv:hep-ph/9504378. 158

[99] G. D. Kribs, T. Plehn, M. Spannowsky, and T. M. P. Tait, "Four generations and Higgs physics," *Phys. Rev.* **D76** (2007) 075016, arXiv:0706.3718 [hep-ph]. 161

[100] **Particle Data Group** Collaboration, K. Nakamura *et al.*, "Review of particle physics," *J. Phys.* **G37** (2010) 075021. 161

[101] M. S. Carena, S. Heinemeyer, C. E. M. Wagner, and G. Weiglein, "Suggestions for benchmark scenarios for MSSM Higgs boson searches at hadron colliders," *Eur. Phys. J.* **C26** (2003) 601–607, arXiv:hep-ph/0202167. 161

[102] A. Dobado, M. J. Herrero, and S. Penaranda, "The Higgs sector of the MSSM in the decoupling limit," *Eur. Phys. J.* **C17** (2000) 487–500, arXiv:hep-ph/0002134. 162

[103] M. Perelstein and C. Spethmann, "A collider signature of the supersymmetric golden region," *JHEP* **04** (2007) 070, arXiv:hep-ph/0702038. 162, 183

[104] I. Low and S. Shalgar, "Implications of the Higgs Discovery in the MSSM Golden Region," *JHEP* **04** (2009) 091, arXiv:0901.0266 [hep-ph]. 162

[105] M. Schmaltz and D. Tucker-Smith, "Little Higgs Review," *Ann. Rev. Nucl. Part. Sci.* **55** (2005) 229–270, arXiv:hep-ph/0502182. 163

[106] M. Schmaltz, "The simplest little Higgs," *JHEP* **08** (2004) 056, arXiv:hep-ph/0407143. 164

[107] G. Marandella, C. Schappacher, and A. Strumia, "Little-Higgs corrections to precision data after LEP2," *Phys. Rev.* **D72** (2005) 035014, arXiv:hep-ph/0502096. 165, 166

[108] N. Arkani-Hamed, A. G. Cohen, E. Katz, and A. E. Nelson, "The littlest Higgs," *JHEP* **07** (2002) 034, arXiv:hep-ph/0206021. 165

[109] T. Han, H. E. Logan, B. McElrath, and L.-T. Wang, "Loop induced decays of the little Higgs: H –> g g, gamma gamma," *Phys. Lett.* **B563** (2003) 191–202, arXiv:hep-ph/0302188. 165

[110] J. Hubisz, P. Meade, A. Noble, and M. Perelstein, "Electroweak precision constraints on the littlest Higgs model with T parity," *JHEP* **01** (2006) 135, arXiv:hep-ph/0506042. 166

[111] A. V. Manohar and M. B. Wise, "Flavor changing neutral currents, an extended scalar sector, and the Higgs production rate at the LHC," *Phys. Rev.* **D74** (2006) 035009, arXiv:hep-ph/0606172. 166, 167

[112] B. Grinstein, D. O'Connell, and M. B. Wise, "The Lee-Wick standard model," *Phys. Rev.* **D77** (2008) 025012, arXiv:0704.1845 [hep-ph]. 167, 169

[113] F. Krauss, T. E. J. Underwood, and R. Zwicky, "The Process $gg \to h(0) \to \gamma\gamma$ in the Lee- Wick standard model," *Phys. Rev.* **D77** (2008) 015012, arXiv:0709.4054 [hep-ph]. 167, 168, 169, 209

[114] T. E. J. Underwood and R. Zwicky, "Electroweak Precision Data and the Lee-Wick Standard Model," *Phys. Rev.* **D79** (2009) 035016, arXiv:0805.3296 [hep-ph]. 169

[115] R. Barbieri, L. J. Hall, and Y. Nomura, "A constrained standard model from a compact extra dimension," *Phys. Rev.* **D63** (2001) 105007, arXiv:hep-ph/0011311. 170

[116] G. Cacciapaglia, M. Cirelli, and G. Cristadoro, "Gluon fusion production of the Higgs boson in a calculable model with one extra dimension," *Phys. Lett.* **B531** (2002) 105–111, arXiv:hep-ph/0111287. 170

[117] G. Cacciapaglia, C. Csaki, G. Marandella, and J. Terning, "The gaugephobic Higgs," *JHEP* **02** (2007) 036, arXiv:hep-ph/0611358. 170, 174

[118] C. Csaki, J. Erlich, and J. Terning, "The effective Lagrangian in the Randall-Sundrum model and electroweak physics," *Phys. Rev.* **D66** (2002) 064021, arXiv:hep-ph/0203034. 170

[119] Y. Hosotani, "Dynamical Mass Generation by Compact Extra Dimensions," *Phys. Lett.* **B126** (1983) 309. 170

[120] G. Cacciapaglia, C. Csaki, and S. C. Park, "Fully radiative electroweak symmetry breaking," *JHEP* **03** (2006) 099, arXiv:hep-ph/0510366. 170, 171, 177

[121] G. Panico, M. Serone, and A. Wulzer, "A model of electroweak symmetry breaking from a fifth dimension," *Nucl. Phys.* **B739** (2006) 186–207, arXiv:hep-ph/0510373. 170, 171, 177, 183

[122] N. Maru and N. Okada, "Gauge-Higgs Unification at LHC," *Phys. Rev.* **D77** (2008) 055010, arXiv:0711.2589 [hep-ph]. 170

[123] K. Agashe and R. Contino, "The minimal composite Higgs model and electroweak precision tests," *Nucl. Phys.* **B742** (2006) 59–85, arXiv:hep-ph/0510164. 170, 174, 183

[124] A. Djouadi and G. Moreau, "Higgs production at the LHC in warped extra-dimensional models," *Phys. Lett.* **B660** (2008) 67–71, arXiv:0707.3800 [hep-ph]. 170

[125] A. Falkowski, "Pseudo-Goldstone Higgs Production via Gluon Fusion," *Phys. Rev.* **D77** (2008) 055018, arXiv:0711.0828 [hep-ph]. 170, 181

[126] N. Maru, "Finite Gluon Fusion Amplitude in the Gauge-Higgs Unification," *Mod. Phys. Lett.* **A23** (2008) 2737–2750, arXiv:0803.0380 [hep-ph]. 170

[127] K. Agashe, A. Delgado, M. J. May, and R. Sundrum, "RS1, custodial isospin and precision tests," *JHEP* **08** (2003) 050, arXiv:hep-ph/0308036. 174

[128] N. Arkani-Hamed and M. Schmaltz, "Hierarchies without symmetries from extra dimensions," *Phys. Rev.* **D61** (2000) 033005, arXiv:hep-ph/9903417. 178

[129] Y. Grossman and M. Neubert, "Neutrino masses and mixings in non-factorizable geometry," *Phys. Lett.* **B474** (2000) 361–371, arXiv:hep-ph/9912408. 180

[130] T. Gherghetta and A. Pomarol, "Bulk fields and supersymmetry in a slice of AdS," *Nucl. Phys.* **B586** (2000) 141–162, arXiv:hep-ph/0003129. 180

[131] **CMS** Collaboration, G. L. Bayatian *et al.*, "CMS physics: Technical design report,". CERN-LHCC-2006-001. 184

[132] D. L. Rainwater and D. Zeppenfeld, "Searching for H –> gamma gamma in weak boson fusion at the LHC," *JHEP* **12** (1997) 005, arXiv:hep-ph/9712271. 184

[133] **CMS** Collaboration, K. Mazumdar, "Search for light Higgs boson at LHC via production through weak boson fusion," arXiv:hep-ex/0308070. 184

[134] ILCcollab., "Ilc reach." for more information and recent pdates, see the talks at the INFN Workshop *LC08: e+e- Physics at the TeW scale*, Laboratori Nazionali di Frascati (Italy), 22-25 September 2008, http://www.lnf.infn.it/conference/lc08, 2008. 185

[135] C. Itzykson and J. B. Zuber, "QUANTUM FIELD THEORY,". New York, Usa: Mcgraw-hill (1980) 705 P.(International Series In Pure and Applied Physics). 198

NOM : LLODRA-PEREZ

Prénoms : Jérémie

DATE de SOUTENANCE

1er juillet 2011

TITRE : **Modèles effectifs de nouvelle physique au Large Hadron Collider**

Numéro d'ordre : 127-2011

DIPLOME DE DOCT.	DOCTEUR-INGENIEUR	DOCTORAT D'ETAT	DOCTORAT DE 3e CYCLE	Spécialité : Physique des Particules Physique Théorique
X	☐	☐	☐	

Cote B.I.U. – Lyon : T 50/210/19 / et bis

CLASSE :

RESUME :

Avec l'exploitation du Large Hadron Collider, débutée en 2010, les physiciens des particules espèrent comprendre plus précisément de la brisure de la symétrie électrofaible et résoudre certaines questions expérimentales et théoriques que soulève encore le modèle standard. S'inscrivant dans cette effervescence scientifique, nous présentons dans cette thèse une paramétrisation indépendante des modèles afin de caractériser les effets d'une éventuelle nouvelle physique sur la production et la désintégration du boson de Higgs. Ce nouvel outil pourra aisément être utilisé dans les analyses des expériences généralistes comme CMS et ATLAS afin de valider ou d'exclure de manière significative certaines théories au delà du modèle standard.

Ensuite, dans une approche fondée sur la construction de modèles, nous avons considéré un scenario avec un espace plat à six dimensions dont deux sont compactifiées sur un Plan Projectif Réel. A six dimensions, cet orbifold est l'unique géométrie qui présente des fermions chiraux et un candidat de matière noire dit naturel. Le photon scalaire, particule la plus légère du premier mode de Kaluza-Klein, est en effet stabilisée par une symétrie relique de l'invariance de Lorentz. En utilisant les contraintes cosmologiques actuelles, nous avons estimé la masse caractéristique de cette particule à quelques centaines de GeV. De ce fait les nouveaux états présents dans cette théorie sont assez légers pour produire des signatures observables au LHC. Avec une étude du spectre de masses et des couplages du modèle incluant les corrections radiatives à une boucle, nous pouvons ainsi donner les premières contraintes sur la phénoménologie du LHC.

MOTS-CLES : dimensions supplémentaires ; compactification ; matière noire ; corrections radiatives ; Boson de Higgs ; Large Hadron Colliders ; phénoménologie

Directeurs de recherches : Aldo Deandrea – Giaccomo Cacciapaglia

Composition du jury : D. Tsimpis – G. Servant – E. Dudas – G. Moreau

224 pages